MODELLING OF FLOWS THROUGH HYDRAULIC STRUCTURES AND INTERACTION WITH SEDIMENT

A thesis submitted to the Cardiff University
In candidature for the degree of
Doctor of Philosophy

by:

Shervin Faghihirad

B.Sc., M.Sc.

Cardiff School of Engineering
Cardiff University

April 2014

DECLARATION

This work has not previously been accepted in substance for degree and is not concurrently being submitted in candidature for any degree.

Signed.....(candidate)

Date.....

STATEMENT 1

This thesis is the result of my own investigations, except where otherwise stated.

Other sources are acknowledged by footnotes giving explicit references. A bibliography is appended.

Signed.....(candidate)

Date.....

STATEMENT 2

I hereby give consent for my thesis, if accepted to be available for photocopying and for interlibrary loan, and for the title and summary to be made available to outside organisations.

Signed.....(candidate)

Date.....

ABSTRACT

A three-dimensional layer integrated morphodynamic model has been developed to predict the hydrodynamic, sediment transport and morphological processes in a regulated reservoir. The model was based on an existing sediment transport model, with improvements being made. A bed evolution module based on the mass balance equation has been developed to determine the bed level change due to sediment transport. The horizontal eddy viscosity coefficient was equated to the depth averaged eddy viscosity, based on the horizontal velocity distribution while the vertical eddy viscosity coefficient was evaluated using the layer integrated form of the k-ε equations. This scheme enhances the accuracy of the computed velocity and suspended sediment concentration distributions.

The highly accurate ULTIMATE QUICKEST scheme was used to represent the advective terms in solving the advective-diffusion equation for suspended sediment transport. An explicit finite difference scheme has been developed for the bed sediment mass balance equation to calculate bed level changes. The numerical model was verified against laboratory data obtained from experiments in a trench and a partially closed channel.

A physical model was constructed to represent the flow, sediment transport and morphodynamic processes in Hamidieh regulated reservoir. The physical model was designed based on the Froude similarity law and was undistorted. The model sediment size was determined in such a manner that the same ratio of particle fall velocity to shear velocity is maintained for both the model and prototype reservoir. Stokes law was used in calculating the particle fall velocity. The physical model results confirmed that the normal water surface elevation in the reservoir should increase by up to 25 cm in order to reach the nominal flow discharge diverted to the intakes.

The numerical model was then applied to the scaled physical model of the reservoir and the associated water intakes and sluice gates. Various scenarios were tested to investigate the effects of different situations of diverting flow and sediment transport regimes, as well as to establish how these operations affect the morphodynamic processes in the reservoir and the vicinity of hydraulic structures. The model predictions agreed with measured data generally well. The numerical model results revealed the possibility of forming sedimentary islands in the regulated reservoir and it is uneconomical to set up a dredging zone near the one of the intakes. In summary, the integrated numerical and physical modelling approach showed many benefits and could help to optimize time and budget for design hydraulic structures.

Key words: morphodynamic numerical model, turbulent flow, regulated reservoir, three-dimensional flow, laboratory tests.

ACKNOWLEDGEMENTS

I would like to express my sincere gratitude to my supervisors Professor Binliang Lin and Professor Roger A. Falconer for the help, guidance and support they were given during this research project. The author wishes to thank the Water Research Institute in Iran for assisting in the laboratory physical model tests.

I am eternally grateful to my parents, my wife and my son for their continuous love, enormous support and encouragement.

Table of Contents

List of Figures

List of Tables

Notations

A	cross-sectional area
a	reference level
B	channel width
C	Chézy - coefficient
C_d	vegetation drag coefficient
C_e	eddy viscosity coefficient
C_p	suspended sediment concentration in the prototype
C_v	coefficient of approach velocity
C_w	air/fluid resistance coefficient
C'	grain roughness coefficient
$c_\mu, c_{1\varepsilon}$, $c_{2\varepsilon}$,σ_k, σ_ε	empirical constants in $k-\varepsilon$ turbulence model
D	representative sediment grain size
D_*	dimensionless particle parameter
D_H	hydraulic diameter
D_r	sediment particle size scale ratio
d_{20}	20% particle diameter
d_{50}	50% particle diameter
d_{90}	90% particle diameter
f	Coriolis parameter
f	Darcy–Weisbach friction factor
Fr	Froude number
F_r	force scale ratio
Fr_*	grain (Densimetric) Froude number
g	gravitational acceleration
H	total depth of flow
h	depth of flow
k_s	bed roughness length
$L_r (or\ \lambda)$	scale ratio (inverse of scale $1:\lambda$)
lh	layer thickness
$lhxm, lhxu$	layer thicknesses in the x-direction for pervious and current time step

$lhym, lhyu$	layer thicknesses in the y-direction for pervious and current time step
n	Manning coefficient
n_r	Manning's roughness scale ratio
$p(=UH)$	discharges per unit width in the x direction
p	porosity of the sediment material
$q(=VH)$	discharges per unit width in the y direction
q_m	source discharge per unit horizontal area
$q_{s,x} + q_{b,x}$	total sediment load transport rates per unit width in the x direction
$q_{s,y} + q_{b,y}$	total sediment load transport rates per unit width in the y direction
Q_r	discharge scale ratio
Q_{sm}	suspended sediment load discharge in the model
Q_{wm}	water discharge in the model
q_b	bed load transport rate
Re	Reynolds number
Re_*	grain size Reynolds number
R	hydraulic radius
S	slope of the energy gradient
S_{ae}	equilibrium concentration at a reference level
S_b	bed load concentration
S_P	effective correlation the shape factor
s_s	specific gravity
T	dimensionless bed-shear stress parameter (or transport stage parameter)
t_r	time scale ratio
U,V	depth averaged velocity components in the x and y directions respectively
U_*	depth averaged shear velocity
U_a	effective particle velocity
U_b	velocity of bed load particles
u, v, w	components of velocity in the x, y, z
u_*	shear velocity

V_s	depth averaged flow speed (=$\sqrt{U^2+V^2}$)
V_r	velocity scale ratio
W	Weber number
W_s	wind speed
W_x,W_y	wind velocity components in the x, y directions, respectively
w_s	settling (fall) velocity
Z	dimensionless suspension parameter
z_b	bed level
z_c	distance to the wall at the first grid point
α	contraction coefficient
α_1	relaxation coefficient
β	momentum correction factor for a non-uniform vertical velocity profile
γ	specific weight of water
γ_s	specific weight of sediment particles
$\frac{\partial}{\partial t}(H\bar{s})$	storage term
δ_b	siltation height
ε_h, ε_v	horizontal and vertical eddy viscosities, respectively
$\varepsilon_x, \varepsilon_y, \varepsilon_z$	sediment mixing coefficient in x, y, z direction, respectively
η	water surface elevation above datum
ϑ	turbulent velocity
ℓ	turbulent length scale
ℓ_m	a new turbulence length scale
κ	von Karman's constant
μ	dynamic viscosity
ν	kinematic viscosity
ρ	fluid density
ρ_a	air density
ρ_s	sediment density
σ_h, σ_v	Schmidt numbers is the horizontal and vertical directions respectively

$\sigma_{yy}, \tau_{xy}, \tau_{xz}, \tau_{yx}, \sigma_{yy}, \tau_{yz}$	components of the stress tensor in the $x-z$ and $y-z$ plane, respectively
τ_b	bed shear stress
$\tau_{b.cr}$	critical bed shear stress

Chapter One

Introduction

1.1 The essence of the research

The central concern of the dissertation is to study hydraulic flows and sediment phenomena through hydraulic structures in a regulated reservoir. The flow patterns in and around most hydraulic structures are complex, three-dimensional, and highly turbulent. Furthermore, the use of a three-dimensional (3-D) numerical model instead of a two-dimensional (2-D), depth-averaged one is strongly recommended where sediment concentration changes in the vertical profile are considerable such as near intakes and sluice gates. For these reasons, in order to understand the impact of hydraulic structures on the hydrodynamic, sediment transport processes and morphological changes in regulated reservoirs it is often necessary to investigate these processes in three dimensions. The main goal of this research is to refine existing numerical (3-D) model and develop a proposed mathematical scheme for predicting the bed level changes in the vicinity of hydraulic structures where complex geometry, flow pattern, turbulence and sediment concentration distribution have important effects on the simulation results.

The type of the research is an application research and how uses a mathematical knowledge in order to simulate natural process correctly for a real case study. In design a real and complex water regulated reservoir both physical and numerical models are used. Currently, physical models are still widely used as an essential tool to obtain information about the above processes. Generally speaking, physical models need a long time to construct and are expensive to run, particularly if large scale models are involved. Numerical models offer the possibility to test various scenarios which are difficult to test in a physical model and this ability will be used for the future operation of the regulated reservoir. Besides, the project cost can be reduced and more options considered.

1.2 Reservoirs

1.2.1 General synthesis

Dams have been constructed worldwide to reduce risks associated with flood hazards, to harness energy for industry and commerce, and to help secure a reliable source of water for domestic, industrial and/or agricultural use.

Most of the existing dams are single-purpose dams, but the number of multipurpose dams is increasing. According to the most recent publication of the World Register of Dams (ICOLD, http://www.icold-cigb.org/GB/Dams/role_of_dams.asp), irrigation is by far the most common purpose of dams. Among the single purpose dams, 50 % are for irrigation, 18% for hydropower (production of electricity), 12% for water supply, 10% for flood control, 5% for recreation and less than 1% for navigation and fish farming.

Presently, irrigated land covers about 277 million hectares (ICOLD, http://www.icold-cigb.org/GB/Dams/role_of_dams.asp), i.e. about 18% of world's arable land but it is responsible for around 40% of crop output and employs nearly 30% of population spread over rural areas. With the large population growth expected for the next decades, irrigation must be expanded to increase the food production capacity. It is estimated that 80% of additional food production by the year 2025 will need to come from irrigated land (ICOLD, http://www.icold-cigb.org/GB/Dams/role_of_dams.asp). Even with the widespread measures to conserve water by improvements in irrigation technology, the construction of more reservoirs will be required.

Runoff waters are a natural resource. For developing countries, storing water is often vital and in many cases, the only means to conserve economically this natural resource (http://icold-cigb.org/GB/World_register/general_synthesis.asp). Reservoirs mainly give guarantee of water supply for irrigation, domestic and industrial use during droughts and reduce negative impacts of floods. Figures 1.1, 1.2 and 1.3 present the purpose of dams constructed worldwide and their attitudes. Referenced dams can be broken in two main categories:

- Single-purpose dams (26938) or 71.6% dams.
- Multi-purpose dams (9321) or 24.8% dams.

Those data are gathered by International Commission on Large Dams (ICOLD, http://www.icold-cigb.org/GB/World_register/general_synthesis.asp) and a basic criterion is a structural dam not less than 15 meters higher than its foundation.

Demand for water is steadily increasing and would reach 2-3 percent per year over the coming decades. With their present aggregate storage of about 14913 km^3, dams clearly

make a significant contribution to the efficient management of the finite water resources that are unevenly distributed and subject to large seasonal fluctuations. Many more dams need to be built to ensure proper use of these resources, in accordance with ICOLD policy (ICOLD, http://www.icold-cigb.org/GB/World_register/general_synthesis.asp) set out in the "Position Paper Dams and Environment".

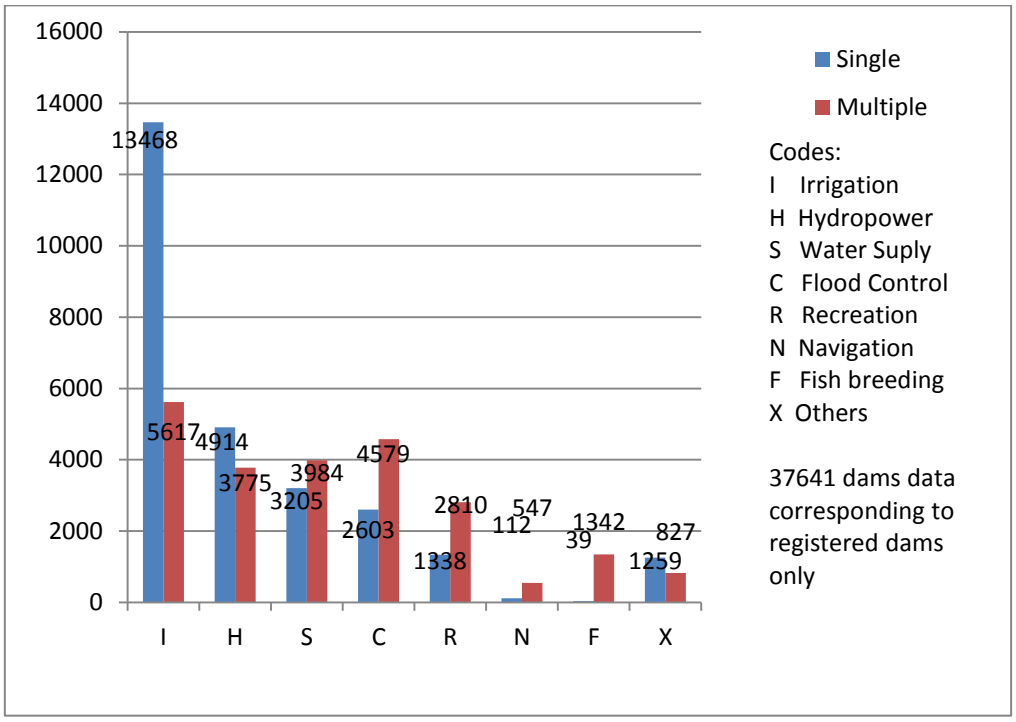

Figure 1.1 Number and purpose of registered dams in ICOLD

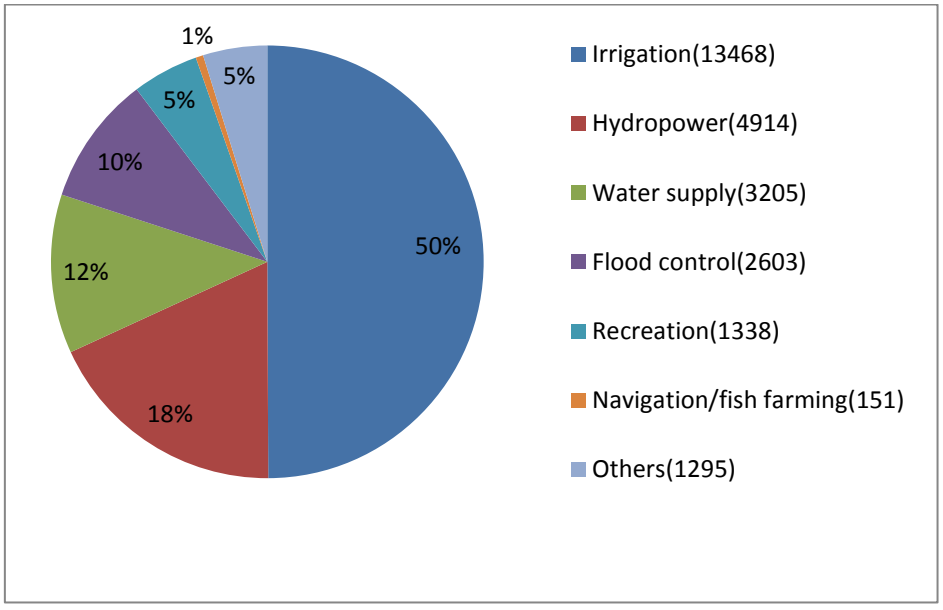

Figure 1.2 The distributed single-purpose dams related to objectives

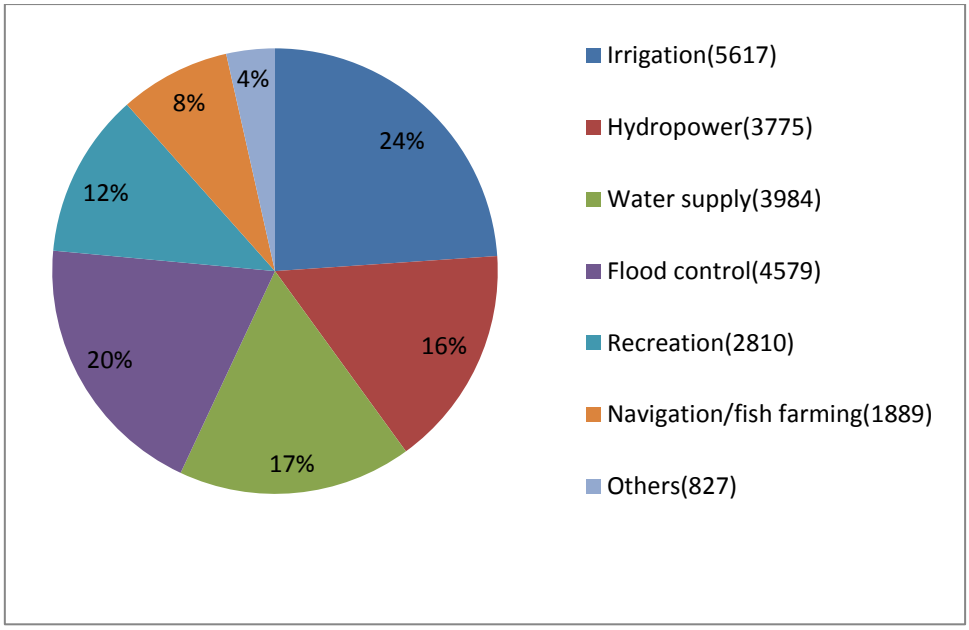

Figure 1.3 The distributed multiple-purpose dams related to objectives

The total of the single-purpose dams could be calculated by the summation of the number of dams belong to different roles. For the multi-purpose dams has to be consider some dams have different role and might be repeated in every group more than one.

1.2.2 Regulated reservoirs

When a regulated reservoir is formed in a river cross section by constructed a low height dam, the natural system would be changed significantly. This type of dam raises the water surface elevation for diverting water flow into an artificial water intake or canal, which be provided and regulated mainly for irrigation networks and agriculture demands. Regulated reservoirs are often constructed downstream of large dams of relatively low elevations (with a low height of the spillway), thereby enabling the flow to be distributed for water supply purposes. However, there are major differences between these regulatory reservoirs and those associated with normal high head dams, in that strong turbulent flows are generated in the regulated reservoir due to the high volumes of flow diversion.

In this research, the role of regulated reservoir would be investigated. Two major hydraulic changes generally occur with the construction of a reservoir. Firstly, the water area upstream of the dam will change from lotic (i.e., running water) to lentic (i.e., still water) in nature, with associated changes in hydrologic, morphological and ecological processes. Secondly, diurnal and seasonal variations in the demand for water will cause short- and long-term variations in discharge.

Regulated reservoirs can modify the sediment regime of a river through retention of material within the reservoir and through modifications of downstream erosion and deposition processes. Short reservoir life expectancies are associated with small-scale dams that impound water with high levels of sediment concentration. Continued deposition of sediment in such reservoirs will result in a decreased water-retention capacity, and may lead to an inability to retard the passage of floodwater downstream.

When water surface elevation rises in the reservoir, intakes could pass water flow to irrigation systems. Sedimentation near the intakes is a major problem for diverting flows during the operation time of regulated reservoirs. Sediments are entered to irrigation networks and caused two main issues. Firstly, bed elevation in irrigation canals rises with the impact of sedimentation and might be need to dredging periodically. Secondly, mineral materials are carried by fine sediments (as wash load) and those are so useful for fertilization. Generally, sediment transport as form of wash load depends on different hydraulic conditions (such as flood times) in the upstream of the regulated reservoirs. Water engineers have to understand the positive and negative issues and try to make a balance between those for presenting a sustainable design of hydraulic structures. Operation and maintenance of irrigation canal need to identify and more understanding about sediment phenomena near and through the hydraulic structures such as intakes and sluice gates in the regulated reservoir. Analysis of those problems is so valuable for water engineers. Understanding flow behaviors and the sediment phenomena in the regulated reservoir and especially near sluice gates and intakes make a platform to propose and design the best scenarios during operation time to reduce the impact of sedimentation for the future in the reservoir and irrigation canal.

Scouring of a river channel immediately downstream of a reservoir commonly occurs, but the patterns of morphological change are very complex. Changes in the flow and flood regimes have many implications relative to the capability of the channel to carry sediment and to flush sediment deposited during low-flow events.

When for water supply to irrigation canals and other water demands need to raise water surface elevation of the river in a certain river cross section and form a regulated reservoir by constructing a low height dam, many subjects has to investigate in designing processes. Some of the most important hydro-environmental and hydraulic concepts are as follows:

- Geomorphology and river morphology
- Hydraulic operations
- Environmental issues
- Type of material and construction

- Economical and social investigations
- Downstream ecology and eco-morphodynamic
- Water quality
- Sediment regime changes
- Morphological changes in the reservoir
- Useful life of a regulated reservoir

In this research, efforts will be focused on simulating hydraulic behavior, sediment transport and morphological changes in regulated reservoirs by making a combination between physical and numerical modelling.

1.3 Goals

The primary objective of this research programme is to study the hydrodynamic, sediment transport and morphodynamic processes in the vicinity of hydraulic structures of a regulated reservoir. Fluid flows in nature are three dimensional and usually turbulent. In many cases the geometry of the flow boundaries is also very complex. Solving the governing equations of water and sediment motion in these conditions is very difficult. Numerical modelling of fluid flow is generally based on the principles of conservation of mass and momentum. In many cases, the flow is governed by the Reynolds-averaged Navier-Stokes equations, which describe the three-dimensional turbulent motion of the incompressible fluid. In many water bodies where the width of the flow is large compared to its depth, the vertical acceleration of water is negligible compared to the gravitational acceleration. In this condition, the pressure distribution along the depth can be assumed to be hydrostatic and the equations of motion can be integrated along the depth to obtain two-dimensional depth averaged equations. The sediment is generally classified as being either cohesive (mud) or non-cohesive (sand and silt), and with these two types of sediment being described by difficult formulations. As a result of fluid flow over loose material, sediment particles will move from one location to another. This movement of the bed material causes the geometry and the bathymetry to change in the region. This may subsequently cause the flow field to change again which in turn affects the sediment transport rate. The typical equation for representing bed level change due to sediment transport in rivers and reservoirs is based on the assumption of conservation of sediment mass. It is generally a nonlinear equation.

In this study, an existing numerical model will be modified and enhanced to include the capability in predicting the effects of hydraulic structures such as sluice gates and intakes on

the hydraulic regime and bed level. The refined model will be validated and verified against experimental data.

The main objectives of this research are as follows:

- To study of hydraulic flows and sediment transport phenomena in the vicinity of hydraulic structures.
- To determine the effect of hydraulic structures such as sluice gates and intakes on the flow regime for different hydraulic conditions.
- To investigate the distributions of the concentration of sediments and the different fluxes between upstream and downstream reaches.
- To study the morphological changes in the reservoir and especially in the vicinity of hydraulic structures.
- To make a combination between numerical and physical modelling on designing procedure of a complex hydraulic structure.

1.4 The structure of thesis

The thesis has seven chapters. Chapter 2 comprises a literature review on numerical and physical models and their applications to reservoirs. Chapter 3 describes physical model theories and criteria for determining an appropriate scale for a hydraulic model briefly. Chapter 3 also presents an experiment study which comprises project background, model design, different hydraulic scenarios, model construction, results and discussions. Chapter 4 explains the governing equations of the hydrodynamic (including turbulence), sediment transport and morphodynamic process, respectively. In this chapter different boundary conditions and simplifications of 2D and 3D numerical models are also discussed. Turbulence has an important role on the above processes and it is discussed in a single section. Besides, mathematical solutions for the different equations (hydrodynamic, sediment transport and bed level change equation) are given in detail in chapter 4. In chapter 5, the capability of the numerical model is evaluated with two sets of experimental data by van Rijn (1986 and 1987). Chapter 6 presents the application of the numerical model to the experiment explained in chapter 3 and comparisons made between the physical and numerical model results. Finally, Chapter 7 summarises the main findings. The possible limitations of the study are considered and future research is suggested in the last chapter.

Chapter Two

Literature Review

2.1 Introduction

This chapter presents a general overview of the literature relating to modelling flows through hydraulic structures and interaction with sediments. In the recent years numerical modelling of the hydrodynamic process in the vicinity of hydraulic structures has become one of the key research interests in the field of river and dam engineering. Because of the complexity of this subject, our knowledge of this process is still limited in terms of model accuracy in describing the process. With recent progress in computing science and numerical methods many researchers have focused on developing numerical models or improving and enhancing existing numerical models to predict the hydrodynamic and sediment transport behaviors in the vicinity of hydraulic structures and the role of cross structures. A large number of physical and numerical models have been developed and deployed for predicting the fundamental physical parameters involved in such processes. These models which have usually been verified and validated against experimental or field data can be applied to a range of case studies. A numerical morphodynamic model often consists of a number of sub-modules, including the hydrodynamic, sediment transport and bed level change modules.

This literature review is divided into seven sections. Section 2.2 introduces various existing hydrodynamic numerical models and their abilities whilst Section 2.3 describes sediment transport numerical models. Section 2.4 emphasizes morphodynamic numerical models and explains the main features and key points related to the subject. In Section 2.5 the application of these numerical models (hydrodynamic, sediment transport and morphodynamic) to reservoirs is investigated. Section 2.6 describes different physical models investigations. Section 2.7 is a summary of the review.

2.2 Hydrodynamic numerical models

It has been a common practice to divide the mathematical flow models into different classes according to the dimensionality of the problem involved. For example, a flow in which the

motion is predominantly confined to one direction as may occur in a straight channel is called one-dimensional flow. Consequently, the continuity equation that describes this motion in a mathematical model is formulated in one independent space variable.

Similarly, the flow in a well-mixed shallow estuary or reservoir is predominantly two-dimensional, whereas the flow near structures (with separation and reattachment) essentially is three-dimensional.

One-dimensional (1D) flow simulations are of interest in situation where the flow field shows little variation over the cross-section. Examples are river flows and flow in irrigation network systems.

Two-dimensional depth-averaged (2DH) flow simulations are of particular interest in situations where the flow field shows no significant variations in vertical direction and where the fluid density is constant. Examples are tidal flow in well-mixed estuaries, seas and shallow reservoirs and wind-driven circulation in shallow flows.

Two-dimensional flow simulations in the vertical plane (2DV) are of interest in situations where the flow is uniform in one horizontal (lateral) direction, but with significant variations in the vertical direction. Examples are the flow across a trench navigation channel, wind-driven circulation perpendicular to the coast, narrow reservoirs and flow over long-term sand dunes.

Three-dimensional (3D) flow simulations are of particular interest in situations where the flow field shows significant variations in vertical and horizontal directions. Examples are salt intrusion in estuaries, fresh water discharge in bays, thermal stratifications in lakes and seas, water flow near hydraulic structures, wind-driven circulations in lakes, seas and oceans, etc.

Sometimes, for reasons of simplicity, a flow model makes use of the assumption that the vertical pressure distribution is hydrostatic. This restricts the range of applications of the model because it cannot be used to compute the flow in the vertical direction. Strictly speaking, such a model is not a three-dimensional model. It is more close to a two-dimensional model, even though it has three independent space variables.

There are many one-dimensional models and most new ones would be pointed here. FLOWS model developed by Delft University of Technology (DUT 1983), HEC-RAS was developed at the Hydrologic Engineering Center (HEC), U.S. Army Corps of Engineers. The new version of HEC-RAS system contains four one-dimensional river analysis components for: (1) steady flow water surface profile computations; (2) unsteady flow simulation; (3) movable boundary sediment transport computations; and (4) water quality analysis (HEC 2008). HEC-RAS is designed to perform one-dimensional hydraulic calculations for a full

network of natural and constructed channels. The major hydraulic capability of the HEC-RAS contains steady flow water surface profiles, unsteady flow simulation, sediment transport/movable boundary computation and water quality analysis.

The one-dimensional (1D) hydrodynamic model ISIS has been extensively used for designing river engineering and irrigation schemes and mapping flood risks. ISIS Flow is used for modelling steady and unsteady flows in networks of open channels and flood plains (Halcrow/HR Wallingford 1999). In ISIS, free surface flow is represented by the Saint Venant equations. Two methods are available for flow problems: the Direct Method and the Pseudo Time-stepping Method. Muskingum and Muskingum-Cunge based flood routing methods are also provided. In addition to channels and flood plains, ISIS Flow contains units to represent a wide variety of hydraulic structures including several types of sluices and weirs, jagged topped weirs and head losses through bridges. Closed conduits and culverts are represented by cross sections and several standard shapes are available. Other units include reservoirs (to represent flood storage areas, for example) and junctions.

Advances in personal computer capability and computational software technology are making detailed analysis more routine in almost all branches of engineering. In channel and river engineering, two-dimensional (2D), depth averaged models are beginning to join one-dimensional models in common practice. These models are useful in studies where local details of velocity and depth distributions are important. Examples include bridge design, river training and diversion works, contaminant transport, and fish habitat evaluation (Steffler and Blackburn 2002).

With possible high velocities and slopes, and relatively shallow depths, river and stream models present a particularly difficult computational challenge. This fact is likely a significant factor in the lag of application of shallow water models in rivers compared to coastal and estuarine problems. There are a number of commercial and public domain 2D models available. They are based on a variety of numerical schemes and offer a range of graphical pre and post processor modules. The fundamental physics is more or less common, however. All 2D models solve the basic mass conservation equation and two (horizontal) components of momentum conservation. Outputs from the model are two (horizontal) velocity components and a depth at each point or node. Velocity distributions in the vertical direction are assumed to be uniform and pressure distributions are generally assumed to be hydrostatic. 2D model schemes based on finite difference, finite volume, and finite element methods are available.

Two-dimensional flow models were first developed and applied for flows in estuaries (Leendertse 1967). They were based on a finite difference method with a staggered grid arrangement that leads to a conservative and monotone (non-oscillatory) solution for subcritical flow regimes. This kind of model has been widely used to simulate coastal flows and flows in lowland rivers (e.g., Vreugdenhil and Wijbenga 1982; Li and Falconer 1995). However, as these schemes become unstable for critical and supercritical flow conditions, they are unsuitable to model flows in channels with steeper slopes.

The depth-integrated two-dimensional (2-D) tidal circulation model (DIVAST), developed originally by Falconer (1980, 1986) and subsequently refined (Falconer and Chen 1991; Li and Falconer 1995), has been applied extensively to several U.K. and overseas estuarine and coastal water bodies by the Environmental Hydraulics Research Group at Bradford University and several external organizations and universities. Much experience has been gained in applying DIVAST to a range of basins, particularly with regard to the treatment of the advection, diffusion, bed stress and free surface stress terms, as well as flooding, drying and the solute transport equation.

Turbulence causes the appearance in the flow of eddies with a wide range of length and time scales that interact in a dynamically complex way. Given the importance of the avoidance or promotion of turbulence in engineering applications, it is no surprise that a substantial amount of research effort is dedicated to the development of numerical methods to capture the important effects due to turbulence. The methods can be grouped into following three categories (Versteeg and Malalasekara 2007):

- Turbulence models for Reynolds-averaged Navier-Stokes (RANS) equations: attention is focused on the mean flow and the effects of turbulence on mean flow properties. Prior to the application of numerical methods the Navier-Stokes equations are time averaged. Extra terms appear in the time-averaged (or Reynolds-averaged) flow equations due to the interactions between various turbulent fluctuations. These extra terms are modelled with classical turbulence models: among the best known ones are the $k-\varepsilon$ model and the Reynolds stress model. The computing resources required for reasonably accurate flow computations are modest, so this approach has been the mainstay of engineering flow calculations over the last three decades.

- Large eddy simulation: this is an intermediate form of turbulence calculations which tracks the behavior of the large eddies. The method involves space filtering of the unsteady Navier-Stokes equations prior to the computations, which passes the large eddies and rejects the smaller eddies. The effects on the resolved flow (mean flow plus large eddies) due to the

smallest, unresolved eddies are included by means of a so-called sub-grid scale model. Unsteady flow equations must be solved, so the demands on computing resources in terms of storage and volume of calculations are large, but (at the time of writing) this technique is starting to address CFD problems with complex geometry.

- Direct numerical simulation (DNS): these simulations compute the mean flow and all turbulent velocity fluctuations. The unsteady fine that they can resolve the Kolmogorov length scales at which energy dissipation takes place and with time steps sufficiently small to resolve the period of the fastest fluctuations. These calculations are highly costly in terms of computing resources, so the method is not used for industrial flow computations.

Enhancing the ability of the numerical model in simulating turbulence concept is considered in different CFD (Computational Fluid Dynamic) codes specifically.

Three two-dimensional depth-averaged models: CCHE2D developed at the National Center for Computational Hydro-science and Engineering (NCCHE), University of Mississippi; RMA-2 from the U. S. Army Corps of Engineers; and FESWMS-2DH from the U. S. Federal Highway Administration were used to simulate flow in river bends.

CCHE2D is an unsteady, turbulent flow model with non-uniform sediment and conservative pollutant transport capabilities. An efficient element scheme of Wang and Hu (1992) is incorporated to numerically solve the two-dimensional depth-averaged shallow water flow equations. The numerical scheme requires a structured grid with quadrilateral elements. A working element is formed around each node. The working element consists of a central node (the node at which the variables are calculated) and eight surrounding nodes. Quadratic interpolation functions are used to approximate the variables and their derivatives. The solution progresses element by element. For details of the scheme are given by Wang and Hu (1992). A fully implicit scheme is used to solve the discretized set of nonlinear equations. The model employs three turbulence closure schemes: the first one is based on depth-averaged parabolic eddy viscosity model; the second one uses depth-integrated mixing length model; and lastly a depth-averaged $k-\varepsilon$ model is utilized to evaluated the turbulence viscosity. The last two turbulence closure schemes are particularly useful for flow in the vicinity of hydraulic structures and in areas of re-circulating flows. The model allows for wetting and drying of the solution domain using critical depth criteria. A node is considered dry if the flow depth is below the user specified critical depth. Complete details about the model are given by Jia and Wang (1999) and Khan et al. (2000).

RMA-2 is an unsteady, turbulent flow model originally developed by Norton et al. (1973) for the U. S. Army Corps of Engineers. The model has been under continuous development by Resources Management Associates (RMA) and Waterways Experiment Station (WES). The model uses fully implicit Galerkin weighted residual technique to solve the two-dimensional depth-averaged shallow flow equations. The water depth and velocity are discretized using linear and quadratic interpolation respectively requiring six nodes triangular or eight nodes quadrilateral elements. A mesh may contain a combination of triangular and quadrilateral elements. The turbulent eddy viscosity (in the form of dynamic turbulent viscosity) is left as user input parameter and depends on the mesh size. The wetting and drying is achieved either through critical depth criteria or marsh porosity. In case of user specified critical depth criteria, an element is considered dry if water depth at any of its node falls below the critical depth.

FESWMS-2DH is also an unsteady, turbulent flow model. The model was developed by Froehlich (1989) for the U. S. Federal Highway Administration. FESWMS-2DH uses theta-implicit Galerkin weighted residual technique with mixed interpolation (as described above) to discretize the two-dimensional depth-averaged flow equations. The mesh can contain six nodes triangular, nine nodes quadrilateral and eight nodes quadrilateral elements. The user can select one of the following two methods to handle wetting and drying of the elements. The first method checks the submergence of each element, if an element is not fully submerged it is eliminated from the analysis. The second method uses critical depth specified by the user to check the status of an element. If all the nodes of an element are below the specified critical depth the element is considered dry.

Depth-integrated 2D hydrodynamic models based on a regular grid have been used for many years for predicting free surface flows, but they are generally computationally more expensive and less flexible when dealing with channel networks and hydraulic structures. The increasing availability of digital topographic data in recent years provides this type of models with scope for wider application. For flood modelling, 2D models based on the mass balance equation and with the raster grid have been developed and increasingly used (Horritt and Bates 2001). Such models discretize the floodplain according to a regular grid with each floodplain pixel in the grid treated as an individual storage cell. The inter-cell fluxes are treated using uniform flow formulae.

Coupled 1D and 2D models have been developed in recent years and successfully applied to large and complex river systems (Verwey 2001 and Dhondia and Stelling 2002). However, there are still a number of issues, including a huge difference in the computational resource

requirements between the 1D and 2D models. For example, in modelling flood inundation in an urban area, it was found that the computational time required for a 2D model can be 1000 times higher than that required for a 1D model (Wicks et al. 2004). Lin et al. (2006) tried to enhance the capability of the ISIS modelling system by integrating a revised version of the DIVAST 2D model. The model has been tested for idealized test cases, followed by application to the Thames Estuary and the urbanized region of Greenwich. The new model has generally performed well in comparison with other similar models.

Water flow in rivers, lakes, estuaries or coastal is primarily driven by tide, wind, bed-level gradients, density gradients or wave actions, it is also strongly affected by the complex geometry and bathymetry of the water body. A few years ago, quasi three-dimensional models were used to predict flow fields in the estuaries and coastal waters which are combination of two-dimensional horizontal model with a vertical velocity profile (see van Rijn 1987). Three-dimensional models are now increasingly attractive for predicting the hydrodynamic parameters in river and estuarine waters. Most three-dimensional numerical models recently developed are based on a splitting method for horizontal and vertical directions. Falconer has developed a three-dimensional numerical model to study wind driven circulation in shallow homogeneous lakes (see Falconer et al. 1991). The finite difference method was used to discretize the governing equations in this model.

For water bodies with relatively simple geometry and bathymetry, it is economical and possible to develop conformal or orthogonal grids for a finite difference model. However, for the most natural rivers with very complex shoreline and bathymetry, the better way to simulate the water flows is to apply a non-orthogonal (boundary-fitted) curvilinear grid to the hydrodynamic numerical model. The Curvilinear Hydrodynamics in 3 – Dimensions (CH3D) by Waterways Experiment Station (WES) of the U.S. Army Corps of Engineers, USA is one of the most suitable models applied to those rivers with complex river banks and bathymetry (see Chapman 1993). The CH3D model is a fully three-dimensional model with well-tested sediment transport and hydrodynamic algorithms. As its name implies, CH3D allows curvilinear river geometry with complex bathymetry.

Manson (1994) developed a three-dimensional river flow using the fractional step projection method on a Cartesian grid, and using a method similar to that proposed by Viollet (see Manson 1994). Pender et al. (1995) subsequently verified this model against experimental data. Lin and Falconer (1997) developed a three dimensional model for estuarine waters based on a layer integrated modelling approach. In this model the depth integrated equations were first solved in a Cartesian co-ordinate system using the finite difference method. With

the water elevations, obtained from these equations, the three-dimensional momentum and continuity equations were then solved to obtain the velocity components in three-dimensions. Again the finite difference method was used for the second part. Hakimzadeh and Falconer (2007) enhanced an existing 3D layer-integrated model to predict more accurately the secondary tide induced circulation through the water column, associated with marinas and enclosed coastal embayment, where the aspect ratio is large or small. Two different turbulence models were also considered, particularly in the horizontal plane, including the mixing length and $k-\varepsilon$ models. In this study some modifications were made in this numerical model in order to predict the flow, sediment transport in river flow environments

2.3 Sediment transport numerical models

The transport of sediment particles by a flow of water can be in the form of bed-load, or suspended load, or both, depending on the size of the bed material particles and the flow conditions. The suspended load may also contain some wash load, which is generally defined as that portion of the suspended load which is governed by the upstream supply rate and not by the composition and properties of the bed material. Sediment transport plays an important role in the evolution of river beds, estuaries, and the coastlines; consequently it exerts a considerable influence on the evolution of the topography of the earth's surface. Therefore, the mechanism of sediment transport is of great interest to hydraulic engineers, coastal engineers, geologists, hydrologists, geographers, and so on. Integrated modelling of sediment transport from river to marine environment requires a quantitative and universally applicable law governing the motion of the transported sediment in all flow situations ranging from pure current to complex flow in the wave-current situation including irregular and sometimes breaking waves. The equation of sediment transport correlated with local flow parameters such as bed shear stress and near bed velocity is highly demanded by hydrodynamic modelers who are able to precisely determine these flow parameters by solving the Reynolds equations in rivers, estuaries and coastal waters.

Mathematical sediment transport models can be divided based on dimensionality, the same as hydrodynamic numerical models, or based on the model capabilities of calculation suspended load and bed load sediments.

One-dimensional (1-D) modelling of sediment transport in streams has seen extensive development over the past decades. In rivers, using one-dimensional numerical models has many benefits such as short computational time, simple equations and less input data, but with many restrictions. For example when we need to understand sediment profile or

sediment distribution in plan, using 1D sediment transport numerical models do not have any meaning. Steady and stepwise quasi-steady 1-D models, such as HEC-6 (Thomas 1982), Han's (1980) model, Chang's (1982) model, van Niekerk et al.'s (1992) model and others, have been widely tested and applied to sedimentation studies in reservoirs and rivers in which the long wave assumption is valid and the long-term results are mainly considered (Wu et al. 2004). Many unsteady flow models (e.g., Cunge et al. 1980; Tsai and Yen 1982; Rahuel et al. 1989) have been developed and applied to river estuaries and other situations where the unsteadiness of flow prevails. With a lot of enhancement and refinement, 1-D models continue to have their place in engineering applications.

One of the components of the new version of HEC-RAS system contains sediment transport/movable boundary computations, with details being given below (HEC 2008):

Sediment Transport/Movable Boundary Computations: This component of the modelling system is intended for the simulation of one-dimensional sediment transport/movable boundary calculations resulting from scour and deposition over moderate time periods (typically years, although application to single flood events will be possible).

The sediment transport potential is computed by grain size fraction, thereby allowing the simulation of hydraulic sorting and armoring. Major features include the ability to model a full network of streams, channel dredging, various levee and encroachment alternatives, and the use of several different equations for the computation of sediment transport.

The model is designed to simulate long-term trends of scour and deposition in a stream channel that might result from modifying the frequency and duration of the water discharge and stage, or modifying the channel geometry. This system can be used to evaluate deposition in reservoirs, design channel contractions required to maintain navigation depths, predict the influence of dredging on the rate of deposition, estimate maximum possible scour during large flood events, and evaluate sedimentation in fixed channels.

The sediment transport add-on module for ISIS Professional allows us to predict the sediment transport rates and patterns of erosion/deposition in river channels. The module has been applied to many natural and engineered channels around the world and has been used to study sedimentation problems for both uniform and graded sediments.

The module is able to predict sediment transport rates, bed elevations and amounts of erosion/deposition throughout a channel system. In summary, this is achieved with the following calculations at each time step:

- The ISIS hydraulic engine calculates the hydraulic variables of flow, stage, velocity in the usual way;

- Starting at the upstream end of the system, the sediment transport module engine then loops around the nodes calculating the sediment transport capacity and solving the sediment continuity equation for depth of erosion/deposition;
- Finally the module updates the channel conveyance tables to allow for any calculated deposition or erosion ready for the next time step.

Many mathematical studies carried out for simulation of both suspended and bed load transport in the flow. van Rijn (1984, part I & part II) proposed methods for calculating suspended and bed load. The motion of the bed load particles is assumed to be dominated by gravity forces, while the effect of turbulence on the overall trajectory is assumed to be minor importance. For the suspended load, a near bed sediment concentration is used as a reference concentration. Numerical suspended sediment transport models can be classified as follows:

- One dimensional model
- Depth integrated (or depth averaged) models
- Two-dimensional vertical models
- Three-dimensional models

A number of numerical models, including: two-dimensional depth-integrated (e.g. Galppatti and Vreugdenhil 1985; Celic and Rodi 1988) and three dimensional sediment transport models (e.g. O'Connor and Nicholson 1988; Lin and Falconer 1996) have been developed to simulated these transport processes. van Rijn (1986) presented a two-dimensional vertical mathematical model for calculating suspended sediment in non-uniform flows. This numerical model is based on the width-integrated convection-diffusion equation for the sediment particles including settling effects. The local fluid velocities and mixing coefficients are described by a so-called Profiled model, which is based on the application of flexible profiles to represent the vertical distribution of basic variables. Wang and Adeff (1986) developed 2-D and 3-D finite element model using the Petrov-Galerkin method for sediment transport in rivers and estuaries. O'Connor and Nicholson (1988) used the characteristics method to represent the advective terms of the sediment transport equation and also undertook laboratory measurements to validate the numerical model. The process of advective and diffusive transport are three-dimensional, although most currently used estuaries, coastal and reservoirs models are primarily two-dimensional in plan. These models involve solving depth-integrated or depth-averaged 2-D sediment transport equations to describe the governing suspended sediment transport (e.g. Galppatti and Vreugdenhil 1985; Falconer and Owen 1990). Considering that 2-D models need much less data and computer resources in comparison with 3-D models, these models are still very useful for many

practical engineering applications. However, in 2-D sediment transport models, only the depth averaged sediment concentration is available. The value of the near-bed reference concentration which is required to compute the sediment erosion or deposition rate must be related to the depth averaged concentration. A common assumption made to related the reference sediment concentration with the depth averaged concentration is equal to the corresponding value in the equilibrium state. This implies that vertical sediment transport profile adjusts instantly to the equilibrium profile, with this approach therefore being limited to situations where the differences between the local true sediment profile and the local equilibrium profile are relatively small. The current research focuses on understanding sediment behavior in the vicinity of hydraulic structures and for this reason 2-D models may not be suitable, because the sediment profile in that area is generally not in an equilibrium condition.

For those situations where flow conditions change rapidly, it is more appropriate and accurate to use a 3-D model in which the local sediment distribution is calculated using the advective-diffusion equation and the erosion or deposition of sediment is directly related to the near bed reference concentration. van Rijn (1987) and van Rijn et al. (1990) investigated the influence of the basic physical parameters and developed a model for suspended sediment transport in gradually varying steady flows, in which the flow velocities were computed using a two-dimensional depth averaged model in combination with a logarithmic velocity profile. Olsen and Skoglund (1994) used a 3-D $k-\varepsilon$ turbulence model to predict the steady flow and sediment transport in a sand trap. A layer integrated 3-D numerical model was developed to predict suspended sediment fluxes by Lin and Falconer (1996). The hydrodynamic equations of the model were solved using a combine layer integrated and depth integrated scheme, with a two layer turbulence mixing model being used to represent the eddy viscosity distribution. The transport of suspended sediment was solved in the model by using a splitting algorithm, which split the original 3-D advective-diffusion equation into a 1-D vertical equation and a 2-D horizontal equation. An implicit finite volume method used in the vertical sub-equation was able to maintain stability for very small layer thicknesses and the ULTIMATE QUICKSET scheme was used to give highly accurate approximations of horizontal advection process. The model was tested against analytic solutions and laboratory measurements for different types of flow and boundary conditions, and has also been applied to predict suspended sediment fluxes in the Humber Estuary, UK.

The program called Sediment Simulation In Intakes with Multiblock option, or “SSIIM” was developed by Olsen (2002). The program is made for use in

River/Environmental/Hydraulic/Sedimentation Engineering. Initially, the main motivation for creating the program was to simulate the sediment movements in general river/channel geometries. This has been shown to be difficult to do in physical model studies for fine sediment. The main strength of SSIIM compared to other CFD program is the capability of modelling sediment transport with moveable bed in a complex geometry. This includes multiple sediment sizes, sorting, bed load and suspended load, bed forms and effects of sloping beds (Olsen 2011).

The SSIIM program solves the Navier-Stokes equations with the k-ε model on a three-dimensional almost general non-orthogonal grid, then uses a control volume discretization approach together with the power-law scheme or the second order upwind scheme. The SIMPLE method is used when calculating the pressure coupling. An implicit solver is used to produce the velocity field in the geometry. Consequently, these velocities are used when solving the convection-diffusion equations for different sediment sizes.

Ruether et al. (2005) used SSIIM model to predict the flow field and the sediment transport at the Kapunga water intake in Tanzania. The 3-D numerical model was used to predict the suspended sediment distribution in the flow approaching a water intake. In this research, a ratio namely performance ratio was proposed by calculating from the sediment concentration in the river upstream of the intake and passing into the water intake. This ratio makes a platform for comparing and verifying results between the numerical model and measurements. Intake performance can be assessed by a performance ratio PR, defined by equation as follows:

$$PR = 1 - \frac{Concentration\ in\ intake\ canal}{Concentration\ in\ the\ river\ upstream\ of\ the\ intake}$$

A performance ratio of unity indicates the maximum possible sediment exclusion, whereas a performance ratio of zero indicates no concentration reduction between the river and the canal. A performance ratio less than zero indicate that an intake is aggravating sediment concentrations.

It was found that the calculated performance ratios at the Kapunga water intake showed an accuracy of 15–20% when compared with the measurements. A sensitivity analysis in this study showed that a more accurate discretization scheme is more important than doubling the number of grid cells. The use of the second-order upstream scheme instead of the first-order method reduced the average deviation by about 8%, whereas the doubling of the number of grid cells improved the result by only about 3%. When using the combination of these two

measures, the best results were obtained. The study also showed that the results are not very sensitive to the variation of the bed roughness. Three different approaches were investigated; with regard to the average performance ratio, the method of van Rijn (1984, part I) showed the best agreement with the measurements.

In addition, many sediment transport numerical models have an ability to predict morphological changes and those can compute bed level changes. These models will be discussed in the next section.

2.4 Morphodynamic numerical models

The central concern of morphodynamics is the evolution of bed levels of rivers, reservoirs and estuarine and other water bodies where fluid flows interact with sediments fluxes. Numerical morphological models usually involve coupling between a hydrodynamic model, a sediment transport model and a model for bed level change, which expresses the balance of sediment volume and its continual redistribution with time.

In modelling reservoirs and rivers, in order to understand the impact of hydraulic structures on the hydrodynamic and sediment transport processes and morphological changes it is often necessary to investigate these processes in three dimensions. The main goal of the current research is to present a proposed scheme for computing bed level changes in the vicinity of hydraulic structures where complex geometry, flow pattern and sediment concentration distributed have important effect on the simulation results.

Currently, physical models are still widely used as an essential tool to obtain information about these processes. Generally speaking, physical models need a long time to construct and are expensive to run, particularly if large scale models are involved. Use of the numerical model offers the possibility to test various scenarios which are difficult to test in a physical model; the cost can also be reduced and more options considered.

The three dimensionality of turbulence and the effect of turbulence on the sediment transport and morphological process in the vicinity of hydraulic structures form a complex problem which is an open research field yet. Theoretical aspects of one-dimensional morphodynamic models were studied by de Vries (1981). De Vriend (1985, 1986) worked on the theoretical basis of the behavior of two-dimensional geo-morphological models. In the 1980s and 1990s, depth-averaged two dimensional (2DH) models were developed. Originating mainly in river engineering (e.g. Struiksma, 1985) the models often had sophisticated quasi-three-dimensional (quasi-3D) extensions to allow for spiral flow in bends. Later they were used in

coastal areas where waves also play a crucial role in driving currents. For reviews of several such models, see de Vriend et al. (1993) and Nicholson et al. (1997).

van Rijn(1987) used a 2-D width-averaged numerical model to simulate bed level changes in dredged trenches. The numerical model predictions agreed closely with the bed levels measured from physical model tests. In a similar study performed by Martinez et al. (1999) a 2-D depth-averaged model was used to determine the evolution of bed elevations, as well as the suspended sediment concentrations, using a finite element model. Olsen (1999) applied a 2-D depth-averaged numerical model to calculate bed level changes in a reservoir which was flushed by flood flows. Péchon and Teisson (1996) presented a morphological model based on a three-dimensional (3D) flow description, where the near-bed velocity was coupled with a local transport formula. This model produced rather irregular results, which were at least partly due to the assumption of local equilibrium transport.

Olsen and Kjellesvig (1999) studied 3-D numerical modelling of bed changes in a sand trap. They found that the numerical model results compared well with similar measurements obtained from physical model studies. Gessler et al. (1999) developed a 3D model for predicting river morphology, which includes separate solvers for bed load transport and 3D suspended transport. It considers several size fractions of sediment and keeps track of the bed composition and evolution during each time step. Kolahdoozan and Falconer (2003) developed a three-dimensional (3-D) layer-integrated morphological model for estuarine and coastal waters and compared the numerical model predictions with experimental measurements in a laboratory model harbour. They used mixing length theory in simulating turbulence, and recommended that a fine mesh should be used in areas of severe erosion or deposition. Kocyigit et al. (2005) presented the application and refinement of a 2-D, depth-integrated, numerical model for predicting changes in bed level in an idealized model square harbour with an asymmetric entrance. The model predictions were compared with physical model results, obtained from a scaled hydraulic model in a laboratory tidal basin. They reported that under-prediction of the volume of erosion was thought to be due to the model not predicting the lateral movement of sediment.

Olsen (2003) and Rüther and Olsen (2003, 2005a, b) developed a fully 3D model with an unstructured grid. They showed first results from a simulation of meander evolution using no initial perturbation. Their work focused on the formation of alternate bars and the initiation of meandering starting from a completely straight channel.

DHI group developed MIKE 21C software that is a generalized mathematical modelling system for the simulation of the hydrodynamics of vertically homogenous flows, and for the

simulation of sediment transport and morphodynamic in river environments. The modelling system has the capability of utilizing either a rectilinear grid, or a curvilinear computational grid. The modelling system is composed of a number of modules relevant to sediment and morphology studies in rivers including: a hydrodynamic module, an advection-dispersion module, a sediment transport module, a flow resistance module, a bank erosion module and a large scale morphological module. The model components can run simultaneously, thus incorporating dynamic feedback from changing hydraulic resistance, bed topography and bank lines to the hydrodynamic behavior of the river (MIKE 21C River morphology, M21C-SD/0400215/HE, 2004,DHI).

The DELFT3D package developed by WL|Delft Hydraulics is a model system that consists of a number of integrated modules which together allow the simulation of hydrodynamic flow (under the shallow water assumption), computation of the transport of water-borne constituents (e.g., salinity and heat), short wave generation and propagation, sediment transport and morphological changes, and the modelling of ecological processes and water quality parameters. The main advantages of this 3D model are the following: (1) three dimensional hydrodynamic processes and the adaptation of non-equilibrium sediment concentration profiles are automatically accounted for in the suspended sediment calculations; (2) the density effects of sediment in suspension (which may cause density currents and/or turbulence damping) are automatically included in the hydrodynamic calculations; (3) changes in bathymetry can be immediately fed back to the hydrodynamic calculations; and (4) sediment transport and morphological simulations are simple to perform and do not require a large data file to communicate results between the hydrodynamic, sediment transport, and bottom updating modules (Lesser et al. 2004).

TELEMAC-3D is a three-dimensional finite element model developed by Patrick Sauvaget of the Laboratoire d' Hydraulique de France. The modelling system contains a number of modules that are assembled for individual simulations. The TELEMAC-3D's prominent applications can be found in free surface flow, in both seas and rivers; the software can take the following processes into account (TELEMAC modelling system 2007):

• Influence of temperature and/or salinity on density,
• Bottom friction,
• Influence of the Coriolis force,
• Influence of weather elements: air pressure and wind,
• Consideration of the thermal exchanges with the atmosphere,
• Sources and sinks for fluid moment within the flow domain,

• Simple or complex turbulence models (K-Epsilon) taking the effects of the Archimedean force (buoyancy) into account,
• Dry areas in the computational domain: tidal flats,
• Current drift and diffusion of a tracer, with generation or disappearance terms.

The code is applicable to many fields. The main ones are related to the marine environment through the investigations of currents being induced either by tides or density gradients, with or without the influence of such an external force as the wind or the air pressure. It can be applied either to large extent areas (on a sea scale) or to smaller domains (coasts and estuaries) for the impact of sewer effluents, the study of thermal plumes or even sedimentary transport. As regards the continental waters, the study of thermal plumes in rivers, the hydrodynamic behavior or natural or man-made lakes can be mentioned as well. In its basic release, the code solves the three-dimensional hydrodynamic equations with the following assumptions:

• Three-dimensional Navier-Stokes equations with a free surface changing in time,
• Negligible variation of density in the conservation of mass equation (incompressible fluid),
• Pressure-hydrostatic assumption (that assumption results in that the pressure at a given depth is the sum of the air pressure at the fluid surface plus the weight of the overlying water body),
• Boussinesq approximation for the momentum (the density variations are not taken into account in the gravity term).

Both TELEMAC-3D and DELFT3D codes are open source now and researchers can use and enhance the codes directly for any applications.

Because the flow field and the resulting transport rate is a nonlinear function of bed level, the sediment conservation equation is physically a nonlinear conservation equation for the bed level. The same situation occurs in other physics contexts, such as mass conservation equation in hydraulics and aerodynamics as well as traffic flow in highway systems (Whitham 1974). A common feature of these conservation laws is that shock waves, i.e. discontinuities of the respective physical quantities, will develop when particle velocity approaches celerity. Several decades of research effort has been devoted to the development of numerical solution techniques for obtaining accurate and stable simulations of shock behavior. These researchers focus on to propose robust numerical schemes for solving bed level change equation in order to be achieved against instability especially for long-term simulations.

As reviewed in Nicholson et al. (1997), many state-of-art morphodynamic models use classical shock capturing schemes for bed level simulation. For example, Johnson and Zyserman (2002) apply a second-order accurate modified Lax-Wendroff scheme (Abbott 1978). The Delft Hydraulics model Delft2D-MOR (Roelvink and van Banning 1994; Roelvink et al. 1994) uses a FTCS (Forward Time, Central Space) explicit scheme with corrections of the transport rate to compensate negative numerical diffusion resulting from the scheme. The HR Wallingford model PISCES (Chesher et al. 1993) uses a one-step Lax-Wendroff scheme. STC (Service Technique Central des Ports Maritimes et des Voies Navigables) model uses a two-step Lax-Wendroff scheme (Tanguy et al. 1993). The University of Liverpool model (O'Connor and Nicholson, 1988, 1995) also uses a modified Lax–Wendroff scheme with effects of gravity on the sediment transport rate. The Lax-Wendroff scheme suffers from dispersion resulting in spurious oscillations occurring in the numerical results; see, for example, Hudson et al. (2005). Various techniques, including flux-limiter methods, have been used to try to eliminate the spurious oscillations. Unfortunately, the spurious oscillations could not be eliminated and overpowered the numerical results for long computational runtimes as also pointed out by Damgaard and Chesher (1997) and Damgaard (1998).

Long et al. (2008) investigate the stability and performance of several finite difference schemes. They study the evolution (in one horizontal direction) of an initial mound of sediment in an analytically tractable case with a rigid lid, in order to compare the performance of various schemes. Two schemes based on the Weighted Essentially Non-Oscillatory (WENO) formulation of Liu et al. (1994) are found to provide reasonably accurate reproduction of a simple shock structure in one horizontal dimension. Then, an Euler-WENO scheme, based on first order explicit time stepping together with a WENO scheme for spatial discretization, is applied in two examples based on depth integrated, free surface flows. In the first example, a phase resolving sediment transport model is used to study evolution of periodic sand bars in the presence of waves at the resonant Bragg frequency. Finally, the evolution of periodic alternating bars in an otherwise rectangular channel is considered.

Long et al. (2008) found that new shock capturing schemes such as WENO (Weighted Essentially Non-Oscillatory) and TVD (Total Variation Diminishing) schemes are more appropriate for morphodynamics. Tests showed that the Euler-WENO scheme and the TVD-WENO scheme would be able to simulate bed level deformation with very good accuracy and stability in comparison to classical schemes. The Euler-WENO scheme is preferred to the

TVD-WENO scheme because the TVD-WENO scheme requires much more computational cost.

It is also demonstrated briefly that the Euler-WENO scheme is successful in phase resolving sediment transport models under waves. Investigation of alternating bar systems due to channel instabilities shows the Euler-WENO scheme is also capable of modelling 2D morphology change.

A numerical scheme for realistic morphology calculations needs to be stable for extremely long integration times, and also needs to be robust when used in conjunction with a variety of strategies for accelerated morphology updating. They have not addressed these questions systematically in their research (Long et al. 2008). Preliminary calculations for the 1-D Gaussian bump case have been performed using the 'online' formulation as defined by Roelvink (2006) with morphology factors up to 100. For that simple case, the shock front structure is preserved accurately for this level of accelerated updating. They also proposed that much work remains to be done to evaluate this sort of application for the WENO scheme.

Now days, researchers try to use physical and numerical model to understand hydraulic and sediment behavior simultaneously. Stephan and Hengl (2010) used a physical model test which aimed at improving the sediment transport through the backwater of a hydropower plant to reduce the flood risk of the town of Hallein. In addition, the morphodynamic 3D model SSIIM was applied to this case in order to investigate if a 3D model may reproduce erosion and deposition pattern for such a complex situation. The numerical results when using the default values for the transport formula show a good agreement for the main erosion and deposition pattern but not for the absolute bed levels.

2.5 Model applications to reservoir

For the mathematical modelling of sediment deposition in reservoirs, Lopez (1978) approximates the partial derivatives of the flow continuity and momentum equations with the Preissmann implicit scheme of finite differences, whereas an explicit scheme is used for solving the sediment continuity equation. For one and quasi-two-dimensional models, there are some classical works, such as Alvim (1987) and Cogollo and Villela (1988), the latter based on the mathematical model of Lopez (1978), for the prediction of sedimentation in Urra II reservoir, Sinu River, Colombia.

Dhamotharan et al. (1981) utilized a one dimensional unsteady numerical model to establish the important reservoir sedimentation variables for trap efficiency as a Peclet number, using depth and turbulent diffusion coefficient, and a Courant number. Ziegler and Nisbet (1995)

simulated 30 years of cohesive sediment transport (from 1961 to 1991) with the SEDZL model, in the Watts Bar reservoir - Tennessee, which is a part of the Tennessee Valley Authority reservoir system. Bathymetry data from 1946, 1951, 1956, 1961 and1991, done in 64 cross-sections of the reservoir were used to calibrate the model. Although a quantitative comparison with the actual bathymetry resulted in an error of 46%, the simulation was considered satisfactory by the authors. This software was also used in the study of fine sediment transport in other aquatic systems, such as Fox River - Wisconsin (Gailani et al. 1991), Pawtuxet River - Rhode Island (Ziegler and Nisbet 1994), and Lake Irie (Lick et al. 1994).

A study with FLUVIAL-12 was developed by Chang et al. (1996) to analyze the efficiency of flushing operations in reservoirs along the North Fork Feather River, U.S.A. The study pointed to a deficiency in electric energy generation due to sedimentation in the near future. The three-dimensional model CH3D-SED was described by Gessler et al. (1999). The model simulated non-cohesive sediment transport in open channels with an application in the project Deep Draft Navigation, in the Lower Mississippi River. Olsen (1999) applied the three-dimensional model SSIIM to predict sedimentation in the Kali Gandaki Hydropower Reservoir, Nepal. Results from a physical model built in scale 1:50 (12m long and 6m wide) and from the numerical model estimated that the reservoir volume of 0.4 million cubic meters would be filled in a short period of time if flushing operations were not run.

Other numerical models have been successfully applied to river and reservoir morphology, such as FAST3D at the University of Karlsruhe (Demuren 1991); HEC-6 from the U.S. Army Corps of Engineers (Nicklow and Mays 2000); and Delft3D, with application to Senbiri reservoir, Toshibetsu river, Japan (Sloff et al. 2004).

Fang and Rodi (2000) used a 3D model to simulate flow and sediment transport in the Three Gorges Project (TGP) reservoir in the Yangtze River. Olsen (2000) used a 3D model to compute the flow field and bed level changes during reservoir flushing. Khosronejad and Salehi Neishabouri (2006) used a vertical two-dimensional finite volume model to study the effects of various parameters on quantity of sediment released from a reservoir in the reservoir flushing process. Khosronejad et al. (2008) developed a fully three-dimensional hydrodynamic model, using a finite volume method to solve the Reynolds averaged Navier-Stokes equations, and combined with a three-dimensional sediment transport model. The hydrodynamic model was based the equations of mass and momentum conservation along with a standard $k-\varepsilon$ turbulence closure model. The sediment transport model was based on the equation of convection/diffusion of sediment concentration and sediment continuity

equation for calculating the sediment concentration and bed level change in the reservoir flushing process, respectively. Both the hydrodynamic and sediment transport models was developed in a boundary-fitted curvilinear coordinate system. The grid is adaptive in the vertical direction, and changes according to the calculated bed level. The hydrodynamic section of the model was verified using experimental and direct numerical simulations data, and the sediment concentration calculations compare well with the experimental results. Also a physical model study was carried out to verify the results of bed evolution at the upstream of a sluice gate. Good agreement was found between bed evolution in the numerical and physical models.

Souza et al. (2010) compares laboratorial sedimentation experiments in a shallow reservoir and predictions using a 2D numerical model with depth-averaged Navier-Stokes equations and a sediment transport code. The reservoir in operation, with a width of 1.5m and length of 3.00m, is used for the laboratory tests. Velocity measurements where conducted with the laser sheet crossing the side walls and a CCD (Charged Coupling Devices) camera positioned under the bed of the reservoir. Two prismatic channels, 2.0m long, 0.15m wide and0.25m high, originally supplied water to the reservoir. The experiments were conducted using only the left supply channel. The sand supply structure, with an elevated reservoir, had a volume of $0.40m^3$ with its bottom positioned 1.50m above the reservoir. A pressurized air system fed the channels with a constant sediment discharge of 0.002kg/s. The PIV (Particle Image Velocimetry) technique could not be applied, evidently, during the sedimentation process. The images were taken with the CCD camera positioned beneath the reservoir, so the sand deposition did not permit the acquisition of flow images. Therefore, instantaneous and mean velocity fields were obtained in several reservoir regions during the water flow, before the addition of sand at the inlet. The numerical simulation was conducted using MIKE21C (Olesen 1987; Talmon 1992) which uses mass and momentum equations reduced to 2D vertically integrated Navier-Stokes equations in this study. Three-dimensional effects of secondary flows are kept in simplified form through the addition of a helical flow tool to the model, described by de Vriend (1981). A number of sediment transport equations were tested which is described in Souza (2006). The Engelund and Fredsøe formulation best reproduced the experimental results. Flows without sediment transport or without bed dunes could be simulated using Smagorinski's turbulence model, while flows with sediment occurring over dunes needed the use of a constant turbulent viscosity. The similarity obtained between experimental data and numerical results, for both flow pattern and sediment deposition,

confirms that the models and numerical codes used in this work are useful for the analysis and prediction of reservoir sedimentation (Souza et al. 2010).

As can been seen from above descriptions, little works focused on understanding hydrodynamic and morphodynamic behavior in the vicinity of hydraulic structures (River regulated structures) and this field has some complexity that need to more investigations in the numerical model. My experiences in the physical model and some difficulties to run the hydraulic model encourage me to study and develop an enhanced numerical model for this case.

2.6 Physical models

Physical modelling is based on dimensional analysis knowledge. Dimensional analysis is a most useful tool in experimental fluid mechanics, allowing for the implicit formulation of criteria for dynamic similarity in a simple and direct manner (Kobus 1980). It is based on the Π-theorem of Buckingham (1914), as described by, for example, Raghunath (1967), Yalin (1971), Novak and Cabelka (1981), Spurk (1992) and Hughes (1993).

A physical problem with n independent parameters $q_1, q_2, \dots, q_n$ can be reduced to a product of $n - r$ independent, dimensionless parameters $\Pi_1, \Pi_2, \dots, \Pi_{n-r}$ with r as the minimum number of reference dimensions (length [L], mass [M] or time [T]) required describing the dimensions of these n parameters. Similarity requires that each of these dimensionless parameters quantitatively agree between model and real-world prototype. The dimensionless parameters include the geometrical ratios as well as the force ratios such as Fr (Froude number), Re (Reynolds number), W (Weber number), C (Cauchy number) and E (Euler number).

These dimensionless parameters allow for a general presentation of results and since they are related as a function of dimensionless parameters, no scale ratios are required to up-scale them. The number of necessary tests is normally reduced since the number of physical parameters characterizing the phenomenon is reduced from n to $n - r$. However, in contrast to inspectional analysis, the relative importance of the dimensionless parameters on the phenomenon remains unknown. The dimensional analysis results in arbitrariness in determining the conditions of similitude if the phenomenon includes more than six parameters n and it is strongly criticized, for example, by Le Méhauté (1990). Nevertheless, it is widely applied in hydraulic modelling. It is recommended using dimensional analysis only

if the level of theoretical understanding of a phenomenon allows no inspectional analysis (Heller 2011).

Depending upon the sediment supply from the watershed and flow intensity in terms of velocity and turbulence, river flows usually carry sediment particles within a wide range of sizes. When the water flows into a reservoir, the coarser particles deposit gradually and form a delta in the headwater area of the reservoir that extends further into the reservoir as deposition continues. Sediment transport from riverine sediments can be investigated via physical and mathematical models. This can give practitioners an insight of the potential transport processes, which affect the movement of sediments across the sediment-water interface (Vanoni 1975). A general objective of physical modelling is to fill the gaps in the existing knowledge of transport processes of non-cohesive sediments in the vicinity of hydraulic structures and to find suitable parameterizations of those processes which will lead to improvements in hydraulic structure operations.

The lifetime of man-made reservoirs often depends on the magnitude of sedimentation. Reservoirs play a significant role on the retention of water and sediments during floods, which contribute to the protection of the population and the land downstream (Chanson and James 1999). In addition, the accumulation of the sediments in reservoirs can affect intake and outlet devices and reduce the storage capacity (Boillat and De Cesare 1994).

As water intakes are designed to extract and deliver water, it is necessary to test a series of design considerations in order to arrive at a desirable concept that can obtain and deliver the water economically with the least environmental impact (ASCE 1982). Therefore, environmental hydraulic engineers are faced with a number of challenges while selecting and designing water intakes. These are site access, site hydrologic conditions, ease of construction, operation and maintenance without which an intake may be designed and constructed but may not be efficiently operable due to lack of adequate water supply (Knauss 1987) or may be adversely operated due to degraded environment (PIANC 1991).

Physical model experiments have been applied to study the performance of reservoirs and related hydraulic structures; this includes the adaptation of them as part of study process for sediment control measures at intakes (Nakato and Ogden 1998). Physical model are useful in predicting river morphological changes related to an intake (Neary et al. 1994). However, physical models are only able to determine sediment control qualitatively (Atkinson 1995); this is due to the scaling effect. As sediment particles are modelled in proportion to the main model scale ratio, those appear so fine which may become cohesive and exhibit different properties from the prototype sediment particles. Therefore, only the coarser sediments can

be scaled. Yalin (1971) suggested that the use of lightweight sediment is impossible to satisfy all the physical scaling laws, particularly, when water is used as the fluid in the model. These may cause the sediment particles in the model to represent coarse material in the prototype. The sediment, therefore, moves in the model as bed load and any correctly designed device for sediment exclusion shows in result reported in Atkinson (1989) illustrate this problem. This is particularly noticeable when sediment control at intakes is studied (Avery 1989).

Grain size gradation can also be found a problem associated with physical models. As the sediment material in rivers can range from fine sand to gravels or even boulders, it is not practical to model such a range. In fact, a physical model with more than one sediment size fraction is exceptional and may not be economical.

When modelling river cross or parallel structures such as groins, dikes and intakes; to investigate their impacts on the river regime, it is imperative to note that when the river bed and banks are composed of non-cohesive coarse material with a wide range of sediment grain sizes, the median grain size could be many times greater than the sediment in motion under normal conditions. In these circumstances, the performance of the structures can only be determined by the material in motion. However, the single sediment size to be selected for modelling must represent prototype bed material to model bed morphology and roughness correctly. This represents inaccuracies involved in the modelling of sediment in motion, which may lead to inaccurate performance of modelling river structures (Atkinson et al. 1993).

A hydraulic model cannot reproduce an equal ratio of all the prototype forces and satisfy perfect similarity. Also practical limitations of available space, funds and bed materials make it necessary in many studies to deviate from the desired scale ratios. Therefore, it depends on the engineer to use his knowledge, experience and even intuition to determine what laws of similarity must be satisfied and what special modelling techniques must be applied. The engineer must first determine the type of problem to be studied, dominant natural process to be simulated and the type of data to be obtained from the model. This information will dictate the type of model to be used, the space to be reproduced and the range of scales suitable for the study.

There are generally two types of river models, which are fixed-bed and moveable-bed. The fixed-bed model is constructed of concrete, pea gravel or some other material that cannot be moved by the force of the fluid in the model. The moveable-bed model has usually fixed bank-lines and overbank areas with a moveable-bed of crushed-coal, sand, light weight

material and some other materials that can be moved by the forces developed in the model stream (Ivicsisc 1975).

In addition, models may be constructed with the same horizontal and vertical scales (undistorted) or with different horizontal and vertical scales (distorted). Even though it is desirable in most cases to have an undistorted model, in some cases distortion is necessary. It necessitates as the prototype area is so large that if the vertical scale was made the same as the horizontal scale, the changes in water surface elevation would be of such small magnitude that accuracy would be lost (French 1986).

Where hydraulic performance of river channels as well as the cross-structures to be predicted, it is appropriate to apply models with fixed-bed. These are used mainly when problems of water levels and flow patterns are only investigated (Chadwick and Morfett 1986).

Physical models are still particularly attractive for investigating non-cohesive sediment transport processes, since many aspects of sediment transport processes are still unclear (Shen 1990). Physical models are attractive but there are difficulties associated with scaling and they may not represent the prototype situation. Several other difficulties are often encountered during laboratory studies associated with sediment transport research. One of the main problems is the degree of turbidity, which can be high in sediment-laden flows and can cause difficulties in direct observation and measurement of sediment fluxes. Chien and Wan (1998) stated that the trend in recent years towards using plastic granular material in flume experiments is an attempt to circumvent this difficulty. They suggested that additional experimental studies of the deposition process under various complicated dynamic conditions should be conducted alongside the development of physical modelling techniques and the use of lightweight modelling materials.

Kocyigit et al. (2005) used a lightweight material called Cation Resinto to represent the bed sediments in laboratory model experiments. The use of this material was aimed at overcoming the difficulties in observing the erosion or deposition phenomena caused by the small magnitude of the flow velocities. A series of laboratory tests were undertaken in a square scaled model harbour, in which bed level changes due to tidal motion were measured.

Mefford et al. (2008) published a physical model study report on Robles Diversion Dam High Flow and Sediment Bypass Ventura, California. This research was carried out in the Bureau of reclamation's Water Resources Research Laboratory, Colorado. Robles Diversion Dam is located on the Ventura River, approximately 14 river miles from the Pacific Ocean. A 1:20 Froude-scale model of the proposed facility was tested to determine the interaction of flows and bed load sediments near the facility following decommissioning and removal of Matilija

Dam located about two river miles upstream. The HFB (High Flow Bypass) spillway was proposed to enhance sediment movement through the diversion pool thereby reducing the impacts of elevated bed load levels resulting from the upstream dam removal. A new auxiliary fish way and 1.5ft dam raise associated with the HFB was also proposed to improve upstream fish passage at the diversion dam during HFB operation. The primary objectives of the model study were to evaluate the HFB spillway's effectiveness for reducing the impact of future increases in sediment load on canal operation and fish passage.

Noor Shahidan and Abu Hasan (2010) investigated the usability of mathematical and physical model for simulation of sediment pattern near the Ijok intake, Ijok River Perak. Ijok Intake is facing sedimentation problem at the inlet that reduced the flow capacity into Ijok Canal. CCHE2D (a two-dimensional numerical model) was used in the study, while a physical model was designed and constructed with a 1:15 undistorted scale at REDAC (River Engineering and Urban Drainage Research Center) physical laboratory in University Sains Malaysia. A comparative study using both models was performed by running simulations without and with an intake structure. Results proved that sediments were accumulated in front of the intake structure, where good agreement was obtained between the numerical and physical simulations. Further simulation with design work of dike structure was carried out using the CCHE2D model, and result showed that proposed dike could reduce and control sedimentation near the intake structure. This research demonstrated that combination of physical and mathematical model can give advantages in analyzing the river sedimentation problem near an intake structure or design mitigation works. As can been seen from the above literature, the role of physical model is undeniable for simulating the hydrodynamic and sediment transport processes.

2.7 Summary

Previous researches in hydrodynamic, sediment transport and morphodynamic processes concerning numerical and physical models have been reviewed in this chapter.

The application of numerical models on simulating hydrodynamic, sediment transport and morphodynamic phenomena for different real case studies could improve and enhance existing methods. Lessons obtained from the numerical simulation of a real case study are very valuable. Besides, this approach needs to investigate accuracy of the mathematical model seriously. Making a comparison between numerical and physical modelling results could reveal joint key features in a same case study. Those are so useful in calibrating and motivating the abilities of the mathematical scheme. This method proposes to design

combined hydraulic structures (such as intakes, sluice gates in a regulated reservoir) in order to find and cover strengths and weaknesses of numerical and physical schemes. Making a combination between numerical and physical modelling also prepares a platform to reduce the cost of designing procedure for a real case study and prevent to construct large scale physical model and run more laboratory tests. Besides this combination enhance our knowledge and abilities for better operation and management of hydraulic structures for the future.

As can been seen from the literature review presented in this chapter, physical and numerical modelling in the design of hydraulic structures can be jointly used. Little works focused on implementing this idea for a real case study comprehensively.

Attempts have been made to investigate procedures for developing a 3-D morphodynamic model to predict natural and hydraulic processes in the vicinity of hydraulic structures accurately. In the current study, A combined numerical and physical modelling approach will be adopted to study the design procedure of hydraulic structures and to assess economic objectives. The essence and complexity of hydraulic flow, sediment transport and morphological changes in the adjacent of hydraulic structures dictate us for simulating these phenomena in three dimensions. For this reason, developing an accurate 3-D numerical model is the focal point of my study.

Chapter Three

Physical Modelling (Theory and Experimental Study)

3.1 Introduction

The present chapter comprises two main parts including physical model theory and an experimental study. The first part including sections 3.2 to 3.4 describes key points of physical model theory related to flow and sediment transport. The second part including sections 3.5 to 3.12 explains an experimental study that is carried out to investigate the flow and sediment transport processes in a regulated reservoir, i.e. the Hamidieh Reservoir, located in Iran.

3.2 Hydraulic simulation theory

A physical scale model is similar to its real-world prototype and involves no scale effects if it satisfies mechanical similarity according to the following three criteria (Yalin 1971, Kobus 1980):

- geometric similarity
- kinematic similarity
- dynamic similarity

Geometric similarity requires similarity in shape, i.e. all length dimensions in the model are λ ($\lambda = L_P/L_m$, where the subscripts p and m refer to prototype (full-scale) and model parameters respectively and L describes characteristic length) times shorter than of real-world prototype. Model lengths, areas and volumes therefore scale with λ, λ^2 and λ^3, respectively, in relation to the prototype.

Kinematic similarity implies geometric similarity and in addition indicates a similarity of motion between model and prototype particles. It requires constant ratios of time, velocity, acceleration and discharge in the model and its prototype at all times.

Dynamic similarity requires in addition to geometric and kinematic similarities that all force ratios in the two systems are identical.

In fluid dynamics, the most relevant forces are (Hughes 1993):

Inertial force = mass × acceleration = $(\rho L^3)\left(\frac{V^2}{L}\right) = \rho L^2 V^2$ (3-1)

Gravitational force = mass × gravitational acceleration = $\rho L^3 \mathrm{g}$ (3-2)

Viscous force = dynamic viscosity × (velocity / distance) × area = $\mu\left(\frac{V}{L}\right)L^2 = \mu VL$ (3-3)

The parameters in Eqs. (3-1) to (3-3) are fluid density ρ, characteristic length L, characteristic velocity V, gravitational acceleration g and dynamic viscosity μ.

Dynamic similarity requires constant ratios of all forces, namely $(\text{inertial force})_\text{P}/(\text{inertial force})_\text{M}$ = $(\text{gravitational force})_\text{p}/(\text{gravitational force})_\text{M}$ = …= constant. A direct consequence is that the corresponding ratios among the various forces in Eqs. (3-1) to (3-3) must be identical in the model and real-world prototype (Kobus 1980). The inertial force is normally the most relevant in fluid dynamics and is therefore included in all common force ratio combinations:

Froude number Fr =$(\text{inertial force}/\text{gravity force})^{1/2} = \frac{V}{(gL)^{1/2}}$ (3-4)

Reynolds number Re = $\text{inertial force}/\text{vicous force} = \frac{LV}{\nu}$ (3-5)

In Eq. (3-5), the kinematic viscosity $\nu = \frac{\mu}{\rho}$ is used instead of the dynamic viscosity μ.

In open channel flows, the presence of the free-surface mean that gravity effects are important. The Froude number is always significant. Secondary scale ratios such as velocity, time and discharge can be derived from the constancy of the Froude number.

Froude scaled modelling is typically used when friction losses are small and the flow is highly turbulent: e.g. spillways, over flow weirs, flow past bridge piers. It is also used in studies involving large waves: e.g. breakwater or ship models.

In river modelling, gravity effects and viscous effects are basically the same order of magnitude. For example, in uniform equilibrium flows, the gravity force component counterbalances exactly the flow resistance and the flow conditions are deduced from the continuity and momentum equations.

In practice, river models are scaled with a Froude similitude ($(\mathrm{Fr})_M = (\mathrm{Fr})_P$) and viscous scale effects must be minimized. The model flow must be turbulent with the same relative roughness as for the prototype (Chanson 1999):

$Re_m > 5000$ (3-6)

$(k_s) = L_r$ (3-7)

where the Reynolds number is defined in terms of the hydraulic diameter (i.e. $Re = \rho V D_H/\mu$ and $D_H = \frac{4A}{P}$, where A is the cross-sectional area and P is the wetted perimeter of the cross-section)

For internal flows or flow through intake structures, the viscous force may be dominant and the Reynolds similarity therefore applies i.e. $(Re)_M = (Re)_P$. A serious disadvantage of the Reynolds similarity is its inconvenient scaling ratios such as λ^{-1} for velocity (Hughes 1993). A phenomenon with a velocity of 1 m/s in a real-world prototype has to be modelled with a model velocity $(1/\lambda^{-1})1$= 25*1=25 m/s at a scale 1:25. For those reasons, Froude similarity is generally used for simulating hydraulic phenomena in rivers and reservoirs.

3.3 Undistorted model attitudes

Undistorted models are those in which all geometric lengths are scaled by the same ratio, and the first several items in this section are simply scaled as products of the geometric length ratio. Since the significant processes in most open channel flow problems are dominated by the forces of gravity and inertia, the remaining ratios are the consequence of requiring that the Froude numbers of the model and prototype be equal:

$$(Fr)_M = (Fr)_P \tag{3-8}$$

Resistance scaling

The modelling of flow resistance is not a simple matter. Often the geometric similarity of roughness height and spacing is not enough. For example, it is observed sometimes that a model does not reproduce the flow patterns in the prototype because the model is too 'smooth' or too 'rough'. In some cases (particularly with a large scale ratio), the model flow is not as turbulent as the prototype flow. A solution is to use roughness elements (e.g. mesh, wire, vertical rods) to enhance the model flow turbulence, hence to simulate more satisfactorily the prototype flow pattern.

Another aspect is the scaling of the resistance coefficient. The flow resistance can be described in terms of the Darcy friction factor or an empirical resistance coefficient (e.g. Chezy or Gauckler-Manning coefficients).

In uniform equilibrium flows, the momentum equation implies:

$$V_r = \sqrt{L_r} = \sqrt{\frac{(D_H)_r (Sin\theta)_r}{\mathrm{f_r}}} \tag{3-9}$$

where the subscripts r refer to scale ratio, D_H = hydraulic diameter, $\sin\theta$ = hydraulic slope and f = Darcy friction factor.

For an undistorted model, a Froude similitude (equations (3-8) and (3-9)) implies that the model flow resistance is similar to that in the prototype:

$$f_r = 1 \tag{3-10}$$

Most prototype flows are fully-rough turbulent and the Darcy friction factor is primarily a function of the relative roughness.

Another approach is based upon the Gauckler-Manning coefficient. The Chezy equation implies that, in gradually-varied and uniform equilibrium flows, the following scaling relationship holds:

$$V_r = \sqrt{L_r} = \frac{1}{(n_{Manning})}((D_H)_r)^{2/3}\sqrt{(\sin\theta)_r} \tag{3-11}$$

For an undistorted scale model, equation (3-11) becomes:

$$\left(n_{Manning}\right)_r = {L_r}^{1/6} \tag{3-12}$$

In summary, a physical model (based upon a Froude similitude) has proportionally more resistance than the prototype. If the resistance losses are small (e.g. at a weir crest), the resistance scale effects are not considered. In the cases of river and harbour modelling, resistance is significant. The matter may be solved using distorted models.

Fixed bed models

For river or channel studies in which the motion of the bed is unimportant a fixed bed model can be used. In practice, an important rule, in model studies is that the model Reynolds number (Re_m) should be kept as large as possible, so that the model flow is rough turbulent (if prototype flow conditions are rough turbulent which is generally occurred).

Various criteria for rough turbulent flow in open channels have been proposed and some of these are listed in Table 3.1.

The most reliable criteria are those, in which Reynolds number is specified in terms of the shear velocity, u_*, and the equivalent roughness size, k, e.g. (Henderson 1966).

$$\frac{u_* k}{\nu} > 100 \tag{3-13}$$

Shear velocity is the ratio of bed shear stress/fluid density and is given by

$$u_* = \frac{\tau_b}{\rho} = \sqrt{gSR} \tag{3-14}$$

where g is gravitational acceleration, R is the hydraulic radius and S is the slope of the energy gradient.

Table 3.1 Criteria for rough turbulent flow

de Vries (1971)	$\frac{Vh}{\nu} > 400\ to\ 800$
Russell (1964)	$\frac{VR}{\nu} > 1000$
Chow (1959)	$\frac{VR}{\nu} > 500$
Henderson (1966)	$\frac{u_* k}{\nu} > 100$
Yalin (1971)	$\frac{u_* k}{\nu} > 70\ approximately$

It is rarely possible to use this criterion directly because it can be difficult to determine the equivalent roughness size. If the channel bed is relatively flat and consists of closely packed pebbles of about equal size (i.e. approximating to the arrangement used by Nikuradse) the equivalent roughness size is related directly to the grain size. In all other cases there is no simple relationship and the value of k must be obtain by other means. The alternative criteria given in Table 3.1 are generally easier to use. In these criteria the length term is specified as the hydraulic radius or depth if the channel is relatively wide, and the velocity is taken to be the mean velocity.

Similarity of frictional resistance will be ensured provided the model and prototype both obey the same resistance law. Once again various equations have been developed to describe the frictional resistance and one of those has been described in a previous section.

Mobile bed experiments

When the movement of the materials which compose the banks and bed of a channel is of paramount importance, a movable-bed model is used.

In comparison with fixed-bed models, the design and operation of a moveable-bed model are much more complex. Two major difficulties are:

1. The boundary roughness of the model is not constant but is a dynamic variable controlled by the motion of the sediment and the bed forms.
2. The model must correctly simulate not only the prototype water movement but also the prototype sediment movement.

Sediment scaling

Sediment transport scaling is a complex problem. It is generally assumed that perfect similitude in both the bed-load and suspended load sediment transport may not be achieved. Therefore a compromise between a bed-load or a suspended load dominated model must be chosen.

Similarity in sediment transport models is obtained by fulfilling similitude in the following dimensionless parameters (Kamphuis1996; Hughes1993):

Grain (or Densimetric) Froude number:

$$Fr_* = \frac{\rho u_*^2}{\gamma_i d_{50}} = \frac{u_*^2}{g d_{50}(s_s - 1)} \quad (3\text{-}15)$$

where u_* = bottom shear velocity ($\sqrt{gSR}$), γ_i = submerged sediment specific weight $[= (\rho_s - \rho)g]$, d_{50} = medium grain size and s_s = specific gravity.

Grain size Reynolds number:

$$Re_* = \frac{u_* d_{50}}{\nu} \quad (3\text{-}16)$$

where ν is water viscosity. These two parameters make reference to forcing (Fr_*) and resting (Re_*) forces acting on a sand particle as represented on Shields diagrams.

Kamphuis (1996) and Hughes (1993) classified bed-load scale models in terms of the requirements they fulfill. The best bed-load model can maintain similitude in grain (densimetric) Froude number, Relative density of the sediment and Relative length number.

Grain (densimetric) Froude number similitude results in geometrical scaling of the median, d_{50}, sediment size:

$$D_{50} = L_r \quad (3\text{-}17)$$

Several authors have proposed different scaling relations assuming suspended load dominates the transport (see Hughes, 1993 for a comprehensive review). These relations determine the scaling using the sediment settling velocity instead of the sediment size and require similitude in both the relative fall speed and relative density.

Zwamborn (1966, 1967 and 1969) has developed a set of similarity criteria for movable-bed models which have been validated by model-prototype correlations. The similarity criteria are:

1. Flow in natural rivers is always fully turbulent. To ensure that the flow in the model is also fully turbulent, the Reynolds number (k_s is length scale) for the model should exceed 600.

2. Dynamic similarity between the model and prototype is achieved when the model-to-prototype ratios of the inertial, gravitational, and frictional forces are equal. Similarity is achieved when:
   a. The Froude numbers for the model and prototype are equal.
   b. The friction criteria are satisfied when the following three conditions are met. First, the product of the grain roughness coefficient and the inverse square root of the slope are equal in the model and prototype or

$$C'_r = \frac{1}{\sqrt{S_r}} \tag{3-18}$$

where C'= grain roughness coefficient

$$C' = 5.75\sqrt{g}\ log\left(\frac{12R}{d_{90}}\right) \tag{3-19}$$

d_{90} = 90 percent smaller grain diameter. Second, the ratio of the shear to the settling (fall) velocity in the model and prototype are equal or

$$\left(\frac{u_*}{w_s}\right)_r = 1 \tag{3-20}$$

where u_* = shear velocity ($\sqrt{gSR}$), w_s = settling (fall) velocity. The settling velocities of selected model sediment materials are summarized in Fig. 3.1 as a function of grain size, shape function and water temperature. The size of particle can be determined by sieve or visual-accumulation tube analyses. The U.S standard sieve series is used for this approach. Shape refers to the form or configuration of particle regardless of its size or composition. Corey (see Schulz et al., 1954) investigated several shape factors, and concluded that from the viewpoint of simplicity and effective correlation the shape factor was the most significant expression of shape.

$$S_P = c/(ab)^{1/2} \tag{3-21}$$

In Eq. (3-21), *a*, *b*, and *c* are the lengths of the longest, the intermediate, and the shortest mutually perpendicular axes through the particle, respectively; and S_P is the shape factor. The shape factor is 1.0 for a sphere. Naturally worn quarts particles have an average shape factor of 0.7. Third, the Reynolds number based on the sediment grain diameter in the model should be about one-tenth of the grain Reynolds number for the prototype or

$$(Re_*)_r < \frac{1}{10} \tag{3-22}$$

3. Sediment motion is closely related to the bed form type which is, in turn, a function of $\frac{u_*}{w_s}$, Re_* and r. For specific values of $\frac{u_*}{w_s}$ and Fr, similar bed forms and consequently similar models of bed movement are ensured when the value of Re_* for the model falls within the range as determined by $\frac{u_*}{w_s}$ and the appropriate range of Fr defining a type of bed form (Fig. 3.2.)

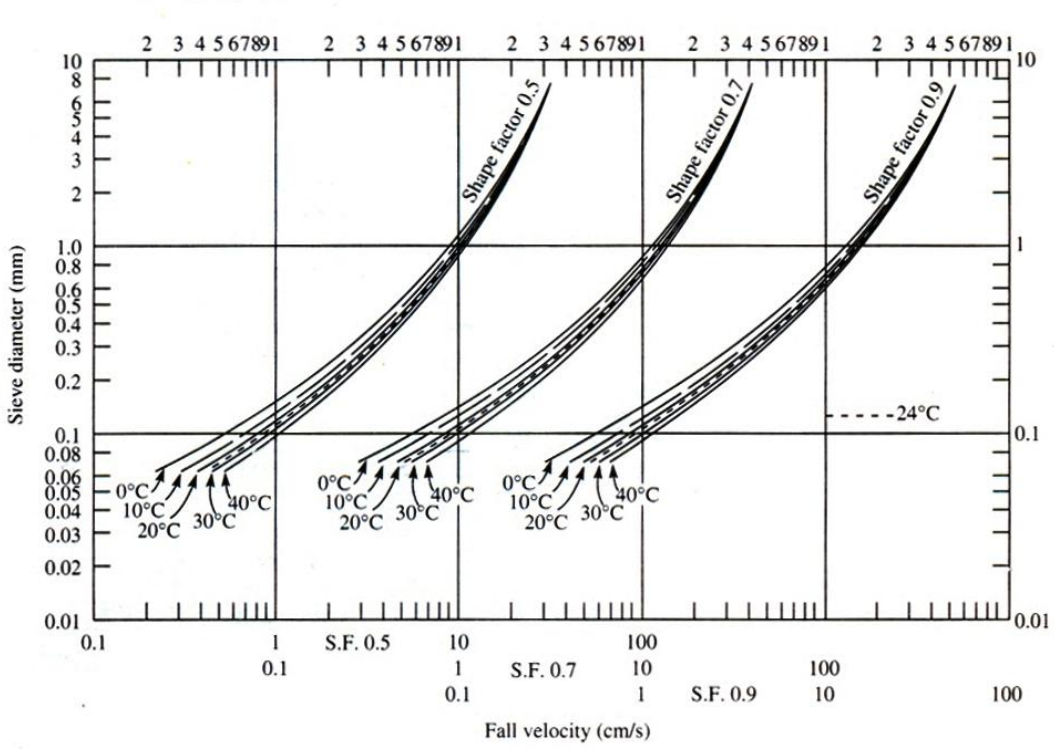

Figure 3.1 Relation between sieve diameter and fall velocity for naturally worn quartz particles falling alone in quiescent distilled water of infinite extent (U.S. Inter-Agency Committee on Water Resources, Subcommittee on Sedimentation, 1957)

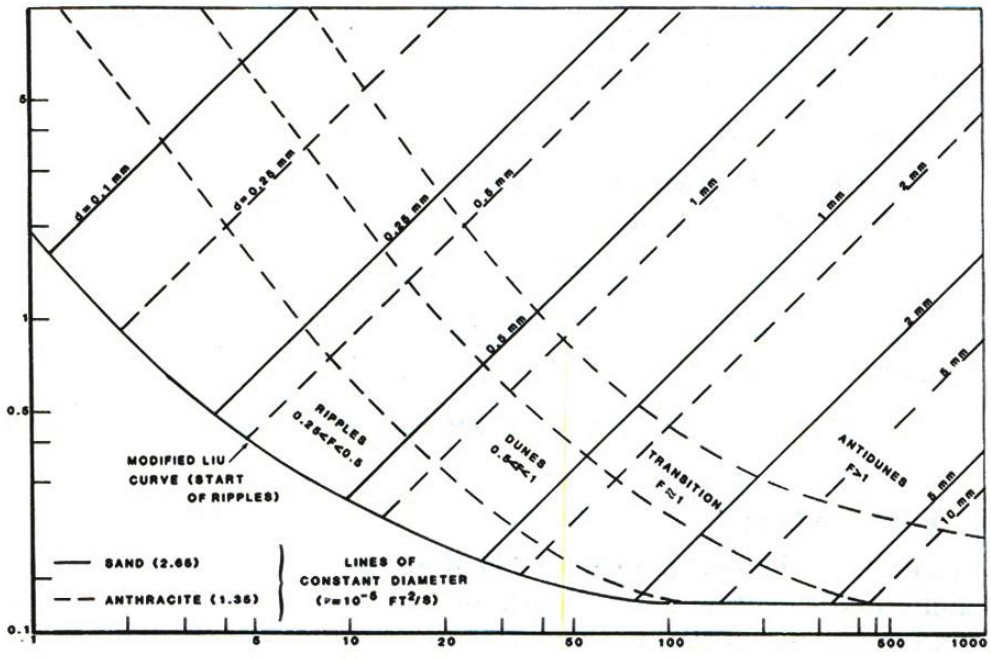

Figure 3.2 Bed shape criteria (Zwamborn 1969)

3.4 Introduction to Hamidieh regulated reservoir study

A physical model was constructed to represent the flow, sediment transport and morphodynamic processes in Hamidieh regulated reservoir. The experiments, including designing scale, constructing and measuring tests of the physical model were carried out in the Water Research Institute in Iran by the author. Efforts were made to simulate the hydrodynamic, sediment transport and morphological processes in one model. The physical model was designed based on Froude similarity (undistorted), with non-cohesive material being used. Although a physical model cannot answer all of the hydraulic questions, it can reveal some key features.

In the next sections, details are given of the criteria for surface water physical model simulations, and the application to the Hamidieh regulated reservoir to investigate fluid, sediment interactions and to optimize the operation of the intake structures. Designing the scale of the model, hydraulic testing programme and scientific judgments will be presented in the following sections.

3.5 Project background

Hamidieh regulated reservoir is located 11 km away from Hamidieh Town. It has been constructed along the Karkheh River, downstream of Karkheh reservoir dam (Figure 3.3). Figure 3.4 also shows an aerial photo of current situation of Hamidieh regulated reservoir and relative hydraulic structures. Currently, there are two water intakes, namely Ghods and Vosaileh. Vosaileh water intake channel, located on the left side of the Hamidieh dam body (regarding to flow direction) is 10.8 km long with a maximum discharge of 60 m^3/s, while Ghods, located on the right side, of dam body operates with a 25 km long channel, with a maximum carrying capacity of 13 m^3/s (WEOKP, 2001). The layout of current situation of Hamidieh regulated reservoir including dam body, irrigation channels, Ghods and Vosaileh intakes is presented in Figure 3.5. Figure 3.6 shows pictures about existing hydraulic structures of Hamidieh regulated reservoir.

Figure 3.3 Location map of Hamidieh town

Figure 3.4 Aerial photo of current situation of Hamidieh regulated reservoir

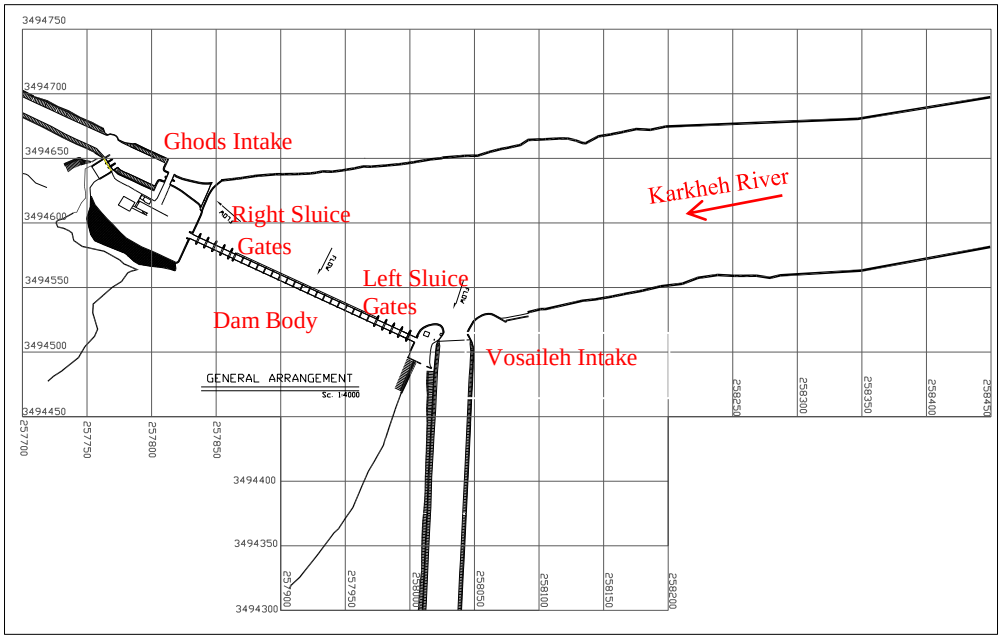

Figure 3.5 The layout of current situation of Hamidieh regulated reservoir and associated structures (WEOKP 2001)

Figure 3.6 Pictures of existing hydraulic structures of Hamidieh regulated reservoir

Due to the development in irrigation and drainage networks of Azadegan and Chamran plains, the two water intakes are no longer able to meet the water demand. Hence, it is necessary to increase the rate of flow by designing new intakes with improved dimensions and geometric characteristics.

Hamidieh reservoir dam is 192 m long, 4.5 m high with 19 spillway bays opening and 10 floodgates. The Azadegan intake, with an inlet width of 56 m, 8 bays opening and 4 under sluice gates, is to replace the Ghods water intake. It is designed to increase the carrying capacity from 13 m^3/s to 75 m^3/s. The Vosaileh water intake is replaced by the Chamran intake, with an inlet width of 86.6 m, 16 bays opening and 13 trash racks opening, to increase the carrying capacity from 60 m^3/s to 90 m^3/s (Figure 3.7).

An undistorted 1:20 scale model of Hamidieh regulated reservoir and its associated structures were constructed to investigate the operation of the entire system to improve the understanding of the flow and sediment processes in the vicinity of the structures.

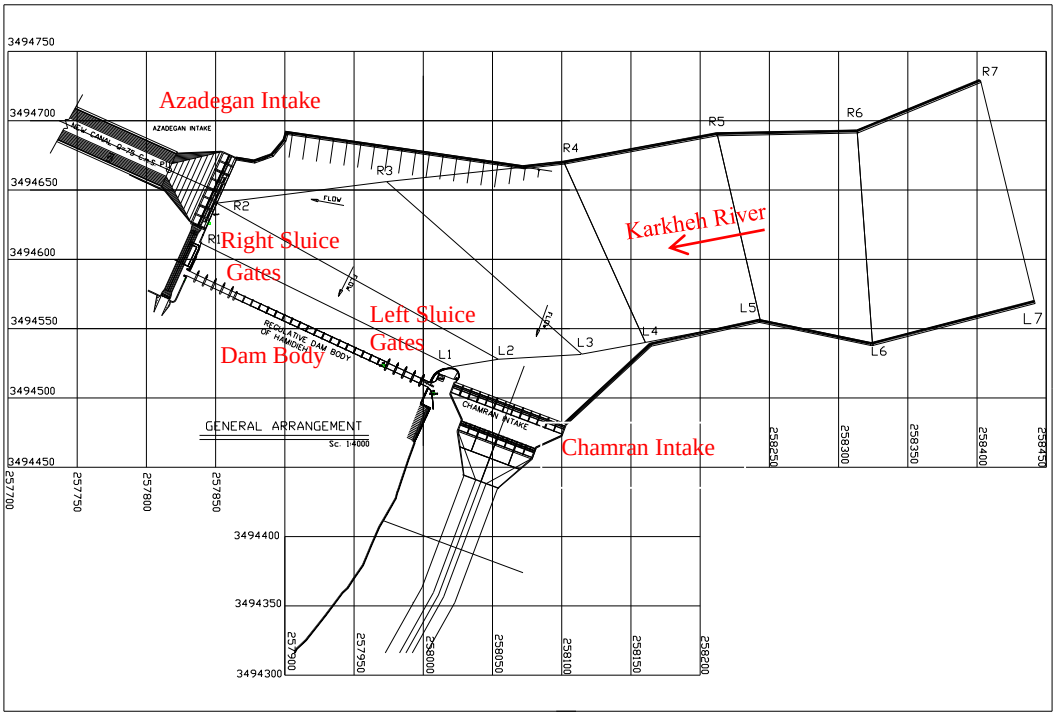

Figure 3.7 Plan view of Hamidieh regulated reservoir and associated structures

In addition, the present condition of the project and also the expectations of new developments, which made the physical model study more significant. The key issues to be considered are:

- Water supply to two main irrigation and drainage networks situated both sides of the regulated reservoir with an area of about 2 x 10^6 hectares (100 hectare =1 km^2),

- Irregular water intake from the river, which can reach up to 90% of the river flow (when water demands rise during farming season significantly),
- Inappropriate location of Hamidieh regulated dam regard to flow pattern (dam was not located perpendicular of upstream flow direction),
- Lack of sufficient discharge through intakes in normal water levels in the reservoir,
- Possibility of creating sedimentary islands in front of the intakes and making impacts on diverting flow discharge forward the intakes,
- Complex pattern of sediment distribution in the reservoir and the amount of sediment passing through the intakes for different operation scenarios,
- Intensive sedimentation observed in Vosaileh water intake (an existing intake).

3.6 Model design and testing

3.6.1 Designing scale

Application of empirical relations in many hydraulic phenomena may lead to some degrees of errors. This could be on account of the complex nature of them or the simplistic approach by which they are treated (De Vries 1993). In river engineering projects, it is necessary to understand the interaction between water and sediment discharge resulted from complex morphological processes in three dimensions (De Vries and Van Der Zwaard 1975). Physical models of rivers offer as essential tools to enable us to obtain more accurate and reliable data, particularly, where these changes are made by cross-structures.

To validate model results in comparison with prototype, the set of conditions associated with each other must be dynamically similar. For free surface flow models, it is necessary to consider both the gravity and friction forces to achieve dynamic similarity. Therefore, the Froude and Reynolds numbers should ideally have the same values in both the prototype and models (Henderson 1966).

To match both Froude and Reynolds number in the physical model simultaneously, need to use a liquid whose kinematic viscosity satisfies the equation as follows:

$$\frac{\nu_m}{\nu_p} = \left(\frac{L_m}{L_p}\right)^{3/2} \tag{3-23}$$

Although it is sometimes possible to find an appropriate liquid for use with the model, in most cases it is either impractical or impossible. Therefore, scaling of the model results must be carried out in accordance with a selected primary criterion with consideration given to the other criterion as a second priority (Sharp 1981).

As the Reynolds number more and more increases, the thickness of the viscous sub-layer

decreases and finally it has no covering effect in the end. Additionally the tenacity has no influence on the flow resistance anymore. Only the size of the relative roughness has to be considered for the calculation of the friction coefficient. Flow in natural channels are usually within the "hydraulically rough" range (see Eq. 3-30) so that the roughness coefficient only depends upon the relative roughness, and the magnitude of the Reynolds number is of no importance (Kobus 1980). Therefore, the model conditions are derived from the Froude number similarity criterion as gravity provides the driving force in river mechanics. Accordingly, satisfaction of the Froude law will make the model operate at a much smaller Reynolds number than the prototype, but care must be taken to ensure that the model operates within the same flow regime as the prototype; as energy losses associated with laminar and turbulent flow cannot be easily scaled (Yalin 1971).

For Froude number similarity with a scale ratio of hydraulic parameters may be derived (Table 3.2). However, it is important to simulate sediment transport processes as accurately as possible, as this reflects the sediment behavior in the prototype. French (1986), following Zwamborn (1966), argues that when particle in solution for mass transport of sediment is not large enough or investigation is concerned with transport en-masse, the dependence on the particles' Reynolds number is limited for suspended sediment load and $\alpha = (w_s \,/\, (\kappa u_*))$ may be a more appropriate parameter to obtain satisfactory scales. Therefore, α values must be the same in both the model and prototype as

$$\left(\frac{w_s}{\kappa u_*}\right) = 1 \tag{3-24}$$

where w_s = particles fall velocity (m/s)

u_*= shear velocity (m/s)

κ = von Karman's constant = 0.407

Stokes' law states that if the particles' Reynolds number ($\frac{u_* D}{\nu}$) is small, w_s is expressed as

$$w_s = \frac{D^2}{18\mu}(\gamma_s - \gamma) \tag{3-25}$$

where γ_s = specific weight of sediment particles (N/m^3)

γ = specific weight of water (N/m^3)

μ = dynamic viscosity ($N.s/m^2$)

D = representative sediment grain size (m)

At a high value of α, the fall velocity increases and only little material is kept in suspension and their distribution becomes non-uniform over the water depth; while at a low value of α,

the fall velocity decreases leading to more material in suspension and their distribution becomes more and more uniform over the water depth (Kobus 1980).

By considering the suspended sediment specific weight and dynamic viscosity of the prototype to be the same as that of the injected sediment into the model (Yalin and MacDonald 1987), Equations (3-24) and (3-25) are applied to work out particle size frequency distribution on the basis of the length ratio in the model as Table 3.2.

$$\left[\frac{D^2}{L^{1/2}}\right]_r = 1 \tag{3-26}$$

Table 3.3 shows the size frequency distribution of suspended sediment in the model. It is also noticed that similar specific weights of the sediment in the model and prototype ($\rho_r = 1$) lead to the similar concentration values in the model and prototype. Hence the suspended sediment discharge is calculated as

$$Q_{sm} = \left(C_p/\rho_r\right).Q_{wm} \tag{3-27}$$

where Q_{sm} and Q_{wm} are the suspended sediment load and water discharge in the model, respectively, while C_p is the suspended sediment concentration in the prototype.

Table 3.2 Ratios of hydraulic and sediment parameters

Quantity	Symbols	Ratio	Scale ratio=(1/20)
Length	L_r	L_r	1:20
Height	h_r	L_r	1:20
Area	A_r	$(L_r)^2$	1:400
Slope	S_r	1	1
Velocity	V_r	$(L_r)^{1/2}$	1:4.472
Discharge	Q_r	$(L_r)^{5/2}$	1:1788.85
Manning's roughness	n_r	$(L_r)^{1/6}$	1:1.648
Sediment particle size	D_r	$(L_r)^{1/4}$	1:2.1147

Table 3.3 Suspended sediment size frequency distribution in prototype and the model

Attitudes	Sediment Size		
	D_{20} (mm)	D_{50} (mm)	D_{90} (mm)
Prototype	0.074	0.121	0.370
Model	0.035	0.057	0.175

In order to model turbulent flow in natural streams more accurately, effect of bed roughness (k) on water depth must be considered. This can be achieved by coupling up Manning-Strickler with Darcy-Weisbach to obtain (Chadwick and Morfett, 1986)

$$\frac{1}{\sqrt{\lambda}} = 2.9\left(\frac{k}{R}\right)^{-\frac{1}{6}} \quad (3\text{-}28)$$

where λ = Darcy factor, and R = hydraulic radius.

In wide channels R may be replaced by water depth y. A comparison of this empirical formula for the roughness coefficient with the general function based on the experiments by Nikuradse yields relative roughness (k/y) in a range of $2x10^{-3} < (k/y) < 2x10^{-1}$ (Kobus 1980). The majority of natural open channels fall within these limits, with the exception of the very large streams and of rivers in coastal regions. Flows in natural channels are usually within the hydraulically rough range so that the roughness coefficient only depends upon the relative roughness hence the magnitude of the Reynolds number is of no importance (French 1986).

According to Moody (1944), the limit between the hydraulically rough flow regions and the transition is given by

$$\frac{\mathbf{Re}\sqrt{\lambda}}{4y}\mathrm{k} = 200 \quad (3\text{-}29)$$

According to equation (3-28), the condition for a hydraulically rough flow is

$$\mathbf{Re} \geq 2.35\times10^{3}\left(\frac{\mathrm{k}}{\mathrm{y}}\right) \quad (3\text{-}30)$$

3.6.2 Construction and material

The design of the physical model for the Hamidieh regulated reservoir and associated structures was categorized on three sections: selecting type of model, calculating model scale and preparations. With reference to the similarity theories, a fixed-bed undistorted physical model seemed appropriate to enable us to observe hydraulic phenomena in the model. However, the flow must be turbulent even at low discharges.

In general, the model scale is selected with consideration of laboratory space so that the constructed model is to be fitted in the area. Then it is possible to determine hydraulic model parameters such as the water discharge, bed roughness and flow hydraulic characteristics. An appropriate scale is selected to meet all these criteria. If not, the above procedure has to be repeated. A 1:20-scale model of the Hamidieh regulated reservoir dam was constructed, as this meets all the above requirements regarding flow hydraulic conditions. The relationship between the hydraulic parameters of the model and the prototype were shown in Table 3.2.

On the basis of 1:500-scale maps, a plan view of the Hamidieh regulated dam physical model was designed and constructed. This included associated structures, such as stilling and

sedimentation basins as well as Azadegan and Chamran water intakes. A laboratory setup was then established based on the designed dimensions of the physical model and associated structures at the Water Research Centre in Iran.

The water discharge was adjusted by a pump control system through an inlet channel and an outlet channel linked to a storage tank. The reservoir bed topography was made by concrete and masonry. Both the two intakes (Chamran and Azadegan) and all of the gates were constructed by wood. Different workshops such as those for carpentry, painting, ironing and turning were involved for constructing and assembling the whole system of this large physical model. It took more than 5 months for construction and installation of the Hamidieh physical model. Figures 3.8 to 3.11 show the constructing stages of this hydraulic model.

a) Chamran Intake b) Azadegan Intake

Figure 3.8 Two intakes physical model

Figure 3.9 The installation stage of the physical model

Figure 3.10 Constructing bed topography for the reservoir model

Figure 3.11 Completed physical model

3.6.3 Measuring systems

Three types of parameters have been measured in the physical study, including the hydrodynamic (discharge, velocity, water level and flow pattern), sediment (distribution of sediment concentration and sediment grain size distribution) and morphological (bed evolution and erosion) parameters. The discharge measurements were made by rectangular and triangular weirs installed in different locations (at the end of each intake and in the final outlet channel). The water level was maintained by a tailgate, while the stream pattern was observed by tracers and the velocity distribution was measured by the means of mechanical current meter (A.OTT KEMPTEN, type: $C_2.''10.150''$, NO.52051 and meter support on rod of 9 mm diameter). The sampling of suspended sediment concentration was taken over the whole depth and calculated using a depth integrating formula. This decision was made because of the low water depth in the physical model. Previous studies and measurements for

the Hamidieh regulated dam (existing condition) have showed that the suspended sediment transport was the dominant process in this reservoir. The majority of sediment found belonged to the non-cohesive type in the prototype (WEOKP 2001). In this physical model study, sampling works at different locations in the reservoir and also at the ends of both intakes were carried out in order to understand the grain size distributions of the sediment entering into the reservoir and pass though the intakes. The particle size distribution was measured and calculated by sieve analysis (or gradation test) and hydrometer analysis. Sediment material using in this physical model was obtained from broken pottery (baked clay). This material is non-cohesive and has a similar specific gravity as that of the prototype. A sediment injection system was used which was designed by the Water Research Institute. This system has the ability for injecting different amounts of dry sediments to the flow. A gearbox was used to move several shafts with different speeds and many slots were arranged on the shafts for better control of the amounts of sediment injection. Bed level changes (topography of the bed reservoir) were measured with surveying operations in different times (initial time and after running morphodynamic scenarios individually) in order to determine the sedimentation and erosion zones and the movements of sediments in the reservoir and the vicinity of hydraulic structures. The following pictures (Figures 3.12 to 3.17) show the measuring tools and sediment injection system used in the physical model study.

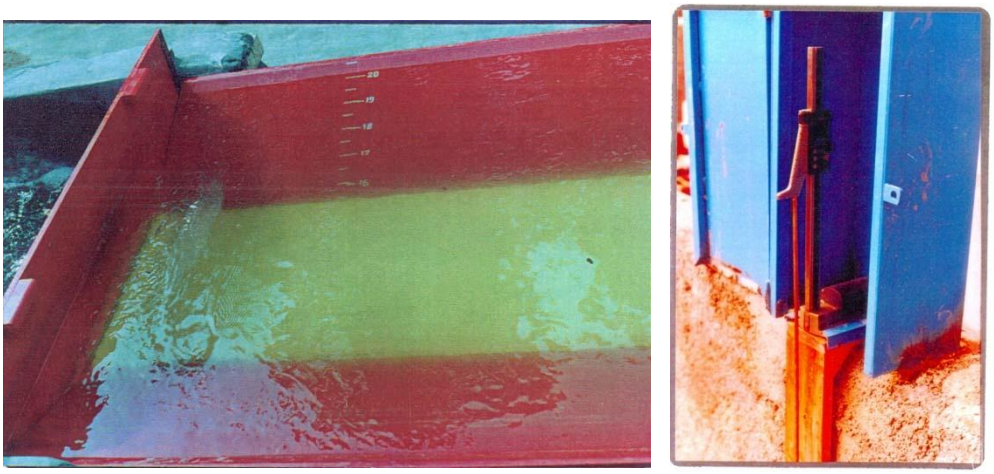

Figure 3.12 Tail gate for regulating and measuring water level, gage mark in trapezoidal channel and digital limnimeter for measuring head water on weir

Figure 3.13 Putting gage marks in the physical model

Figure 3.14 Mechanical current meter system (A.OTT KEMPTEN, type: $C_2.''10.150''$, NO.52051-meter support on rod of 9 mm diameter)

Figure 3.15 Sediment injection system and accessories (gearbox, shaft and storage box)

Figure 3.16 Hydrometer analysis for sediment samples

Figure 3.17 Determination of sediment concentration

3.7 Scenarios and results of physical model

3.7.1 Flow and hydrodynamic section

Experiments were undertaken with different water discharges to simulate three different conditions containing regulatory conditions, high flow and flooding

Similarity of frictional resistance will be ensured provided the model and prototype both obey the same resistance law. The Manning equation is probably most widely used. However, the model roughness must be considered in conjunction with the reduction in Reynolds number (Sharp 1981). The roughness coefficient in the prototype was estimated in the range of 0.023 to 0.025 (refer to proposing $n_{Manning}$ for various types of channels by Chow 1959), these were converted to 0.014 to 0.015 in the physical model ($(n_{Manning})_r = {L_r}^{1/6} = (20)^{1/6} = 1.648$, refer to Table 3.2), which could easily be obtained by a plane concrete surface.

Intake structures are used where water abstraction from rivers or reservoirs is required. Therefore, the design of the inlet structures should be handled with care and attention. In prototype generally, the inlet velocity varies in the range of 0.5-1.0 m/s (Kobus 1980), while any transition or bending at the entrance should occur gradually to minimize the energy losses in the inlet channel. A uniform velocity distribution is also recommended at the entrance, as a non-uniform velocity distribution and unstable water surface upstream of the intake channel, as well as vortex generated near the intakes could reduce the rate of flow into the system.

In the study the hydraulic performance of the intake structures is assessed by the velocity measurements as well as flow pattern behavior in the vicinity of the structures. The velocity distribution could also been determined by velocity profile variations in plane, which is obtained by point velocity measurements using a current meter.

In the physical model study measurements of flow velocity were made at several points in front of the intakes .by current-meters. These measure points are situated at 20 m and 40 m upstream of the intakes respectively. The location of these points is shown in the Figures 3.18 and 3.19.

The velocity was measured by a current-meter at $0.6D$ (D = water depth) from the water surface and fitted to the physical scale and prototype. This depth was chosen based on the velocity logarithmic profile assumption.

Table 3.4 indicates the velocity values for different locations that were shown in Figures 3.18 and 3.19 for the physical and converted to the prototype scale, respectively.

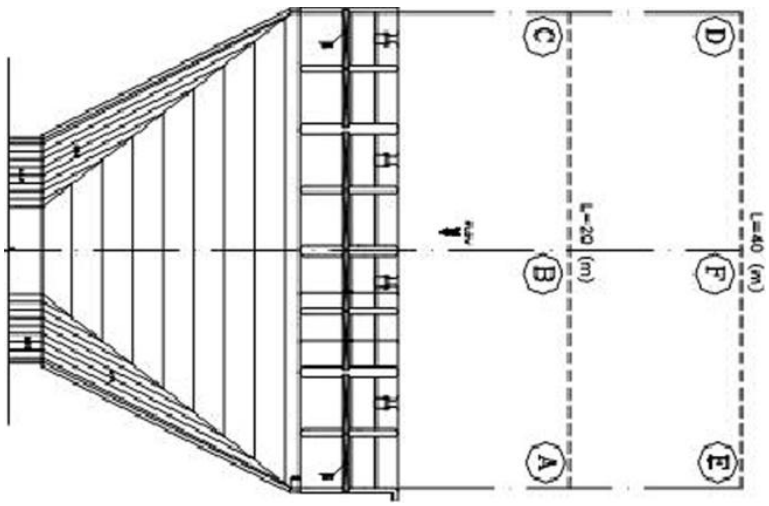

Figure 3.18 Location of velocity measuring points in vicinity of Azadegan intake

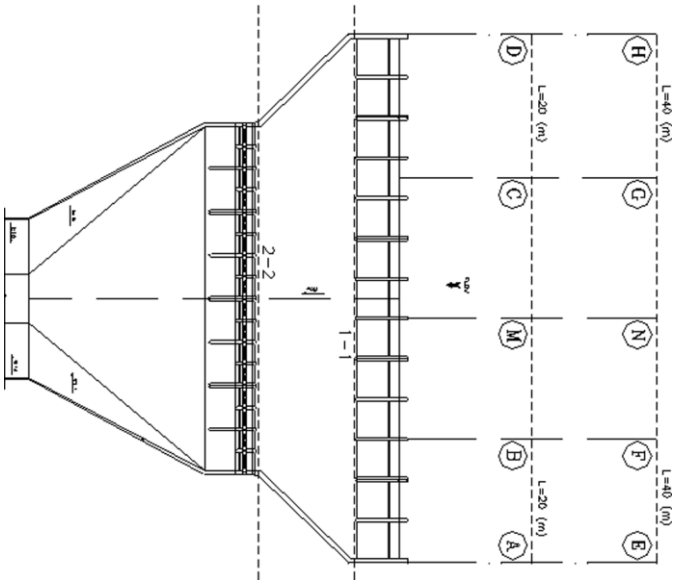

Figure 3.19 Location of velocity measuring points in the vicinity of Chamran intake

Table 3.4 Velocity values obtained from physical model and converted to prototype

Location	Points	Measured Physical Scale (cm/s)	Converted to Prototype Scale (m/s)
Chamran	A	3.09	0.138
	B	5.91	0.264
	M	6.59	0.295
	C	5.91	0.264
	D	3.10	0.139
	E	3.08	0.138
	F	5.27	0.236
	N	6.40	0.286
	G	5.18	0.232
	H	3.59	0.161
Azadegan	A	3.97	0.178
	B	4.13	0.185
	C	4.46	0.199
	E	3.18	0.142
	F	4.25	0.190
	D	3.18	0.142

The whole flow and hydrodynamic experiments run for this section were carried out in clear water (i.e. water without sediments). The velocity measurements show a uniform flow velocity distribution upstream of Azadegan intake, which stabilizes more by a reduction in distance to confirm proper operation of the system.

Figure 3.20 shows the flow pattern obtained from the physical model in the regulatory condition (Test No. 5 explained in Table 3.5). For this test, wood chips that are floated on the water surface were used to show the flow pattern. According to the observation of the flow

direction, it is noticed that a non-uniform velocity distribution zone exists upstream of Chamran intake on the left bank side. This is thought to be related to the location of Chamran intake.

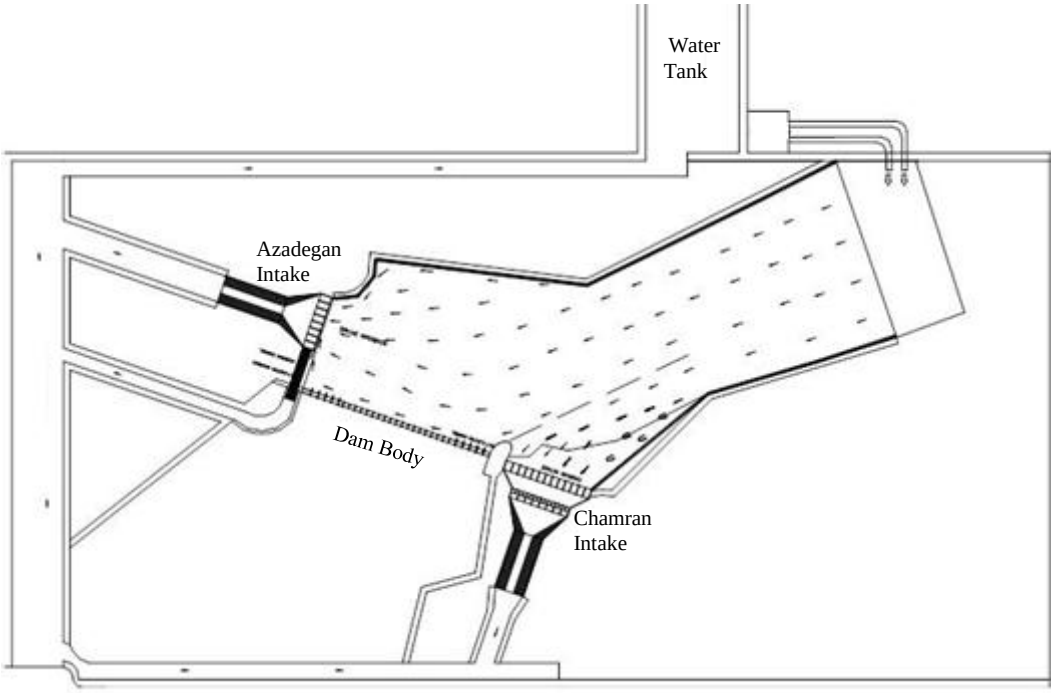

Figure 3.20 Flow pattern in a regulatory condition at normal water level (20.20m) in the Hamidieh reservoir (Test No. 5 explained in Table 3.5)

The water elevation was set to 20.20 m (in the prototype) for the normal condition in the regulated reservoir according to hydraulic designing conditions for these series test.

Tables 3.5 present the results for 20 different scenarios. Water discharge measurements downstream of the intakes indicate that Chamran intake cannot meet the requirement of a nominal carrying capacity of 90 m^3/s, while Azadegan easily achieves 75 m^3/s at 20.20m water elevation in the reservoir (Table 3.5). That is one of the key results for the hydrodynamic study and a solution is required for solving the problem with Chamran intake.

Table 3.5 Results of hydraulic experiments, Discharge (m^3/s), Bay opening (m^2) and Water surface elevation (m) (data transferred to prototype)

Test No.	System / Operation	Hamidieh Reservoir	Az. intake	Ch. intake	Under sluice Az. intake	Right sluice gates	Left sluice gates	Remarks
1	Discharge	48.29	6.97	36.14	5.18	-	-	*
	Bay opening	-	4.60	13.14	4.48	-	-	
	WS. Elevation	20.20	19.30	19.70	-	-	-	
2	Discharge	88.67	27.69	54.17	6.81	-	-	*
	Bay opening	-	14.40	22.50	4.48	-	-	
	WS. Elevation	20.20	19.36	19.77	-	-	-	
3	Discharge	113.02	43.14	62.73	7.15	-	-	*
	Bay opening	-	27.90	33.75	4.48	-	-	
	WS. Elevation	20.20	19.56	19.83	-	-	-	
4	Discharge	166.99	103.89	63.20	-	-	-	*
	Bay opening							
	WS. Elevation	20.20	20.00	20.00	-	-	-	
5	Discharge	179.66	107.99	71.67	-	-	-	*
	Bay opening	-	144	52.8	-	-	-	**
	WS. Elevation	20.20	20.00	20.00				***
6	Discharge	194.21	40.26	63.27	4.10	38.58	48.00	*
	Bay opening	-	14.40	27.75	4.48	6.51	9.11	
	WS. Elevation	20.20	19.46	19.83	-	-	-	
7	Discharge	159.55	74.86	73.54	4.65	-	6.50	*
	Bay opening	-	36.00	49.2	2.24	-	1.04	
	WS. Elevation	20.25	20.00	20.00	-	-	-	
8	Discharge	167.04	74.02	81.67	4.65	-	6.7	*
	Bay opening	-	34.2	49.8	2.24	-	1.04	
	WS. Elevation	20.30	20.00	20.00	-	-	-	
9	Discharge	179.81	74.02	94.34	4.65	-	6.8	*
	Bay opening	-	28.80	50.40	2.24	-	1.04	
	WS. Elevation	20.35	20.00	20.00	-	-	-	
10	Discharge	186.33	76.50	98.10	4.65	-	7.08	*
	Bay opening	-	29.70	52.80	2.24	-	1.04	
	Elevation	20.40	20.00	20.00	-	-	-	
11	Discharge	189.17	80.40	95.56	4.71	-	8.50	****
	Bay opening	-	43.20	50.40	2.24	-	1.30	
	WS. Elevation	20.45	20.20	20.20	-	-	-	
12	Discharge	186.56	84.53	88.75	4.78	-	8.50	****
	Bay opening	-	46.80	49.80	2.24	-	1.30	
	Elevation	20.40	20.00	20.00	-	-	-	
13	Discharge	174.47	79.44	82.43	4.7	-	7.90	****
	Bay opening	-	43.20	49.20	2.24	-	1.30	
	WS. Elevation	20.35	20.00	20.00	-	-	-	
14	Discharge	147.81	67.02	68.37	4.68	-	7.74	****
	Bay opening	-	45.00	49.2	2.24	-	1.30	
	WS. Elevation	20.30	20.00	20.00	-	-	-	

Continued-Table 3.5 Results of hydraulic experiments, Discharge (m^3/s), Bay opening (m^2) and Water surface elevation (m) (data transferred to prototype)

Test No.	System / Operation	Hamidieh Reservoir	Az. intake	Ch. intake	Under sluice Az. intake	Right flood gates	Left flood gates	Remarks
15	Discharge	137.31	65.74	59.04	4.68	-	7.90	****
	Bay opening	-	45.00	48.00	2.24	-	1.30	
	WS. Elevation	20.25	20.00	20.00	-	-	-	
16	Discharge	125.25	57.17	55.50	4.68	-	7.90	****
	Bay opening	-	43.20	48.00	2.24	-	1.30	
	Elevation	20.20	20.00	20.00	-	-	-	
17	Discharge	180.79	122.23	45.88	4.88	-	7.80	****
	Bay opening	-	86.40	24.00	2.24	-	1.30	
	WS. Elevation	20.45	20.20	20.20	-	-	-	
18	Discharge	215.41	109.48	93.15	4.88	-	7.80	****
	Bay opening	-	57.60	36.00	2.24	-	1.30	
	WS. Elevation	20.45	20.00	20.00	-	-	-	
19	Discharge	224.24	129.23	100.99	5.17	-	8.85	****
	Bay opening	-	86.40	48.00	2.24	-	1.30	
	WS. Elevation	20.45	20.00	20.00	-	-	-	
20	Discharge	256.47	140.53	102.13	5.06	-	8.75	****
	Bay opening	-	115.20	51.00	2.24	-	1.30	
	WS. Elevation	20.45	20.00	20.00	-	-	-	

* without trash racks,
** head loss at Chamran intake gates,
*** nominal carrying capacity for the intakes at the water surface elevation 20.20m,
**** with trash racks and considering bay opening surface trash racks is 80 % of the total surface (These conservative scenarios have been considered for service time operation when trashes were gathered in front of the intakes).
Az. = Azadegan, Ch. = Chamran and WS. Elevation = Water surface elevation

The water surface elevations for the intakes shown in Table 3.5 were measured in the trapezoidal channel at the end of intakes (see Figure 3.12).

After these experiments, several solutions were put forward to enable Chamran to reach its nominal carrying capacity in the normal elevation (20.20 m). Those solutions was made and run in the physical model One of the solutions, which was actually adopted in the experimental model, was to install permeable groins on the opposite bank to deflect the flow, making its direction towards the intakes. The measure could activate stagnant zone to some extent, however, Chamran's carrying capacity was increased only by 5%, see Figure 3.21. Another solution was to make two guide walls for the Chamran intake (Figure 3.22). This method could not enhance the discharge capacity for this intake, neither. When a permeable wall was obstructed across the entire reservoir width, a local increase in the reservoir water elevation was observed, resulting in 90 m^3/s water discharge at Chamran, see Figure 3.23. Nevertheless, this solution is not very practical for implementation, as this would confirm

that the nominal carrying capacity at Chamran can only be obtainable by a raise in water elevation to 20.40 m in the reservoir. Finally, the water elevation of the reservoir was set to 20.45 m for the sediment experiments shown below in order to reach safe and secure water flow distribution for the two intakes for all scenarios.

Figure 3.21 Location of permeable groins on the opposite bank

Figure 3.22 Location of permeable guide wall for Chamran intake

Figure 3.23 Obstruction of reservoir width by a permeable wall

3.7.2 Sediment transport and morphodynamic section

In this research, different scenarios were considered in order to determine the amount of sediments entering the intakes and investigating sediment grain size distribution in the reservoir and through hydraulic structures. Besides, the role of sluice gates on the sediment flashing in front of intakes was investigated in the physical model. Details are given below of the physical model study of sediment transport process. For a better understanding of the implication of the model results to the project, the results were transferred to the prototype like flow and hydrodynamic section. This action would help us to get an overview about engineering judgments. For brevity, the experimental results are presented as a graph and a summarized table. The scenarios have been designed and carried out in the hydraulic laboratory of Water Research Institute based on different operations for the intakes (in percentage of opening of the gates), flow discharge and sediment concentrations put in the reservoir by the author.

Previous studies in the field for existing condition of Hamidieh regulated reservoir have showed that the suspended sediment transport is the dominant process and the majority of sediment found in this region belongs to the non-cohesive type (WEOKP, 2001).

Sediment sampling was carried out in order to determine the sediment concentration and particle size distributions in the physical model. The sampling of suspended sediment concentration in the physical model was taken along the whole depth and calculated using a depth integrated formula. Figure 3.24 presents the sites of the sediment samples at different locations.

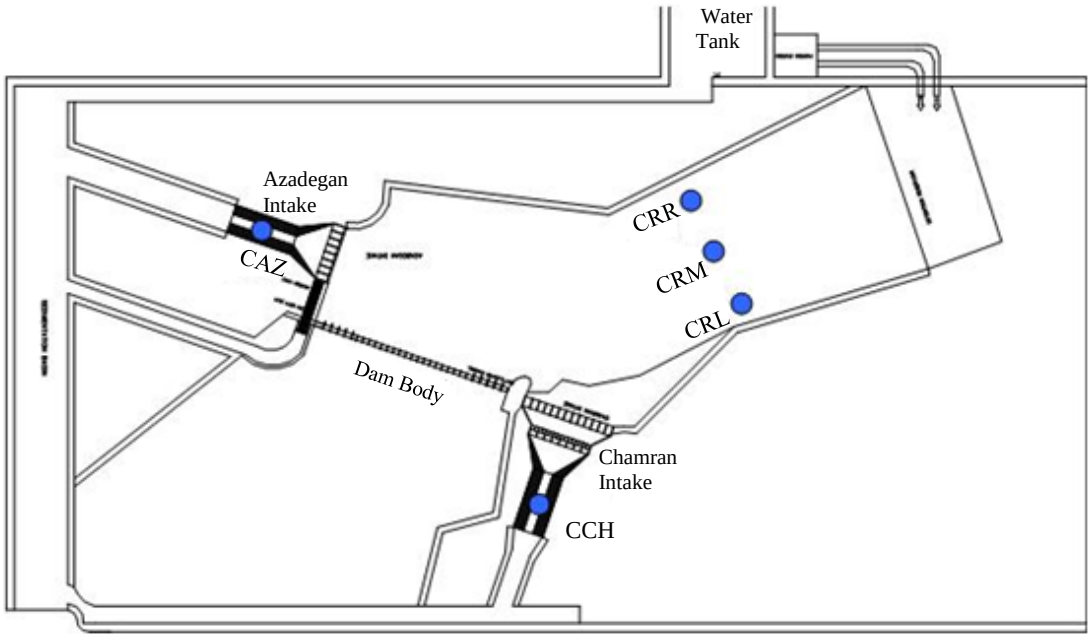

Figure 3.24 Locations of sediment concentration and gradation sampling points (CAZ=Concentration in Azadegan Intake, CCH=Concentration in Chamran Intake and CRR, CRM and CRL=Concentration in the reservoir)

Various sediment transport scenarios have been tested. Figure 3.25 shows the relationship between the sediment discharge in the reservoir ($Q_S - \text{reservoir}$) and sediment discharge in both intakes (Chamran and Azadegan) and pass through the away from under sluice gates belong to the Azadegan intake ($Q_S - \text{systems}$). By this graph (Figure 3.25), we can evaluate the amount of sediment entering the intakes and under sluice gates and the corresponding value in the reservoir. As can be seen from Figure 3.25, sediment entering to Chamran intake is more than same values in Azadegan intake and under sluice gates belong to Azadegan intake during all laboratory tests for this section.

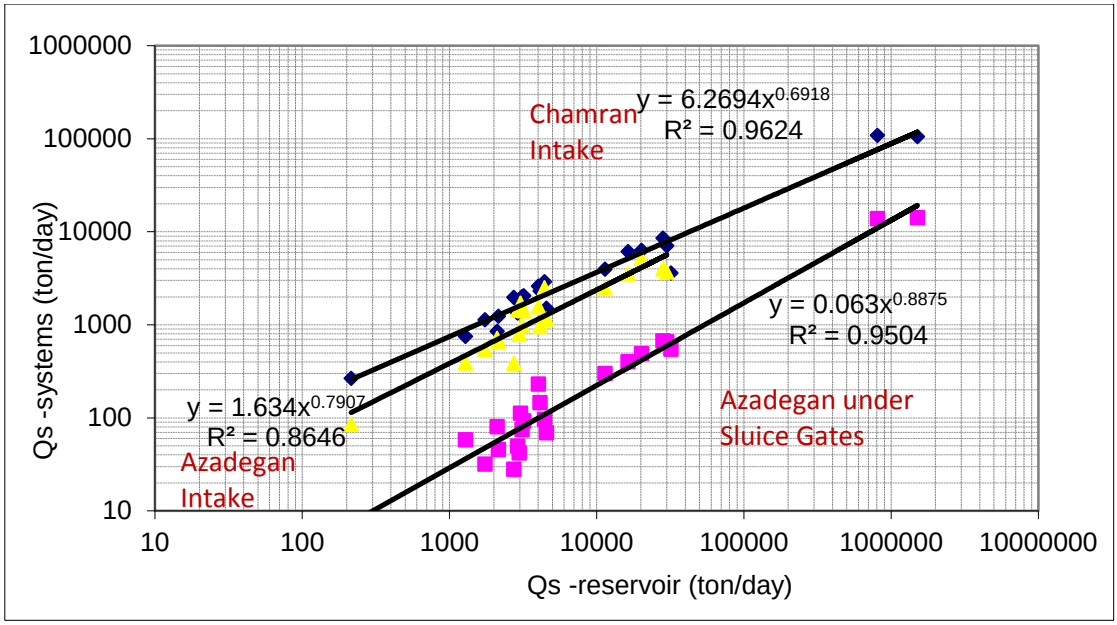

Figure 3.25 Changes sediment dischrage in reservoir and sediment discharge entry to different hydraulic structures

Table 3.6 shows the grain size distributions of the sediments sampled for different scenarios. Three water discharges (or hydraulic condition) were designed in these investigations. The first one is named regulated condition, indicating that a normal water discharge in the reservoir is diverted toward to both intakes and a minimum flow passing through the sluice gates. The second one is named high water condition, indicating a high water discharge to the reservoir, with only a part of it being diverted toward the two intakes and a larger part of flow passing through sluice gates. This situation occurs when the water demands for agriculture and other sectors are less than the existing discharge in the reservoir, or when the upstream dam has to release more water for flood control. The third one is named flood condition. In this situation, the Azadegan intake is closed but the Chamran intake has to open because of drinking water demand and the high capacity of sluice gates.

Table 3.6 Sediment grain size for different hydraulic and sediment transport scenarios

NO.	Locations	Sample Code	D_{10} mm	D_{50} mm	D_{90} mm	Discharge m^3/s	Hydraulic conditions
1	Azadegan intake	DAS3	0.011	0.09	0.36	75.73	Regulated
2		DAS14	0.005	0.081	0.34	41.77 - 42.61	Regulated
3		DAS2	0.0073	0.085	0.3	23.06	Regulated
4		DA13	0.005	0.12	0.6	54.3	High water
5		DA14	0.009	0.062	0.26	75.44	High water
6		DA15	0.009	0.075	0.18	46.4	High water
1	Chamran intake	DGS3	0.0015	0.05	0.18	79.59	Regulated
2		DGS14	0.0035	0.05	0.2	77.45 - 69.39	Regulated
3		DGS2	0.01	0.05	0.18	43.88	Regulated
4		DG13	-	0.046	0.26	67.07	High water
5		DG14	0.006	0.08	0.18	84.5	High water
6		DG15	0.014	0.15	0.4	84.5	High water
7		DG16	0.017	0.13	0.43	47.45	Flood
1	Under sluice gates belong to Azadegan intake	DTS3	0.01	0.046	0.2	3.1	Regulated
2		DTS14	0.0018	0.027	0.09	3.07	Regulated
3		DTS2	0.0013	0.04	0.12	2.87	Regulated
4		DT13	0.0016	0.039	0.17	8.25	High water
5		DT14	-	0.056	0.2	8.32	High water
6		DT15	0.0024	0.077	0.22	8.2	High water
7		DT16	0.0015	0.052	0.26	7.58	Flood

Note: The data have been converted are transferred to prototype

As can been seen from Table 3.6 that the sediment grain size distribution (D_{10}, D_{50} and D_{90}) in Azadegan does not have any significant changes at the regulated condition. For high water condition the sampling results for DA13 was considered wrong which is belong to the sampling error, but for the two other samples (DA14 and DA15) D_{90} reduces and D_{10} increases, with the mean sediment grain size (D_{50}) decreasing for around 10%. This reduction might be related to the flow carrying high concentration sediment passing through the sluice gates at the high water condition.

The sediment transport process near the Chamran intake is dependent more on the location of this hydraulic structure. As can been seen from the above table, the sediment grain size in Chamran is almost uniformly distribution at the regulated condition. When the momentum (or-input flow discharge) of the reservoir increases at the high water and flood test series, D_{50} and D_{90} also rise. This increase growth in the mean sediment grain size (D_{50}) is up to three times in comparison with the regulated condition and it shows that the possibility of large sediment gain sizes entry to this intake is very likely to occur.

The sluice gates associated with the Azadegan intake have a normal role in all conditions and the sediment grain sizes increase at the high water and flood conditions. This process is normally related to the hydrodynamic parameters.

The area located in front of the Azadegan intake and close to the right bank has been recommended as an artificial dredging zone. The aim is to make a stable diversion flow into the intake, thus to enable long term water supply operation. Physical model simulations have been undertaken to investigate the feasibility of this measure in improving the condition for supplying water (Figure 3.26).

A comparison between Figures 3.26 and 3.27 shows that sedimentation rate in the dredging zone is higher than the other areas. The hydrodynamic data also show that the Azadegan intake could pass more than 75 m^3/s (nominal carrying capacity). Due to the above reasons, it is recommended not making the dredging zone in front of Azadegan intake.

Figure 3.26 The dredging zone in front of Azadegan intake before running the sediment transport scenarios

Figure 3.27 The dredging zone in front of Azadegan intake after tests

The role of sluice gates also investigated. Many scenarios were tested to investigate the performance of the hydraulic structures in reducing the rate of sediment entering into the intakes. For brevity, two extreme scenarios' results are discussed here. Table 3.7 shows the parameters related to the scenarios.

Table 3.7 Hydraulic model parameters of sluice gates' testing scenarios

No	Hydraulic Parameters	Left sluice gates					Right sluice gates				
		One	Second	Third	Fourth	Fifth	One	Second	Third	Fourth	Fifth
1	Opening	25%	25%	25%	25%	-	-	30%	30%	-	30%
	Discharge	$124.3\ m^3/s$					$112.6\ m^3/s$				
	Condition	High water					High water				
2	Opening	40%	40%	40%	40%	-	-	40%	40%	40%	40
	Discharge	$228.2\ m^3/s$					$228.2\ m^3/s$				
	Condition	Flood					Flood				

Note: The data have been converted to prototype

When the sluice gates were open a scouring hole in front of those gates could be seen, but they were local and did not have any considerable effects on the sediment flashing and settling processes in front of the intakes (Figures 3.28 and 3.29).

Figure 3.28 Scour zone in front of the right sluice gates

Figure 3.29 Scouring zone in front of the left side sluice gates

The bed level change near the hydraulic structures is one of the most important subjects in our study. The following results show the morphological changes after the sediment transport tests. The sediment transport and morphodynamic tests were carried out in four stages. In the first stage, a scenario (S.1) was run for a very long time compared with other tests and was special condition for this physical study. For this scenario, sediments injection continued until the concentrations at the input and output opening boundaries became the same. Three other scenarios included the regulated, high water and flood condition, as explained before. The physical model results (for scenario S.1) were compared to the initial bathymetry at 6 sections that were shown in the Hamidieh reservoir in Figure 3.7 in section 3.5 (Figure 3.30). Profiles 1, 2 and 3 would be extended to cover the whole area in the vicinity of Chamran intake. Table 3.8 lists the main hydraulic and sediment parameters for morphodynamic scenario S.1.

Table 3.8 Main hydraulic and sediment parameters for morphodynamic scenario

No		Operation	Boundary Condition	Concentration (gr/liter)	Time for simulation (hour)
S.1	Reservoir	Water level 20.45 m	Discharge 126.8m^3/s	0.2321	48.5
	Az Intake	Opened	Discharge 75m^3/s	-	
	Ch Intake	Opened	Water level 20.45 m	-	
	L S	Closed	-	-	
	R S	Closed	-	-	

*Az Intake= Azadegan Intake, Ch Intake= Chamran Intake, L S= Left sluice gate and R S = Right sluice gate
**The whole data are transferred to prototype

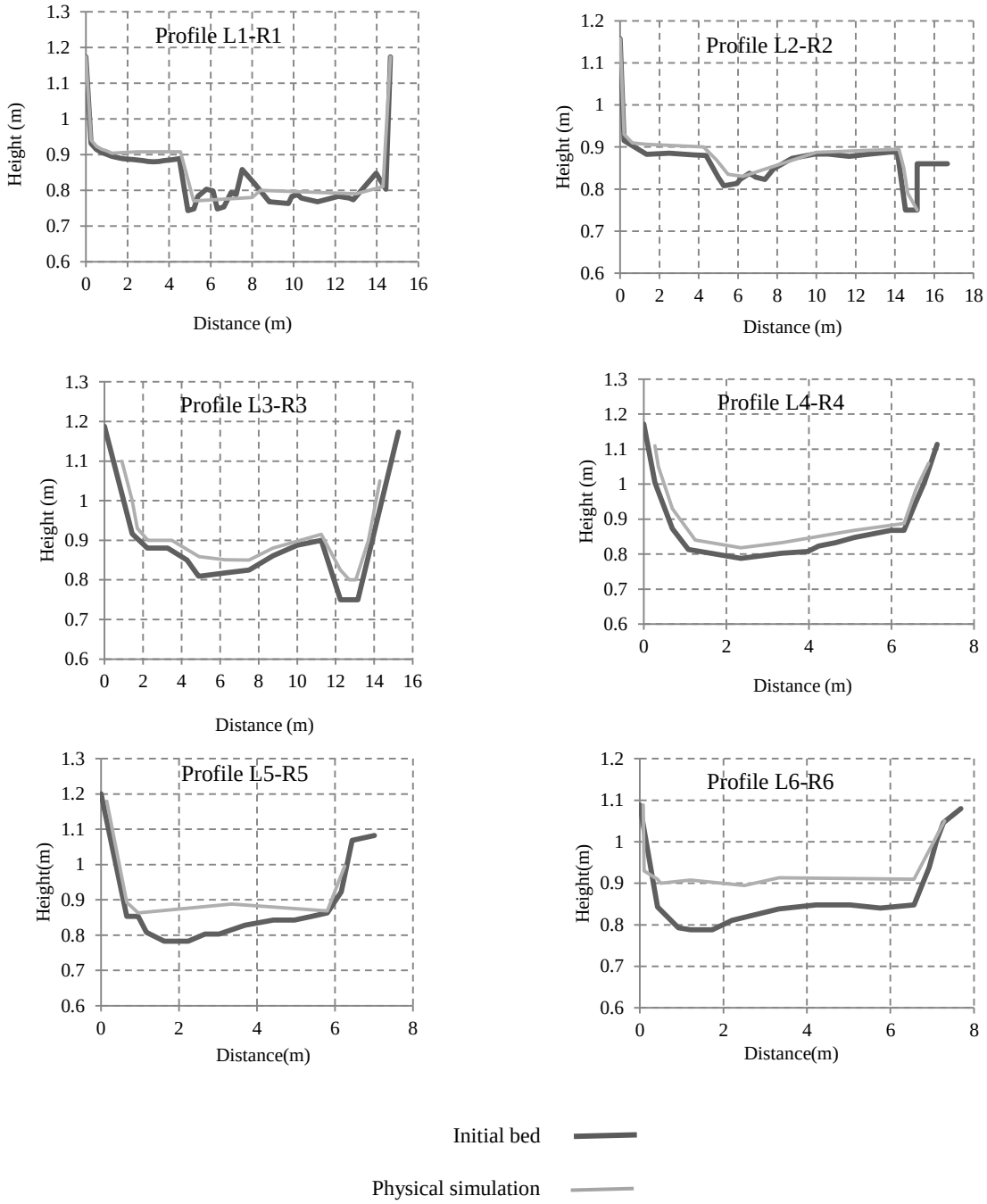

Figure 3.30 Bed level changes after 48.5 hours in 6 section profiles (scenario S.1)

The pictures shown in Figure 3.31 reveal that the morphological changes after running sediment transport scenarios. The physical model results indicate that there is a possibility of sedimentary islands being formed in the upstream of the intakes, since the regulated hydraulic regime resulted in a high value of sediment concentration.

Figure 3.31 Morphological changes in Hamidieh regulated reservoir (physical model) after sediment transport experiments

3.7.3 Considering scale effects for Hamidieh physical model

Scale effects arise due to force ratios which are not identical between a model and its real-world prototype and result in deviations between the up-scaled model and prototype observations. A comprehensive review was carried out on scale effects on physical hydraulic engineering models by Heller (2011). In that review article considers mechanical, Froude and Reynolds model–prototype similarities, describes scale effects for typical hydraulic flow

phenomena and discusses how scale effects are avoided, compensated or corrected. There are some limiting conditions in the hydraulic model scale, which were also paid attention in our physical model.

In hydraulic research the main criteria of similarity are the Froude and Reynolds laws. In hydraulics the Mach or Weber laws are rarely decisive criteria. Problems with the decisive effect of compressibility only occur at velocities greater than sound and are therefore applicable, e.g., in water hammer problems and, above all, in aerodynamics. The forces caused by surface tension are very important in hydraulic models, but in the solution of practical engineering problems they are avoided by not reducing the model below a certain dimension so that they are almost as insignificant on the model as in the majority of cases in prototype. Separate research studies have shown that if the influence of surface tension and capillarity is to be negligible, the following minimum limiting values must be observed on a model operated according to the Froude law (Novak and Cabelka 1981):

- The velocity at the water surface on the model $v \geq 230\ mm/s$ in order that gravity waves might occur (this is important especially for experiments with the resistance of piers and head losses for flow round various bodies), (Zegzhda 1938).
- The depth of flow on the model $h \geq 15\ mm$ to eliminate the effect of capillary and surface tension. This condition can lead to distorted models.

3.8 Conclusion

A series of physical model experiments have been undertaken to study the hydrodynamic, sediment and morphological processes in the Hamidieh regulated reservoir. Laboratory tests were designed based on three hydraulic conditions namely regulated, high water and flood flows and sediment transport processes were investigated (see section 3.7.2). The physical model results could, to a certain extent, reveal the governing processes in the system. It is necessary to remember that the limitations and simplifications of the experiments may affect the results. The capacity and operation time of the pumps, measurement tools, cost of sediment material and construction and maintenance of reservoir bathymetry for running new scenarios were all important aspects in this physical model study. The results obtained from the hydraulic model experiments confirm the following technical features:

- The Chamran water intake could reach its nominal carrying capacity of 90 m^3/s provided that the water elevation is increased from 20.20m (proposed normal water level for regulatory condition) to 20.45m in the reservoir.

- An increase of 30% in discharge in compensation releases downstream of the Hamidieh reservoir (for keeping environment) is necessary; as this can effectively improve the performance of the under sluice gates associated with the Azadegan intake. It could also provide a constant release of water from the left side sluice gates (near Chamran), which is to be applied in normal regulatory conditions.
- Decreasing the number of opening bays of the Chamran intake as well as redesigning a single contraction (Figure 3.32), rather than a double one (Figure 3.19), can reduce energy losses in the Chamran intake system.

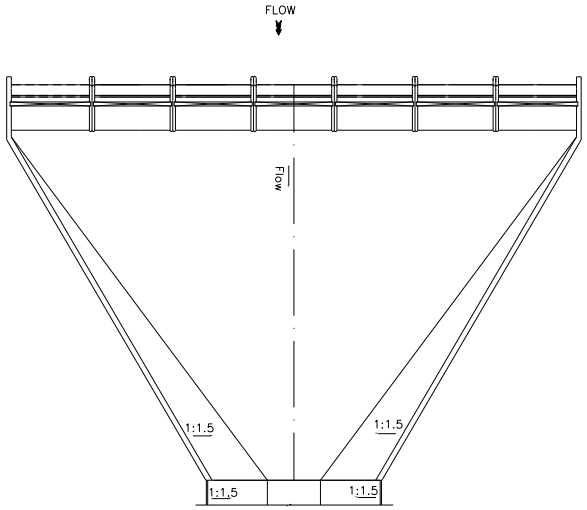

Figure 3.32 The Proposed layout for Chamran Intake

- The Azadegan water intake could operate at the nominal discharge of 75 m^3/s (or even a little more than that) due to its appropriate location and geometric shape. Therefore, it is a reliable flow intake. It is also advisable to keep the present geometric of Azadegan plan as it may be necessary existing capacity discharge of the intake due to the problems raised by the shortage carrying capacity discharge of Chamran intake.
- The recommended artificial dredging zone, located in the front of Azadegan intake, was not affect the hydraulic behavior significantly and there was a high risk of significant sedimentation.
- The location of Chamran intake may result in the formation of the sedimentation zone in the areas adjacent to the intake and sediment entering to the irrigation channel (trapezoidal channel).
- The sluice gates' operation scheme had not any considerable impact on the sediment flashing capability in the areas close to the intakes.

- The movements of sediment in the reservoir were also observed at different scenarios (regulated, high water and flood conditions). It means that the morphodynamic process depends on sediment transport phenomena and hydrodynamic attitudes such as flow pattern, speed and hydraulic operations.
- The dominant sediment transport process in the Hamidieh regulated reservoir was the suspended sediment transport. The major reason for this process was related to existing sediment grain size diameter in the water body.
- In the regulatory conditions the size of sediment entry moves to the Azadegan intake was larger than Chamran intake.

From the analysis the results and methodology find following scientific features:

- The great flexibility of the undistorted physical model allowed easily designing different scenarios without significant scale effects.
- Sediment material using in this physical model was obtained from broken pottery (baked clay). This material is non-cohesive and has a similar specific gravity as that of the prototype and for this reason the performance of sediment scenarios forms well. This material could be proposed for similar studies better than lightweight material especially when the type of model is undistorted and the scale is large.
- In the physical tests when high sediment concentrations were simulated by injecting dry sediments method (existing sediment injection system, see Figure 3.15) observed some problems in managing scenarios. This problem was related to low water depth in the physical model (maximum water depth is around 21cm) and the injection method. In other word, when the rate of injected sediment was increased part of those sediments could not mix well in the water column and settle down near the sediment injection system. It would be suggested making wet injection system for simulating high sediments concentrations. Also, the system has to be installing enough far from the investigation area for getting best results.
- The physical model study reported herein presented that designing same scale for investigation of hydrodynamic, sediment transport and morphodynamic processes in a complicated water body system such as regulated dam raise accuracy of measurements. By this method synchronization of these processes in the physical model keep such as prototype. Besides the potential of using the physical model results in order to simulate, validate and calibrate by the numerical model rises significantly.

3.9 Summary

In this chapter efforts were made to describe physical model theory and an experimental study of a regulated reservoir. Selecting an appropriate scale is very important for a physical model study. Model scale effects, the availability of material for constructing the physical model and a good understanding of the physical processes are the key issues in any physical model study. The result of this part of the research shows that an undistorted model is preferred in the Hamidieh regulated reservoir study. This scheme prevents the significant scale effects on hydrodynamic parameters, such as flow velocity, water depth and sediment size and thus enhances the accuracy of the results. A comprehensive experimental study was carried out to investigate hydrodynamic, sediment transport and morphological changes in Hamidieh regulated reservoir. The results of the experimental study revealed many options for better operation of the regulated reservoir and associated hydraulic structures, such as intakes and sluice gates.

Chapter Four

Numerical Modelling (Governing Equations and Solutions)

4.1 Introduction

With the rapid increase in computer power in recent years, it is not surprising to note that three-dimensional (3-D) numerical modelling of flow and sediment behavior near the hydraulic structures has shifted from academic research to practical applications in order to reduce the cost and time of design of hydraulic structures.

This chapter presents briefly the governing hydrodynamic, sediment transport and bed level changes equations and solution methods. The emphasis of the study is on simulating the three-dimensional hydrodynamic processes because of the complexity of the flow behavior near the hydraulic structures. The main features of the turbulence model used in the current study are discussed.

The numerical model contains three modules representing the hydrodynamic, sediment transport and morphodynamic processes, in which the morphodynamic module is added the first time to this numerical model by the author. Details are given herein of the development and discretization of a three-dimensional layer integrated numerical model to predict morphological changes in the vicinity of hydraulic structures. The effort is on presenting and describing the computational scheme for solving the bed level change equation (in the morphodynamic module) and coupling to other modules (hydrodynamic and sediment transport).

4.2 Governing hydrodynamic equations

The governing equations used to describe flows in reservoirs are generally based on 3-D Reynolds averaged Navier Stokes equations for incompressible and unsteady turbulent flows. If the vertical acceleration of the flow is negligible in comparison with the gravity and the vertical pressure gradient terms, then the hydrostatic pressure distribution assumption can be made. Since the reservoir to be studied in the current study has a relatively shallow water, the density of the water has also been assumed constant throughout the computational domain. In

applying these approximations, the three-dimensional governing equations of mass and momentum can be written respectively in their conservative forms as follows:

$$\frac{\partial u}{\partial x}+\frac{\partial v}{\partial y}+\frac{\partial w}{\partial z}=0 \tag{4-1}$$

$$\frac{\partial u}{\partial t}+\frac{\partial uu}{\partial x}+\frac{\partial uv}{\partial y}+\frac{\partial uw}{\partial z}=fv-\frac{1}{\rho}\frac{\partial p}{\partial x}+\frac{1}{\rho}\left[\frac{\partial \sigma_{xx}}{\partial x}+\frac{\partial \tau_{xy}}{\partial y}+\frac{\partial \tau_{xz}}{\partial z}\right] \tag{4-2}$$

$$\frac{\partial v}{\partial t}+\frac{\partial vu}{\partial x}+\frac{\partial vv}{\partial y}+\frac{\partial vw}{\partial z}=fu-\frac{1}{\rho}\frac{\partial p}{\partial y}+\frac{1}{\rho}\left[\frac{\partial \tau_{yx}}{\partial x}+\frac{\partial \sigma_{yy}}{\partial y}+\frac{\partial \tau_{xz}}{\partial z}\right] \tag{4-3}$$

$$\frac{\partial p}{\partial z}+\rho g=0 \tag{4-4}$$

where t = time, x, y, z = Cartesian co-ordinates, u, v, w = components of velocity in the x, y, z direction, respectively, p = pressure, ρ = density of water, f = Coriolis parameter, g = gravitational acceleration and $\sigma_{yy}, \tau_{xy}, \tau_{xz}, \tau_{yx}, \sigma_{yy}, \tau_{yz}$ are components of the stress tensor in the $x-z$ and $y-z$ plane, respectively.

4.2.1 Layer integrated hydrodynamic equations

The layer integrated numerical model used in this study was based on a model originally developed by Lin and Falconer (1997). The governing equations (Equations 4-1 to 4-4) were solved using the finite difference scheme on a regular square mesh in the horizontal plane, and a layer-integrated finite difference scheme on an irregular mesh in the vertical plane.

A sketch of the 3D grid and relative positions of the governing variables in the $x-z$ plane are illustrated in Figure 4.1. As illustrated, three layer types exist, including top layer, bottom layer and middle layer. The top and bottom layer thicknesses vary with the *x, y* co-ordinates to prescribe both the free surface and bottom topography, respectively. In contrast, the middle layers have a uniform (or non-uniform) thickness.

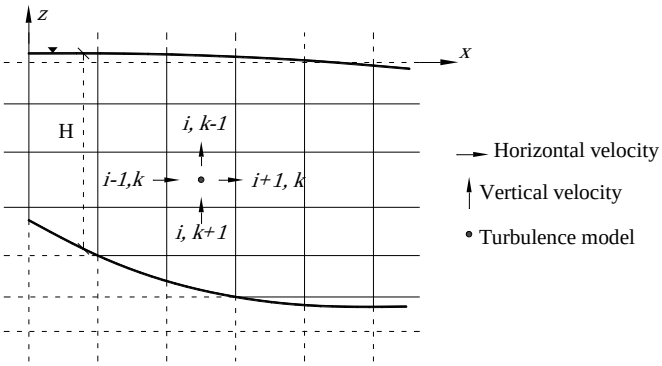

Figure 4.1 Coordinate system for layer integrated equations

The governing equations for mass and momentum are first integrated over the kth layer, k =1, 2, 3, …, K. Letting:

$$\langle o\rangle_k = \int_{k+1/2}^{k-1/2}(o)\,dz \tag{4-5}$$

where o= mass or momentum equations, $k \pm \frac{1}{2}$ refers to the vertical (or z) elevations of the layer interfaces between the k+1, k and k-1 layers, respectively, the continuity equation integrated over layer k becomes:

$$\int_{k+1/2}^{k-1/2}\left(\frac{\partial u}{\partial x}+\frac{\partial v}{\partial y}+\frac{\partial w}{\partial z}\right)dz = 0 \tag{4-6}$$

Giving:

$$w_{k-1/2} - w_{k+1/2} + \int_{k+1/2}^{k-1/2}\left(\frac{\partial u}{\partial x}+\frac{\partial v}{\partial y}\right)dz = 0 \tag{4-7}$$

Using Leibnitz rule (Hall 1987), interchanging the differential operators $\partial/\partial x$ and $\partial/\partial y$ with the integral, and accounting for limits of integration, gives the vertical velocity component *w* at the interface $k-1/2$, as:

$$w_{k-1/2} = -\sum_{k=k}^{K}\left\{\frac{\partial(hu)}{\partial x}+\frac{\partial(hv)}{\partial y}\right\} \tag{4-8}$$

Equation 4-8 is the equation of continuity in differential form for layer *k*. At the water surface (ζ denotes the water surface elevation relative to datum), the continuity equation reduces to:

$$\frac{\partial\zeta}{\partial t}+\sum_{k=k}^{K}\left\{\frac{\partial(hu)}{\partial x}+\frac{\partial(hv)}{\partial y}\right\} \tag{4-9}$$

Similarity, vertical integration of the momentum equations (4-2 and 4-3) for the kth layer gives:

$$\frac{\partial\langle u\rangle}{\partial t}+\frac{\partial\langle uu\rangle}{\partial x}+\frac{\partial\langle uv\rangle}{\partial y}+(uw)_{k-1/2}-(uw)_{k+1/2} = f\langle v\rangle-\frac{1}{\rho}\left\langle\frac{\partial p}{\partial x}\right\rangle+\frac{1}{\rho}\left[\frac{\partial\langle\sigma_{xx}\rangle}{\partial x}+\frac{\partial\langle\tau_{xy}\rangle}{\partial y}\right]+\frac{1}{\rho}\left(\tau_{xz}|_{k-1/2}-\tau_{xz}|_{k+1/2}\right) \tag{4-10}$$

$$\frac{\partial\langle v\rangle}{\partial t}+\frac{\partial\langle uv\rangle}{\partial x}+\frac{\partial\langle vv\rangle}{\partial y}+(vw)_{k-1/2}-(vw)_{k+1/2} = f\langle u\rangle-\frac{1}{\rho}\left\langle\frac{\partial p}{\partial y}\right\rangle+\frac{1}{\rho}\left[\frac{\partial\langle\tau_{yx}\rangle}{\partial x}+\frac{\partial\langle\sigma_{yy}\rangle}{\partial y}\right]+\frac{1}{\rho}\left(\tau_{yz}\big|_{k-1/2}-\tau_{yz}\big|_{k+1/2}\right) \tag{4-11}$$

where $\langle u\rangle, \langle v\rangle$ are layer-integrated velocities in the x, y directions, respectively. Defining the layer-integrated velocity in the x-direction as:

$$\bar{u} = \frac{1}{\Delta Z}\int_{k+1/2}^{k-1/2}u(x,y,z)dz \tag{4-12}$$

where ΔZ=the layer thickness, and similarly for the y-direction, assuming the Boussinesq approximation to give:

$$\sigma_{xx} = \rho\varepsilon_h\left[\frac{\partial\bar{u}}{\partial x}+\frac{\partial\bar{u}}{\partial x}\right],\ \tau_{xy} = \rho\varepsilon_h\left[\frac{\partial\bar{u}}{\partial y}+\frac{\partial\bar{v}}{\partial x}\right],\ \tau_{xz} = \rho\varepsilon_v\left[\frac{\partial\bar{u}}{\partial z}+\frac{\partial\bar{w}}{\partial x}\right] \text{ etc.} \tag{4-13}$$

where ε_h , ε_v= horizontal and vertical eddy viscosities, respectively, assuming a hydrostatic pressure distribution given as:

$$\frac{\partial p}{\partial x} \cong g\rho \frac{\partial \zeta}{\partial x} \, , \frac{\partial p}{\partial y} \cong g\rho \frac{\partial \zeta}{\partial y} \tag{4-14}$$

and defining:

$$\langle u \rangle = q_x = \bar{u}\Delta Z, \langle v \rangle = q_y = \bar{v}\Delta Z \tag{4-15}$$

Then Equations 4-10 and 4-11 can be rewritten as:

$$\left.\frac{\partial q_x}{\partial t}\right|_k + \left[\frac{\partial \bar{u} q_x}{\partial x} + \frac{\partial \bar{v} q_x}{\partial y}\right]_k = f q_y|_k - g\Delta Z \left.\frac{\partial \zeta}{\partial x}\right|_k + \left\{\frac{\partial}{\partial x}\varepsilon_h \Delta Z \left[\frac{\partial \bar{u}}{\partial x} + \frac{\partial \bar{u}}{\partial x}\right] + \frac{\partial}{\partial y}\varepsilon_h \Delta Z \left[\frac{\partial \bar{u}}{\partial y} + \frac{\partial \bar{v}}{\partial x}\right]\right\}_k +$$

$$(w\bar{u})_{k+1/2} - (w\bar{u})_{k-1/2} + \frac{(\tau_{xz}|_{k-1/2} - \tau_{xz}|_{k+1/2})}{\rho} \tag{4-16}$$

$$\left.\frac{\partial q_y}{\partial t}\right|_k + \left[\frac{\partial \bar{u} q_y}{\partial x} + \frac{\partial \bar{v} q_y}{\partial y}\right]_k = f q_x|_k - g\Delta Z \left.\frac{\partial \zeta}{\partial y}\right|_k + \left\{\frac{\partial}{\partial x}\varepsilon_h \Delta Z \left[\frac{\partial \bar{v}}{\partial x} + \frac{\partial \bar{u}}{\partial y}\right] + \frac{\partial}{\partial y}\varepsilon_h \Delta Z \left[\frac{\partial \bar{v}}{\partial y} + \frac{\partial \bar{v}}{\partial y}\right]\right\}_k +$$

$$(w\bar{v})_{k+1/2} - (w\bar{v})_{k-1/2} + \frac{\left(\tau_{yz}|_{k-1/2} - \tau_{yz}|_{k+1/2}\right)}{\rho} \tag{4-17}$$

At the free surface (where k=1), the terms $(w\bar{u})_{k-1/2}$ and $(w\bar{v})_{k-1/2}$ can be eliminated using the kinematic free surface condition and Leibnitz rule. At the bed, the terms $(w\bar{u})_{k+1/2}$ and $(w\bar{v})_{k+1/2}$ become zero due to the no-slip boundary condition.

In applying these equations to large estuaries and reservoirs, the ratio of the vertical length scale to the horizontal length scale is very small. The vertical eddy viscosity terms are generally several orders of magnitude larger than the corresponding horizontal terms. Therefore, it is important to prescribe the vertical eddy viscosity more accurately than for the horizontal viscosity. In the original version of 3D layer-integrated model (TRIVAST), the horizontal eddy viscosity ε_h was assumed to be constant in the vertical, and its value was assumed to be equal to the depth-averaged eddy viscosity. The vertical eddy viscosity ε_v was represented using a two-layer mixing length model (Rodi 1984) written in the following form:

$$\varepsilon_v = l^2 \left[\left(\frac{\partial u}{\partial z}\right)^2 + \left(\frac{\partial v}{\partial z}\right)^2\right]^{1/2} \tag{4-18}$$

where l is mixing length, defined as:

$$\begin{cases} l = \kappa z & for \quad \kappa z \le 0.1H \\ l = 0.1H & for \quad \kappa z > 0.1H \end{cases} \tag{4-19}$$

and κ is von Karman's constant (0.41).

An enhanced version of 3D layer-integrated model is used in the current study; in which the vertical eddy viscosity is calculated using the $k-\varepsilon$ turbulence model. More details of the turbulence model will be discussed in section 4.3.

4.2.2 Depth integrated hydrodynamic equations

Numerical modelling of fluid flow is based on the principles of continuity of mass and conservation of momentum within the body of fluid to be modeled. In many cases, the flow is defined by the Reynolds equations, which describe the three-dimensional turbulent motion of the incompressible fluid. For flows which show little variation in the vertical direction, it is appropriate to integrate these equations over the depth of water, resulting in simplified or 'two-dimensional' equations of motion. When integrated over the depth, the equations governing fluid motion are as follows (Falconer and Lin 2001):

Conservation of mass:

$$\frac{\partial \eta}{\partial t} + \frac{\partial p}{\partial x} + \frac{\partial q}{\partial y} = q_m \tag{4-20}$$

Conservation of momentum:

$$\frac{\partial p}{\partial t} + \frac{\partial \beta p U}{\partial x} + \frac{\partial \beta p V}{\partial y} = fq - gH\frac{\partial \eta}{\partial x} + \frac{\rho_a}{\rho} C_w W_x \sqrt{W_x^{\,2} + W_y^{\,2}} - \frac{gp\sqrt{p^2+q^2}}{H^2 C^2}$$

$$+ \varepsilon\left[2\frac{\partial^2 p}{\partial x^2} + \frac{\partial^2 p}{\partial y^2} + \frac{\partial^2 q}{\partial x \partial y}\right] - C_d mD\frac{p\sqrt{p^2+q^2}}{H} \tag{4-21}$$

$$\frac{\partial q}{\partial t} + \frac{\partial \beta q U}{\partial x} + \frac{\partial \beta q V}{\partial y} = fp - gH\frac{\partial \eta}{\partial y} + \frac{\rho_a}{\rho} C_w W_y \sqrt{W_x^{\,2} + W_y^{\,2}} - \frac{gq\sqrt{p^2+q^2}}{H^2 C^2}$$

$$+ \varepsilon\left[2\frac{\partial^2 q}{\partial x^2} + \frac{\partial^2 q}{\partial y^2} + \frac{\partial^2 p}{\partial x \partial y}\right] - C_d mD\frac{q\sqrt{p^2+q^2}}{H} \tag{4-22}$$

where:

- p (=UH), q (=VH) discharges per unit width in the x and y directions respectively (m^3/s/m);
- q_m source discharge per unit horizontal area ($m^3/s/m^2$);
- U,V depth averaged velocity components in the x and y directions respectively (m/s);
- β momentum correction factor for a non-uniform vertical velocity profile;
- g gravitational acceleration (=9.806 m/s^2);
- H total water depth = $\eta + h$;
- η water surface elevation above datum;
- h water depth below datum;
- ρ_a density of air ($\cong$ 1.292 kg/m^3);
- ρ density of fluid (kg/m^3);

- C Chezy roughness coefficient ($m^{1/2}/s$);
- W_x, W_y wind velocity components in x , y directions
- C_w air/fluid resistance coefficient (assumed to be 2.6x 10^{-3} for W_s >15 m/s , W_s= wind speed (=$\sqrt{W_x^2 + W_y^2}$));
- ε depth averaged turbulent eddy viscosity (m^2/s);
- C_d vegetation drag coefficient;
- m vegetation density;
- D vegetation diameter;
- x, y co-ordinates (m)

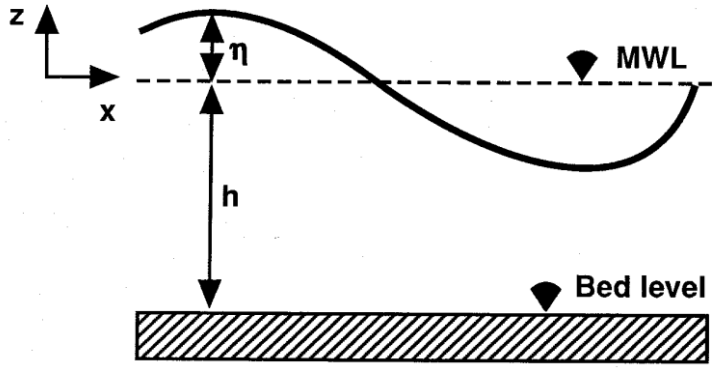

Figure 4.2 Coordinate system for wave profile

DIVAST (Depth Integrated Velocities and Solute Transport) is a two-dimensional model, in which the vertical component is neglected. Such models are valid when the flow is predominantly horizontal with good vertical mixing or if the vertical variations are insignificant. This is mostly the case in shallow, tidal bays and estuaries with moderate freshwater inflow, but not in fjords and lakes at medium latitude. Whether the effects of stratification may be neglected does not only depend on the physical properties of the water body of interest, but also on the scale of the modelling. This model was originally developed by Falconer (1985). Full details of different terms of equations (4-20), (4-21) and (4-22) are given in the reference manual of DIVAST Model (Falconer 2001) and are not included here for brevity.

4.2.3 Boundary conditions for the hydrodynamic model

Two key layers in the layer integrated hydrodynamic model were the surface and bottom layers. At the water surface, the shear stress is equated directly to the wind stress, given as:

$$\tau_{xz}|_{\zeta} = \rho_a C_w W_s W_x \quad (4\text{-}23)$$

$$\tau_{yz}\big|_{\zeta} = \rho_a C_w W_s W_y \quad (4\text{-}24)$$

where C_w= resistance coefficient; ρ_a is air density; W_s = wind speed; and W_x, W_y= wind velocity components in the x, y directions, respectively.

At the bed:

$$\varepsilon_v \frac{\partial u}{\partial z} = \frac{\tau_b}{\rho} = (u_*)^2 \quad (4\text{-}25)$$

where τ_b= bed shear stress; and u_*= bed shear velocity. Assuming a logarithmic velocity profile within the bottom layer (see French, 1986), the following equation can be obtained for the bed shear stress:

$$\frac{\tau_b}{\rho} = \left|\frac{\bar{u}^{n+1/2}+\bar{u}^{n-1/2}}{2}\right| \frac{\bar{u}^{n+1/2}+\bar{u}^{n-1/2}}{2} \left[2.5ln\left(\frac{30d}{2.72k_s}\right)\right]^{-2} \quad (4\text{-}26)$$

where d= thickness of the bottom layer; and k_s= bed roughness length.

The bed stress obtained for the layer-integrated equations is also used in calculating the depth integrated equations [see Lin and Falconer 1997]. In shallow regions where only one layer is wet, the bed resistance stress is represented in the form of Darcy's equation, with the friction factor being evaluated using the Colebrook-White equation (Falconer 1993).

4.2.4 Gates simulation

In this section details are given of the numerical technique added to the existing numerical model (to the hydrodynamic model) for simulating flow through gates by the author. This technique enhance existing numerical model in order to apply it for simulating flow through hydraulic structures. Obstacles in the flow may generate sudden transitions from flow contraction to expansion. The grid resolution is often low compared to the gradients of the water level, the velocity and the bathymetry. The hydrostatic pressure assumption may locally be invalid. Examples of these obstacles in civil engineering projects are: gates, barriers, sluices, groins, weirs, bridge piers and porous plates. The obstacles generate energy losses and may change the direction of the flow. Different methods suggested for simulation the role of hydraulic structures in numerical models. This section has only explained a technique for numerical simulation of gates. These steps are considered to represent the technique in the numerical model:

- Determining the location of gates.
- Determining the head-discharge equation (non-linear) for vertical sluice gates with regard to hydraulic conditions such as free surface, submerged and overtopping.

- Approximation in order to make a linear equation for the head-discharge equation
- Discretizing the resulting linear equation.
- Replacing resulted linear equation instead of momentum equation in the solution procedure for the selected cells (gate locations).

4.2.4.1 Validation of the numerical technique

In the following, a simple example (see Figures 4.3) is simulated by the refined model according to the procedure described above. In this example, three vertical sluice gates with 10m (width) and 5m (height) are located in the middle of rectangular channel. The hydraulic condition is considered submerged for this simulation (Figure 4.4). The all dimensions and hydraulic attitudes are given in Table 4.1.

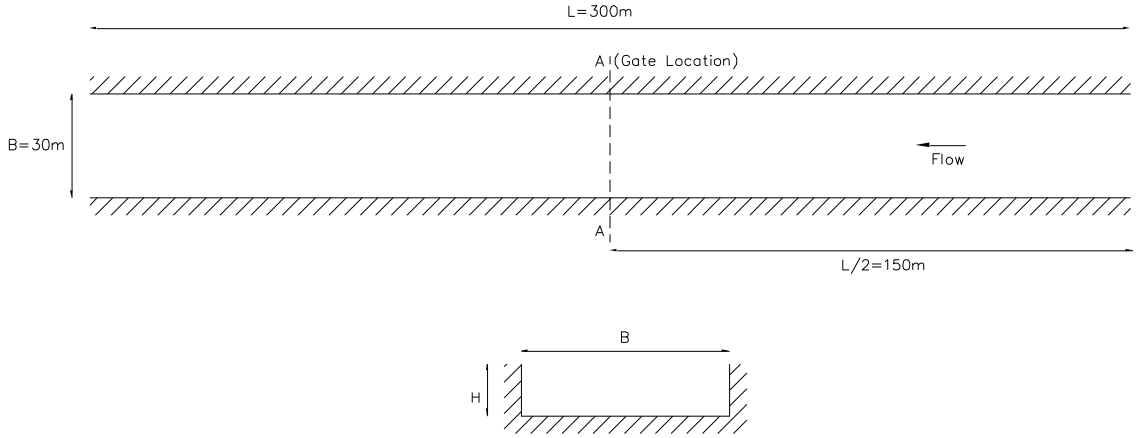

Figure 4.3 Plan and section views of channel

Table 4.1 The characteristics of validation scenario for gates simulation

Upstream Boundary condition	Down stream Boundary condition	L (m)	B (m)	H (m)	Gate location	Gate operation	Remark
Water level (4 m)	Water level (3 m)	300	30	5	Middle of Channel (A-A)	3 gates with 40% opening (1.6m)	Validation Scenario Width of gate= 10 m Gates condition= Submerged Cartesian mesh with Dx=Dy=10 m

L= Length of the channel, **B**= Width of the channel and **H**= Height of the channel

The above example was simulated by the improved numerical model (DIVAST) and the following results have been obtained from the numerical model and subsequently these results were compared with an analytic solution derived by Bos (1989).

For a submerged gate the following formula can be used to estimate the flow rate passing through the gate:

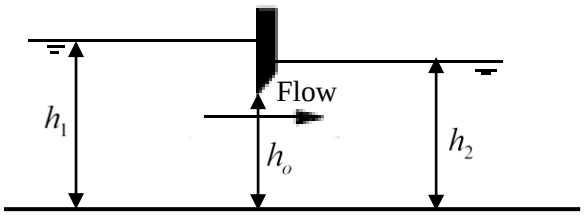

Figure 4.4 Submerged gate flow

$$Q = C_e C_v b h_o \sqrt{2g}\,(h_1 - h_2)^{0.5} \qquad (4\text{-}27)$$

provided that :

$h_o \geq 0.001$;

$h_1 \geq 1.5 h_o$; and

$$h_2 / h_0 > \frac{\alpha}{2}\left\{\sqrt{\left(1+16\left[\frac{h_1}{\alpha h_o}-1\right]\right)}-1\right\}$$

where:

$$C_e = 0.61\left[1+0.15(b+2h_o)/(2b+2h_o)\right] \qquad (4\text{-}28)$$

$\alpha =$ Contraction coefficient (see Bos 1989, Table 8.3)

$C_v =$ Coefficient of approach velocity (see Bos 1989, Fig. 1.12.)

$b =$ Breadth of each vertical sluice gate at control section (m)

In the improved numerical model the above formula was used for simulating the role of sluice gates with regard to the procedure described previously.

4.2.4.2 Results in the validated example

The following data explain the results calculated by the improved numerical model. Table 4.2 presents results obtained from the numerical model. Table 4.3 describes the analytic solution based on formula (4-27).

Table 4.2 Results of the improved numerical model

Location	**Speed (m/s)**	**Depth (m)**	**Q/B (m^3/s/m)**
Gate 1	0.45	3.52	1.584
Gate 2	0.45	3.52	1.584
Gate 3	0.45	3.52	1.584
Total discharge per width unit (q)			**4.752**
Reference	Numerical model	Numerical model	Numerical model

Table 4.3 Results of the analytic solution

Location	**Depth in the cell before the gate (h_1)** (m)	**Depth in the cell after the gate (h_2)** (m)	h_o (m)	C_e	C_v	Q/B $m^3/s/m$
Cells before and after Gate 1	3.745	3.470	1.6	0.66	1.011	1.532
Cells before and after Gate 2	3.745	3.470	1.6	0.66	1.011	1.532
Cells before and after Gate 3	3.745	3.470	1.6	0.66	1.011	1.532
Total discharge per width unit (q)						**4.597**
Reference	Numerical model	Numerical model	-	Equations (4-27) and (4-28)		

As observed in the above tables, the improved numerical model could predict the amount of total discharge per width unit in an acceptable manner with regard to analytic solution based on Bos formula. It means that we can determine flow discharge passing through the gates based on head-discharge equation (4-27) in the numerical solution.

4.3 Turbulence model

River flows are always turbulent and turbulent fluctuations contribute significantly to the transport of momentum, heat and mass. Even in the simplest variant of flow in a straight, smooth channel the turbulence generated near the bed is highly complex, featuring a variety of three dimensional coherent structures (Nezu and Nakagawa 1993). The turbulence is complicated even further by geometrical variations such as those due to bed forms, roughness elements and vegetation, changes in river cross- section, bends causing secondary motions, confluences associated with strong shear layers and all kinds of man-made structures such as dikes, bridge piers, groins and etc. (Rodi 2010). Strong turbulent flows are generated in the regulated reservoir due to the high volumes of flow diversion. The turbulence may introduce complex flow patterns, which can be difficult to predict.

As mentioned in Section 4.2.1, in large estuaries and reservoirs, the vertical eddy viscosity terms are generally several orders of magnitude larger than the corresponding horizontal terms. Therefore, it is important to prescribe the vertical eddy viscosity more accurately than for the horizontal viscosity (Lin and Falconer 1997).

Hakimzadeh and Falconer (2007) refined 3D layer-integrated model and applied model to scaled hydraulic model rectangular tidal basins with using two- and zero-equation turbulence models. For the zero-equation turbulence model the mixing length model was deployed to

calculate the horizontal eddy viscosity coefficient, whereas for the two equation model, the depth integrated $k-\varepsilon$ turbulence model was used. Likewise, the layer integrated $k-\varepsilon$ turbulence model was used to determine the vertical eddy viscosity coefficient.

In current study, the horizontal eddy viscosity was calculated by zero- equation (mixing length) and the vertical eddy viscosity was evaluated using the layer integrated form of the $k-\varepsilon$ equations based on Hakimzadeh and Falconer (2007).

In this section, the main features of the turbulence models which are used in the current numerical model are discussed. The main efforts are focused on the $k-\varepsilon$ turbulence model, with the mixing length model being explained briefly.

4.3.1 Mixing length model

Based on dimensional analysis one can assume that the kinematic viscosity ν_t, which has dimensions m^2/s, can be expressed as a product of a turbulent velocity $\vartheta(m/s)$ and a turbulent length scale $\ell\ (m)$. If one velocity scale and one length scale suffice to describe the effects of turbulence, dimensional analysis yields (Versteeg and Malalasekera 2007):

$$\nu_t = C\vartheta\ell \tag{4-29}$$

where C is a dimensionless constant of proportionality. The dynamic turbulent viscosity is given by

$$\mu_t = C\rho\vartheta\ell \tag{4-30}$$

Most of the kinetic energy of turbulence is contained in the largest eddies, and turbulence length scale ℓ is therefore characteristic of these eddies which interact with the mean flow. If we accept that there is a strong connection between the mean flow and the behavior of the largest eddies we can attempt to link the characteristic velocity scale of eddies with the mean flow properties. This has been found to work well in simple two-dimensional turbulent flows where the only significant Reynolds stress is $\tau_{xy} = \tau_{yx} = -\rho\overline{u'v'}$ and the only significant mean velocity gradient is $\frac{\partial U}{\partial y}$. For such flows it is at least dimensionally correct to state that, if the eddy length scale is ℓ,

$$\vartheta = c\ell\left|\frac{\partial U}{\partial y}\right| \tag{4-31}$$

where c is a dimensionless constant. The absolute value is taken to ensure that the velocity scale is always a positive quantity irrespective of the sign of the velocity gradient.

Combing 4-29 and 4-31 and absorbing the two constants C and c into a new length scale ℓ_m we obtain

$$\nu_t = \ell_m^2 \left|\frac{\partial U}{\partial y}\right| \tag{4-32}$$

Referring to section 4.2.1 in solving for the Reynolds stresses; Boussinesq proposed that they could be represented in a diffusive manner whereby:

$$\sigma_{xx} = -\rho\overline{u'u'} = \rho\varepsilon_h\left[\frac{\partial\bar{u}}{\partial x} + \frac{\partial\bar{u}}{\partial x}\right], \tau_{xy} = -\rho\overline{u'v'} = \rho\varepsilon_h\left[\frac{\partial\bar{u}}{\partial y} + \frac{\partial\bar{v}}{\partial x}\right],$$

$$\tau_{xz} = -\rho\overline{u'w'} = \rho\varepsilon_v\left[\frac{\partial\bar{u}}{\partial z} + \frac{\partial\bar{w}}{\partial x}\right] \tag{4-33}$$

To determine the Reynolds stresses given in equation 4-33, many different and varying computed expressions exist for ε_h , ε_v . The representation most widely used in coastal and estuarine flows is to apply a zero-equation turbulence model similar to that prescribed by Prandtl's mixing length hypothesis (Goldstein 1938) where, for the x-direction:

$$\varepsilon = \ell^2 J \tag{4-34}$$

where ℓ is some characteristic mixing length and

$$J = \left[2\left[\frac{\partial\bar{u}}{\partial x}\right]^2 + 2\left[\frac{\partial\bar{v}}{\partial x}\right]^2 + 2\left[\frac{\partial\bar{w}}{\partial x}\right]^2 + \left[\frac{\partial\bar{w}}{\partial y} + \frac{\partial\bar{v}}{\partial z}\right]^2 + \left[\frac{\partial\bar{u}}{\partial z} + \frac{\partial\bar{w}}{\partial x}\right]^2 + \left[\frac{\partial\bar{v}}{\partial x} + \frac{\partial\bar{u}}{\partial y}\right]^2\right]^{1/2} \tag{4-35}$$

although this expression can usually be simplified due to the dominance of one or more velocity gradients. In determining the mixing length Prandtl suggested:

$$\ell = \kappa y \tag{4-36}$$

near a wall, where κ = von Karman's constant (0.41) and y is the co-ordinate perpendicular to the wall, with y = 0 at the wall. Other expressions are available for ℓ including, for example, the von Karman representation given as

$$\ell = \kappa\left|\frac{\partial\bar{u}}{\partial y}\Big/\frac{\partial^2\bar{u}}{\partial y^2}\right| \tag{4-37}$$

For the zero-equation turbulence model, the horizontal eddy viscosity is evaluated using the following equation outlined in Fischer (1973):

$$\varepsilon_h = \sigma U_* H \tag{4-38}$$

where ε_h= horizontal kinematic eddy viscosity; σ= eddy viscosity constant (typically ≅ 0.15 based upon laboratory data from Fischer. For real flows the value of σ is frequently much larger and $\sigma \approx 1.0$ is used in the current version of the model); U_*= depth averaged shear velocity; H= total depth of flow.

In the current study, the horizontal eddy viscosity was assumed to be constant along the water depth, with the depth-averaged eddy viscosity value being set in every layer. If the turbulent shear stress is dominated by the bottom friction, a relationship between the Chezy coefficient and the eddy viscosity exists. In the numerical model, the depth-integrated horizontal eddy viscosity is calculated (after Fischer et. al 1979) using:

$$\varepsilon_h = \sigma \frac{H}{C} \sqrt{g(U^2 + V^2)} \quad (4\text{-}39)$$

where C= Chezy roughness coefficient: U,V=depth average velocity components in the x and y directions respectively.

An overall assessment of the mixing length model can be found in Table 4.4 (Versteeg and Malalasekera 2007):

Table 4.4 Mixing length model assessment

Advantages:
easy to implement and cheap in terms of computing resources
good predictions for thin shear layers: jets, mixing layers, wakes and boundary layers
well established
Disadvantages:
completely incapable of describing flows with separation and recirculation
only calculates mean flow properties and turbulent shear stress

4.3.2 $k-\varepsilon$ model

In two-dimensional thin shear layers the changes in the flow direction are always so slow that the turbulence can adjust itself to local conditions. In flows where convection and diffusion cause significant differences between production and destruction of turbulence, e.g. in recirculating flows, a compact algebraic prescription for the mixing length is no longer feasible. Therefore it is necessary to consider the dynamics of turbulence. In two-equation models, the turbulence velocity scale is computed from the turbulent kinetic energy, which is provided from the solution of its transport equation. The turbulent length scale is estimated from two properties of the turbulence field, usually the turbulent kinetic energy and its dissipation rate. The dissipation rate of the turbulent kinetic energy is obtained from the solution of its transport equation. The k-ε model focuses on the mechanisms that affect the turbulence kinetic energy. k is the turbulence kinetic energy and is defined as the variance of the fluctuations in velocity. It has dimensions of (L^2T^{-2}); for example, m^2/s^2. ε is the turbulence eddy dissipation (the rate at which the velocity fluctuations dissipate), and has dimensions of k per unit time (L^2T^{-3}); for example, m^2/s^3.The governing equations for the turbulence kinetic energy and dissipation rate can be derived from Navier-Stokes equations (Rodi 1984):

$$\frac{\partial k}{\partial t} + u_i \frac{\partial k}{\partial x_i} = \frac{\partial}{\partial x_i}\left(\frac{\nu_t}{\sigma_k}\frac{\partial k}{\partial x_i}\right) + P - \varepsilon \quad (4\text{-}40)$$

$$\frac{\partial \varepsilon}{\partial t} + u_i \frac{\partial \varepsilon}{\partial x_i} = \frac{\partial}{\partial x_i}\left(\frac{\nu_t}{\sigma_\varepsilon}\frac{\partial \varepsilon}{\partial x_i}\right) + c_{1\varepsilon}\frac{\varepsilon}{k}P - c_{2\varepsilon}\frac{\varepsilon^2}{k} \quad (4\text{-}41)$$

Equations (4-40) and (4-41), together with the continuity equation can be rewritten as:

$$\frac{\partial k}{\partial t} + \frac{\partial k u_i}{\partial x_i} = \frac{\partial}{\partial x_i}\left(\frac{\nu_t}{\sigma_k}\frac{\partial k}{\partial x_i}\right) + P - \varepsilon \quad (4\text{-}42)$$

$$\frac{\partial \varepsilon}{\partial t} + \frac{\partial \varepsilon u_i}{\partial x_i} = \frac{\partial}{\partial x_i}\left(\frac{\nu_t}{\sigma_\varepsilon}\frac{\partial \varepsilon}{\partial x_i}\right) + c_{1\varepsilon}\frac{\varepsilon}{k}P - c_{2\varepsilon}\frac{\varepsilon^2}{k} \quad (4\text{-}43)$$

where P(shear production $= \nu_t\left(\frac{\partial u_i}{\partial x_j} + \frac{\partial u_j}{\partial x_i}\right)\frac{\partial u_i}{\partial x_j}$ and $c_{1\varepsilon}$, $c_{2\varepsilon}$,σ_k, σ_ε are empirical constants.

The eddy viscosity is derived from turbulence parameters k and ε as

$$\nu_t = c_\mu \frac{k^2}{\varepsilon} \quad (4\text{-}44)$$

where c_μ is also an empirical constant. Eqs. (4-40) and (4-41) and the relationship by Eq. (4-44) give the so-called $k-\varepsilon$ turbulence model. Several carefully calibrated empirical coefficients enter the k-ε turbulence model. The values of the constants suggested by the ASCE (1988) can be summarized as follows:

$c_\mu = 0.09$, $c_{1\varepsilon} = 1.44$, $c_{2\varepsilon} = 1.92$, $\sigma_k = 1.0$, $\sigma_\varepsilon = 1.3$

4.3.2.1 Layer integrated $k-\varepsilon$ model

In applying the $k-\varepsilon$ model to the study, two approaches have been considered. In the first approach equations (4-42) and (4-43) were solved directly to give the corresponding homogenous eddy viscosity (i.e. similar velocity scales). In the second approach equations (4-42) and (4-43) were selected in some way so that they gave horizontal and vertical eddy viscosity values separately (i.e. different velocity scales) as proposed by Jin and Kranenburg (1993). In the numerical model proposed by Falconer and Hakimzadeh (2007) the second approach was used, i.e. for the vertical eddy viscosity, equations (4-42) and (4-43) were written as proposed by Rodi (1993), to give:

$$\frac{\partial k}{\partial t} + \frac{\partial k u}{\partial x} + \frac{\partial k v}{\partial y} + \frac{\partial k w}{\partial z} = \frac{\partial}{\partial z}\left(\frac{\nu_t}{\sigma_k}\frac{\partial k}{\partial z}\right) + P - \varepsilon \quad (4\text{-}45)$$

$$\frac{\partial \varepsilon}{\partial t} + \frac{\partial \varepsilon u}{\partial x} + \frac{\partial \varepsilon v}{\partial y} + \frac{\partial \varepsilon w}{\partial z} = \frac{\partial}{\partial z}\left(\frac{\nu_t}{\sigma_\varepsilon}\frac{\partial \varepsilon}{\partial z}\right) + c_{1\varepsilon}\frac{\varepsilon}{k}P - c_{2\varepsilon}\frac{\varepsilon^2}{k} \quad (4\text{-}46)$$

where $P = \left[\left(\frac{\partial u}{\partial z}\right)^2 + \left(\frac{\partial v}{\partial z}\right)^2\right]$

By assuming that $\hat{\text{var}} = (1/\Delta z)\int_{m+1/2}^{m-1/2}(\text{var})dz$, where $m \pm 1/2$ refer to the vertical elevations of the layer interface between the m+1 and m, and m and m-1 layers respectively such as

$\hat{k} = (1/\Delta z)\int_{m+1/2}^{m-1/2} k\,dz$, then the vertical eddy viscosity can be evaluated using the layer integrated form of the $k-\varepsilon$ equations, as derived in Falconer and Hakimzadeh (2007), giving

$$\left.\frac{\partial \hat{k}\,\Delta z}{\partial t}\right|_m + \left(\frac{\partial \hat{k}\,q_{1x}}{\partial x} + \frac{\partial \hat{k}\,q_{1y}}{\partial y}\right)_m + \left(w\hat{k}\right)_{m-1/2} - \left(w\hat{k}\right)_{m+1/2}$$

$$= \left(\frac{\hat{\nu}_{tv}}{\sigma_k}\cdot\frac{\partial \hat{k}}{\partial z}\right)_{m-1/2} - \left(\frac{\hat{\nu}_{tv}}{\sigma_k}\cdot\frac{\partial \hat{k}}{\partial z}\right)_{m+1/2} + \hat{p}\,\Delta z - \hat{\varepsilon}\,\Delta z \qquad (4\text{-}47)$$

$$\left.\frac{\partial \hat{\varepsilon}\,\Delta z}{\delta t}\right|_m + \left(\frac{\partial \hat{\varepsilon}\,q_{1x}}{\partial x} + \frac{\partial \hat{\varepsilon}\,q_{1y}}{\partial y}\right)_m + \left(w\hat{\varepsilon}\right)_{m-1/2} - \left(w\hat{\varepsilon}\right)_{m+1/2}$$

$$= \left(\frac{\hat{\nu}_{tv}}{\sigma_\varepsilon}\cdot\frac{\partial \hat{\varepsilon}}{\partial z}\right)_{m-1/2} - \left(\frac{\hat{\nu}_{tv}}{\sigma_\varepsilon}\cdot\frac{\partial \hat{\varepsilon}}{\partial z}\right)_{m+1/2} + c_{1\varepsilon}\frac{\hat{\varepsilon}}{\hat{k}}\hat{p}\,\Delta z - c_{2\varepsilon}\frac{\hat{\varepsilon}^2}{\hat{k}}\Delta z \qquad (4\text{-}48)$$

where $\sigma_k, \sigma_\varepsilon, c_\mu, c_{1\varepsilon}, c_{2\varepsilon}$ =constant coefficient;

$$\hat{p} = \hat{\nu}_{tv}\left[\left(\frac{\partial \bar{u}}{\partial z}\right)^2 + \left(\frac{\partial \bar{v}}{\partial z}\right)^2\right] \qquad (4\text{-}49)$$

$$\hat{\nu}_{tv} = c_\mu \frac{\hat{k}^2}{\hat{\varepsilon}} \qquad (4\text{-}50)$$

and q_{1x}, q_{1y} =layer integrated velocity components in the x, y directions. Full details of a range of widely used formulas for the eddy viscosity representation have been outlined in Rodi (1993) and Versteeg and Malalasekera (2007).

4.3.2.2 Boundary conditions for the turbulence model

For the $k-\varepsilon$ turbulence equations the following boundary conditions were used:

(i) inlet: distribution of k and ε were given.

Demuren and Rodi (1983) suggested two formulas for fully developed channel flows:

$$k_d = 0.004u_d^2 \qquad (4\text{-}51)$$

$$\varepsilon_d = c_\mu^{3/4}\frac{k_d^{3/2}}{0.09b} \qquad (4\text{-}52)$$

where u_d = inflow velocity, and b= inlet width

(ii) outlet: $\frac{\partial k}{\partial n} = 0$ and $\frac{\partial \varepsilon}{\partial n} = 0$

(iii) free surface: k and ε given

Krishnappan and Lau (1986) suggested for ε the following condition should be used:

$$\varepsilon_f = \frac{c_{f\varepsilon}\left(\frac{k_f}{\sqrt{c_\mu}}\right)^{3/2}}{\kappa z_f} \tag{4-53}$$

where z_f = distance from the free surface to the centre of surface grid, and k_f = the corresponding value for the turbulent energy. The value of $c_{f\varepsilon}$ used in equation (4-53) is 0.164, $c_\mu = 0.09$ and $\kappa = 0.41$ is the von Karman constant.

(iv) near wall regions and bottom layers:

With regards to the wall boundary conditions for k and ε, the hypothesis of equilibrium of production and dissipation ($P = \varepsilon$) yields expressions for k and ε as follows (Rodi 1984):

$$k_w = \frac{{u_*}^2}{\sqrt{c_\mu}} \tag{4-54}$$

$$\varepsilon_w = \frac{{u_*}^3}{\kappa z_c} \tag{4-55}$$

where u_*= shear velocity and z_c= distance to the wall at the first grid point. The above expressions for k and ε can be applied to both near wall regions and the bottom layer.

A summary of the performance assessment for the standard $k - \varepsilon$ model is given in Table 4.5 (Versteeg and Malalasekera 2007).

Table 4.5 Standard $k-\varepsilon$ model assessment

Advantages:
simplest turbulence model for which only initial and/or boundary conditions need to be supplied
excellent performance for many industrially relevant flows
well established, the most widely validated turbulence model
Disadvantages:
more expensive to implement than mixing length model
poor performance in a variety of important cases such as: (i) some unconfined flows (ii) flows with large extra strains (e.g. curved boundary layers, swirling flows) (iii) rotating flows (iv) flows driven by anisotropy of normal Reynolds stresses (e.g. fully developed flows in non- circular ducts)

4.4 Sediment transport

One of the main factors responsible for erosion and deposition at the Earth's surface is sediment transport in flowing water. Water flow induces sediment transport and changes in the surface morphology, which in turn modifies the flow. The study of natural river changes and the interference of man in natural water bodies such as reservoirs is a difficult but important activity, as increasing and shifting populations place more demands on the natural sources of fresh water. The transport of sediment particles by a flow of water can be in the form of bed-load and suspended load, depending on the size of the bed material particles and the flow conditions. The suspended load may also contain some wash load, which is governed by the upstream supply rate and not by the composition and properties of the bed material. The next sections explain the mathematical scheme for suspended load and bed-load sediment transport.

4.4.1 Suspended sediment transport model (3D)

In general, sediment is described as being cohesive if the particle (or grain) diameter is less than about 60 μm (0.06 mm), with the particles having cohesive properties due to electrostatic forces comparable with gravity forces active between the particles (van Rijn 1993). The total load for non-cohesive sediment transport is subdivided into two different modes of transport: bed load and suspended load. The bed load is defined as that part of the

total load where the sediment is almost continuously in contact with the bed, being carried by rolling, sliding or hopping, whereas the suspended load is that part of the total load which is maintained in suspension for considerable periods of time by the turbulence of the flow (van Rijn 1993). These two components of total load transport are also represented by two different formulations, since the transport mechanisms are different.

The transport of sediment particles in the water column can be expressed in the form of both suspended and bed load transport. In formulating the fluxes of suspended and bed load sediment transport, numerous theories and empirical equations have been postulated based on both field and laboratory measured data. The formulations outlined by van Rijn (1984 a, b) have been widely accepted for modelling both the suspended and bed load transport. From the mathematical point of view, it is necessary to separate these two types of particle transport, although in reality there is no sharp division between the bed load layer and the suspended load layer.

Depending upon the size and density of the bed material and the flow conditions, sediment particles can be transported by the flow in the form of bed load and suspended load. The 3-D mass equation for sediment in suspension is written as (Lin and Falconer 1996):

$$\frac{\partial S}{\partial t}+\frac{\partial}{\partial x}(uS)+\frac{\partial}{\partial y}(vS)+\frac{\partial}{\partial z}[(w-w_s)S]-\frac{\partial}{\partial x}\left(\varepsilon_x\frac{\partial S}{\partial x}\right)-\frac{\partial}{\partial y}\left(\varepsilon_y\frac{\partial S}{\partial y}\right)-\frac{\partial}{\partial z}\left(\varepsilon_z\frac{\partial S}{\partial z}\right) \qquad (4\text{-}56)$$

where $S=$ sediment concentration, $w_s=$ particle settling velocity, $\varepsilon_x, \varepsilon_y$ and $\varepsilon_z=$ sediment mixing coefficient in x, y, z direction, respectively.

In a clear, still fluid the particle fall velocity (w_s) of a solitary sand particle smaller than about 100 μm (Stokes-range) can be described by (van Rijn, 1984b):

$$w_s=\frac{(S_s-1)gD_s^{\,2}}{18\nu} \qquad (4\text{-}57a)$$

For suspended sand particles in the range of 100-1000 μm, the following type of equation as proposed by Zanke (1977) can be used:

$$w_s=10\frac{\nu}{D_s}\left\{\left[1+\frac{0.01(s-1)gD_s^3}{\nu^2}\right]^{0.5}-1\right\} \qquad (4\text{-}57b)$$

For particles larger than about 1000 μm the following simple equation can be used (van Rijn, 1984b):

$$w_s=1.1[(S_s-1)gD_s]^{0.5} \qquad (4\text{-}57c)$$

where $\nu =$ kinematic viscosity for clear water, $s =$ specific density of suspended sediment, and $D_s =$ representative particle diameter of the suspended sediment particles which may be smaller than D_{50} of the bed material (for computing D_s, see van Rijn 1984b)

The mixing coefficients were related to the turbulent eddy viscosity through the equations:

$$\varepsilon_x = \frac{\nu_{th}}{\sigma_h},\ \varepsilon_y = \frac{\nu_{th}}{\sigma_h} \text{ and } \varepsilon_z = \frac{\nu_{tv}}{\sigma_v} \tag{4-58}$$

where $\sigma_h, \sigma_v =$ Schmidt numbers is the horizontal and vertical directions respectively, with values ranging from 0.5 to 1.0.

In solving Eq. (4-56), four type of boundaries (open boundary, bank boundary, water surface and sediment bed boundary) need to be specified. In the next section, more details will be given of the specification of different boundary conditions.

Full details of the depth-integrated formation of Eq. 4-56 were given in Falconer and Chen (1996) and are not included here for brevity.

4.4.1.1 Boundary conditions for suspended the sediment transport model

In solving the governing Equation 4-56, four types of boundary conditions needed to be prescribed. These included:

a. Open boundary condition

In regulated reservoir with different hydraulic structures (intakes, sluice gates, etc.), flow velocities may be directed inwards or outwards across the open boundaries of the computational domain. For an inflow condition (inlet boundary) the concentration profiles are specified using either field measurements that are available or using the equilibrium concentration profiles corresponding to the local bed shear stresses. The general expression for the equilibrium concentration is (van Rijn 1984):

$$w_s S + \varepsilon_z \frac{\partial S}{\partial z} = 0 \tag{4-59}$$

The equilibrium sediment concentration profile follows from Eq. 4-59 by integration (van Rijn 1984):

$$\frac{S_a}{S_{ae}} = \left[\left(\frac{a}{z}\right)\left(\frac{h-z}{h-a}\right)\right]^{\mathrm{Z}} \qquad \text{for } \frac{z}{h} < 0.5 \tag{4-60a}$$

$$\frac{S_a}{S_{ae}} = \left[\left(\frac{a}{h-a}\right)\right]^{\mathrm{Z}} [e]^{-4\mathrm{Z}(z/h-0.5)} \qquad \text{for } \frac{z}{h} > 0.5 \tag{4-60b}$$

in which:

$Z = w_s/\beta\kappa u_*$ = dimensionless suspension parameter

S_{ae} = equilibrium concentration at a reference level

The sediment concentration profile can be computed when the reference concentration is known. The following expression has been proposed for this latter variable (van Rijn 1984):

$$S_{ae} = 0.015 \frac{D_{50}}{a} \frac{T^{1.5}}{D_*^{0.3}} \quad (4\text{-}61)$$

where D_{50} =sediment diameter of which 50% of the bed material is finer. T= transport stage parameter, and D_* = dimensionless particle parameter. The reference concentration S_{ae} is a function of the bed shear stress τ_b and the critical bed shear stress $\tau_{b.cr}$ for the initiation of sediment motion. If the bed shear stress exceeds the critical bed shear stress $\tau_{b.cr}$, then particles settled on the bed will suspend into the flow and S_{ae} is therefore positive. If the bed shear stress is less than $\tau_{b.cr}$, no erosion occurs and S_{ae} becomes zero. The definition of the transport stage and dimensionless particle parameter D_* can be found in van Rijn (1984). Equation (4-61) specifies a dimensionless volume concentration; multiplying it by ρ_s yields a value in kg/m^3. Equation (4-61) is valid for particles in the range of 100 to 500 μm.

The reference level (z = a) is proposed to be equal to half the bed form height. The inlet boundary should be selected at a location where no or only minor morphological changes are expected.

For an outflow condition (outlet boundary) the concentration profiles are obtained by extrapolation using a first – order upwinding scheme. The location of the outlet boundary should be far away from the area of interest.

b. Bank boundary condition

At bank boundaries the sediment flux is set to zero, i.e., the normal derivatives of the concentration are zero.

c. Water surface boundary condition

At the free surface, the net vertical sediment flux was assumed to be zero, giving:

$$\left[w_s S + \varepsilon_z \frac{\partial S}{\partial z}\right]_\zeta = 0 \quad (4\text{-}62)$$

where subscripts ζ denotes the water surface elevation relative to datum.

d. Sediment bed boundary condition

The sediment bed boundary is usually given at a small height "*a*" (the reference level) above the bed, and then the reference concentration or gradient of the concentration is prescribed by its equilibrium value at this elevation. Both of these options are included in the present model giving, respectively:

(i) $S_a = S_{ae}$ or (4-63a)

(ii) $E_a = \left(-\varepsilon_z \frac{\partial S}{\partial z}\right)_{z=a} = E_{ae}$ (4-63b)

At the reference level "*a*" in which the subscript *ae* denotes the equilibrium value at the reference level "*a*".

A wide variety of relationships exist in the literature for predicting the near-bed reference concentration of suspended sediment, from which entertainment rate of bed sediment flux into suspension can be obtained. Garcia and Parker (1991) carried out a detailed comparison of seven relationships against a common set of experimental data, for which direct measurements of the near-bed concentration were available. They found that relationship given by van Rijn (1984) and Smith and Mclean (1977) performed best. The expression for S_{ae} used in this study and described in Eq. (4-61) was given by van Rijn (1984).

The upward diffusive sediment flux is given by:

$E_{ae} = -w_s S_{ae}$ (4-64)

van Rijn (1984) proposed that if the bed-form dimensions are not know can be used form the equivalent roughness height (k_s), while a minimum value $a = 0.01H$ is used for reasons of accuracy.

When the flow velocity is varying rapidly (steep bottom slope), the application of a bed-concentration type of boundary condition may result in a positive concentration gradient near the bed ($\partial S_a/\partial t > 0$) at a certain location (x_i). This is physically not realistic for a movable bed situation. In that case the concentration at the location (x_i) is recomputed using a zero-bed concentration gradient ($\partial S_a/\partial t = 0$) as bed-boundary condition (van Rijn, 1986).

Finally, it is noted that the bed-boundary condition is specified at small height (say half the bed-form height) above the mean bed level. This approach is attractive because in that case the bed concentration or sediment flux may be represented by its equilibrium value assuming that there is an almost instantaneous adjustment to equilibrium conditions close to the bed. Detailed experimental research has shown that these assumptions are reasonable (Delft Hydraulics Laboratory, 1981 and 1983).

4.4.2 Bed load transport

The bed load sediment flux q_b is calculated using the following equation (Lin and Falconer 1995):

$$q_b = S_b U_b \delta_b = S_a U_a a \tag{4-65}$$

where S_b= bed load concentration, U_b= velocity of bed load particles, δ_b=siltation height, and U_a= effective particle velocity, given as:

$$U_a = \alpha U_b \tag{4-66}$$

where $U_b = [(1-s)gD_{50}]^{0.5} \times 1.5T^{0.6}$ $\quad and \quad$ $\alpha = 2.3$.

4.5 Bed level change equation

When sediment particles move within the fluid and along the bed boundary, in the form of suspended or bed load, then bed level changes will generally occur. The depth-integrated mass balance equation due to sediment transport can be derived using a control volume in the water body from the bed to the water surface and applying the mass conservation law, given as (Kolahdoozan 1999):

$$\frac{\partial z_b}{\partial t} + \frac{1}{1-p}\left\{\frac{\partial}{\partial t}(H\bar{s}) + \frac{\partial}{\partial x}\left(q_{s,x} + q_{b,x}\right) + \frac{\partial}{\partial y}\left(q_{s,y} + q_{b,y}\right)\right\} = 0 \tag{4-67}$$

where z_b = bed level (Fig. 4.5), p= porosity of the sediment material, and $q_{s,x} + q_{b,x}$ and $q_{s,y} + q_{b,y}$ = total sediment load transport rates per unit width in the x and y directions, respectively. The storage term $\frac{\partial}{\partial t}(H\bar{s})$ in equation (4-67) can be neglected if a quasi-steady flow condition is assumed, to give:

$$\frac{\partial z_b}{\partial t} + \frac{1}{1-p}\left\{\frac{\partial}{\partial x}\left(q_{s,x} + q_{b,x}\right) + \frac{\partial}{\partial y}\left(q_{s,y} + q_{b,y}\right)\right\} = 0 \tag{4-68}$$

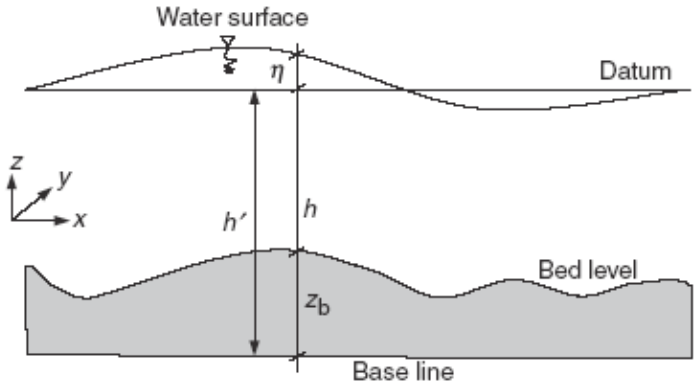

Figure 4.5 Relationship between bed level above base line and depth below datum

Bed level changes can be defined in terms of the mean water level (h) using the following geometrical relationship (see Fig. 4.5), where

$$\frac{\partial z_b}{\partial t} = \frac{\partial(h' - h)}{\partial t} = \frac{\partial h'}{\partial t} - \frac{\partial h}{\partial t} \text{ and } \frac{\partial h'}{\partial t} = 0 \tag{4-69}$$

Leading to

$$-\frac{\partial h}{\partial t} + \frac{1}{1-p}\left(\frac{\partial}{\partial x}\left(q_{s,x} + q_{b,x}\right) + \frac{\partial}{\partial y}\left(q_{s,y} + q_{b,y}\right)\right) = 0 \tag{4-70}$$

4.6 Discretization and numerical solution for hydrodynamic equations

The main procedure for modelling the hydrodynamic processes including the turbulence in this numerical model can be summarized as follows:

I- For the first half time step the depth integrated hydrodynamic equation is first solved using the ADI scheme for the first iteration to obtain the water surface elevation gradient. Turbulence modelling is based on equation 4-39.

II- When the layer number is greater than one, the layer integrated hydrodynamic equation in the x-direction and the layer integrated turbulence equations are solved to give layer averaged velocity $\bar{u}$ and turbulent parameters $\hat{k}$ and $\hat{\varepsilon}$.

III- The momentum correction factor is then found by vertical integration of the layer averaged velocity and the stresses are evaluated from the layer integrated equations to give the corresponding terms for the depth integrated equations.

IV- The vertical velocity w, the horizontal eddy viscosity and the vertical eddy viscosity are then determined using the layer integrated continuity equation and the corresponding eddy viscosity relationships.

V- For the next iteration the procedure repeats steps I to IV inclusive before proceeding to the second half time step.

VI- Likewise, for the second half time step, steps similar to I to V are repeated for the y-direction.

VII- The check for flooding and drying is undertaken at this stage, with the surface layer thickness being modified to take into account of the new water surface elevation.

These computational schemes explain in the following flow chart.

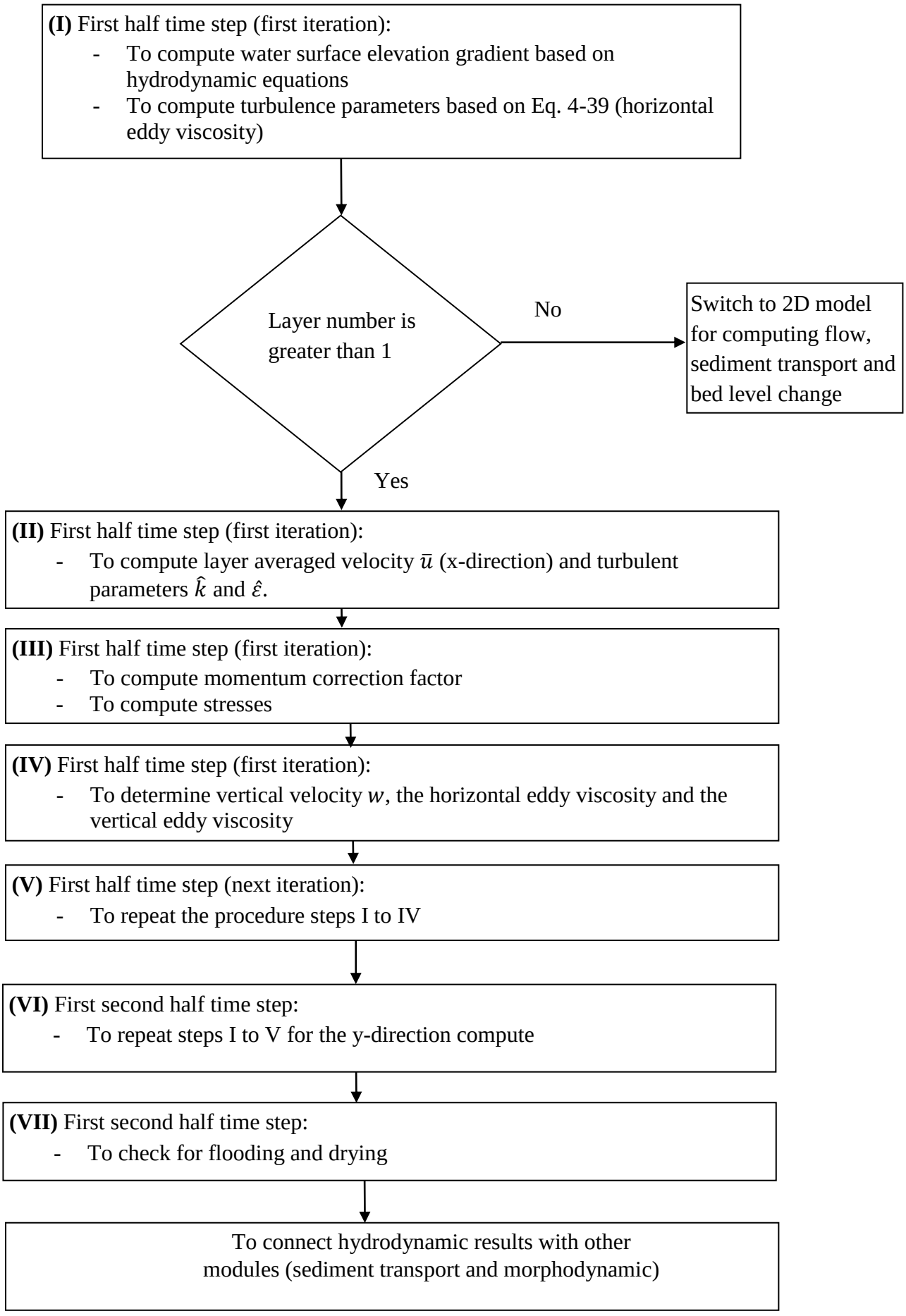
(I) First half time step (first iteration):
- To compute water surface elevation gradient based on hydrodynamic equations
- To compute turbulence parameters based on Eq. 4-39 (horizontal eddy viscosity)
Layer number is greater than 1
No
Switch to 2D model for computing flow, sediment transport and bed level change
Yes
(II) First half time step (first iteration):
- To compute layer averaged velocity $\bar{u}$ (x-direction) and turbulent parameters $\hat{k}$ and $\hat{\varepsilon}$.
(III) First half time step (first iteration):
- To compute momentum correction factor
- To compute stresses
(IV) First half time step (first iteration):
- To determine vertical velocity w, the horizontal eddy viscosity and the vertical eddy viscosity
(V) First half time step (next iteration):
- To repeat the procedure steps I to IV
(VI) First second half time step:
- To repeat steps I to V for the y-direction compute
(VII) First second half time step:
- To check for flooding and drying
To connect hydrodynamic results with other modules (sediment transport and morphodynamic)

In solving the layer-integrated equation (Equation 4-16), this was rewritten in the form:

$$\frac{\partial \bar{u}\Delta Z}{\partial t} - \left[\left(\varepsilon_v \frac{\partial \bar{u}}{\partial z}\right)_{k-1/2} - \left(\varepsilon_v \frac{\partial \bar{u}}{\partial z}\right)_{k+1/2}\right] = S_{x0} \tag{4-71}$$

where S_{x0} incorporates the terms solved explicitly. The finite difference representation used for Equation 4-71 was as follows:

$$\left((\bar{u}Z)_k^{n+1/2} - (\bar{u}Z)_k^{n-1/2}\right) - \Delta t \left(\frac{\varepsilon_v}{\Delta z}\right)_{k-1/2} \left[\left(\bar{u}_{k-1}^{n+1/2} - \bar{u}_k^{n+1/2}\right) + \left(\bar{u}_{k-1}^{n-1/2} - \bar{u}_k^{n-1/2}\right)\right]/2 +$$

$$\Delta t \left(\frac{\varepsilon_v}{\Delta z}\right)_{k+1/2} \left[\left(\bar{u}_k^{n+1/2} - \bar{u}_{k+1}^{n+1/2}\right) + \left(\bar{u}_k^{n-1/2} - \bar{u}_{k+1}^{n-1/2}\right)\right]/2 = S_x \tag{4-72}$$

where

$$S_x = ADV + COR + PRE + DIF + VTC$$

where

$$ADV = -\frac{\Delta t}{\Delta x}\Big[\bar{u}' q_x'\big|_{i+1,j,k}^n - \bar{u}' q_x'\big|_{i,j,k}^n + q_y\big|_{i+1/2,j+1/2,k}^n \bar{u}'\big|_{i+1/2,j+1/2,k}^n - q_y\big|_{i+1/2,j-1/2,k}^n \bar{u}'\big|_{i+1/2,j-1/2k}^n\Big]$$

$$COR = \Delta t.f.q_y\big|_{i+1/2,j,k}^n$$

$$PRE = -\frac{g\Delta t}{2\Delta t} Z_{i+1/2,j,k}^n [\zeta_{i+1,j}^{n+1/2} + \zeta_{i+1,j}^{n-1/2} - \zeta_{i,j}^{n+1/2} - \zeta_{i,j}^{n-1/2}]$$

$$DIF = \frac{\Delta t}{(\Delta x)^2}\{2\big[\varepsilon_h Z_{i+1/2,j,k}^n \big(\bar{u}'_{i+3/2,j,k} - \bar{u}'_{i+1/2,j,k}\big) - \varepsilon_h Z_{i,j,k}^n \big(\bar{u}'_{i+1/2,j,k} - \bar{u}'_{i-1/2,j,k}\big)\big] + \big[\varepsilon_h Z_{i+1/2,j+1/2,k}^n \big(\bar{u}'_{i+1/2,j+1,k} - \bar{u}'_{i+1/2,j,k}\big) - \varepsilon_h Z_{i+1/2,j-1/2,k}^n \big(\bar{u}'_{i+1/2,j,k} - \bar{u}'_{i+1/2,j-1,k}\big)\big] + \big[\varepsilon_h Z_{i+1,j,k}^n \big(\bar{v}_{i+3/2,j,k} - \bar{v}_{i+1/2,j,k}\big) - \varepsilon_h Z_{i,j,k}^n \big(\bar{v}_{i+1/2,j,k} - \bar{v}_{i-1/2,j,k}\big)\big]\}$$

$$VTC = \Delta t\big[(w\bar{u}')_{i+1/2,j,k+1/2} - (w\bar{u}')_{i+1/2,j,k-1/2}\big]$$

Thus, we have:

$$p\bar{u}_{k-1}^{n+1/2} + q\bar{u}_k^{n+1/2} + r\bar{u}_{k+1}^{n+1/2} = s + S_x \tag{4-73}$$

where

$$p = -\frac{\Delta t}{2}\left(\frac{\varepsilon_v}{\Delta z}\right)_{k-1/2}$$

$$q = \Delta z_k + \frac{\Delta t}{2}\left[\left(\frac{\varepsilon_v}{\Delta z}\right)_{k-1/2} + \left(\frac{\varepsilon_v}{\Delta z}\right)_{k+1/2}\right]$$

$$r = -\frac{\Delta t}{2}\left(\frac{\varepsilon_v}{\Delta z}\right)_{k+1/2}$$

$$s = \Delta z_k \bar{u}_k^{n-1/2}$$
$$+ \frac{\Delta t}{2}\left\{\left(\frac{\varepsilon_v}{\Delta z}\right)_{k-1/2} \bar{u}_{k-1/2}^{n-1/2} - \left[\left(\frac{\varepsilon_v}{\Delta z}\right)_{k-1/2} + \left(\frac{\varepsilon_v}{\Delta z}\right)_{k+1/2}\right]\bar{u}_k^{n-1/2}\right.$$
$$\left. + \left(\frac{\varepsilon_v}{\Delta z}\right)_{k+1/2} \bar{u}_{k+1}^{n-1/2}\right\}$$

Horizontally, a space-staggered grid representation was used, with the velocities and depths being located at the centre of the sides of the grid cell, and with the other main variables being located at the centre of the grid cell. For the horizontal differential terms, the same basic finite difference scheme and grid representations were used both for the layer- and depth integrated equations, thus the velocities obtained from these two set of equations were consistent.

The discrete form of the layer integrated $k-\varepsilon$ equations can be written in a similar manner to the hydrodynamic equations. Therefore the layer integrated turbulent kinetic energy equation can be written as (just for keeping the format of turbulence Equations 4-47 and 4-48 the notation of vertical eddy viscosity ν_{tv} , is the same ε_v (Hamkinzadeh 1997)):

$$(\hat{k}\Delta z)_{i,j,k}^{n+1/2} - (\hat{k}\Delta z)_{i,j,k}^{n} + \frac{\Delta t}{2\Delta x}\left[\hat{k}' q'_{lx}|_{i+1/2,j,k}^{n} - \hat{k}' q'_{lx}|_{i-1/2,j,k}^{n} + \hat{k} q_{ly}\big|_{i,j+1/2,k}^{n} - \right.$$
$$\left. \hat{k} q_{ly}\big|_{i,j-1/2,k}^{n}\right] + \frac{\Delta t}{2}\left[\left(w\hat{k}'\right)_{i,j,k-1/2} - \left(w\hat{k}'\right)_{i,j,k+1/2}\right] = \frac{\Delta t}{2\Delta z_{i,j,k-1/2}}\left[\frac{\hat{\nu}'_{tv}}{\sigma_k}\left(\hat{k}_{i,j,k-1}^{n+1/2} - \right.\right.$$
$$\left.\left.\hat{k}_{i,j,k}^{n+1/2}\right)\right]_{k-1/2} - \frac{\Delta t}{2\Delta z_{i,j,k+1/2}}\left[\frac{\hat{\nu}'_{tv}}{\sigma_k}\left(\hat{k}_{i,j,k}^{n+1/2} - \hat{k}_{i,j,k+1}^{n+1/2}\right)\right]_{k+1/2} + \frac{\Delta t}{2\Delta z_{i,j,k}}\hat{\nu}'_{tv}\left[\left(\bar{u}_{i,j,k-1/2}^{n+1/2} - \right.\right.$$
$$\left.\left.\bar{u}_{i,j,k+1/2}^{n+1/2}\right)^2 + \left(\bar{v}_{i,j,k-1/2}^{n+1/2} - \bar{v}_{i,j,k+1/2}^{n+1/2}\right)^2\right]_k - \frac{\Delta t \Delta z_{i,j,k}}{2}\hat{\varepsilon}'_{\mathrm{i,j,k}} \qquad (4\text{-}74)$$

Similarly, the discrete form of the layer integrated equation for the dissipation rate of the turbulent kinetic energy can be written as (Hakimzadeh 1997):

$$(\hat{\varepsilon}\Delta z)_{i,j,k}^{n+1/2} - (\hat{\varepsilon}\Delta z)_{i,j,k}^{n} + \frac{\Delta t}{2\Delta x}\left[\hat{\varepsilon}' q'_{lx}|_{i+1/2,j,k}^{n} - \hat{\varepsilon}' q'_{lx}|_{i-1/2,j,k}^{n} + \hat{\varepsilon} q_{ly}\big|_{i,j+1/2,k}^{n} - \right.$$
$$\left. \hat{\varepsilon} q_{ly}\big|_{i,j-1/2,k}^{n}\right] + \frac{\Delta t}{2}\left[(w\hat{\varepsilon}')_{i,j,k-1/2} - (w\hat{\varepsilon}')_{i,j,k+1/2}\right] = \frac{\Delta t}{2\Delta z_{i,j,k-1/2}}\left[\frac{\hat{\nu}'_{tv}}{\sigma_k}\left(\hat{\varepsilon}_{i,j,k-1}^{n+1/2} - \right.\right.$$
$$\left.\left.\hat{\varepsilon}_{i,j,k}^{n+1/2}\right)\right]_{k-1/2} - \frac{\Delta t}{2\Delta z_{i,j,k+1/2}}\left[\frac{\hat{\nu}'_{tv}}{\sigma_k}\left(\hat{\varepsilon}_{i,j,k}^{n+1/2} - \hat{\varepsilon}_{i,j,k+1}^{n+1/2}\right)\right]_{k+1/2} + \frac{\Delta t}{2\Delta z_{i,j,k}} c_{1\varepsilon} c_\mu \hat{k}'_{i,j,k}\left[\left(\bar{u}_{i,j,k-1/2}^{n+1/2} - \right.\right.$$
$$\left.\left.\bar{u}_{i,j,k+1/2}^{n+1/2}\right)^2 + \left(\bar{v}_{i,j,k-1/2}^{n+1/2} - \bar{v}_{i,j,k+1/2}^{n+1/2}\right)^2\right]_k - \frac{\Delta t \Delta z_{i,j,k}}{2} c_{2\varepsilon}\frac{\hat{\varepsilon}'^2_{i,j,k}}{\hat{k}'_{i,j,k}} \qquad (4\text{-}75)$$

For the layer integrated finite difference equations for the turbulence model, then these equations can be solved by the Thomas Algorithm in a similar method in hydrodynamic section. Hence, equation (4-73) can be written as (Hakimzadeh 1997):

$$p(k).\hat{k}_{k-1}^{n+1/2} + Q(k).\hat{k}_{k}^{n+1/2} + Q(k).\hat{k}_{k+1}^{n+1/2} = S(k) \quad (4\text{-}76)$$

where

$$p(k) = -\frac{\Delta t}{2\Delta z_{k-1/2}}\left(\frac{\hat{v}'_{tv}}{\sigma_k}\right)_{k-1/2}$$

$$Q(k) = \Delta z_k + \frac{\Delta t}{2\Delta z_{k-1/2}}\left(\frac{\hat{v}'_{tv}}{\sigma_k}\right)_{k-1/2} + \frac{\Delta t}{2\Delta z_{k+1/2}}\left(\frac{\hat{v}'_{tv}}{\sigma_k}\right)_{k+1/2}$$

$$R(k) = -\frac{\Delta t}{2\Delta z_{k+1/2}}\left(\frac{\hat{v}'_{tv}}{\sigma_k}\right)_{k+1/2}$$

$$S(k) = s_0 + ADV + PRO + VTC + DIS$$

where

$$s_0 = \left(\hat{k}.\Delta z\right)_k^n$$

$$ADV = -\frac{\Delta t}{2\Delta x}\left[\hat{k}' q'_{lx}|_{i+1/2,j,k}^{n} - \hat{k}' q'_{lx}|_{i-1/2,j,k}^{n} + \hat{k} q_{ly}\Big|_{i,j+1/2,k}^{n} - \hat{k} q_{ly}\Big|_{i,j-1/2,k}^{n}\right]$$

$$PRO = \frac{\Delta t}{2\Delta z_k}\hat{v}'_{th}\left[\left(\bar{u}_{i,j,k-1/2}^{n+1/2} - \bar{u}_{i,j,k+1/2}^{n+1/2}\right)^2 + \left(\bar{v}_{i,j,k-1/2}^{n+1/2} - \bar{v}_{i,j,k+1/2}^{n+1/2}\right)^2\right]$$

$$VTC = \frac{\Delta t}{2}\left[\left(w\hat{k}'\right)_{i,j,k-1/2} - \left(w\hat{k}'\right)_{i,j,k+1/2}\right]$$

$$DIS = -\frac{\Delta t}{2}\hat{\varepsilon}'_k \Delta z_k$$

Using the Thomas algorithm the unknown parameter $\hat{k}$ can be calculated as outlined in Hakimzadeh (1997). Likewise, the same procedure can be used for the equation for the dissipation rate of the turbulence kinetic energy.

4.6.1 Representation of closed boundary conditions

Three closed boundary representations were considered to evaluate the second derivative for the turbulent diffusion terms adjacent to solid boundaries and the advective acceleration representations along the boundary.

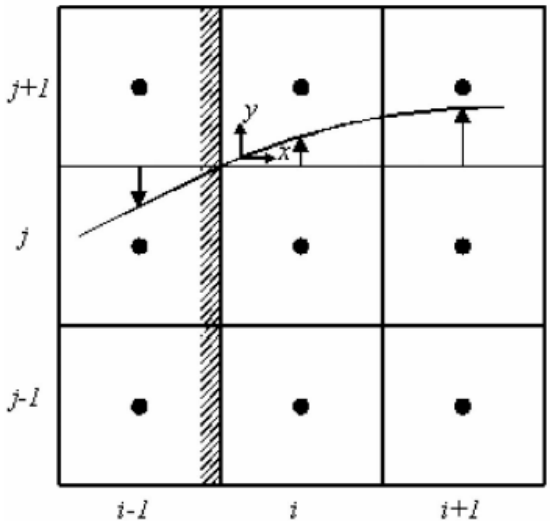

Figure 4.6 Finite-difference notation for closed boundary

Using the notation illustrated in Fig. 4.6, where the boundary wall was located along the axis $i - 1/2$ and with the node $i-1$ being external to the domain, then the second derivative of the *y*-direction velocity (*V)*, with respect to *x*, is required at the velocity point $i, j + 1/2$ and with the *V* velocity at the location $i - 1,\ j + 1/2$ being a "fictitious point" and external to the domain, i.e., this point is outside of the domain and has no physical value. In representing this velocity in the second derivative the three methods adopted can be summarized as follows:

1. *No-slip condition*. In this case a linear variation in velocity is assumed between $i - 1$, $j + 1/2$ and $i, j + 1/2$, thereby giving zero velocity at the solid boundary, that is

$$V_{i-1,j+1/2} = -V_{i,j+1/2} \tag{4-77}$$

2. Semi-slip condition. In this case the wall shear stress τ_w is represented in the form of a quadratic friction law as given by Li and Falconer (1995)

$$\tau_w = \rho \frac{\mathrm{f}}{2} V^2 \tag{4-78}$$

where f = Darcy–Weisbach friction factor; and *V*= undisturbed velocity. Assuming that the side wall shear stress can be represented by Newton's viscosity law, then the normal velocity gradient yields

$$\frac{\partial V}{\partial x} = \sqrt{\frac{\mathrm{f}}{2}} \frac{V}{\sigma H} \tag{4-79}$$

where σ= eddy viscosity constant. Thus, using a forward difference representation at the lower boundary gives

$$V_{i-1,j+1/2} = V_{i,j+1/2} \left[1 - \sqrt{\frac{\mathrm{f}}{2}} \frac{\Delta x}{\sigma H} \right] \cong 0.9 V_{i,j+1/2} \tag{4-80}$$

which is close to the free-slip boundary condition.

3. *Partial-slip condition*. In this case the velocity profile is assumed to follow a seventh power law distribution between the free stream velocity, at some point $i+n$ and the wall [see Alstead (1994)] giving

$$V(x) = V_{i+n,j+1/2}\left[\frac{x}{(n+1/2)\Delta x}\right]^{1/7} \quad (4\text{-}81)$$

Differentiating both for the first and second derivatives, this approach gives

$$V_{i-1,j+1/2} = 0.340 V_{i,j+1/2} \quad (4\text{-}82)$$

In section 4.6, discretization of the 3D hydrodynamic and turbulence equations of the numerical model was explained. The 2D form of the numerical model can be found in the reference manual of DIVAST model by Falconer and Lin (2001).

4.7 Discretization and numerical solution for sediment transport equations

An operator splitting was used to solve the suspended sediment transport equation 4-56. The basic principle of this method is to split the advective –diffusion equation into several smaller and simpler sub-equations, with each sub-equation being solved using the most efficient numerical algorithm (Lin and Falconer 1997). For expressing the advective-diffusion equation in the form of an initial value equation, with appropriate initial and boundary conditions are referred to Lin and Falconer (1996) and are not included here for brevity

The main attraction of using this method is the flexibility in the choice of how to split the original equation. Basically there are two ways of splitting an equation; one is to split the governing equation according to the nature of physical processes of the terms, and the other is to split the governing equation according to the direction of the partial differential terms. Therefore a multi-dimensional sediment transport equation may be split into an advection equation, a diffusion equation and a reaction equation (Ding and Liu, 1989) or into several one-dimensional sub-equations for each direction. In an estuarine or reservoir study the horizontal dimension is generally much larger than the vertical dimension, thus equation 4-56 could be rearranged into the following two equations:

$$\frac{\partial S}{\partial t} + \frac{\partial}{\partial z}(w_z S) - \frac{\partial}{\partial z}\left(\varepsilon_z \frac{\partial S}{\partial z}\right) = 0 \quad (4\text{-}83a)$$

$$\left[w_s S + \varepsilon_z \frac{\partial S}{\partial z}\right]_\zeta = 0 \qquad \text{at the water surface ,}$$

and:

$$S_a = S_{ae} \; or \; E_a = \left(-\varepsilon_z \frac{\partial S}{\partial z}\right)_{z=a} = E_{ae} \qquad \text{at the bed}$$

where $w_Z = w - w_s$, and other equation being:

$$\frac{\partial S}{\partial t} + \frac{\partial}{\partial z}(uS) + \frac{\partial}{\partial z}(vS) - \frac{\partial}{\partial x}\left(\varepsilon_z \frac{\partial S}{\partial x}\right) - \frac{\partial}{\partial y}\left(\varepsilon_z \frac{\partial S}{\partial y}\right) = 0, \quad \text{(4-83b)}$$

for $i = 1,2,\ldots, I_{max},\ j = 1,2,\ldots, J_{max},\ k = 1,2,\ldots, K_{max}$ and $t \in (t_n,\ t_{n-1})$, with the open and closed boundary conditions being as highlighted previously.

Equation (4-83a) is a one dimensional equation and was discretized using an unequally spaced grid in the vertical direction. Since the diffusion term is the most important term in this equation, and some of the grid sizes may become very smaller near the bed and water surface, the equation was solved an implicit finite volume method to avoid very small time steps. In the study carried out by Lin and Falconer (1996), the total mass flux was approximated by a power law scheme (Patankar 1988). This scheme used a combination of an exponential function and a linear function to approximate the analytical solution of the 1-D advective-diffusion equation and only three vertical grid points are used in its differential form. Since a sigma co-ordinate system was not used in this numerical model, the number of vertical layers may be very small in the shallow part of an estuary or reservoir and thus the power-law scheme is particularly attractive. The discretization equation for equation (4-83a) is therefore:

$$-a_s S_{k-1}^{n+1} + a_p S_k^{n+1} - a_N S_{k+1}^{n+1} = b \quad \text{(4-84)}$$

where

$$a_N = D_N A(|Pe_n|) + [-F_n, 0]$$

$$a_s = D_s A(|Pe_s|) + [-F_s, 0]$$

$$b = \frac{\Delta z}{\Delta t} S_k^n$$

$$a_p = a_N + a_s + \frac{\Delta z}{\Delta t}$$

where

$$A(|P_e|) = [0, (1 - 0.1|P_e|^5)] \quad \text{(4-85)}$$

The symbol $[a, b]$ is used to denote the greater of a and b, subscripts n and s denote the control volume face, P_e = grid Peclet number, D = diffusion coefficient and F = mass flow rate, with full definitions being given in Patankar (1988).

Equation (4-84) has a tridiagonal matrix of coefficients and has therefore been solved using a tridiagonal matrix algorithm. Equation (4-83b) has first integrated over the layer thickness Δz to give:

$$\frac{\partial(\Delta z s)}{\partial t} + \frac{\partial}{\partial x}(\Delta z u S) + \frac{\partial}{\partial y}(\Delta z v S) + \frac{\partial}{\partial x}\left(\Delta z \varepsilon_x \frac{\partial S}{\partial x}\right) + \frac{\partial}{\partial y}\left(\Delta z \varepsilon_y \frac{\partial S}{\partial y}\right) = 0 \quad \text{(4-86)}$$

for $k = 1,2, \ldots, k_{max}$

Since a uniform grid square has been deployed horizontally and the grid size relatively large, the advection terms (of order Δx^{-1}) are likely to dominate over the diffusion terms (of order Δx^{-2}). Numerical experiments show that using traditional higher-order accurate finite difference schemes, such as the QUICK scheme (Leonard 1991), pose difficulties in dealing with advection dominated flows in that negative concentrations can arise as the result of undershoot. Undershoot and overshoot usually occur in regions where the gradients of the concentration are relatively large. One approach to overcome this problem is to introduce a limiter function; such that undershoot and overshoot are first detected and then prevented. There are a number of schemes documented for this purpose, with TVD (Total Variance Diminishing) scheme being one of most popular for solving advective-diffusion problem. Cahyono (1993) carried out a detailed study by comparing 36 finite difference schemes and applying them to six numerical test cases for both one-dimensional and two-dimensional flows. His comparisons showed that the ULTIMATE scheme, originally proposed by Leonard (1991), was particularly attractive since it was more general than the other schemes considered and was easier to apply. Lin and Falconer (1997), in their 2D depth integrated estuarine model, used both splitting and non-splitting methods for third order QUIKEST scheme combined with ULTIMATE limiter, to predict solute and sediment transport.

In the numerical reported herein, the ULTIMATE QUICKSET scheme has been used to present the advective terms in equation (4-86), with the central difference scheme being used to represent the diffusion terms and with the source term being represented by a first order accurate difference approximation in time. For simplicity, only a brief discussion of discretization of the advective terms will be given here.

For a typical cell *i, j* at layer *k,* the advection terms in equation (4-86) was expressed as the sum of the four face values, i.e., west face, east face, south face and north face values. The fluxes across these faces were then evaluated using the two-dimensional form of the third-order QUIKSET scheme. These face values were then rewritten in the non-dimensional form and a universal limiter was applied to check and eliminate any unphysical oscillations. Further details of the scheme are given elsewhere (see Lin and Falconer 1996).

4.8 Discretization and numerical solution for bed level change equation

As the aim of this research was to model the morphodynamic processes, in this section emphasis will be focused on the numerical solution method for predicting bed level changes.

In solving the governing equation for predicting bed level changes, an explicit finite difference scheme has been deployed. Whereas the hydrodynamic and sediment transport modules were solved with an alternating direction implicit finite difference scheme and each time step has been divided into two half time steps, the scheme for the morphological model has be designed to follow the general scheme. It means that for the first half time step, bed level parameter in x-direction is updated and the second half time step bed level parameter in y-direction is updated.

To discretize the bed level change equation using a staggered grid, the bed level has been specified at the side center of grids in each direction, see Figure 4.7.

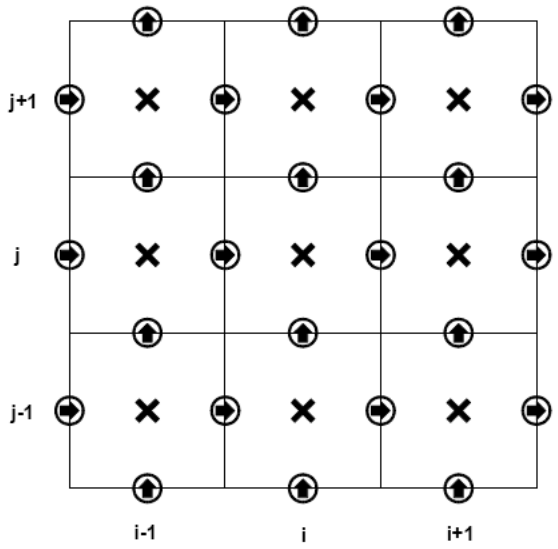

water elevation above datum (η) and solute (S)

x-component discharge per unit width (p)

y-component discharge per unit width (q)

depth below datum (h)

Figure 4.7 Computational space staggered grid system

In this section, numerical schemes for both of the depth integrated (2D) and layer integrated (3D) bed level change equations (Eq. 4-70) will be presented.

1. Depth integrated 2D equation

For the first half time step the resulting discretized equation of mass balance (Eq. 4-70) the terms in the x-direction ($\Delta x = \Delta y$) can be written as follows:

$$-\frac{\partial h}{\partial t}=\frac{-h^{n+\frac{1}{2}}_{i+\frac{1}{2},j}+h^{n}_{i+\frac{1}{2},j}}{0.5*\Delta t} \tag{4-87}$$

$$\frac{1}{1-p}\left(\frac{\partial}{\partial x}\left(q_{s,x}+q_{b,x}\right)\right)=\frac{1}{1-p}\frac{\partial q_{t,x}}{\partial x}=\frac{1}{(1-p)*\Delta x}\left[u^{n}_{i+\frac{1}{2},j+\frac{1}{2}}s^{n}_{i+\frac{1}{2},j+\frac{1}{2}}\left(h^{n}_{i+\frac{1}{2},j+\frac{1}{2}}+\eta^{n}_{i+\frac{1}{2},j+\frac{1}{2}}\right)-u^{n}_{i-\frac{1}{2},j+\frac{1}{2}}s^{n}_{i-\frac{1}{2},j+\frac{1}{2}}\left(h^{n}_{i-\frac{1}{2},j+\frac{1}{2}}+\eta^{n}_{i-\frac{1}{2},j+\frac{1}{2}}\right)\right] \tag{4-88}$$

$$\frac{1}{1-p}\left(\frac{\partial}{\partial y}\left(q_{s,y}+q_{b,y}\right)\right)=\frac{1}{1-p}\frac{\partial q_{t,y}}{\partial y}=\frac{1}{(1-p)*\Delta y}\left[v^{n}_{i+\frac{1}{2},j+\frac{1}{2}}s^{n}_{i+\frac{1}{2},j+\frac{1}{2}}\left(h^{n}_{i+\frac{1}{2},j+\frac{1}{2}}+\eta^{n}_{i+\frac{1}{2},j+\frac{1}{2}}\right)-v^{n}_{i+\frac{1}{2},j-\frac{1}{2}}s^{n}_{i+\frac{1}{2},j-\frac{1}{2}}\left(h^{n}_{i+\frac{1}{2},j-\frac{1}{2}}+\eta^{n}_{i+\frac{1}{2},j-\frac{1}{2}}\right)\right] \tag{4-89}$$

Likewise for the second half time step (y-direction): ($\Delta x = \Delta y$)

$$-\frac{\partial h}{\partial t}=\frac{-h^{n+1}_{i,j+\frac{1}{2}}+h^{n+\frac{1}{2}}_{i,j+\frac{1}{2}}}{0.5*\Delta t} \tag{4-90}$$

$$\frac{1}{1-p}\left(\frac{\partial}{\partial x}\left(q_{s,x}+q_{b,x}\right)\right)=\frac{1}{1-p}\frac{\partial q_{t,x}}{\partial x}=\frac{1}{(1-p)*\Delta x}\left[u^{n+\frac{1}{2}}_{i+\frac{1}{2},j+\frac{1}{2}}s^{n+\frac{1}{2}}_{i+\frac{1}{2},j+\frac{1}{2}}\left(h^{n+\frac{1}{2}}_{i+\frac{1}{2},j+\frac{1}{2}}+\eta^{n+\frac{1}{2}}_{i+\frac{1}{2},j+\frac{1}{2}}\right)-u^{n+\frac{1}{2}}_{i-\frac{1}{2},j+\frac{1}{2}}s^{n+\frac{1}{2}}_{i-\frac{1}{2},j+\frac{1}{2}}\left(h^{n+\frac{1}{2}}_{i-\frac{1}{2},j+\frac{1}{2}}+\eta^{n+\frac{1}{2}}_{i-\frac{1}{2},j+\frac{1}{2}}\right)\right] \tag{4-91}$$

$$\frac{1}{1-p}\left(\frac{\partial}{\partial y}\left(q_{s,y}+q_{b,y}\right)\right)=\frac{1}{1-p}\frac{\partial q_{t,y}}{\partial y}=\frac{1}{(1-p)*\Delta y}\left[v^{n+\frac{1}{2}}_{i+\frac{1}{2},j+\frac{1}{2}}s^{n+\frac{1}{2}}_{i+\frac{1}{2},j+\frac{1}{2}}\left(h^{n+\frac{1}{2}}_{i+\frac{1}{2},j+\frac{1}{2}}+\eta^{n+\frac{1}{2}}_{i+\frac{1}{2},j+\frac{1}{2}}\right)-v^{n+\frac{1}{2}}_{i+\frac{1}{2},j-\frac{1}{2}}s^{n+\frac{1}{2}}_{i+\frac{1}{2},j-\frac{1}{2}}\left(h^{n+\frac{1}{2}}_{i+\frac{1}{2},j-\frac{1}{2}}+\eta^{n+\frac{1}{2}}_{i+\frac{1}{2},j-\frac{1}{2}}\right)\right] \tag{4-92}$$

2. Layer integrated 3D equation

For the first half time step the resulting discretized equation of mass balance (Eq. 4-70) the terms in the x-direction ($\Delta x = \Delta y$) can be written as follows:

$$-\frac{\partial h}{\partial t}=\frac{-(lh)^{n+\frac{1}{2}}_{i+\frac{1}{2},j,k_{\max}}+(lh)^{n}_{i+\frac{1}{2},j,k_{\max}}-\sum_{k=1}^{k=k_{\max}-1}(lh)^{n+\frac{1}{2}}_{i+\frac{1}{2},j,k}+\sum_{k=1}^{k=k_{\max}-1}(lh)^{n}_{i+\frac{1}{2},j,k}}{0.5*\Delta t} \tag{4-93}$$

$$\frac{1}{1-p}\left(\frac{\partial}{\partial x}\left(q_{s,x}+q_{b,x}\right)\right)=\frac{1}{1-p}\frac{\partial q_{t,x}}{\partial x}=\frac{1}{(1-p)*\Delta x}\left[\sum_{k=1}^{k=k_{\max}}u^{n}_{i+\frac{1}{2},j+\frac{1}{2},k}S^{n}_{i+\frac{1}{2},j+\frac{1}{2},k}(lh)^{n}_{i+\frac{1}{2},j+\frac{1}{2},k}-\sum_{k=1}^{k=k_{\max}}u^{n}_{i-\frac{1}{2},j+\frac{1}{2},k}S^{n}_{i-\frac{1}{2},j+\frac{1}{2},k}(lh)^{n}_{i-\frac{1}{2},j+\frac{1}{2},k}\right] \quad (4\text{-}94)$$

$$\frac{1}{1-p}\left(\frac{\partial}{\partial x}\left(q_{s,y}+q_{b,y}\right)\right)=\frac{1}{1-p}\frac{\partial q_{t,y}}{\partial y}=\frac{1}{(1-p)*\Delta y}\left[\sum_{k=1}^{k=k_{\max}}v^{n}_{i+\frac{1}{2},j+\frac{1}{2},k}S^{n}_{i+\frac{1}{2},j+\frac{1}{2},k}(lh)^{n}_{i+\frac{1}{2},j+\frac{1}{2},k}-\sum_{k=1}^{k=k_{\max}}v^{n}_{i+\frac{1}{2},j-\frac{1}{2},k}S^{n}_{i+\frac{1}{2},j-\frac{1}{2},k}(lh)^{n}_{i+\frac{1}{2},j-\frac{1}{2},k}\right] \quad (4\text{-}95)$$

Likewise for the second half time step (y-direction): ($\Delta x = \Delta y$)

$$-\frac{\partial h}{\partial t}=\frac{-(lh)^{n+1}_{i,j+\frac{1}{2},k_{\max}}+(lh)^{n+\frac{1}{2}}_{i,j+\frac{1}{2},k_{\max}}-\sum_{k=1}^{k=k_{\max}-1}(lh)^{n+1}_{i,j+\frac{1}{2},k}+\sum_{k=1}^{k=k_{\max}-1}(lh)^{n+\frac{1}{2}}_{i,j+\frac{1}{2},k}}{0.5*\Delta t} \quad (4\text{-}96)$$

$$\frac{1}{1-p}\left(\frac{\partial}{\partial x}\left(q_{s,x}+q_{b,x}\right)\right)=\frac{1}{1-p}\frac{\partial q_{t,x}}{\partial x}=\frac{1}{(1-p)*\Delta x}\left[\sum_{k=1}^{k=k_{\max}}u^{n+\frac{1}{2}}_{i+\frac{1}{2},j+\frac{1}{2},k}S^{n+\frac{1}{2}}_{i+\frac{1}{2},j+\frac{1}{2},k}(lh)^{n+\frac{1}{2}}_{i+\frac{1}{2},j+\frac{1}{2},k}-\sum_{k=1}^{k=k_{\max}}u^{n+\frac{1}{2}}_{i-\frac{1}{2},j+\frac{1}{2},k}S^{n+\frac{1}{2}}_{i-\frac{1}{2},j+\frac{1}{2},k}(lh)^{n+\frac{1}{2}}_{i-\frac{1}{2},j+\frac{1}{2},k}\right] \quad (4\text{-}97)$$

$$\frac{1}{1-p}\left(\frac{\partial}{\partial x}\left(q_{s,y}+q_{b,y}\right)\right)=\frac{1}{1-p}\frac{\partial q_{t,y}}{\partial y}=\frac{1}{(1-p)*\Delta y}\left[\sum_{k=1}^{k=k_{\max}}v^{n+\frac{1}{2}}_{i+\frac{1}{2},j+\frac{1}{2},k}S^{n+\frac{1}{2}}_{i+\frac{1}{2},j+\frac{1}{2},k}(lh)^{n+\frac{1}{2}}_{i+\frac{1}{2},j+\frac{1}{2},k}-\sum_{k=1}^{k=k_{\max}}v^{n+\frac{1}{2}}_{i+\frac{1}{2},j-\frac{1}{2},k}S^{n+\frac{1}{2}}_{i+\frac{1}{2},j-\frac{1}{2},k}(lh)^{n+\frac{1}{2}}_{i+\frac{1}{2},j-\frac{1}{2},k}\right] \quad (4\text{-}98)$$

where *lh* = layer thickness and *k*= number of layers. Three groups of variables directly affect each other. Therefore, the complete mathematical model for the morphodynamic process should contain a set of coupled equations linking the processes of flow, sediment transport and bed level changes.

When only one layer is conserved, the computational domain switches automatically from 3D to 2D.

A FORTRAN subroutine has been developed based on equations (4-93) to (4-98) and this subroutine has been integrated into the numerical model by the author. For each iteration, the input parameters mentioned above were first obtained based on local hydrodynamic and sediment transport parameters at each grid point of the computational domain. These input parameters were then used by the morphodynamic subroutine to determine the bed level

changes. Thus, the main numerical solution procedure of the morphodynamic model is as follows:

1. To define initial and boundary condition for the hydrodynamic, turbulence and sediment transport modules.

Uploading the flow rate for the input boundary needed to be implemented gradually from zero to T_0 (initial time steps). This technique is useful against instability in 3D numerical model. This soft start interval (or warm-up period) was undertaken for a number of time steps over which the input boundary flow rate was gradually increased from zero to 100% of its true value. For implementing this idea, a half sinusoidal function was used for forming these gradually changes (see Figure 4.8).

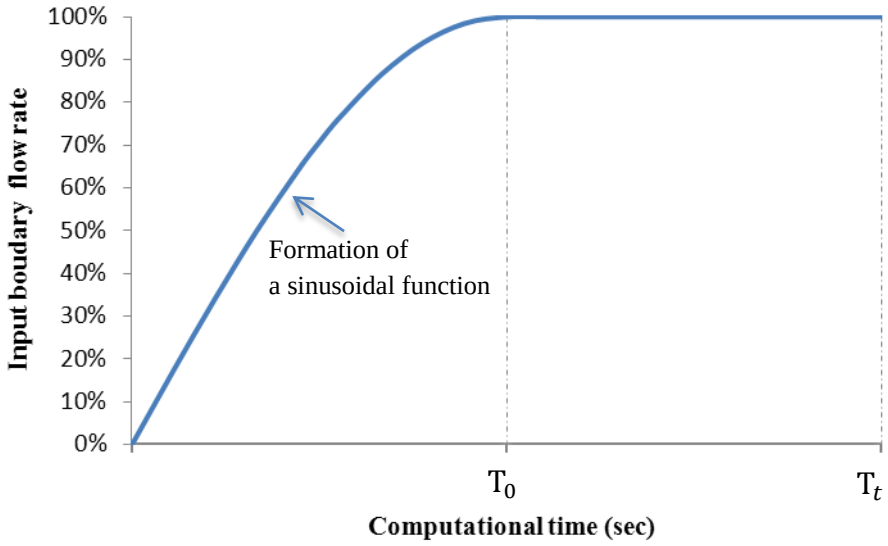

Figure 4.8 Plotted warm-up period (T_0= initial time steps and T_t= total computational time)

The length of warm-up period was chosen based on initial conditions and numerical experiences for every scenario. This time interval used at the start of a simulation for a smooth transition between initial and boundary conditions.

2. To solve the layer-integrated hydrodynamic equations in the x-direction for the first half time step, to obtain the water elevations and velocity components across the domain.

3. To solve the layer-integrated advection-diffusion equation to obtain the concentration values for the first half time step.

4. To solve the mass balance equation for the bed level changes (i.e. Eq. 4-70) to obtain the thickness of the bed layer across the domain.

5. To update the layer thickness in the x-direction as follows:

$$lhxu = \alpha_1 lhxm + (1-\alpha_1) lhxu \quad (4\text{-}99)$$

where $lhxm, lhxu$ are layer thicknesses in the x-direction for pervious and current time step respectively, $\alpha_{1,}$ is a relaxation coefficient, $0 \leq \alpha_1 \leq 1$

Using equation 4-99 is a technique to avoid generating a "chock" in the computational scheme.

6. To update the values of the velocity components, sediment concentration and bed levels for the next half time step.

7. To repeat steps 2-6 for the y-direction.

4.9 Summary

The hydrodynamic governing equations of flows in reservoirs have been reviewed in this chapter. The original numerical model was designed for coastal and estuarine flows (see Lin and Falconer 1997) and the mixing length model was used in the original version. Effort has been made to enhance the ability of hydrodynamic model for using in the reservoir environment. The depth integrated and layer integrated equations of water flow have been reviewed and the scheme for simulating the role of the gates for the numerical model has been introduced.

Also, the turbulence models, including the mixing length and $k-\varepsilon$ models have been reviewed briefly. The turbulence kinetic energy and dissipation rate of kinetic energy equations have been explained. The constants and the boundary condition used in the above turbulence models have been also outlined.

Besides, the governing sediment transport and bed level change equations have been discussed. The morphodynamic process was the focus in this research and the governing equation describing the bed level changes was derived by integrating the mass balance equation over the full depth, including both the suspended and bed load layers

The layer integrated governing equations of the hydrodynamic (including the $k-\varepsilon$ model), sediment transport and morphodynamic processes were discretized in this chapter. This was followed by the representation of suitable boundary conditions for both the open and closed boundaries. Then the numerical solution of the layer integrated equations and solution procedure for different modules (hydrodynamic, turbulence, sediment transport and morphodynamic) were explained. The essence of this research lies in the three-dimensional processes and for this reason the main emphasis has been placed on the 3D layer integrated equations.

Chapter Five

Model Verification

5.1 Introduction

The aims of this chapter were to test and verify the numerical model described in Chapter 4. The model was verified against laboratory data from two experiments carried out by van Rijn (1987). Also, efforts have been made to compare model predictions with results obtained by other researchers, i.e. Wang (1989) and Kolahdoozan and Falconer (2003). The chapter is divided two main sections: (i) To investigate flow, sediment transport and bed level changes in a trench, and (ii) To study hydrodynamic, sediment transport and morphodynamic in partially closed channel. All of the main modules, involving the hydrodynamic, sediment transport and morphological processes were tested.

5.2 Test Case 1: flow, sediment transport and bed level changes in a trench

The trench experiment undertaken by van Rijn (1986) was used as the first test case of the 3D layer-integrated morphodynamic model (see Figure 5.1).

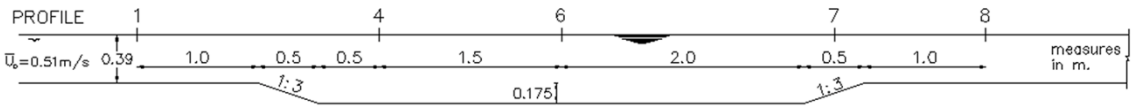

Figure 5.1 The layout of model trench

In this test the mean velocity and water level at the upstream boundary were 0.51 m/s and 0.39 m, respectively. Sediments were supplied at a rate of 0.04 kg/sm at the upstream boundary to maintain an equilibrium condition. It was found that the equilibrium suspended sediment transport rate was $S_{s,0} = 0.03\,kg/sm$ and the bed load transport rate was $S_{b,0} = 0.01\ kg/sm$. The characteristic diameter of the sediment material was: D_{50} = 0.16 mm and D_{90} = 0.2 mm. The bed-form height was in a range of 0.015-0.035 m and the roughness

coefficient was k_s = 0.025 m. More details of the model configuration and hydraulic parameters can be found in van Rijn (1986).

In applying the 3D layer-integrated morphodynamic model to this case study the depth of the (Equation 5-1) was used to compute the thickness of layers. The minimum thickness was 0.02 m near of the bed and the thickness of the upper layers was gradually changed to reach 0.078 m at the top (first layer).

$$Z(k) = k.a + bSin\,(\pi(k.a)) \quad (5\text{-}1)$$

$$lt(k) = Z(k) - Z(k-1) \quad (5\text{-}2)$$

where

$Z(k)$ = the vertical elevation of the kth layer from the top surface (see Figure 5.1)

$Lt(k)$ = the kth layer thickness

k = the number of layer

a, b = coefficients

This method provides a greater resolution in the zone where large velocity and concentration gradients exist (i.e. near the bed surface) and the sediment transport process can be simulated more precisely. The most important point in this method is the consideration of a similar bottom layer thickness for the upstream, excavation zone and downstream of the trench. Comparisons between the model predicted and measured velocity profiles and sediment concentration profiles at five cross sections shown in Figure 5.1 are given in Figures 5.2 and 5.3. It can be seen that the velocity profiles has been well predicted by the 3D layer-integrated morphodynamic model, with the shape of the velocity curves following the measured ones.

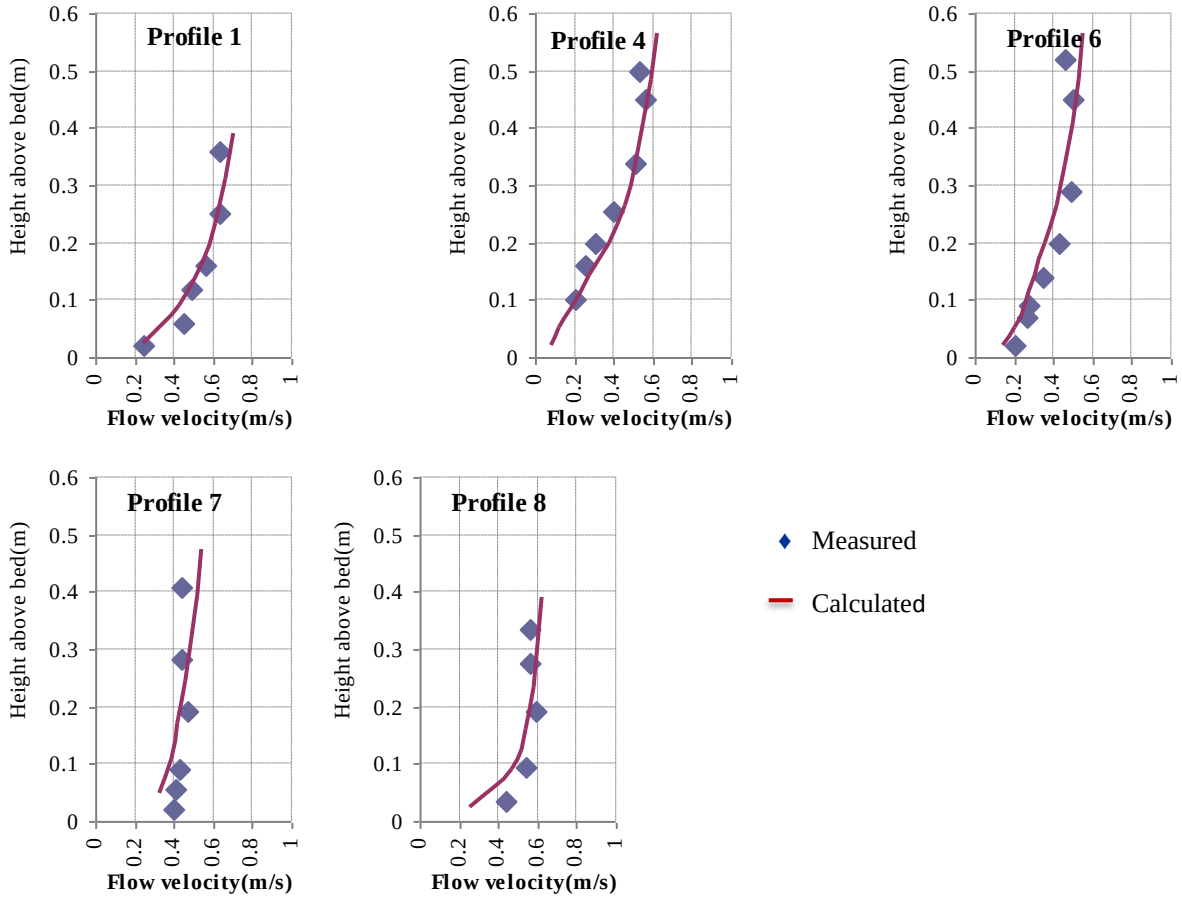

Figure 5.2 Comparisons of velocity profiles in the trench

The agreement between measured and computed velocity profile in the deceleration zone (profile 4) is reasonably good in comparison with acceleration zone (profile 7). It is noted that the measurements have been made in the center line of the flume, while the computations are based on cross section-layer integrated values.

The longitudinal distributions of the measured sediment concentration profiles have been simulated rather well by the 3D layer-integrated morphodynamic model both in the middle zone of the trench (profile 6) and in the acceleration zone (profiles 7 and 8) where a rapid increase of the near-bed concentrations can be observed. At the deceleration zone (profile 4) the model predicted concentrations are smaller than the measured ones, particularly near the bed. The results have shown that the technique used for the set up the layers in different sizes evaluated significantly useful.

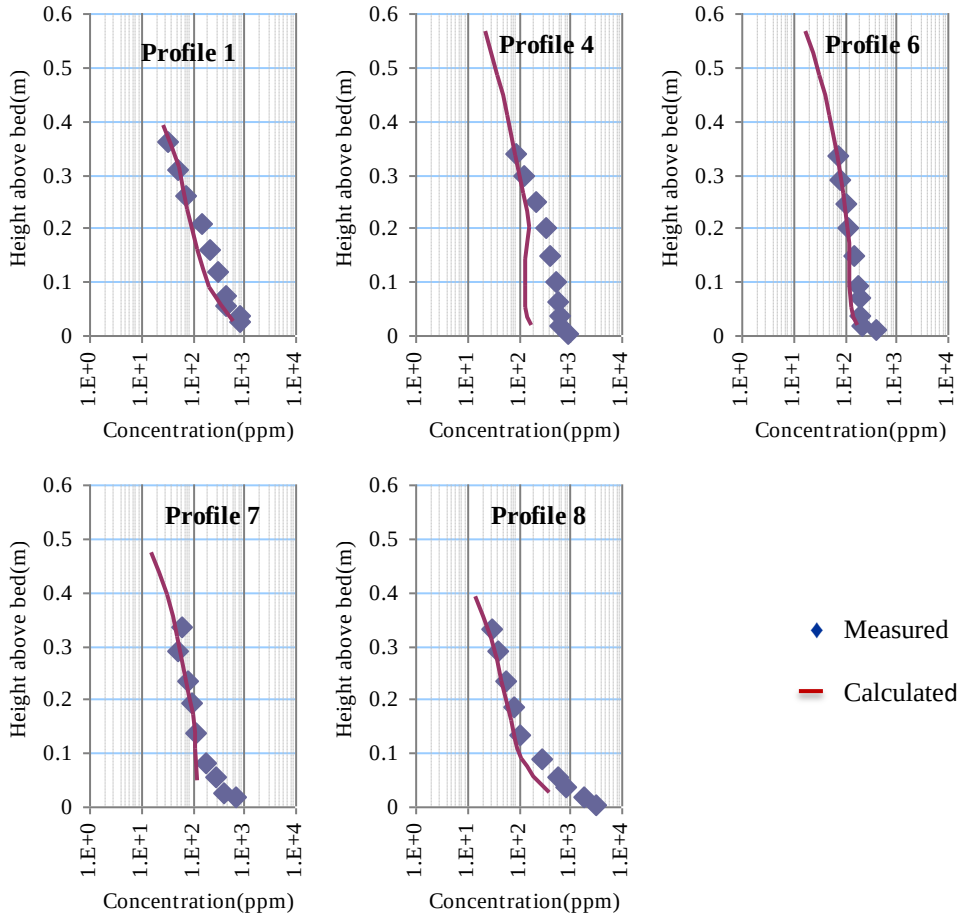

Figure 5.3 Comparisons of sediment concentration profiles in the trench

One of the reasons for the under-prediction of sediment concentration may be due to the fact that in the present model an equilibrium near-bed concentration (see Lin and Falconer, 1996) was used to specify the bed sediment boundary condition. Although this assumption has widely been used and shown to be valid from some numerical model studies with non-equilibrium conditions (van Rijn 1986; Olsen and Kjellesvig 1998), it may still cause error when flow condition change rapidly at the deceleration zone in the trench

The model predicted and measured bed level changes in the trench are shown in Figure 5.4. In this figure model predictions were also compared with two other numerical models. SUTRENCH was developed by Delft Hydraulics (van Rijn 1987); GEOTRIVAST was developed by Kolahdoozan and Falconer in 2003. Figure 5.4 shows a reasonable degree of similarity between three sets of data.

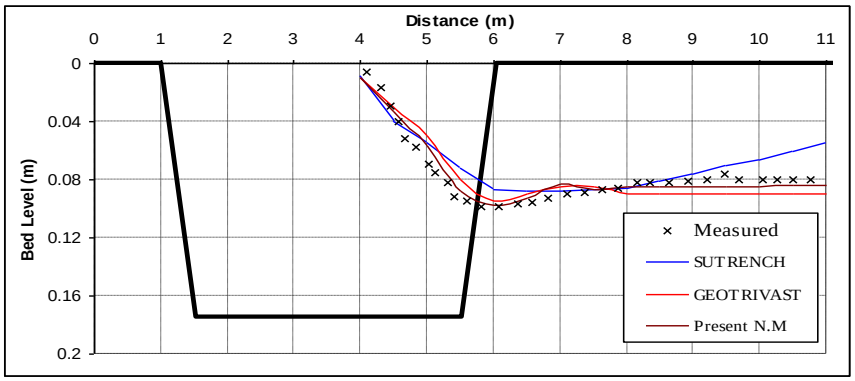

Figure 5.4 Bed level profiles in the trench after 15 hours (Present N.M =Present Numerical Model)

5.2.1 A sensitive analysis on vertical layers

The influence of the number (n) of vertical layers on the computed flow velocity and sediment concentration has been investigated for this case study. The number (n) of vertical layers is specified as an input parameter in this sensitive analysis. The model was run for 10 layers and explained in above section. For the second run, the depth of the channel is divided into 20 layers with different thickness. The minimum thickness is 0.02 m near of the bed and the thickness of the upper layers is gradually changed to reach 0.033 m at the top (first layer). The computed velocity and sediment concentration profiles (for two runs, 10 layers and 20 layers) at five cross sections shown in Figure 5.1 are presented and compared with the measured data in Figures 5.5 and 5.6.

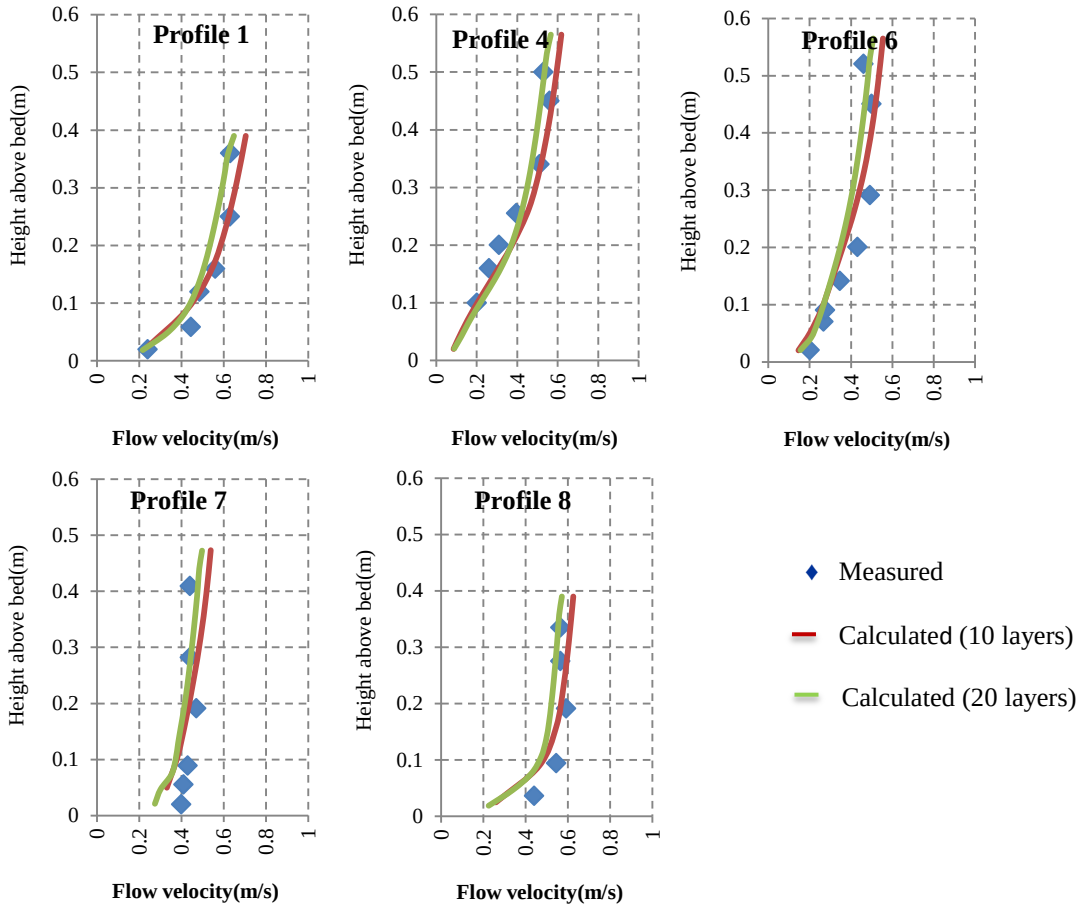

Figure 5.5 Comparisons of velocity profiles in the trench for sensitive analysis

As can be seen from Figure 5.5, increasing the number of vertical layers rises the agreement between measured and computed velocity profiles at the upper and middle layers (i.e. layers are cited upper than 0.1 m of bed) in the deceleration zone (profile 1 and 4), the middle zone of the trench (profile 6) and the acceleration zone (profile 7 and 8). Based on the calculations, the accuracy of the computed velocity profiles enhances 6% average at the upper and middle layers for all zones.

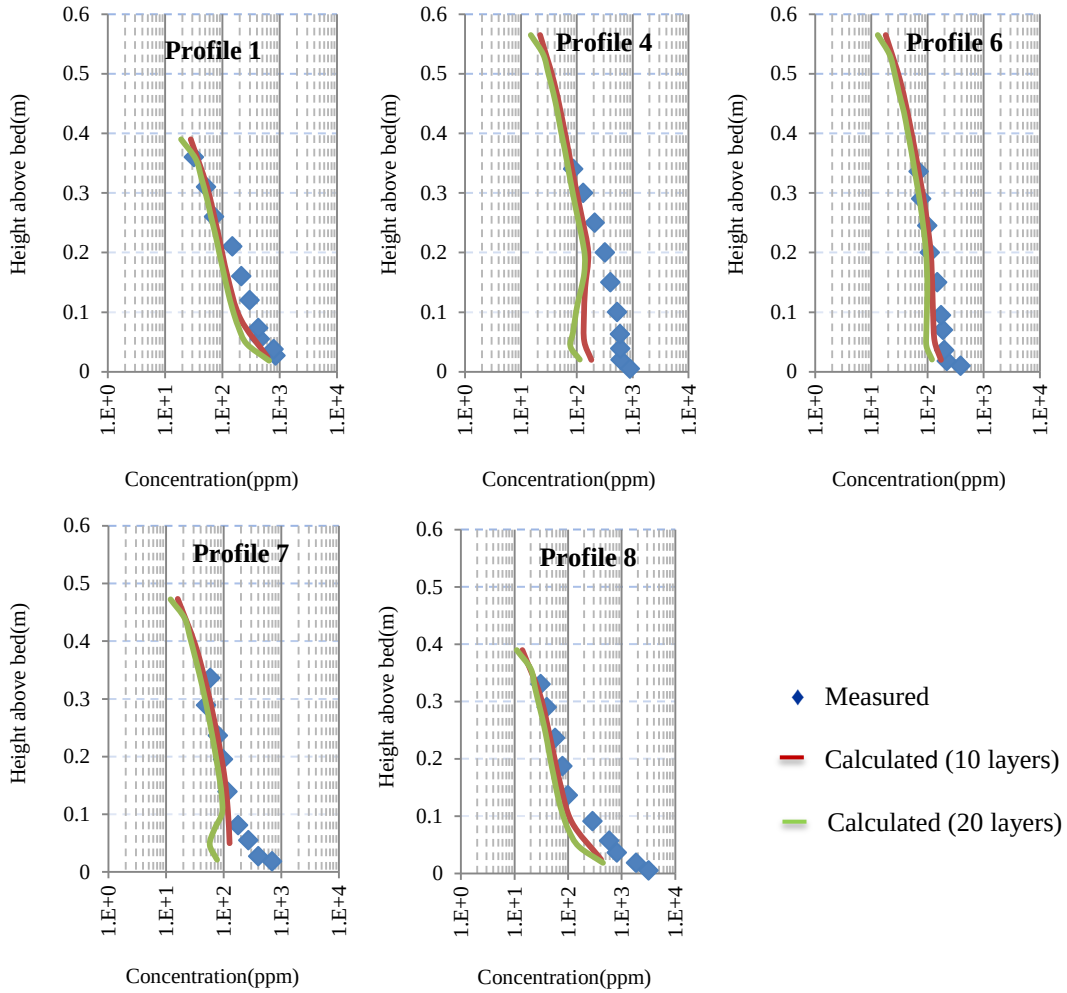

Figure 5.6 Comparisons of sediment concentration profiles in the trench for sensitive analysis

Figure 5.6 shows that comparison between measured and computed sediment concentration profiles in different zones. By increasing the number of vertical layers, the errors between measured and computed sediment concentration profiles at the upper and middle layers (i.e. layers are cited upper than 0.1 m of bed) does not change considerably for all zones (profile 1, 4, 6, 7 and 8). The errors occur at the bottom layers (i.e. layers are cited lower than 0.1 m of bed) of the acceleration zone (profile 7). This error might be related to an equilibrium assumption in the numerical model near the bed that explained before in the end of section 5.2 (see Lin and Falconer 1996). For sediment concentration profiles, increasing the number of vertical layers does not show any considerable influences on the results at the upper and middle layers while the trend (vertical gradient) of the computed results is generally closer to the trend of measured data at the bottom layers for profiles 1, 4, 6 and 8. Consequently, only a greater resolution in vertical grid could not enhance the computed sediment concentration

profiles near the bed and for this area other parameters such as bed boundary conditions might be considered for further accuracy.

5.3 Test Case Two: partially closed channel

To verify and test the 3D layer-integrated morphodynamic model, the fluid flow, sediment transport and initial bed level changes in channel were studied. The most objective was to evaluate the numerical performance of the model.

5.3.1 Hydraulic conditions

Test computations have been made for a unidirectional flow in a channel of constant width (=1000 m) and a horizontal bed. The channel was partially closed by a dam with a length of 400 m and a width of 100 m, as shown in Figure 5.7. The discharge was 4000 m^3/s. The water depth at the outlet boundary was 6 m. The bed material was assumed to be sand with $d_{50} = 200\ \mu m$ and $d_{90} = 300\ \mu m$. This test case was presented by van Rijn (1987).

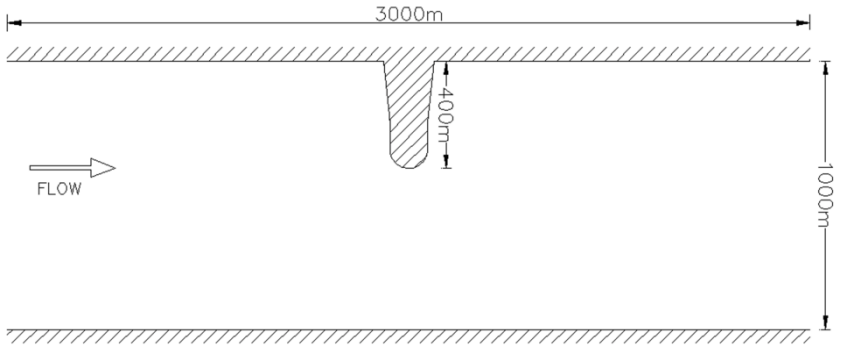

Figure 5.7 Schematic view of partially closed channel

5.3.2 Boundary conditions and input parameters

5.3.2.1 Fluid velocities

The 3D layer-integrated morphodynamic model was used to predict the fluid velocity. The flow field in the SUTRENCH computation was calculated with the WAQUA model (van Rijn, 1987). The numerical WAQUA-model was based on a curvilinear grid schematization consisted of 20x40 grid points. In the study carried out by Wang (1989) using the ESMOR model a grid size of 25 m in a staggered grid system was used, in order to produce comparable results with the original study and other numerical models, the grid size in the present computation was set to be about the same as the minimum grid size with that used in SUTRENCH and equal to those in ESMOR, GEO-DIVAST and GEO-TRIVAST

(Kolahdoozan and Falconer 1999) models. Therefore, Δx=Δy was set to 25m, which led to 41x125 grid points. In vertical direction 10 layers were selected, the same as the original study. As a rectangular staggered grid system in the 3D layer-integrated model, the widths of grids cells were gradually reduced for simulating the shape of dam (Figure 5.8a).

At the inflow boundary a uniform specific discharge $q = 4\ m^2/s$ was prescribed. At the outflow boundary a constant water depth of 6 m was prescribed. The bed roughness height was assumed to be constant, i.e. 0.25m, as suggested by van Rijn (1987).

5.3.2.2 Sediment concentration and transport rate

The 3D layer-integrated morphodynamic model has been used to compute the sediment concentration and bed level changes. The suspended sediment boundary condition was prescribed the equilibrium concentration at the inlet boundary and a zero gradient boundary condition was chosen at the outlet boundary. The applied horizontal sediment mixing coefficients for both the x and y-directions were assumed to be constant, with $\varepsilon_{s,x} = \varepsilon_{s,y} = 0.5\ m^2/s$ (van Rijn, 1987). The bed material porosity and density were set to 0.4 and 2650 kg/m^3, respectively.

5.3.3 Model results

5.3.3.1 Flow pattern and fluid velocity

The model predictions were compared with those by four existing numerical models, i.e. ESMOR, SUTRENCH, GEO-TRIVAST and GEO-DIVAST. The model SUTRENCH was developed by Delft Hydraulics (van Rijn 1987) and in this model two versions, including a 2DV model and a quasi-3D finite element model with a variable grid size. For the quasi-3D model the velocity field was obtained by using the depth averaged velocity components accompanied by a logarithmic velocity profile in the vertical direction. The model ESMOR was developed by Delft Hydraulics (Wang 1989) and is a two-dimensional depth averaged model. GEO-TRIVAST and GEO-DIVAST were developed by Kolahdoozan and Falconer (2003) and those numerical models are a 2DH depth integrated and 3D layer-integrated morphodynamic forms, respectively.

The present model predicted flow field is shown in Figure 5.8, together with the original flow fields obtained by (SUTRENCH and ESMOR).The maximum velocity in the accelerating zone near the head of the headland was 1.66 m/s. This value was calculated 1.72 m/s in the study by SUTRENCH model (van Rijn, 1987).

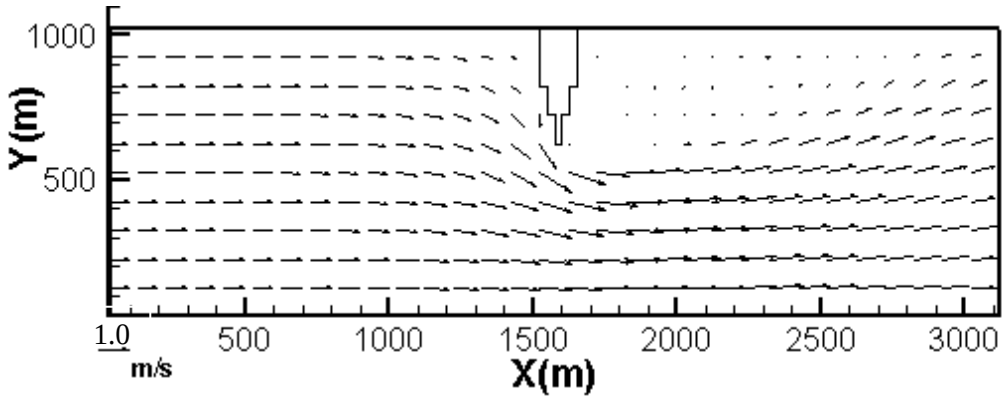

a) By the present model

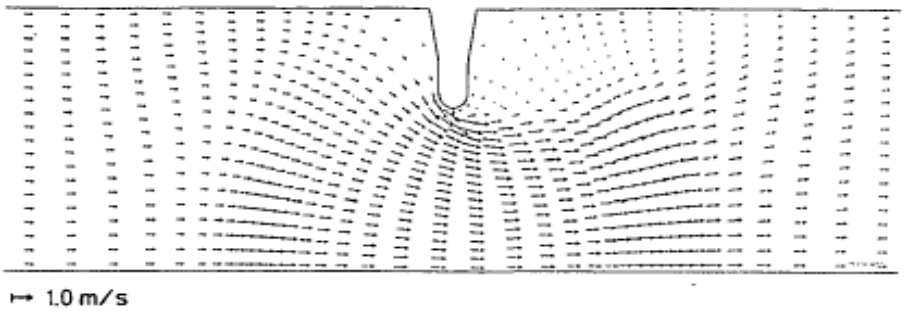

b) By SUTRENCH

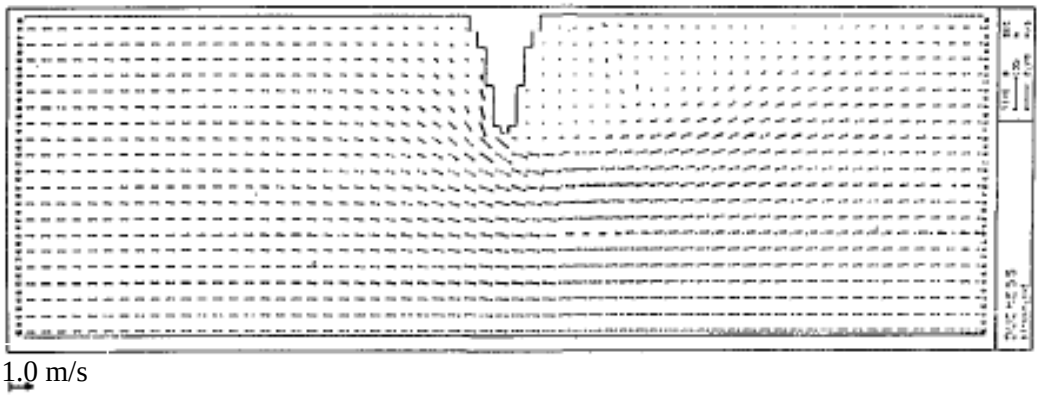

c) By ESMOR

Figure 5.8 The velocity field

Also, the streamline pattern in detail for the presented numerical model and SUTRENCH model along the channel are shown in Figure 5.9. As can be seen from Figure 5.9, a high agreement exists between both numerical results. Several nodes along the streamlines A and B, and in the recirculating zone were chosen for comparing the results of present model with those from the numerical models reported before. Due to high agreement between the streamline patterns, the locations of these nodes are physically same (see Figure 5.9). Besides, this arrangement of nodes (situated in a stream line) makes a platform for presenting sediment transport results in a same stream tube of flow. Besides, the present model predicted

depth averaged velocity and concentration profiles along the streamline B and C were compared with the other models to show the accuracy and applicability of each model.

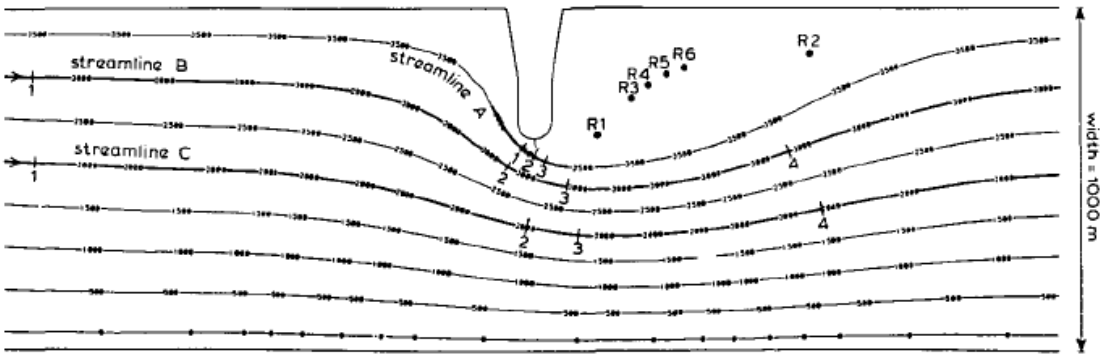

a) By SUTRENCH

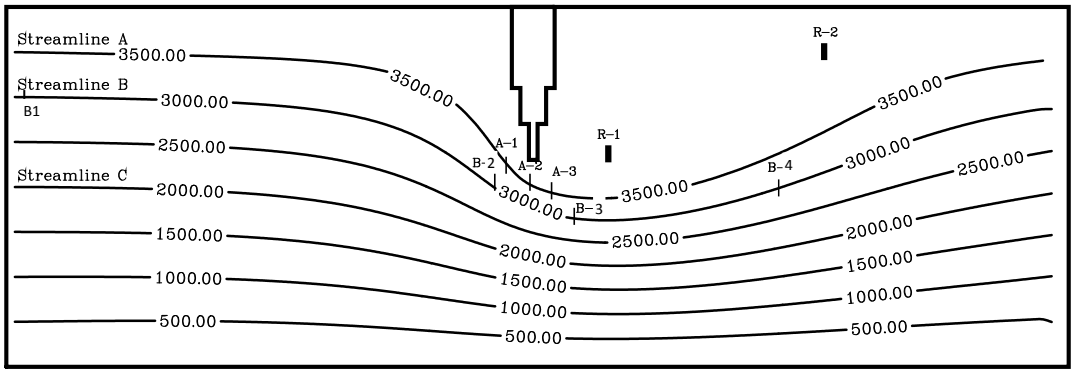

b) By the presented model

Figure 5.9 Streamline pattern along the channel

For more detailed comparisons, the depth averaged velocities along streamlines B and C obtained from four different models are shown in Figures 5.10 and 5.11, respectively. A good degree of similarity between the different models can be seen. It can be concluded from Figures 5.10 and 5.11 that the depth averaged velocity predicted by the present model has higher values beyond the headland. Generally the 3D layer-integrated morphodynamic model gave closer agreement with the other models.

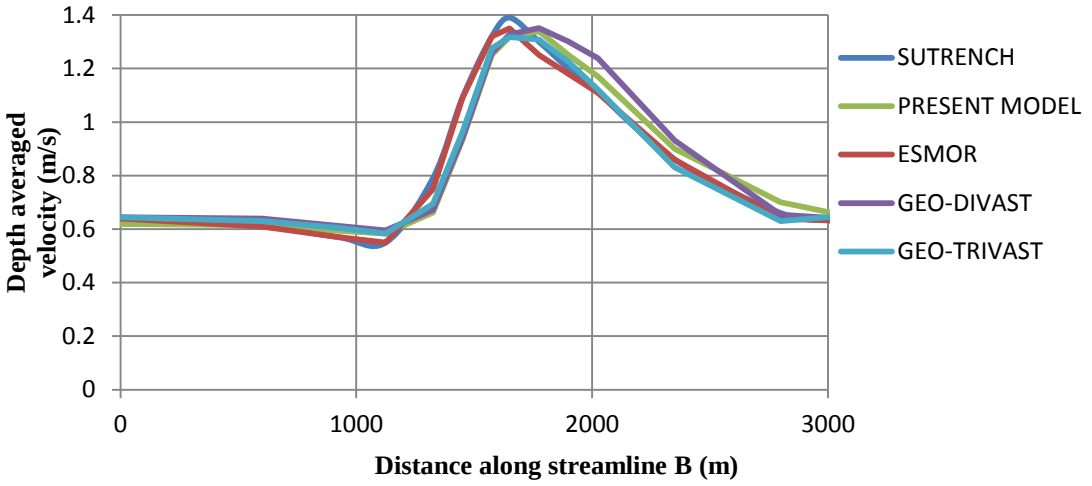

Figure 5.10 Comparison of depth averaged velocities along streamline B for different models

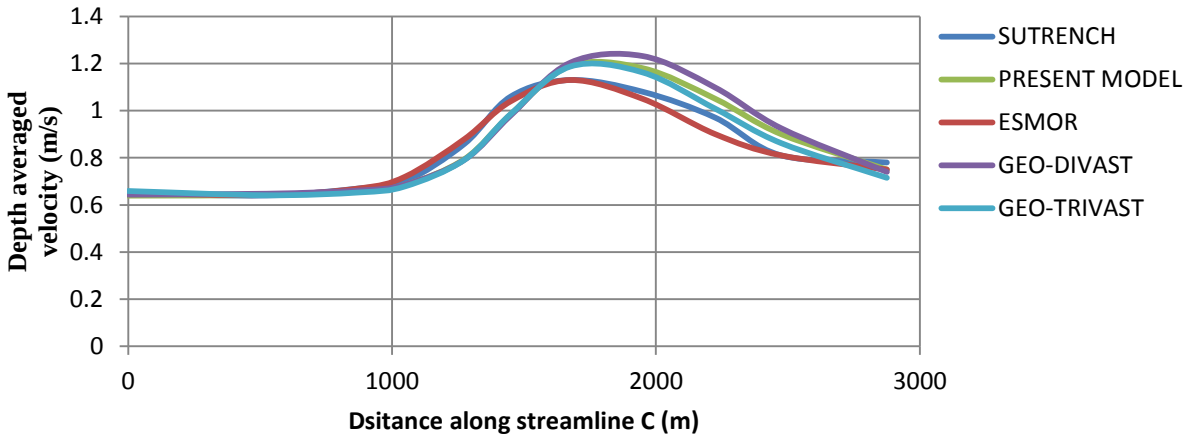

Figure 5.11 Comparison of depth averaged velocities along streamline C for different models

5.3.3.2 Sediment concentration

For calculating the sediment concentration distribution, the 3D layer-integrated morphodynamic model was set for one layer. Figure 5.12 shows the model predicted sediment concentration distribution. Figure 5.13 presents the sediment concentration distribution calculated by the ESMOR model. As can be seen from these figures, there is a good agreement between the two predictions.

Figures 5.14, 5.15 and 5.16 show computed sediment concentration profiles along the water depth at several points along streamlines A and B and in the recirculation zone by the present model (for locations see Figure 5.9b). In those figures the predictions by the SUTRENCH 3D model is also shown. The equilibrium concentration profiles (assumptions: steady and horizontal uniform conditions; $\frac{du}{dx} = 0$, $\frac{dc}{dx} = 0$) are also shown. As can be observed for

streamlines A and B, the non-equilibrium concentrations are smaller than the equilibrium values for increasing velocities ($\frac{du}{dx} > 0$, acceleration zone) and larger for decreasing velocities ($\frac{du}{dx} < 0$, deceleration zone). van Rijn' studies in 1987 revealed that horizontal distribution of the local equilibrium transport rates near the head of the dam are much larger (up to a factor of 5!) than horizontal distribution of the depth-integrated suspension sediment transport computed by the SUTRENCH-3D. Based on these results, he did not recommend to apply an equilibrium transport formula to compute morphological variations in horizontal directions in the case of fine sand conditions ($d_{50} < 300\mu m$) and large velocity gradients. It is noted that the equilibrium concentrations in the recirculation zone are zero because the velocities are below those for initiation of motion (Fig. 5.16).

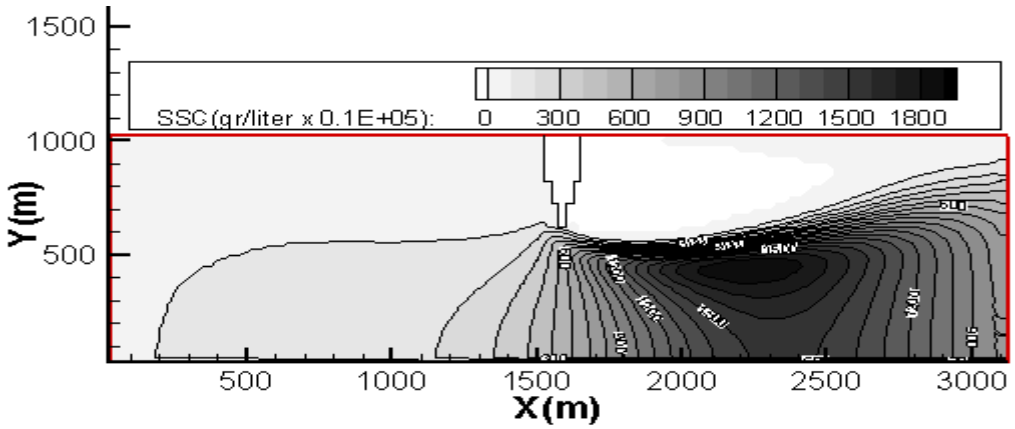

Figure 5.12 Sediment concentration distribution obtained from the present model

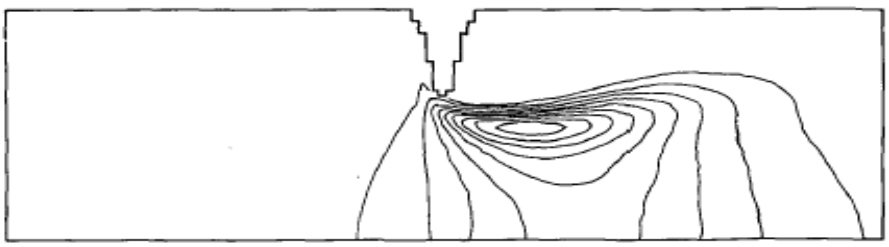

Figure 5.13 Sediment concentration distribution obtained from ESMOR

As can be concluded from Figures 5.14, 5.15 and 5.16 the results obtained from the 3D layer-integrated morphodynamic model are in most cases close to non-equilibrium scheme (SUTRENCH). The results using the above two numerical models are much closer to each other near the bed of the channel, but near of the water surface a major differences is

observed, especially along streamline A and at B2 & B3 in streamline B. These errors are, however, of minor importance because most of the suspended sediment material is transported in the lower part of the flow. Nevertheless, further research is necessary to improve the numerical schematization of the gradient type boundary conditions in 3D model.

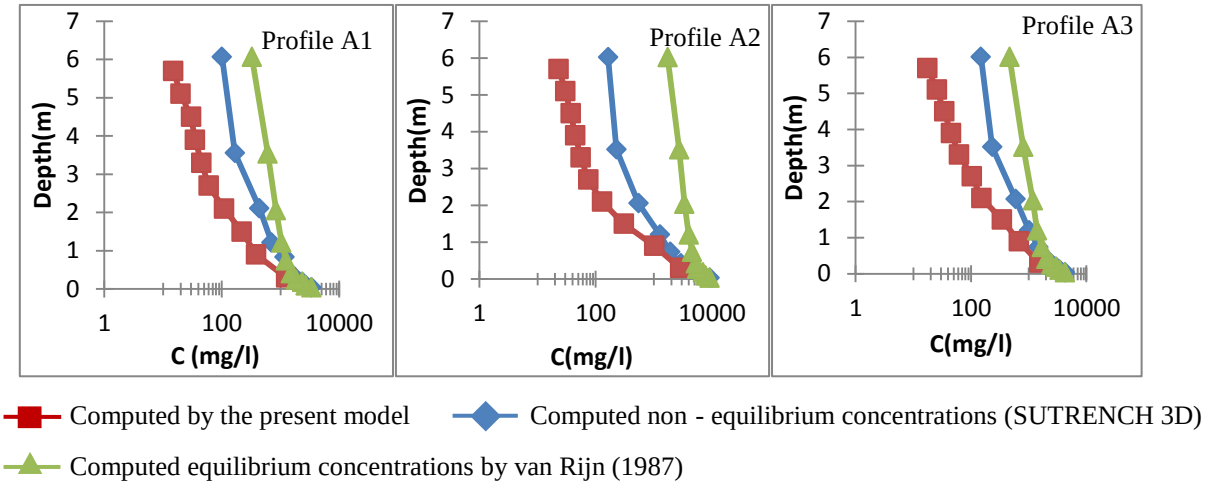

Figure 5.14 Concentration profiles in streamline A

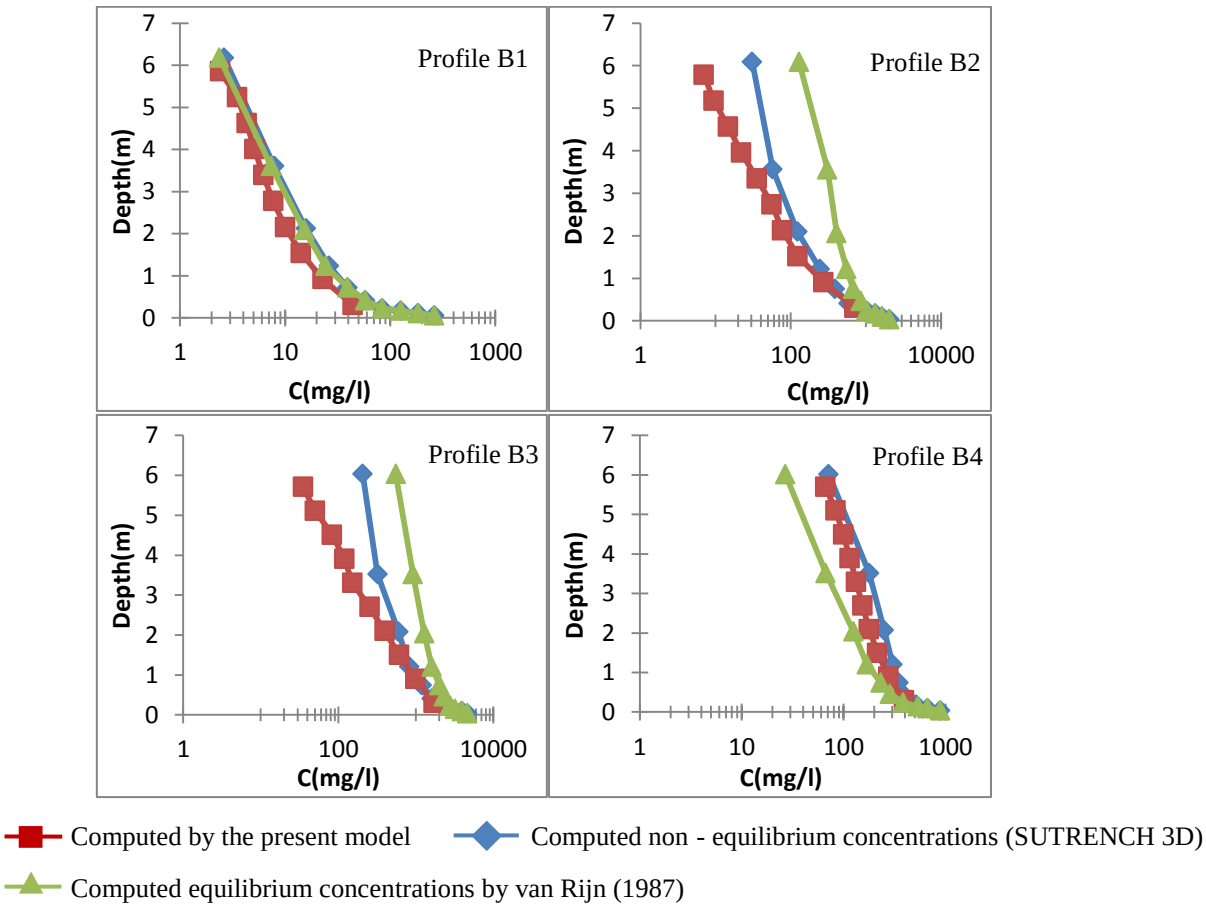

Figure 5.15 Concentration profiles in streamline B

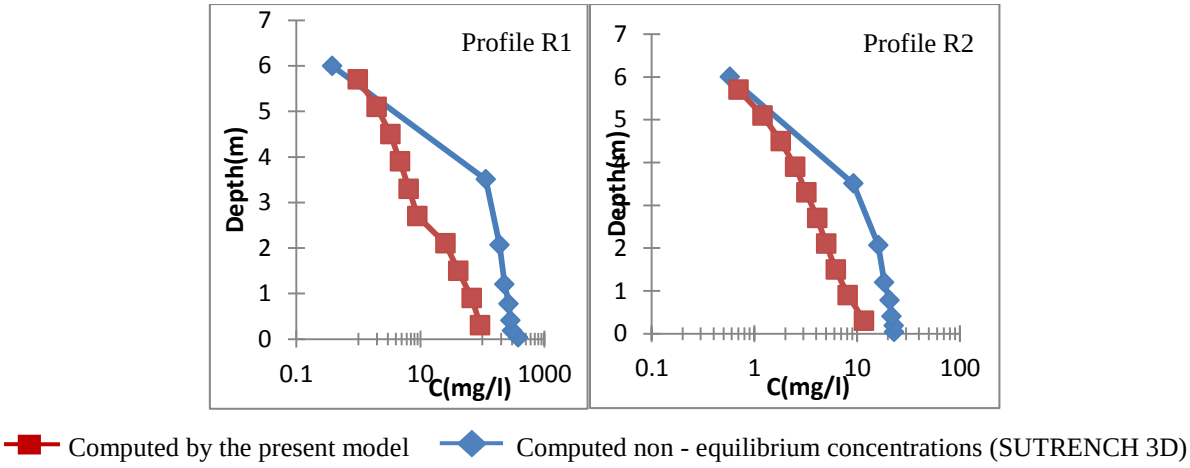

Figure 5.16 Concentration profile in recirculation zone

The present model and SUTRENCH 3D agreed well along whole depth at B1 and B4 in streamline B and both nodes are located far from the headland (see Figure 5.9b). At R1 and R4 in the recirculation zone, the present model shows reasonable agreement with SUTRENCH 3D (Figure 5.16).

5.3.3.3 Sediment transport

Figures 5.17 and 5.18 show the depth-integrated suspended sediment transport rates computed by the present model, the SUTRENCH-2D and 3D models for streamlines B and C. One key difference between the two model results is that the concentration is lower than those from other models in the vicinity of headland. Most of the differences are likely caused by the numerical diffusion of the 3D-model (relatively large grid sizes). This could be improved by reducing locally the model grid size in recirculation zones.

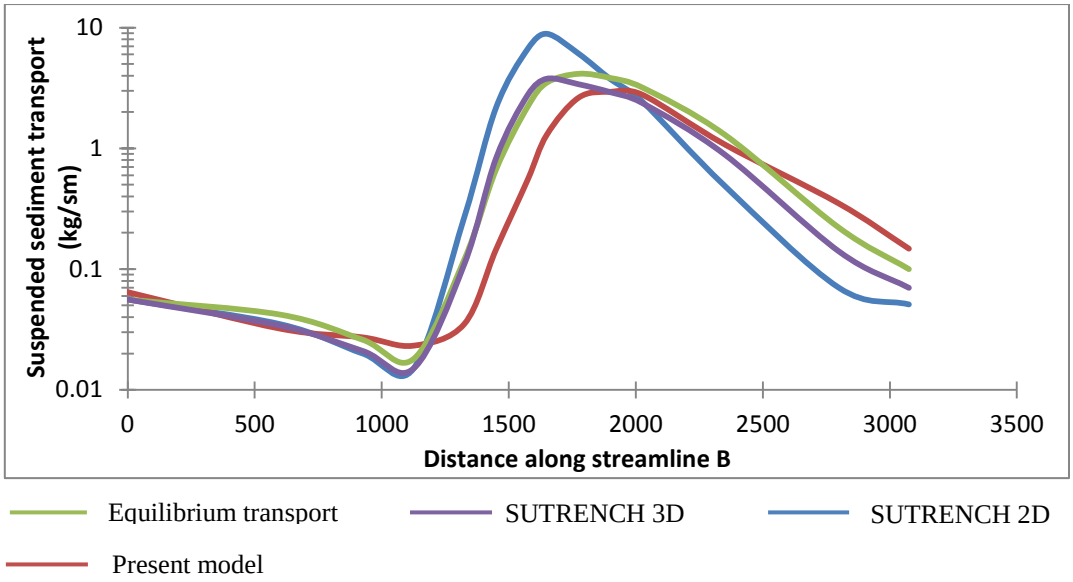

Figure 5.17 Suspended sediment transport in streamline B

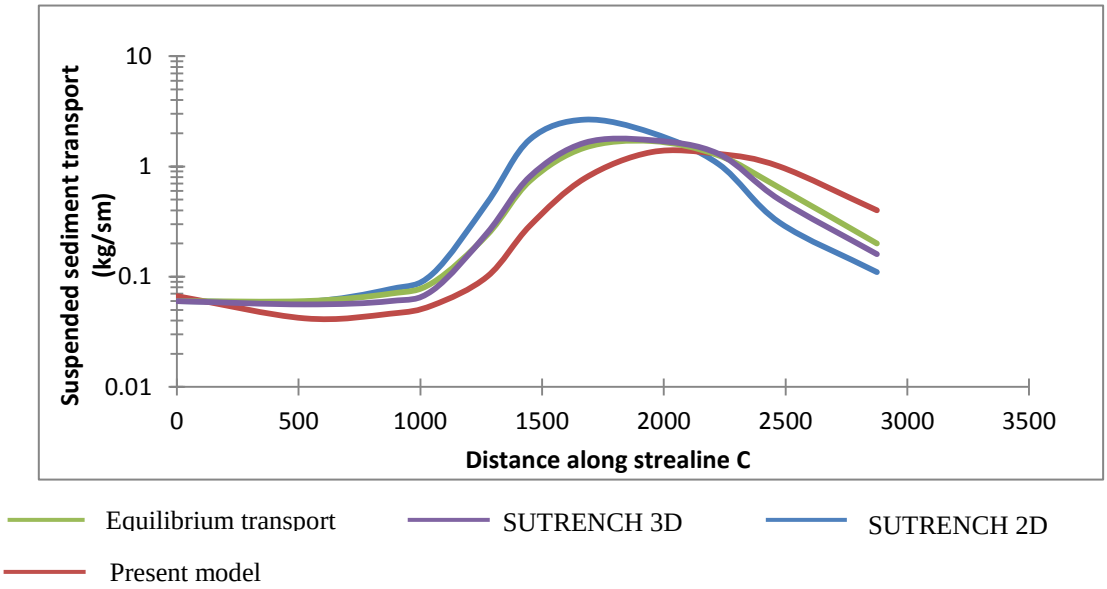

Figure 5.18 Suspended sediment transport in streamline C

5.3.3.4 Bed level changes

In this case study predictions of bed level changes were obtained based on the depth integrated sediment mass balance equation. Figure 5.19 shows the rate of bed level change predicted using the 3D layer-integrated morphodynamic model. A combination of Figures 5.20 and 5.21 shows the rate of bed level change (erosion + sedimentation) calculated using the ESMOR model. As can be seen from Figure 5.19 and the combination of Figures 5.20 and 5.21, a good agreement exists between the present model and ESMOR.

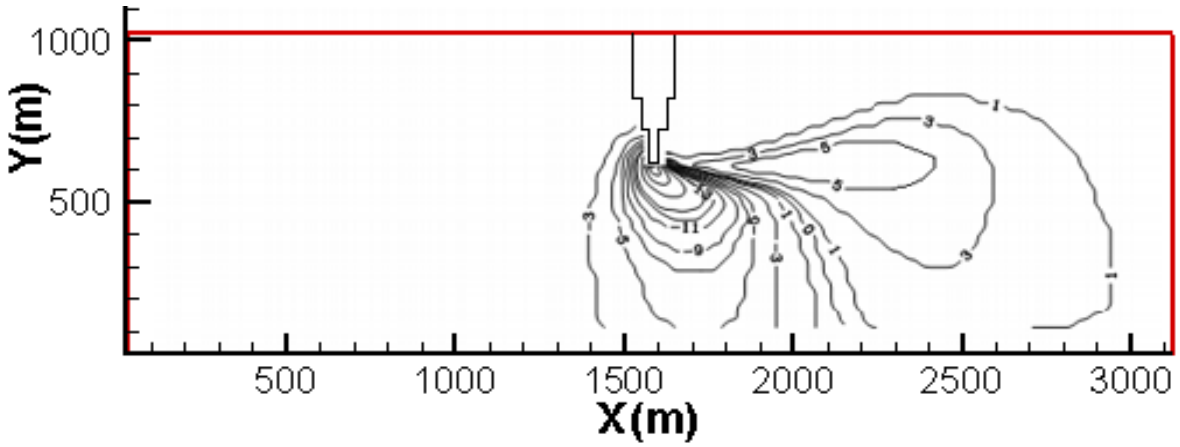

Figure 5.19 The rate of bed level change (mm/hr) obtained using the present model

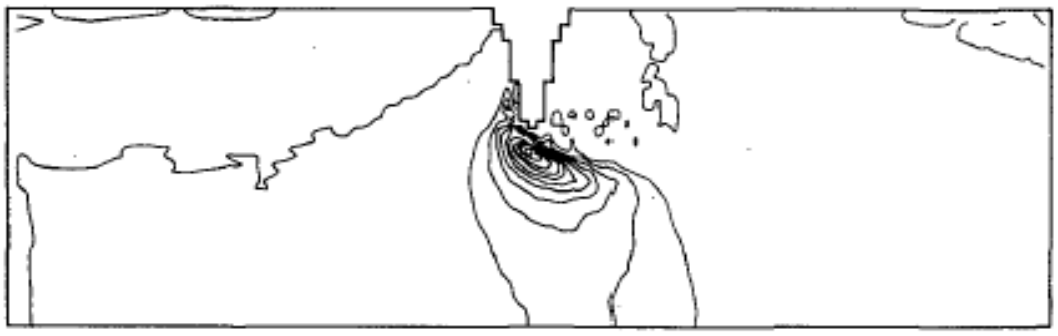

Figure 5.20 Erosion (interval=4mm/hr) in ESMOR model

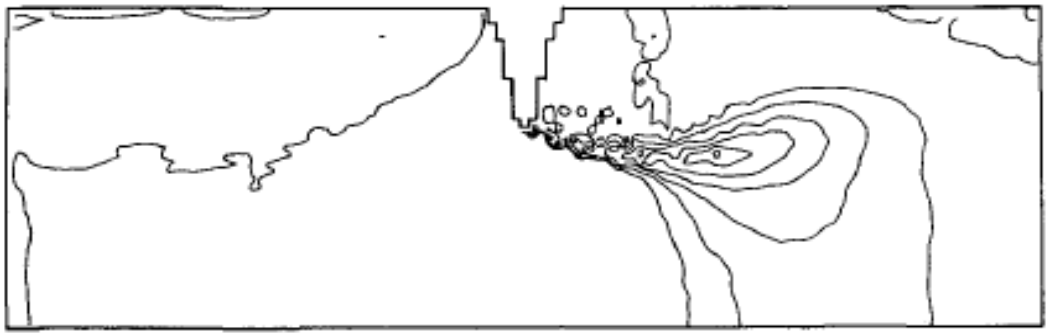

Figure 5.21 Sedimentation (interval=2mm/hr) in ESMOR model

The maximum erosion and deposition rates predicted in the headland vicinity using the different models are presented in Table 5.1

Table 5.1 The maximum rates for erosion and deposition in different numerical models

Maximum / Models	Erosion mm/hr	Deposition mm/hr
ESMOR	43	10.5
SUTRENCH	100	25
GEODIVAST	40.7	3.9
GEOTRIVAST	45.5	12.8
Presented model	40	11

The differences among the results depend on different model grids and the essence of different computational methods used in the model but generally the predictions are acceptable. By applying the 3D layer-integrated morphodynamic model for this case study, it was shown that the results obtained using the present model could reveal hydrodynamic, sediment transport and morphological changes process with a reasonable agreement with other numerical models.

5.4 Summary

This chapter presents two examples used to test the ability of the numerical model developed to compute hydrodynamic behavior, sediment transport and morphological processes. The numerical model has been set up based on geometry data and hydraulic parameters (boundary conditions and initial conditions) for flow and sediment transport belong to two cases and the model simulation involves all main modules (i.e. hydrodynamic, sediment transport and morphodynamic processes). The model results have been compared with laboratory measured data and other numerical model results and the present numerical model performed generally well.

Chapter Six

Model Application

6.1 Introduction

The central goal of this research is applying the enhanced numerical model for a real case study, i.e. Hamidieh regulated reservoir. In this chapter the abilities of the numerical model to predict hydrodynamic, sediment transport and morphodynamic phenomena for the complex hydraulic structure is demonstrated. Firstly, the chapter starts with a general description about Hamidieh regulated reservoir and relative hydraulic structures such as intakes, sluice gates and dam body, and the objectives and hydraulic attitudes. The chapter continues with an explanation of different scenarios on hydrodynamic, sediment transport and morphological changes, showing results and comparing them with the laboratory data. Finally, analyzing the results and evaluating the performance of the numerical model are presented.

6.2 A case study (Hamidieh Regulated Reservoir)

Hamidieh regulated reservoir is located 11 km away from Hamidieh town in the south-west of Iran. It has been constructed on Karkheh River downstream of Karkheh reservoir dam. There are two water intakes, one located on each side of the river, named Ghods and Vosaileh. Currently, Vosaileh water intake channel is 10.8 km long with a maximum discharge of $60\,m^3/s$, while Ghods intake channel is 25 km long with a maximum carrying capacity of $13\,m^3/s$ (see Figures 3.3 to 3.6).

Due to the development in irrigation and drainage networks of Azadegan and Chamran plains, the present conditions of the water intakes are not able to meet the water demand. Hence, it is necessary to increase the flow rates by designing new intakes.

Hamidieh reservoir dam is 192 m long, 4.5 m high with 19 spillway bays and 10 sluice gates. Azadegan water intake replaces Ghods, with an inlet width of 56 m, 8 bays under 4 sluice gates. It is intended to increase the carrying capacity from $13\,m^3/s$ to $75\,m^3/s$. Vosialeh water intake is replaced by Chamran, which has an inlet width of 86.6 m, 16 bays and 13

trash racks to increase the carrying capacity from $60\,m^3/s$ to $90\,m^3/s$ .Figure 6.1 showed a plan view of Hamidieh regulated reservoir and associated structures, see also chapter four.

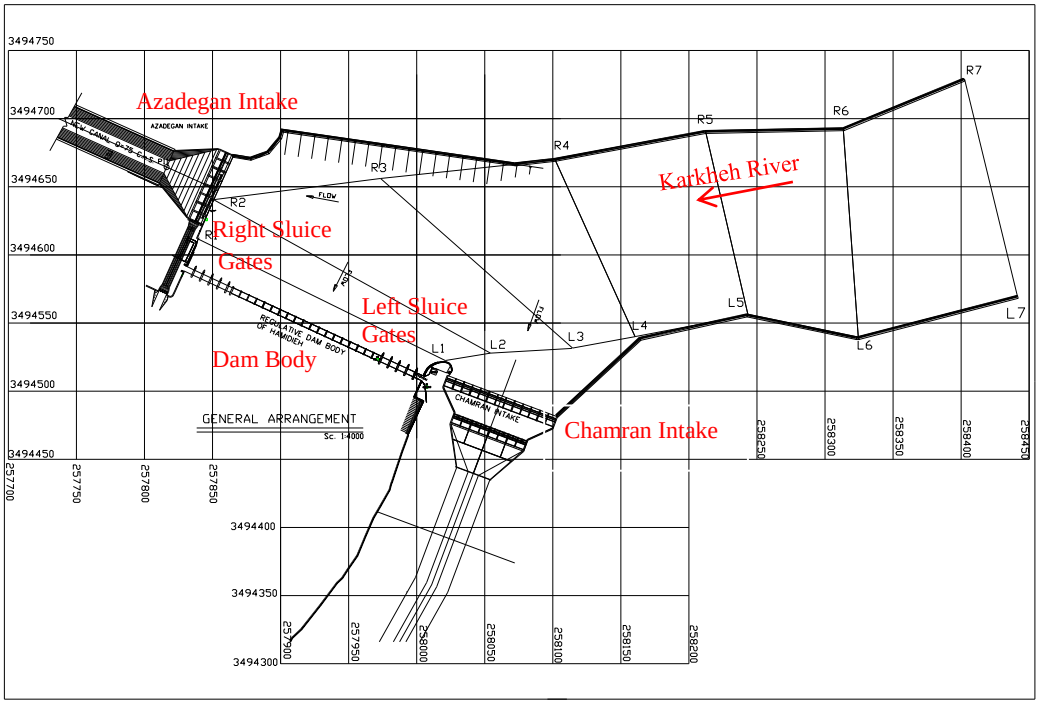

Figure 6.1 Plan view of Hamidieh regulated dam and associated structures

An undistorted 1:20-scale physical model of Hamidieh regulated reservoir and its relevant structures were constructed to investigate the operation of the entire system to improve the understanding of hydraulic flow and sedimentation process in the vicinity of the structures, see Chapter 3.

6.2.1 Objectives

A detailed numerical modelling investigation has been undertaken to simulate water flows through hydraulic structures and their interaction with sediments. Using a numerical model it is possible to examine various scenarios that are difficult to test in physical models. These scenarios are useful for hydraulic structure design, operation schemes and future maintenance. The main objectives of this numerical model investigation are as follows:

- To evaluate the numerical model for a practical engineering application with real and complex geometry, boundary conditions and different operation scenarios.
- To assess the capabilities of the 3D layer-integrated scheme on simulating hydraulic process.

- To reduce time and costs using numerical model to aid hydraulic structure designing and to test for various scenarios that are generally more difficult to test with a physical model.

6.3 Numerical model study

Physical and numerical models can be used jointly for designing hydraulic structures in order to understand better natural processes. This approach makes a joint platform for solving engineering problems and eliminates the cost. The numerical model has been set based on the size of physical model to gain same simulation on hydraulic parameters (Reynolds number, velocity and sediment sizes, grain Reynolds number and etc.) theoretically.

In recent years, several 3-D numerical models have been developed, for predicting hydrodynamic, sediment transport and morphodynamic processes and applied in different cases. Olsen and Kjellesvig (1999) undertook a 3-D numerical model study of bed changes in a sand trap. The numerical model results compared well with the measurements obtained from the physical model studies. Gessler et al (1999) developed a 3-D model of river morphology, which included separate solvers for bed load transport and suspended sediment transport. It considered several size fractions of sediment and recorded the bed composition and evolution during each time step. Kolahdoozan and Falconer (2003) developed a three-dimensional (3-D) layer-integrated morphological model for estuarine and coastal waters and compared the numerical model predictions with experimental measurements in a laboratory model harbour. They used the mixing length model for turbulence closure, and recommended that a fine mesh should be used in areas of severe erosion or deposition. Olsen (2003) and Rüther and Olsen (2003, 2005a, b) developed a fully 3-D model with an unstructured grid to represent the domain. They showed results from a simulation of meander evolution. Their work focused on the formation of alternate bars and the initiation of meandering starting from a completely straight channel.

In many research projects physical and numerical model were used jointly to understand the hydrodynamic and sediment transport behaviors. Stephan and Hengl (2010) used a physical model test aimed at improving the sediment movement through the backwater of a hydropower plant to reduce the flood risk of the town of Hallein. The 3D morphodynamic model SSIIM was applied to this case in order to investigate if the 3D model could reproduce the erosion and deposition pattern for such a complex situation. The numerical results agreed with the measured erosion and deposition patterns but not the absolute bed levels.

This part of research explains the main results of the numerical model and compares some of these results with the physical model results which is applied for a real case study namely Hamidieh regulated reservoir.

6.4 Flow and hydrodynamic simulation

The numerical model was set up based on the measurement data obtained from the physical model for various operation conditions of the intakes and sluice gates. The data included the general flow patterns and more detailed velocity distributions within the reservoir and in the vicinity of hydraulic structures. The bathymetry data and hydrodynamic scenarios were defined by using field surveyed data and laboratory data. Figure 6.2 shows the initial bathymetry of the reservoir and the intakes for the physical model scale.

One dredging zone located in front of Azadegan intake and close to the right bank, has been recommended in order to make a stable diversion flow into the intake for long term water supply operation. Numerical and physical model simulations have been undertaken to investigate the feasibility of this measure in improving the condition for supplying water.

Table 6.1 lists the hydraulic parameters used to set-up the numerical model for testing hydrodynamic model scenario. These parameters were chosen on the basis of the data obtained from the physical model experiments, in which the velocity distribution was measured in front of the two intakes.

Table 6.1 Hydrodynamic parameters of scenario S.1

NO		Hydraulic Boundary Condition	Turbulence Boundary Condition	Operation
S.1	Reservoir	Discharge 82.2 liter/s	Surface and Inlet	Water level (1.01 m)
	Az. Intake	Discharge 41.9 liter/s	Outlet	
	Ch Intake	Water Level (1 m)	Outlet	
	L S	Closed	-	
	R S	Closed	-	

Az Intake= Azadegan Intake, Ch Intake= Chamran Intake,
L S= Left sluice gate and R S = Right sluice gate

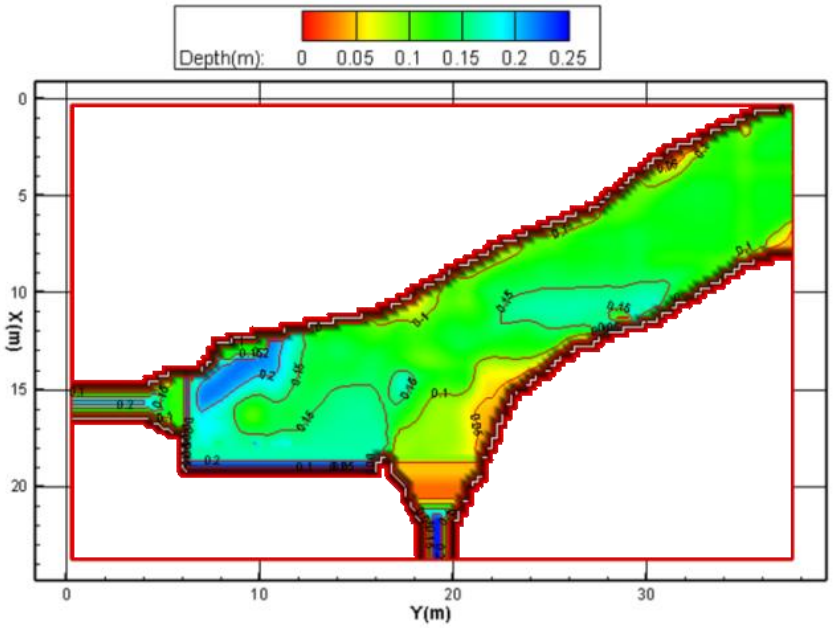

Figure 6.2 The initial bathymetry of Hamidieh, physical model scale

In the physical model study the velocity was measured at several points in front of the intakes by current-meters. The locations of these points were shown in the Figures 3.18 and 3.19. In this study, the velocity measurements at these points, together with the observed water surface levels were used for calibrating the hydrodynamic model.

In the physical model study, the velocity was measured by a current-meter at $0.6D$ (D= water depth) from the water surface and fitted to the physical scale. This depth had been chosen based on velocity logarithmic profile assumption.

In applying the 3D layer integrated model to this case study the water depth was divided into 5 vertical layers. The thickness of the layers was all set to 0.057m except for the top layer, which was set to 0.051m in the main channel. The grid size was set to 0.25m. The water surface level was calibrated by comparing the water surface levels obtained from the physical model and those predicted by the numerical model, with the difference being found to vary between 0.0022m and 0.0055m. Roughness height was used as the calibration parameter. Table 6.2 lists the velocity values for different locations shown in Figures 3.18 and 3.19 for both the physical and the numerical models.

Efforts have been made to use the measured data for better calibration but it was not possible to test and measure hydraulic parameters for more scenarios and locations. Despite these limitations, the comparisons made using the available data in Table 6.2 shows that the trend and quantities of velocity values obtained from the numerical and physical models are in an

acceptable level of agreement for this complicated situation. In this hydrodynamic scenario 24 gates operated simultaneously and with a real bathymetry being used. The numerical model results show that the magnitude of the vertical eddy viscosity is from 10 up to 50 times larger than the corresponding horizontal eddy viscosity in different areas (see Figure 6.6).

The results obtained from both physical and numerical models are presented for the undistorted 1:20-scale model of Hamidieh regulated reservoir. The flow pattern and velocity contours in the reservoir were calculated by the numerical model and illustrated in Figure 6.3 (for scenario S.1). The speed profiles along the depth predicted by the numerical model for scenario S.1 at 4 points near of the intakes (B&F for Azadegan and M&N for Chamran) were shown in Figure 6.4. The measured velocity at $0.6D$ from the water surface in the physical model is also shown in this diagram.

Table 6.2 Comparison between velocity values obtained from numerical and physical models for scenario S.1

Location	Points	Measured (cm/s)	Calculated (cm/s)
Chamran	A	3.09	4.0
	B	5.91	6.08
	M	6.59	7.21
	C	5.91	6.63
	D	3.10	3.89
	E	3.08	3.86
	F	5.27	5.94
	N	6.40	7.24
	G	5.18	6.53
	H	3.59	3.89
Azadegan	A	3.97	4.70
	B	4.13	4.31
	C	4.46	5.15
	E	3.18	3.54
	F	4.25	3.73
	D	3.18	3.59

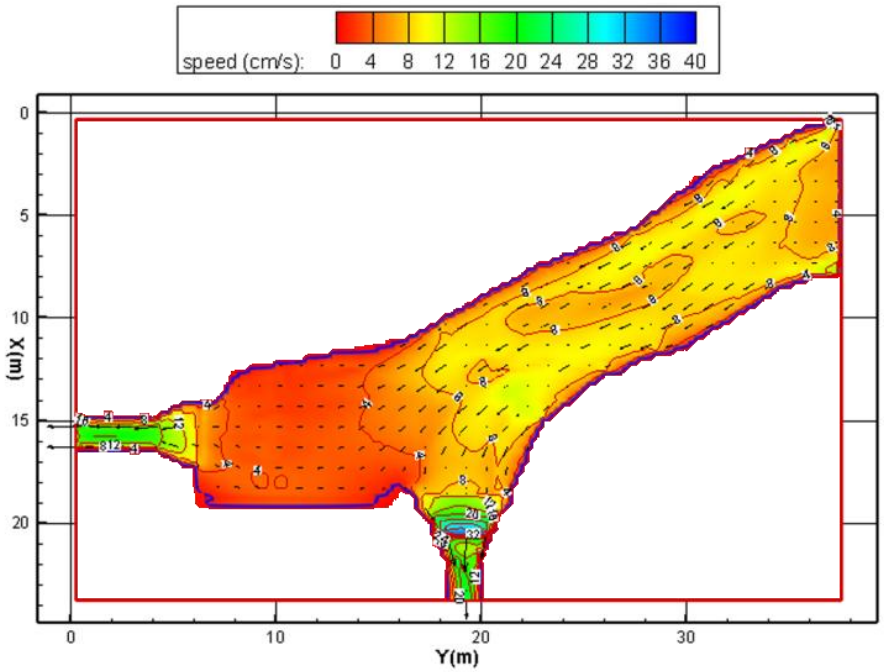

Figure 6.3 Numerical model predicted flow pattern and speed contours for scenario S.1

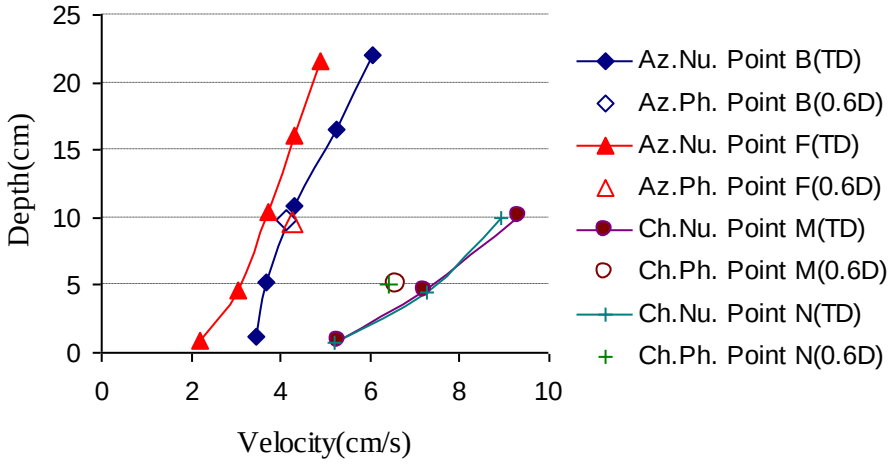

Figure 6.4 Model predicted velocity distributions and measured velocities at 0.6D from water surface for scenario S.1 (Az=Azadegan Intake, Ch=Chamran Intake, Nu=Numerical, Ph=Physical and TD=Total Depth (i.e. calculated by 3D layer-integrated numerical model along whole depth))

From Figure 6.4 it can be seen that the mathematical model predicted velocity values agree reasonably well with measured ones from the physical model although some variations can be observed. The type of turbulence model has an important role in predicting the speed parameters. For the model simulations reported herein, predictions were obtained using a layer integrated three-dimensional hydrodynamic and sediment transport model and also

switched to one layer for calculating depth-integrated flow and sediment transport parameters. In this model a two-equation turbulence model was used, with details of the governing equations and boundary conditions being given in Chapter 4. The original mathematical model was developed by Hakimzadeh and Falconer (2007) for simulating re-circulating flows in tidal basins. Some improvements were made in the model in order to predicting the flow, sediment transport and morphological processes in a river flow regulated reservoir (added a module for calculating morphodynamic and numerical techniques for running different boundary conditions). These improvements enhance the abilities of the existing numerical model. During the early stage of this research, 2D DIVAST model was also used, in which the mixing length theory was used to model turbulent flow. The results were not encouraging, especially for predicting velocity distributions in front of the two intakes. For this reason, the numerical simulation was carried out based on computing vertical eddy viscosity by using $k - \varepsilon$ turbulence model.

After calibrating the numerical model with the result of physical model (scenario S.1), two scenarios have also been designed for better understanding about the flow pattern and velocity parameter in the regulated reservoir. Different turbulence boundary conditions were set for the numerical model based on the formulas explained in Chapter 4. The attitudes of those scenarios are presented in Table 6.3. The numerical model is been switched to 1 layer for these two scenarios (i.e. depth-integrated).

Table 6.3 The characteristic for extra hydrodynamic scenarios

NO		Hydraulic Boundary Condition	Turbulence Boundary Condition	Operation
S.2	Reservoir	Discharge 92.2 liter/s	Surface and Inlet	Water level (1.0225 m)
	Az. Intake	Discharge 41.9 liter/s	Outlet	
	Ch Intake	Water Level (1 m)	Outlet	
	L S	Discharge 5.6 liter/s	Outlet	
	R S	Closed	-	
S.3	Reservoir	Discharge 135 liter/s	Surface and Inlet	Water level (1.0225 m)
	Az. Intake	Discharge 41.9 liter/s	Outlet	
	Ch Intake	Water Level (1 m)	Outlet	
	L S	Discharge 25.2 liter/s	Outlet	
	R S	Discharge 25.2 liter/s	Outlet	

Az Intake= Azadegan Intake, Ch Intake= Chamran Intake,
L S= Left sluice gate and R S = Right sluice gate

The flow pattern and velocity contours in the regulated reservoir for these two scenarios were calculated by the numerical model and illustrated in Figure 6.5 (a, b). As can be seen from the results (scenarios S.2 and S.3), when sluice gates could release more water discharge flow velocity near Chamran intake rises significantly and this condition will improve the performance of this intake. In other word, the possibility of sedimentation in the vicinity of this intake would be reduced.

(a)

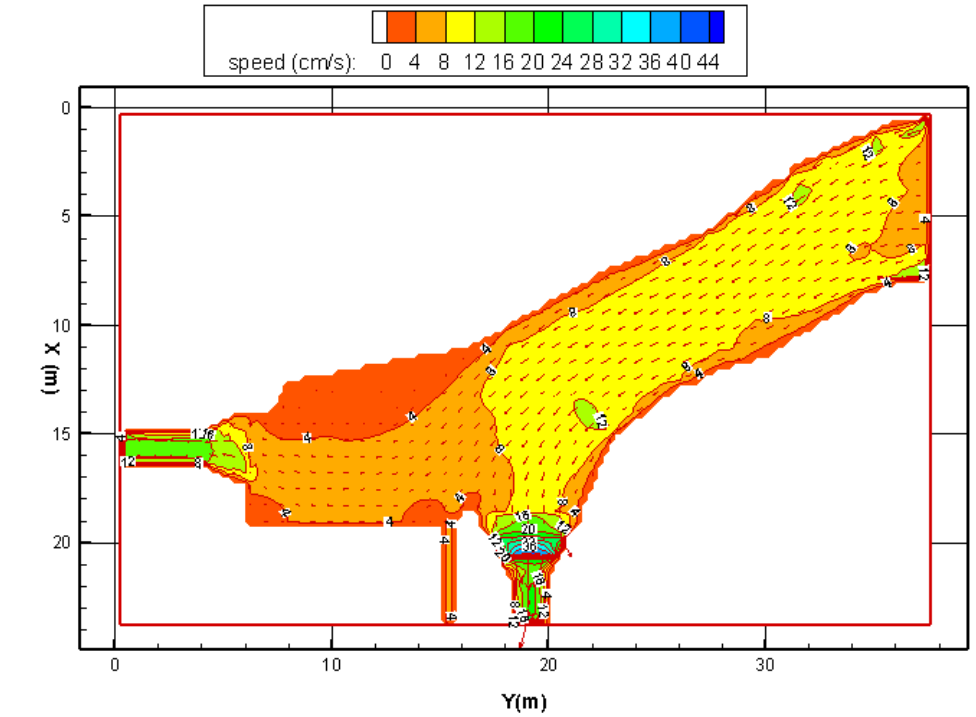

(b)

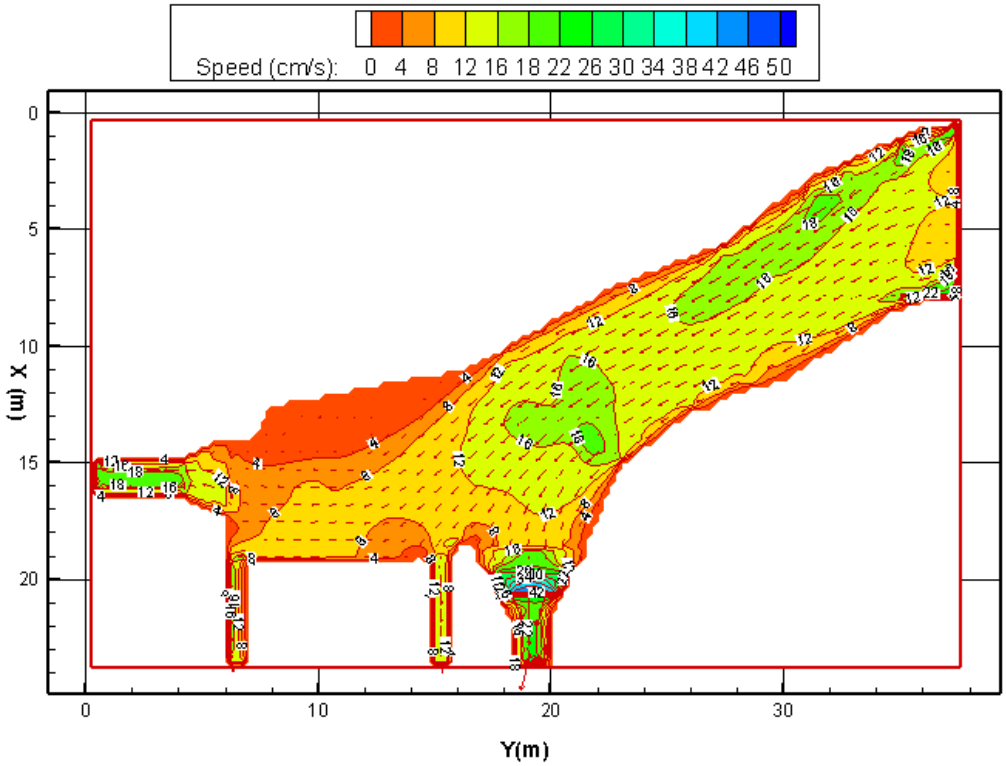

Figure 6.5 Numerical model predicted flow pattern and speed contours for (a) Scenario S.2 and (b) Scenario S.3

Figure 6.6 contains the results of depth integrated horizontal eddy viscosity and layer integrated vertical eddy viscosity for each layer in this case study (For scenario S.1). The layer integrated vertical eddy viscosity is calculated by the $k-\varepsilon$ turbulence model.

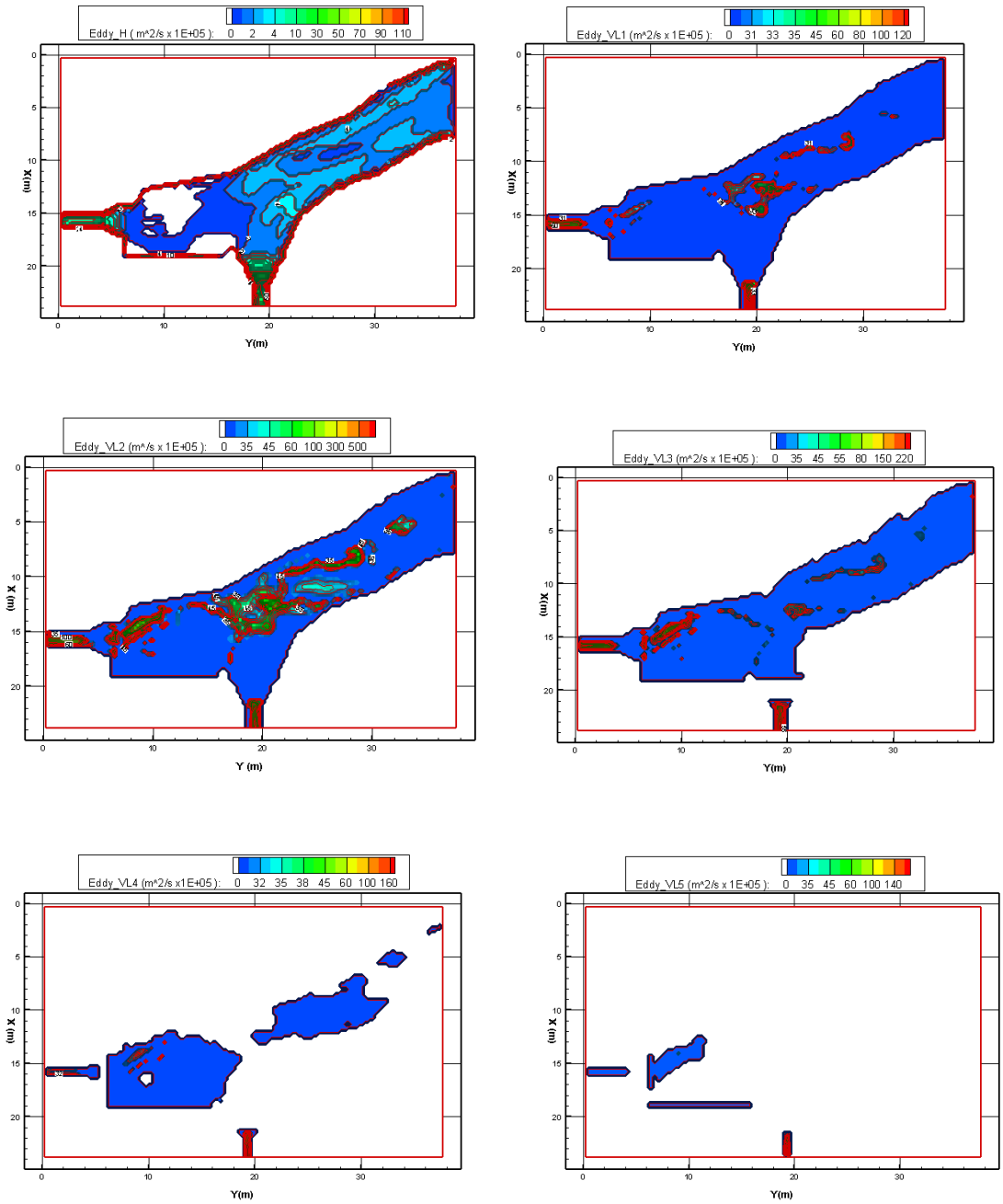

Figure 6.6 Eddy viscosity results (Eddy_H= depth integrated horizontal eddy viscosity and Eddy_VL1…5= layer integrated vertical eddy viscosity for each layer) for hydrodynamic scenario S.1

An analysis of the hydrodynamic results identifies two main issues:

-According to the observation of the flow direction, it is noticed that a non-uniform velocity distribution zone exists upstream of Chamran intake on the left bank. This is thought to be related to the location of the intake.

- The velocity pattern for the regulatory condition at the artificial dredging zone (in front of Azadegan intake) indicates that this is a location for high potential sedimentation.

6.5 Sediment transport simulation

For simulating sediment transport in hydraulic systems information such as particle size distribution, inflow discharge and associated sediment discharge, type of sediments (cohesive or non-cohesive) and understanding the dominant process of sediment transport (suspended load or bed load) in the nature are required. Previous studies have showed that the suspended transport is the dominant process for existing situation in this case (WEOKP 2001). The majority of sediment found in this region belongs to non-cohesive type. One of the most important tasks is to prevent sediments from entering the intakes. Any sediment particles deposited into the irrigation canals would cause a decrease in the flow rate. Currently, the stakeholders of the irrigation network have to dredge the canals periodically. In designing the new system of Hamidieh regulated reservoir a great effort has been made to mitigate the sedimentation problem in canals.

In this research, various scenarios were considered in order to determine the amount of sediments entering the intakes (see Table 6.4). Details are given below of the numerical model study of the sediment transport process. The numerical model predictions were compared with the physical model results at five sites. The plan of these sites was shown in Chapter 3 at Figure 3.24.

Table 6.4 Main parameters for sediment transport scenarios

No		Operation	Boundary Condition	Concentration gr/liter
S.4	Reservoir	Water level 1.0225 m	Discharge 87.2 liter/s	0.4724
	Az Intake	-	Discharge 41.9 liter/s	-
	Ch Intake	-	Water level 1 m	-
	L S	-	-	-
	R S	-	-	-
S.5	Reservoir	Water level 1.0225 m	Discharge 92.2 liter/s	0.6724
	Az Intake	-	Discharge 41.9 liter/s	-
	Ch Intake	-	Water level 1 m	-
	L S	-	Discharge 5.6 liter/s	-
	R S	-	-	-
S.6	Reservoir	Water level 1.0225 m	Discharge 135 liter/s	1.3391
	Az Intake	-	Discharge 41.9 liter/s	-
	Ch Intake	-	Water level 1 m	-
	L S	-	Discharge 25.2 liter/s	-
	R S	-	Discharge 25.2 liter/s	-
General data	d_{16}, d_{50}, d_{84} & $d_{90} = 0.035, 0.057, 0.139$ & $0.175\ mm$ *Specific gravity= 2.67, Grid size= 0.25 m* and *Computational time=360 min with Intel(R) Core(TM)2 Quad CPU Q8400 @ 2.66 GHz*			

Az Intake= Azadegan Intake, Ch Intake= Chamran Intake,
L S= Left sluice gate and R S = Right sluice gate

The numerical model scenarios were selected based on the laboratory tests. The model predicted patterns of the suspended sediments concentrations are shown in Figures 6.7, 6.8 and 6.9, for scenarios S.4, S.5 and S.6, respectively. The suspended sediment concentrations computed by the numerical model agreed quite well with the ones measured from the physical mode. The maximum error is less than 21.3% and the averaged error is less than 8.3%, which seems acceptable considering the overall complexity of the sediment transport processes. The sampling of suspended sediment concentration in the physical model was taken along the whole depth and calculated using a depth integrated formula. Table 6.4 shows a comparison between the measured (in the physical model) and calculated (by the numerical model) suspended sediment concentrations at the locations shown in Figure 3.24. From Figures 6.7, 6.8 and 6.9, the movement of suspended sediment in the reservoir, over the intakes and sluice gates can be clearly seen.

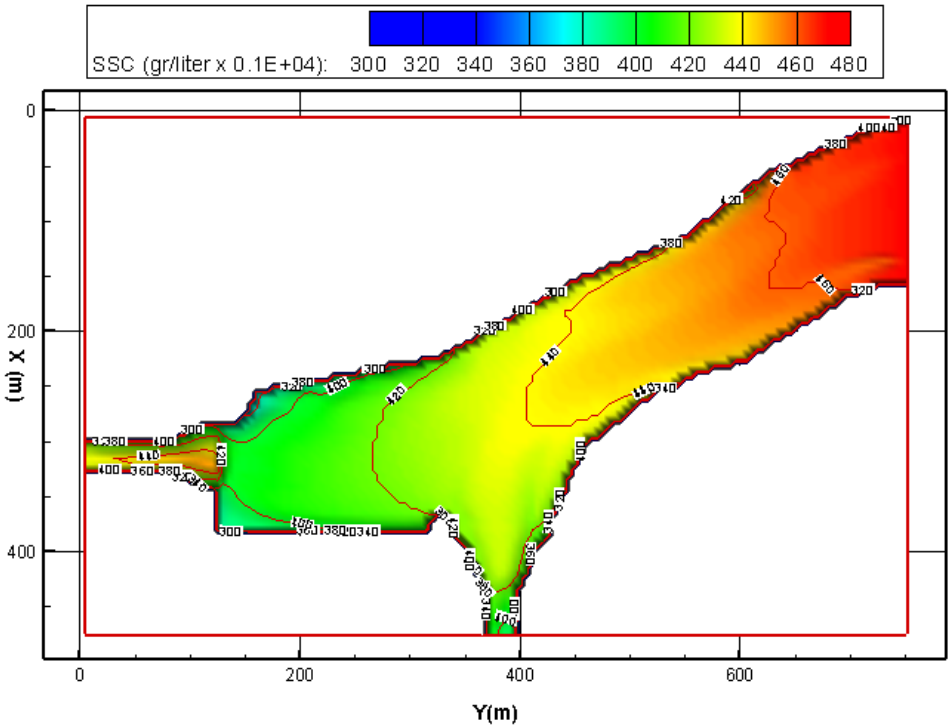

Figure 6.7 Pattern of suspended sediments concentrations (SSC), scenario S.4

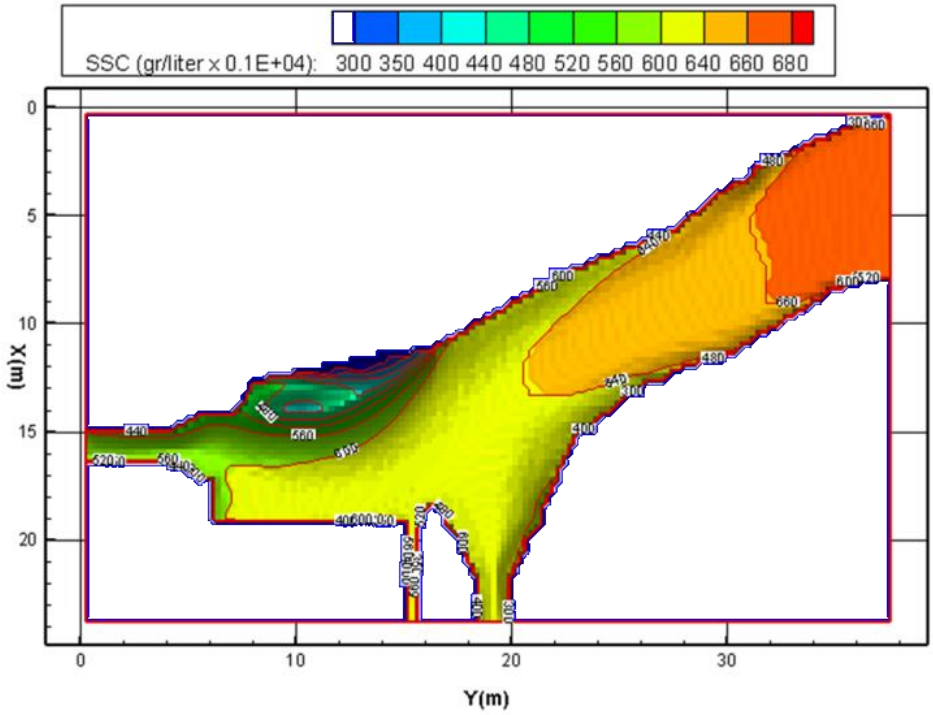

Figure 6.8 Pattern of suspended sediments concentrations (SSC), scenario S.5

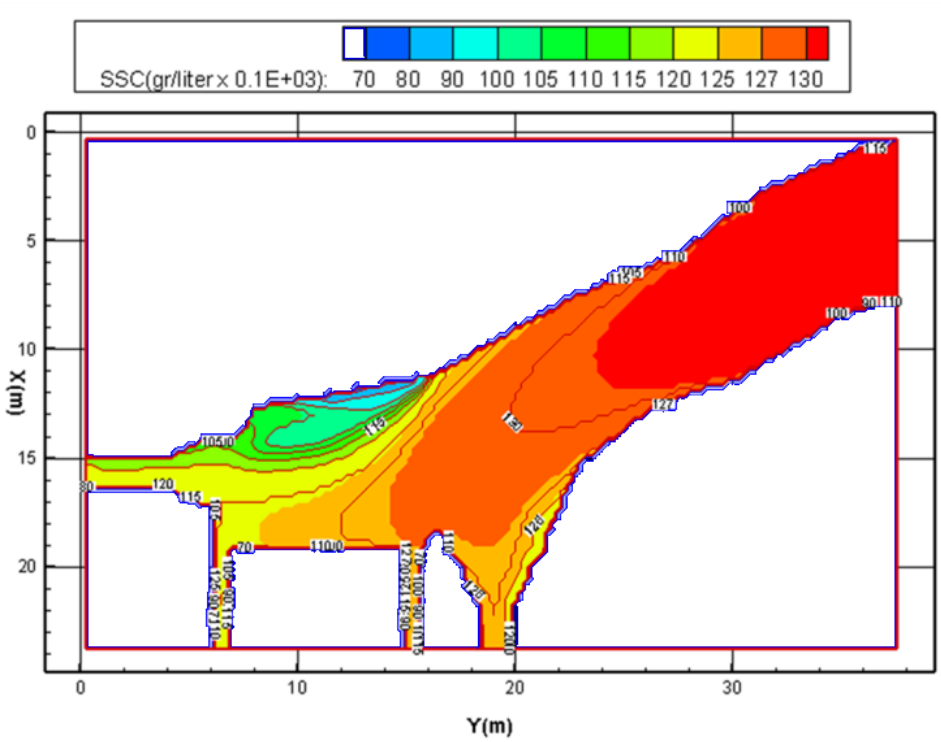

Figure 6.9 Pattern of suspended sediments concentrations (SSC), scenario S.6

Table 6.5 SSC measured and predicted at sampling points

No	Points	SSC (Measured) gr/liter	SSC (Calculated) gr/liter	|Error|* %
S.4	CRL	0.401	0.452	12.72
	CRM	0.423	0.456	7.8
	CRR	0.417	0.452	8.39
	CAZ	0.396	0.401	1.26
	CCH	0.433	0.434	0.23
S.5	CRL	0.563	0.645	14.56
	CRM	0.638	0.651	2.04
	CRR	0.605	0.645	6.61
	CAZ	0.618	0.589	4.69
	CCH	0.681	0.619	9.10
S.6	CRL	1.18	1.3	10.17
	CRM	1.38	1.31	5.07
	CRR	1.12	1.3	16.07
	CAZ	0.99	1.20	21.21
	CCH	1.11	1.25	12.61

* |Averaged Error|=8.28%, SSC= sediment suspended sediment, Measured= measured in the physical model and Calculated= calculated by the numerical model

The scenarios are designed in three categories. The characteristics of these scenarios are:

- Low flow condition without sluice gates (scenario S.4).

- Low flow condition with one sluice gate (scenario S.5).

- High flow condition with sluice gates along both sides of the dam in operation (scenario S.6).

The attributes of the scenarios are presented in Table 6.4. The results showed that the suspended load has an important role in the sediment transport process and is closely related to particle size. A good agreement has been observed between the SSCs obtained from numerical and the physical models. The analysis of the sediment transport results identifies that:

(i) The suspended sediment concentration in Chamran intake is higher than the one in Azadegan intake. The main reason is thought to be the location of the intakes. Chamran intake is located in the internal curve position when considering the layout of the system.

(ii) The pattern of the suspended sediment movement in the reservoir has showed that the sediment entering rate to Chamran intake is affected very little by the sluice gate operation schemes. It means that the sluice gates on the left side do not have a considerable effect on reducing the suspended sediment concentration moving through Chamran intake.

(iii) It seems that the problem of sediment entering the intakes is remained. The layout of these hydraulic structures is only part of the reason for this problem. The natural system of sediment transport and the size of the sediments have an important role for this situation.

6.6 Morphodynamic

Details are first given below of the numerical model predictors of the morphological changes in the Hamidieh regulated reservoir. The model simulation was based on field surveyed data and laboratory data obtained from the physical model for various operation conditions of the intakes and sluice gates. The hydrodynamic and sediment transport studies were presented in the two above sections before. The bathymetry data and morphodynamic scenarios were defined by using field surveyed data and laboratory measured data. The initial bathymetry of the reservoir and the intakes in the physical model scale was plotted in Figure 6.2. Table 6.6 lists the hydraulic and sediments parameters used to set-up the numerical model for testing the morphodynamic model scenarios. These parameters were chosen on the basis of the data obtained from the physical model experiments.

Table 6.6 Main hydraulic and sediment parameters for morphodynamic scenarios

No		Operation	Boundary Condition	Concentration (gr/liter)	Time for simulation (hour)
S.7	Reservoir	Water level 1.0225 m	Discharge 70.9 liter/s	0.2321	48.5
	Az Intake	Opened	Discharge 41.9 liter/s	-	
	Ch Intake	Opened	Water level 1.0225 m	-	
	L S	Closed	-	-	
	R S	Closed	-	-	
S.8	Reservoir	Water level 1.0225 m	Discharge 95.3 liter/s	0.679	8
	Az Intake	Opened	Discharge 39.7 liter/s	-	
	Ch Intake	Opened	Water level 1.0225 m	-	
	L S	Opened	Water level 1.0225 m	-	
	R S	Closed	-	-	
S.9	Reservoir	Water level 1.0225 m	Discharge 167.7 liter/s	2.122	8
	Az Intake	Opened	Discharge 39.7 liter/s	-	
	Ch Intake	Opened	Water level 1.0225 m	-	
	L S	Opened	Water level 1.0225 m	-	
	R S	Opened	Water level 1.0225 m	-	
General data	d_{16}, d_{50}, d_{84}& $d_{90} = 0.035, 0.057, 0.139$ & $0.175\ mm$, *Specific gravity= 2.67, Grid size= 0.25 m*				

Az Intake= Azadegan Intake, Ch Intake= Chamran Intake, L S= Left sluice gates and R S = Right sluice gates

The investigation is focused on the bed level changes in the areas close to the intakes and sluice gates. In this section, efforts have been also made to use the measured data for better calibration and to test the capability of the numerical model. The results obtained from both physical and numerical models are presented for the 1:20-scale model of Hamidieh regulated reservoir. For simulating the morphodynamic processes information such as particle size distribution, inflow discharge and associated sediment discharge, type of sediments (cohesive or non-cohesive) is required. An understanding of the dominant process of sediment transport (suspended load or bed load) in the field is also important. Previous studies showed that the suspended transport is the dominant process for this case. The majority of sediment found in this region belongs to non-cohesive type. In the numerical model, the scenarios were selected on the basis of the laboratory tests. van Rijn's (1984) formula was used to calculate the sediment transport rate. As can be seen from Table 6.6, scenario S.7 was run for much longer time compared with scenarios S.8 and S.9 and was a special condition for this physical test. For this scenario, sediments injection has continued until the same concentrations among input and output opening boundaries in the hydraulic model being reached. The bed level changes were computed by the morphodynamic module. The numerical model predictions (for scenario S.7) were compared to the physical model results at 6 section profiles that

recognized in the Hamidieh reservoir in Figure 6.1 before. Profiles 1, 2 and 3 would be extended for covering the whole area in the vicinity of Chamran intake.

From Figures 6.10 it can be seen that the mathematical model predicted bed level changes agree reasonably well with the measured ones from the physical model, although some differences can be observed. In most locations computational results of bed level changes are less than the physical results. The predicted bed level change at L6-R6 is greater than the measured one. This is thought to be due to a problem in the sediment injection system. It was observed that some dry sediment injected into the reservoir from the river boundary (section L7-R7) could not mix well initially and are settled and deposited near the injection system (section L6-R6).

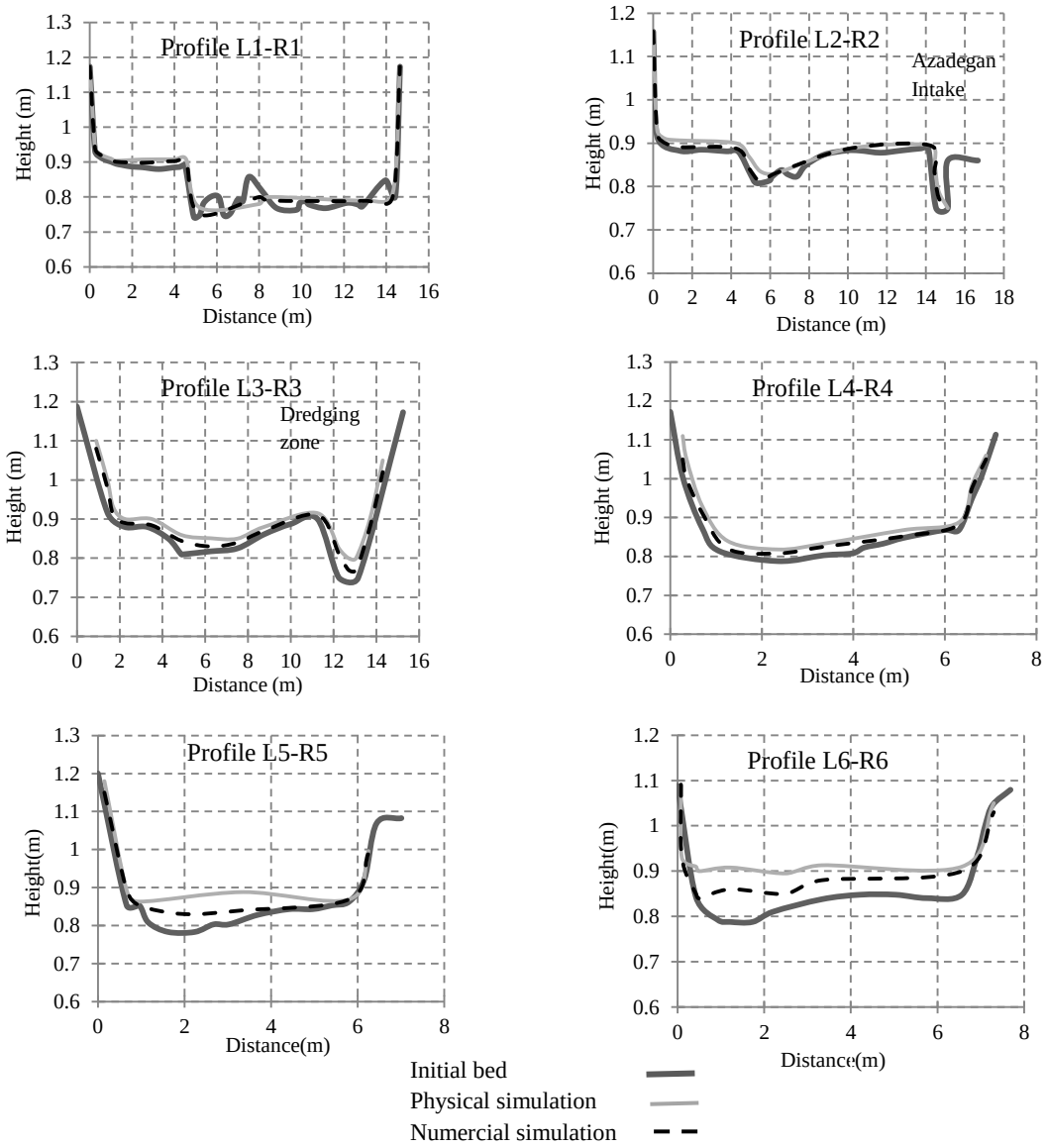

Figure 6.10 Bed level changes after 48.5 hours in 6 section profiles (scenario S.7)

Figure 6.11 shows the initial bathymetry used for simulating scenarios S.8 and S.9. The morphological changes were computed by the developed numerical model and the results related to scenarios S.8 and S.9 have been presented in Figures 6.12 and 6.13. A general investigation on the results shows that the mathematical morphodynamic model can reveal the all main features observed in the physical model with an acceptable accuracy range.

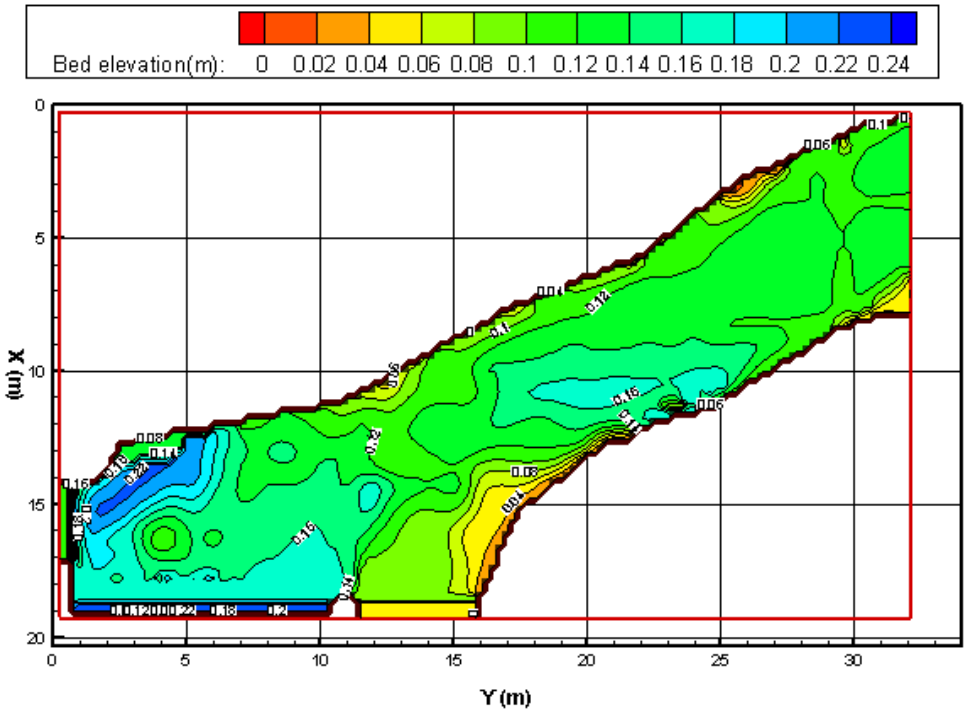

Figure 6.11 Initial bathymetry for scenarios S.8 and S.9

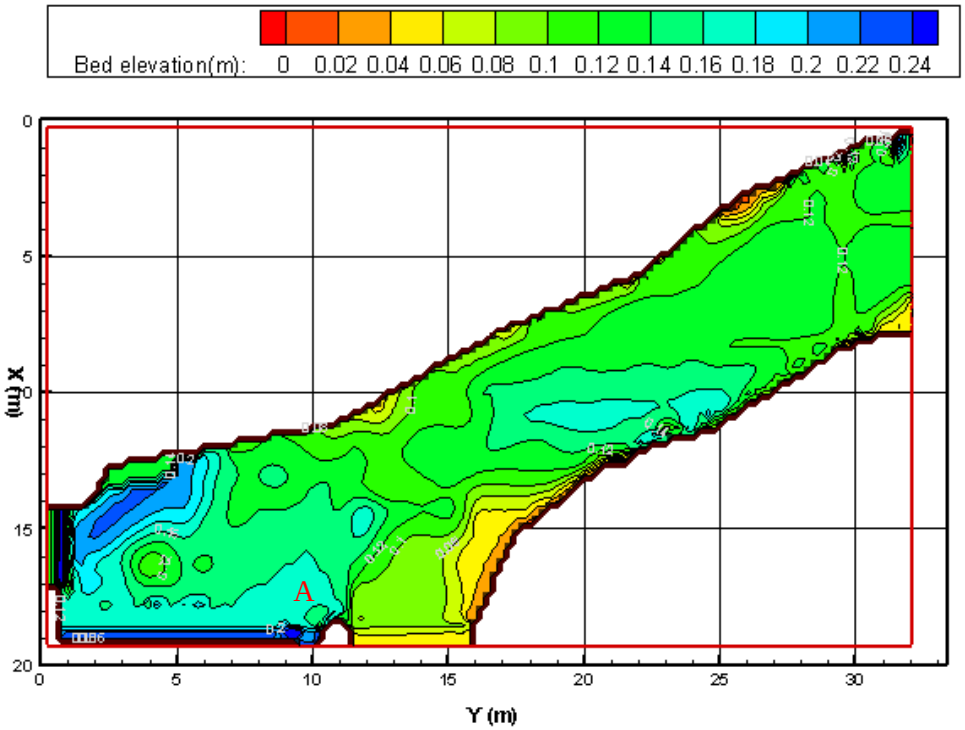

Figure 6.12 Computed bathymetry after 8 hours for scenario S.8

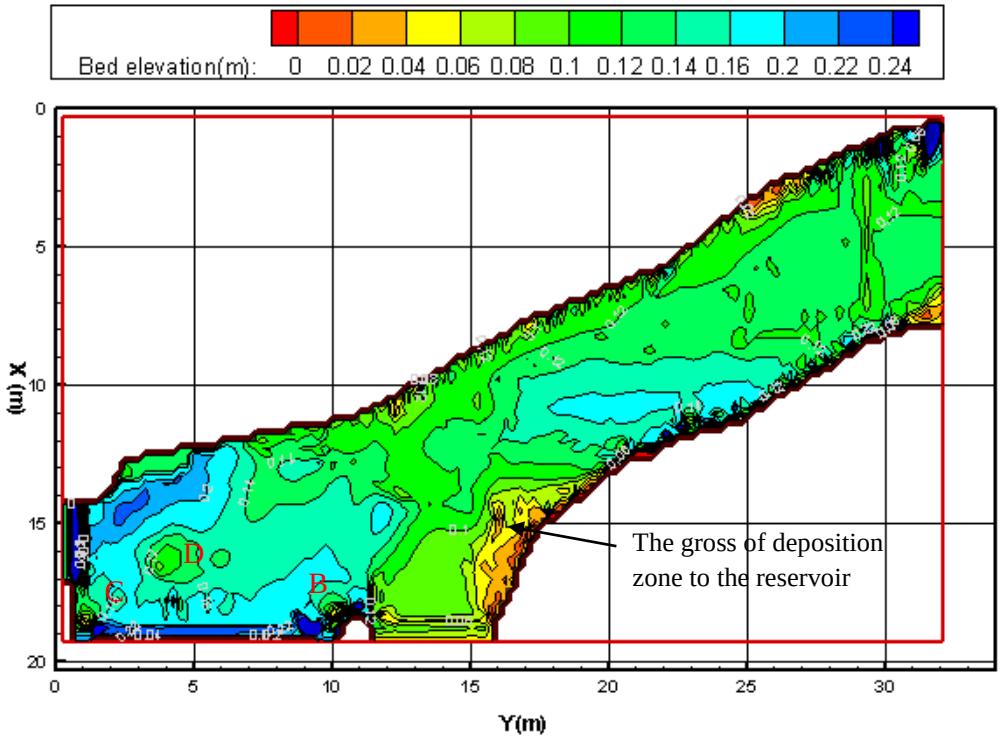

Figure 6.13 Computed bathymetry after 8 hours for scenario S.9

The analysis of the morphological results identifies that:

(i) A deposition zone is formed in front of Chamran intake (right corner) and the prong of this sedimentation zone moves to the reservoir and it will reduce the amount of diverted flow into this intake. This consequence has occurred for all of scenarios (S.7, 8 & 9), but the rate of sedimentation in this zone was predicted in difference values according to hydraulic and sediment conditions for every scenario. This bed evolution trend is presented in Figure 6.13 and profiles L1-R1, L2-R2 and L3-R3 in Figure 6.10 obviously.

(ii) When the sluice gates are open the numerical model predicted a scour hole in front of those gates. This hole is local and does not have any considerable effect on the sediment flashing and settling processes in front of the intakes (Figures 6.12, Location A and 6.13, Locations B & C).

(iii) One dredging zone in front of Azadegan intake close to the right bank has been recommended in order to make stable diversion flow into the intake for the long term water supply operation (see Figure 6.2). The results related to scenario S.9 shows that the sedimentation rate in this zone is much higher than other locations. There is a high potentially of sedimentation at the artificial dredging zone.

(iv) The model predictions indicate that there is a possibility of sedimentary islands being formed in the upstream of the intakes, since the regulated hydraulic regime resulted in a high value of sediment concentration (see Figure 6.13, Location D).

6.7 Conclusion and discussion for the results of numerical model

This chapter presents the application of a three-dimensional numerical morphodynamic model to predict the flow, sediment transport and the morphological changes in a river regulated reservoir, named Hamidieh Reservoir. The aim of the study was to present the understanding of the abilities of the numerical model in simulating these complex processes in a real case. In order to represent the complex turbulent flows in the vicinity of hydraulic structures, a two-equation turbulence model was used. A physical model measurement was also undertaken. Detailed laboratory measurements were conducted to measure velocity distributions at a number of points near the intakes, and suspended sediment concentrations were measured at different points in the reservoir. Also, specific laboratory measurements were made to determine the bed level changes at 6 cross-sections in the reservoir. Numerical model predictions were compared with the laboratory measured data. A series of scenario runs of the operation schemes revealed the governing phenomena in the system to a certain extent. The results obtained from the investigation confirm these technical issues:

(i) A non-uniform velocity distribution zone exists upstream of Chamran intake on the left bank side.

(ii) In the recommended dredging zone, located in front of Azadegan intake, there is a high risk of significant sedimentation.

(iii) The location of Chamran intake has a considerable impact on the suspended sediment moving through the intake and making the formation of the sedimentation zone in the areas adjacent to the intake.

(iv) The sluice gates operation scheme did not have any considerable impact on the sediment flushing capability in areas close to the intakes.

(v) The possibility of forming island in the reservoir is predicted by the numerical model.

(vi) The results of this research indicate that the calibrated numerical model could be used in the hydraulic design. By this method, the laboratory tests are reduced and thus time and budget are optimized.

It should be pointed out that simplifications and assumptions have been made in both the physical and numerical models presented in this paper and they will have an impact on the accuracy of the model results.

From the evaluation of the numerical results the following scientific features were found:

i) The 3D layer-integrated scheme used in the mathematical model revealed the main hydrodynamic, solute transport and morphodynamic issues with a high degree of accuracy for the cases considered and, in essence, the flow was basically fully three dimensional. By using the layer integrated scheme the computational time reduces significantly in comparison with fully 3-D scheme and the accuracy of the results are in an acceptable range. This is thought to be the first time using this numerical model for simulating in regulated dam case study.

ii) The computed suspended sediment concentrations by the 3D layer-integrated model for this case study agreed well with the ones measured from the physical model (see Table 6.5). To acquire this level of accuracy, the hydrodynamic computational scheme and the selected turbulence model play an important role. The results of this research showed that the selection of the $k-\varepsilon$ turbulence model in regulated reservoir where the Reynolds number is high but without any significant local vortex near hydraulic structures (such as gates) was the correct choice.

iii) An explicit method was used for discretizing the bed level change equation. This scheme is compatible with the structure of mathematical solution for hydrodynamic and sediment transport modules of the numerical model.

6.8 Summary

This chapter presents the application of the developed numerical model to compute the hydrodynamic behavior, sediment transport and morphological changes for an engineering case study. River regulated reservoirs are often constructed downstream of dams, with relatively low elevations, thereby enabling the flow to be distributed for water supply purposes. However, there are major differences between these regulatory reservoirs and those associated with normal high head dams, in that strong turbulent flows are generated in the regulated reservoir due to the high volumes of flow diversion. An enhanced turbulence model ($k-\varepsilon$) was used to represent the complex flow pattern in the vicinity of hydraulic structures. In this research, the numerical model is developed and applied to a regulated reservoir dam, associated with water intakes and sluice gates, and the model is used to investigate the flow patterns, sediment transport processes and morphodynamic in the vicinity of the various hydraulic structures. Calibration of the model was undertaken using previously made scaled physical model measurements. In this context different scenarios were introduced to study the effect of different intake and sluice gate configurations, as well as establishing how their operation affected the flow, sediment transport processes and morphodynamic in Hamidieh Reservoir. The results related to all modules (hydrodynamic, sediment transport and morphodynamic) have been computed. The numerical results were agreed with laboratory tests in a reasonable accuracy.

Chapter Seven

Conclusions and Recommendations

7.1 Summary of the research

In the thesis a 3D layer-integrated morphodynamic model has been presented. The governing equations used to describe the morphodynamic processes include: the hydrodynamic, sediment transport and bed-sediment mass balance equations, with the two-equation $k-\varepsilon$ model being used for turbulence closure. The hydrodynamic governing equations are solved based on a combined layer-integrated and depth-integrated scheme, in which the finite difference scheme for a regular square mesh is used in the horizontal plane, and a layer-integrated finite difference scheme is used on an irregular mesh in the vertical. The operator splitting technique and a highly accurate finite difference scheme have been used to solve the suspended sediment transport equation. The depth-integrated mass balance equation for sediment transport is derived using a control volume in the water body from the bed to the water surface and applying the mass conservation law.

In this research study a new version of the TRIVAST model has been developed to predict the hydrodynamic, sediment transport and morphological changes in a regulated reservoir. This model was applied to a scaled hydraulic model using the two- and zero-equation turbulence models as outlined by Hakimzadeh and Falconer (2007).

Some improvements, including numerical techniques for running different boundary conditions and irregular mesh sizing in the vertical layer, were included in the model. These improvements enhanced the ability of the existing numerical model and to the author's knowledge this is the first time a 3D layer-integrated model has been applied to a regulated reservoir case study.

A numerical module including a proposed mathematical scheme has been developed and added to the 3D layer-integrated model (TRIVAST) for solving the bed level change equation. In solving the governing equations for predicting bed level changes, an explicit finite difference scheme was deployed. In contrast the hydrodynamic and sediment transport modules were solved with an alternating direction implicit finite difference scheme.

The verification of the numerical model has been done by applying the model to two widely used test cases. The numerical model results were also compared with the results obtained from other numerical models, such as by Wang (1989) and Kolahdoozan and Falconer (1999). The model predictions agreed generally closely with the measured data and the other numerical model results.

A physical model was constructed to represent the flow, sediment transport and morphodynamic processes in Hamidieh regulated reservoir. The study procedures, including the design scale, model construction and measurements, were carried out in the Water Research Institute in Iran by the author. The physical model was designed based on the Froude law of scaling and was undistorted. The model sediment size was determined in such a manner that the same ratio of the particle's fall velocity to shear velocity was maintained for both the model and prototype reservoir. Stokes law was used in calculating the particle fall velocity.

The enhanced numerical model was then applied to the scaled physical model of the regulated reservoir. Regulated dams are often constructed downstream of large reservoirs, with relatively low elevations, thereby enabling the flow to be distributed for water supply purposes. There are major differences between these regulatory reservoirs and those associated with normal high head dams, in that strong turbulent flows are generated in the regulated reservoir due to high volumes of flow with low head differences.

A combined numerical and physical modelling approach has many benefits for designing a hydraulic structure. In this thesis, especially in chapters 3, 5 and 6, these benefits are discussed in detail. In the physical model study many techniques were designed for better performance of the model. Sediment material used in this physical model was obtained from broken pottery (baked clay). This material is non-cohesive and has a similar specific gravity as that of the prototype and for this reason the performance of sediment scenario runs worked well.

7.2 The main findings of the research

The main findings of this research study are:

I) The physical model study reported herein showed that designing with the same scales for investigating the hydrodynamic, sediment transport and morphodynamic processes in a complicated water system, such as a regulated dam, enhanced the accuracy. By this method, synchronization of these processes in the physical model relates closely to conditions in the

prototype. The potential of using the physical model results in order to simulate, validate and calibrate the numerical model is also significantly enhanced.

II) Physical model results of Hamidieh regulated dam confirm that Chamran Intake could reach its nominal carrying capacity of 90 m^3/s provided that the water elevation is increased from 20.20m (i.e. the proposed normal water level for regulatory conditions) to 20.45m in the reservoir. This is a key result of the physical model study on determining the normal water elevation for diverting the flow into both intakes.

III) Based on the physical model results of Hamidieh regulated dam in the regulatory conditions, the size of sediment entering the Azadegan intake is larger than that entering the Chamran intake. This issue was obtained specifically from the physical model simulation studies.

IV) The 3D layer-integrated scheme used in the mathematical model revealed the main hydrodynamic, solute transport and morphodynamic issues with a high degree of accuracy for the cases considered and, in essence, the flow was basically fully three dimensional. Due to the important role of the near-bed layer (with high sediment concentration), for the processes of sediment transport and morphological changes, the idea of a 3D layer-integrated calculation was very close to the natural environment. By using this concept the computational time was reduced significantly.

V) The calibrated numerical model of Hamidieh regulated dam revealed many hydraulic aspects which were in reasonable agreement with the physical model study results. Some of these important aspects are summarized below:

- The possibility of forming sedimentary islands in the reservoir;
- The sluice gates operation scheme did not have any considerable impact on the sediment flushing capability in areas close to the intakes;
- To reveal deposition and erosion zones near the hydraulic structures and their impacts on diverting flow into the intakes.
- There was no need to excavate the reservoir bed for making the proposed artificial dredging zone, located in front of Azadegan intake, as there was a high risk of significant sedimentation.

The whole aspects and points have been presented in the chapter 6 precisely.

VI) The results of this research have indicated that the calibrated numerical model could be used in the hydraulic design and making decisions for management of the regulated reservoir, with this being a real case study. By this method, the laboratory tests were reduced and thus time and budget were optimized.

7.3 The novelties of the research

The research reveals many sound scientific points that would be so useful for considering in similar studies.

The main novelty aspects of this research are summarized below**:**

I) Baked clay is a very useful material for non-cohesive sediment transport studies in the physical model when the dominant process is suspended sediment transport. This material is cheap and provided a desired grain distribution when a sieving technique is carried out. The specific gravity for this material is around 2.67, the same as the sediment material in the prototype. This means that by using this material scale effete could reduce significantly.

II) The computed suspended sediment concentration by the numerical model in Hamidieh regulated reservoir case study agreed well with the measured results from the physical model (averaged error is less than 8.3%, see Table 6.5). To acquire this level of accuracy, the hydrodynamic computational scheme and the selected turbulence model play an important role. The results of this research showed that the selection of the $k-\varepsilon$ turbulence model in regulated reservoirs where the Reynolds number is high, but without any significant local vortex near hydraulic structures (such as gates) was the correct choice. An accurate estimation of the eddy viscosity has a direct impact on the calculated flow velocity distribution (both horizontally and vertically) and the mixing coefficient which is a key parameter in calculating the sediment transport fluxes. This concept clearly showed the capability of the refined numerical model.

III) A proposed algorithm has been implemented for 2D and 3D morphodynamic module. An explicit method was used for discretizing the bed level change equation. The morphodynamic model was validated across a range of processes and process interactions. The explicit method reduced the computational time and enhanced the accuracy of the results significantly.

IV) Experience showed that in order to prevent instability in the numerical model (especially in the 3-D form), uploading the flow rate for the input boundary needed to be implemented gradually from zero to T_0 (initial time steps). This soft start interval (or warm-up period) was undertaken for a number of time steps over which the input boundary flow rate was gradually increased from zero to 100% of its true value. For implementing this idea, a half sinusoidal function was used for forming these gradually changes (see Figure 4.8). Also, it was proposed to choose a water elevation for output boundaries. Both techniques were useful for enhancing the stability of the numerical model

V) Using an irregular mesh sizing for the vertical direction in the computational domain increased accuracy. This technique was used for investigating the flow, sediment transport and bed level changes in a trench (see test case 1 in Chapter 5) and the results were particularly encouraging. The first layer thickness (from the bed) was proposed to be set to greater than the thickness of the reference level (a).

7.4 Recommendation for further study

In the integrated research study reported herein, efforts have been focused on presenting a new way to apply numerical and physical modelling and combinations of these approaches for solving engineering problems. A joint platform has been designed to obtain accurate results from the numerical and physical model simulations. During the research programme, many techniques and ideas have been reviewed and proposed in order to enhance the ability of the numerical model and to run the physical model for a complicated and real case study (Hamidieh regulated dam). In view of these findings, this research can be seen as a status report of work in progress. This research will be continued with consideration of the suggestions and recommendations that are presented in this section. In extending this research study in the future, the following suggestions are proposed for further consideration:

I) **To use large eddy simulation.** The turbulent flow is complicated even further by geometrical variations due to bed forms, roughness elements and vegetation changes in river cross-section, bends causing secondary currents, confluences associated with strong shear layers and all kinds of man-made structures such as dikes, bridge piers, groins etc. The Large-Eddy Simulation (LES) technique is increasingly used in river flow calculations. Rodi (2010) showed that LES can be applied to river flow problems and allows predicting and studying situations with a particularly complex flow behavior. The method not only yields information on complex mean-flow features but also in unsteady features by resolving the large scale eddies of turbulent motion. The 3D time-dependent LES calculations are computationally expensive, but they are affordable on modern high-performance computers and increasingly on clusters of PCs. By using the LES technique, the velocities and suspended sediment transport fluxes will be computed more accurately, especially in the vicinity of hydraulic structures that engender highly three dimensional flow fields. Enhancing the ability of the numerical model in simulating the level of turbulence is needed for further research.

II) **To discretize the bed level change equations with other methods and make comparisons among the numerical results.** Existing morphological models use classical lower order Lax–Wendroff or modified Lax–Wendroff schemes for morphology. These

schemes are not very stable for simulating long time sediment transport processes. Filtering or artificial diffusion are often added to achieve stability. Long et al. (2008) addressed this with the Euler-WENO scheme and showed it to have significant advantages over schemes with artificial viscosity and filtering processes. Hence, this scheme is highly recommended, especially for phase-resolving sediment transport models. They made their comparisons for a number of numerical examples. The implementation of this idea in simulating morphological changes for different real case studies will strengthen the capabilities of numerical schemes.

III) **Making a new system to inject sediment input for the physical model.** In the physical tests when high sediment concentrations are simulated by injecting dry sediments the method led to some problems in managing the scenarios. This problem was related to a low water depth in the physical model (less than 20cm water depth) and the injection method. It is suggested that a wet injection system be used for simulating high sediments concentrations. Also, the system needs to be installed far enough upstream from the investigation area for best results.

IV) **Further application study of the numerical model**. The 3D layer-integrated model developed should be applied to more real case studies, such as: regulated dams, diversion dams having field measurement data or laboratory data for further investigation of the flow patterns, sediment transport and morphodynamic processes.

References

Abbott, M.B. 1978, Computational hydraulics. Elements of theory of free surface flows. Pitman Publishing, London.

Alstead, R. D. 1994, Numerical modelling of tidal flow using nested and patched grid schemes. Ph.D. thesis, Univ. of Bradford, Bradford, U.K.

Alvim, A.M. 1987, Modelo matemático bidimensionalde assoreamento em reservatórios. (2-D mathematical model for reservoir sedimentation) M.Sc. dissertation, Engineering School of Sao Carlos − University of Sao Paulo, Sao Carlos, Brazil (in Portuguese).

ASCE. 1982, Design of Water Intake Structures for Fish Protection. American Society of Civil Engineers, New York, NY. pp. 69-73.

ASCE. 1988, Task Committee on Turbulence Models in Hydraulic Computations, Turbulence modelling of surface water flow and transport, Parts I-III, Journal of Hydraulic Engineering, ASCE, 114(9), 970-1051.

Atkinson, E. 1989, Predicting the performance predicting method for canal sediment extractors. Hydraulic Research Wallingford, UK, Report no. OD/TN 41.

Atkinson, E., Lawson, JD. and Tosswell, P. 1993, Comparison of physical and computer modelling of the Kapunga intake with performance of the prototype. Paper R 106, 15th Congress of the Int. Comm. on Irrig. and Drain, The Hague.

Atkinson, E., Lawson, JD. and Tosswell, P. 1994, Comparison of physical and computer modelling of the Kapunga intake with performance of the prototype. Hydraulic Research Wallingford, UK, Report no. ODP121.

Atkinson, E. 1995, A numerical model for predicting sediment exclusion at intakes. Hydraulic Research Wallingford, UK, Report no. OD130.

Avery, P. 1989, Sediment control at intakes. British Hydromechanics Research Association, The Fluid Engineering Center, Cranfield, Bedford, England.

Boillat, J.-L. and De Cesare, G. 1994, Dichteströmungen im Bereich des Grundablasses des Stausees Luzzone – Modellversuche. Tagungsband (proceedings) des Symposiums "Betrieb, Erhaltung und Erneuerung von Talsperren und Hochdruckanlagen", pp. 183-192, Graz, Austria.

Bos, M. G. 1989, Discharge Measurement Structures – ILRI Publication 20, Netherlands.

Buckingham, E. 1914, On physically similar systems – Illustrations of the use of dimensional equations. Physical Review 4, 345–376.

Cahyono. 1993, Three-dimensional numerical modelling of sediment transport processes in non-stratified estuarine and coastal waters, PhD. Thesis, Dept. of Civil Engineering, University of Bradford, Bradford, January, pp.315.

Celic, I. and Rodi, W. 1988, Modelling suspended sediment transport in non-equilibrium situation. J. Hydraul. Eng., ASCE, 114(10), 1157-1191.

Chadwick, A. J. and Morfett, J. C. 1986, Hydraulics in civil engineering. Allen & Unwin, London, 492p.

Chang, H. H. 1982, Mathematical model for erodible channels. J. Hydraul. Div., Am. Soc. Civ. Eng., 108(5), 678–689.

Chang, H.H., Harrison, L. L., Lee, W. and Tu, S. 1996, Numerical modeling for sediment-pass-through reservoirs. Journal of Hydraulic Research 122(7).

Chanson, H. 1999, The Hydraulics of Open Channel Flow. Published by Arnold, 338 Euston Road, London NW1 3BH, UK.

Chanson, H. and James, D.P. 1999, Siltation of Australian Reservoirs: some Observations and Dam Safety Implications. Proc. 28th IAHR Congress, Graz, Austria, Session B5, 6 pages (CD-ROM).

Chapman, R. S. 1993, Modification of the momentum diffusion algorithm within CH3D. Final Report to the Coastal Engineering Research Center. U.S. Army Corps of Engineers, Waterways Experiment Station, Vicksburg, MS, USA.

Chien, N. and Wan, Z. 1998, Mechanics of Sediment Transport. ASCE Press, Reston, VA, USA.

Chesher, T.J., Wallace, H.M., Meadowcroft, I.C., Southgate, H.N. 1993, PISCES. A morphodynamic coastal area model, First annual report, Report SR 337. HR Wallingford.

Chow, V. T. 1959, Open Channel Hydraulics. McGraw-Hill New York.

Cogollo, P.R.J. and Villela, S.M. 1988, Mathematical model for reservoir silting. Proceedings of the Porto Alegre Symposium of Sediment Budgets, IAHS Publication, Porto Alegre, Brazil.

Cunge, J. A., Holly, F. M., Jr., and Verwey, A. 1980, Practical aspects of computational river hydraulics, Pitman Publishing Inc., Boston.

Damgaard, J.S. and Chesher, T.J. 1997, Morphodynamic simulations of Helwick Bank, Report TR 31. HR Wallingford.

Damgaard, J.S. 1998, Numerical schemes for morphodynamic simulations, Report IT 459. HR Wallingford.

Delft Hydraulics Laboratory, 1981 and 1983, Development of sediment concentration profiles in a steady uniform flow without initial sediment load, report M 1531 II and III, Delft, The Netherland.

Demuren, A.O., Rodi, W. 1983, Side discharges into open channels: Mathematical Model. Journal of Hydraulic Engineering, v 109, n 12, p 1707-1722.

Demuren, A.O. 1991, Development of a mathematical model for sediment transport in meandering rivers. Report. no. 693, Institute for Hydromechanics, University of Karlsruhe, Karlsruhe, Germany.

De Vriend, H.J. 1981, Steady flow in shallow channel bends. Communication on Hydraulics 81-3, Department of Civil Engineering, Delft University of Technology, Netherlands.

De Vriend, H.J., 1985, Flow formulation in mathematical models for 2DH morphological changes, Report No. R1747-5, Delft Hydraulic Laboratory, Delft, The Netherlands.

De Vriend, H.J. 1986, Two- and three-dimensional mathematical modelling of coastal morphology, Report No. H284-2, Delft Hydraulic Laboratory, Delft, The Netherlands.

De Vriend, H.J., Zyserman, J., Nicholson, J., Roelvink, J.A., Pechon, P. and Southgate, H.N. 1993, Medium-term 2DH coastal area modelling. Coastal Engineering 21 (1–3), 193–224.

De Vries, M. 1971, Solving river problems by hydraulic and mathematical models. Delft Hydraulic Laboratory, Publ. No. 76 II, September.

De Vries, M. and Van Der Zwaard, J. J. 1975, Movable-bed river-models, ASCE Symp. On Modelling, Pub. No. 156. San Francisco, pp.1-17.

De Vries, M. 1981, Morphological computations, Delft University of Technology, Dept. of Civil Eng, Lecture notes f10a.

De Vries, M. 1993, Use of models for river problems, Int. Hydro. Prog. Studies and Reports on Hydrology, 51, Paris, UNESCO Pub.

Dhamotharan, S., Gulliver, J.S. and Stefan, H.G. 1981, Unsteady One-Dimensional Settling of Suspended Sediment. Water Resources Research 17(4), 1125-1132.

Dhondia, J. F. and Stelling, G. S. 2002, Application of one dimensional–two dimensional integrated hydraulic model for flood simulation and damage. Proceedings of the 5thInternational Conference on Hydroinformatics, Cardiff, 265–276.

Ding, D. and Liu, P. L. 1989, An operator-splitting algorithm for two-dimensional convection-dispersion –reaction problems. International Journal for Numerical methods in Engineering, Vol. 28, pp.1023-1040.

DUT. 1983, Flow user's guide, Delft University of technology, Dept. of civil Eng.

Faghihirad, S., Lin, B. and Falconer, R. A. 2010, 3D layer-integrated modelling of flow and sediment transport through a river regulated reservoir. International Conference on Fluvial Hydraulics, IAHR, Braunscheweig, Germany Volume 2, p1573-1580.

Faghihirad, S., Lin, B. and Falconer, R. A. 2011, 3D layer-integrated modelling morphological changes in a river regulated reservoir. The 7th IAHR Symposium on River, Coastal and Estuarine Morphodynamics (RCEM), Beijing, China.

Falconer, R. A. 1980, Numerical modelling of tidal circulation in harbours. Journal of the Waterway, Port, Coastal and Ocean Division, ASCE 106, 31–48.

Falconer, R. A. 1986, A two-dimensional mathematical model study of the nitrate levels in an inland natural basin. Proceedings of the International Conference on Water Quality Modelling in the Inland Natural Environment, BHRA Fluid Engineering, Bournemouth, England, Paper J1, June, pp. 325–344.

Falconer, R. A. and Owen, P. H. 1990, Numerical modelling of suspended sediment fluxes in estuarine waters. Estuarine and Coastal and Shelf science, 31, 745-762.

Falconer, R. A., George, G.D. and Hall, P. 1991, Three-dimensional numerical modelling of wind-driven circulation in a shallow homogeneous Lake. Journal of Hydrology, Elsevier Science Publishers, Vol. 124, pp. 59-79.

Falconer, R. A. and Chen, Y. P. 1991, An improved representation of flooding and drying and wind stress effects in a 2-D numerical model. Proceedings of the Institution of Civil Engineers, Part 2, Research and Theory 91, 659–687.

Falconer, R. A. 1993, An introduction to nearly horizontal flows. In Coastal, Estuarial and Harbour Engineers' Reference Book (Abbott, M. B. & Price, W. A., eds). E & FN Spon Ltd., London, 736 pp.

Falconer, R. A. and Chen, Y. 1996, Modelling Sediment Transport and Water Quality Processes on Tidal Floodplains. In: Floodplain Processes, Malcom G. Anderson, Des E. Walling and Paul D. Bates (editors), John Wiley & Sons Ltd.

Falconer, R. A. and Lin, B. 2001, DIVAST model Reference manual, Cardiff University.

Fang, H.W., Rodi, W. 2000, Three-Dimensional Calculation of Flow and Sediment Transport in the Neighborhood of the Dam for the Three Gorges Project (TGP) reservoir in the Yangtze River. Report of the Institute for Hydromechanics, No. 762, University of Karlsruhe, Germany.

Fischer, H. B. 1973, Longitudinal dispersion and turbulent mixing in open channel flow. Annu. Rev. Fluid Mech., 5, 59–78.

Fischer, H.B. 1976, Mixing and dispersion in estuaries. Annual Review of Fluid Mechanics, 8, 107-133.

Fischer, H.B. List, E. G., Koh, R. C. Y., Imberger, J. and Brooks, N. H. 1979, Mixing and Dispersion in Inland and Coastal Waters. Academic Press, Inc., California.

French, R. H. 1986, Open channel hydraulics McGraw-Hill, New York.

Froehlich, D. C. 1989, Finite Element Surface Water Modeling System: Two dimensional flow in a horizontal plane. User's Manual, U. S. Federal Highway Administration Report No. FHWA-RD-88-177.

Gailani, J., Ziegler, C.K. and Lick, W. 1991. Transport of suspended solids in the Lower Fox River. Journal of Great Lakes Reservoirs 17(4), 479-494.

Galppatti, G. and Vreugdenhil, C. B. 1985, A depth-integrated model for suspended sediment transport. J. Hydraul. Eng., ASCE, 127, 30-37.

Garci, M. and Parker, G. 1991, Entrainment of bed sediment into suspension. Journal of Hydraulic Engineering, ASCE, Vol. 117, No. 4, pp. 359-375.

Gessler, D., Hall, B., Spasojevic, M., Holly, F., Pourtaheri, H. and Raphelt, N. 1999, Application of 3D mobile bed, hydrodynamic model. Journal of Hydraulic Engineering 125(7).

Goldstein, S. 1938, Modern developments in fluid dynamics. Vol 1, Oxford University Press, Oxford.

Hakimzadeh, H. 1997, Turbulence modelling of tidal currents in rectangular harbors. Ph.D. Thesis, Univ. of Bradford, Bradford, U.K.

Hakimzadeh, H., Falconer, R. A. 2007, Layer integrated modelling of three-dimensional recirculating flows in model tidal basins. Journal of water, port, coastal and ocean engineering; DOI: 10.1061/(ASCE)0733-950X.

Halcrow/HR Wallingford. 1999, ISIS Flow User Manual, Swindon, Wiltshire, SN4 OQD, UK.

Hall, P. 1987, Numerical Modelling of Wind Induced Lake Circulation. Ph.D. Thesis, University of Birmingham, 292 pp.

Han, Q. W. 1980, A study on the non-equilibrium transportation of suspended load. Proc., 1st Int. Symp. on River Sedimentation, Beijing.

Heller, V. 2011, Scale effects in physical hydraulic engineering models. Journal of Hydraulic Research, Vol. 49, No. 3 (2011), pp. 293–306. doi:10.1080/00221686.2011.578914.

Henderson, F.M. 1966, Open channel flow. Macmillan, NewYork.

Horritt, M.S. and Bates, P.D. 2001, Effects of special resolution on a raster based model of flood flow, Journal of Hydrology, 253, 239-249.

Hudson, J., Damgaard, J., Dodd, N., Chesher, T., Cooper, A. 2005, Numerical approaches for 1D morphodynamic modelling. Coast. Eng. 52, 691–707.

Hughes, S.A. 1993, Advanced series on ocean engineering 7. Physical models and laboratory techniques in coastal engineering, World Scientific, London.

Hydrological Engineering Center. 1997, UNET, One-dimensional unsteady flow through a full network of open channels, User's Manual, U.S. Army Corps of Engineers, Davis, CA.

Hydrological Engineering Center. 2008, HEC-RAS River Analysis System, Hydraulic Reference Manual, Version 4.0, U.S. Army Corps of Engineers, Davis, CA, Report Number: CPD-69.

Interagency Committee on Water Resources, Subcommittee on Sedimentation. 1957, Measurement and Analysis of Sediment Loads in Streams: Report No. 12, Some Fundamentals of Particle Size Analysis. St. Anthony Falls Hydraulic Laboratory, Minneapolis, MN.

Ivicsisc, L. 1975, Hydraulic models. VTTUKI, Budapest.

Jia, Y., and Wang, S. S.-Y. 1999, Numerical model for channel flow and morphological change studies. Journal of Hydraulic Engineering, ASCE, Vol. 125, No. 9.

Jin, X., Kranenburg ,C. 1993, Quasi-3D Numerical modeling of shallow-water circulation. ASCE J. Hydr. Eng. 119 (4) 458-472.

Johnson, H.K., Zyserman, J.A. 2002, Controlling spatial oscillations in bed level update schemes. Coast. Eng. 46, 109–126.

Kamphuis, J. W. 1996, Physical Modeling of Coastal Processes In: LIU, P. L. (ed.), Advance in Coastal and Ocean Engineering, World Scientific, pp.

Khan, A. A., Cadavid, R. and Wang, S. S.-Y. 2000, Simulation of channel confluence and bifurcation using the CCHE2D model. Journal of Water and Maritime Engineering, Proceeding Institution of Civil Engineers, Vol. 142, June.

Khosronejad, A., Salehi Neyshabouri, A. A. 2006, Numerical Simulation of Sediment Release from Reservoirs. Internl. J. Sedim. Res. 21(1), 1-15.

Khosronejad, A., Rennie, C.D. and Salehi Neyshabouri, A. A. 2008, Three-dimensional numerical modeling of reservoir sediment release. Journal of Hydraulic Research Vol. 46, No. 2, pp. 209–223.

Knauss, J., Coordinating editor, IAHR, 1987, Swirling Flow Problems at Intakes.

Kobus, H., ed. 1980, Hydraulic modelling. German association for water resources and land improvement, Bulletin 7. Parey, Hamburg.

Kocyigit, O., Lin, B. and Falconer, R. A. 2005, Modelling sediment transport using a lightweight bed material. Proceeding of the institution of civil engineers, Maritime engineering, p 3-14.

Kolahdoozan, M., 1999, Numerical Modelling of Geomorphological Processes in Estuarine Waters. Ph.D Thesis, University of Bradford, Bradford, UK, pp. 288

Kolahdoozan, M. and Falconer, R. A. 2003, Three-dimensional geo-morphological modeling of estuarine waters. International Journal of Sediment Research, Vol. 18, No. 1, pp. 1-16.

Krishnappan, B. G., Lau, Y. L. 1986, Turbulence modelling of flood plain flows. Journal of hydraulic engineering, v 112, n 4, p 251-266.

Leendertse, J. J. 1967, Aspects of a computational model for long period water wave propagation. Memorandum RM-5294-PR, RAND Corporation, Santa Monica, Calif.

Le Méhauté, B. 1990, Similitude. Ocean engineering science, the sea. B. Le Mehaute, D.M. Hanes, eds. Wiley, New York, 955–980.

Leonard, B. P. 1991, The ULTIMATE conservative difference scheme applied to unsteady one dimensional advection. Computer Methods in Applied Mechanics & Engineering, Vol. 88, pp, 17-74.

Lesser, G.R., Roelvink, J.A., van Kester, J.A.T.M. and Stelling, G.S. 2004, Development and validation of a three-dimensional morphological model. An International Journal for coastal, Harbour and Offshore Engineers. Doi:10.1016/j.coastaleng.2004.07.014

Lick, W., Lick , J. and Ziegler , C.K. 1994, There-suspension and transport of fine-grained sediments in Lake Irie. Journal of Great Lakes Reservoirs 20(4), 599-612.

Lin, B. and Falconer, R. A. 1995b, Three- dimensional layer integrated modelling of estuarine flows with flooding and drying. Estuary and Coastal Shelf Science.

Lin, B. and Falconer, R. A. 1995, Modelling Sediment Fluxes in Estuarine Waters Using Curvilinear Co-ordinate Grid System. Estuary, Coastal and Shelf Science, Vol. 14, pp.413-428.

Lin, B. and Falconer, R. A. 1996, Numerical modelling of three dimensional suspended sediment for estuarine and coastal waters. Journal of hydraulic research. 34(4), 435-456.

Lin, B. and Falconer, R. A. 1997, Tidal flow and transport modelling using ULTIMATE QUICKSET scheme. Journal of Hydraulic Engineering, ASCE, Vol. 123, No. 4, 303-314.

Lin, B. and Falconer, R. A. 1997, Three-dimensional layer integrated modelling of estuarine flows with flooding and drying. Estuarine, coastal and shelf science, 44, 737-751.

Lin, B., Wicks, J., Falconer, R. A. and Adams, K. 2006, Integrated 1D and 2D hydrodynamic models for flood simulations. Proceedings of the Institution of Civil Engineers, Water management 159, Issue WM1,Pages 19–25.

Li, C. W. and Falconer, R. A. 1995, Depth integrated modelling of tide induced circulation in a Square Harbour. Journal of Hydraulic Research, Delft, the Netherlands, 33(3), 321–32.

Liu, X.-D., Osher, S. and Chan, T. 1994, Weighted essentially non-oscillatory schemes. J. Comput. Phys. 115, 200.

Long, W., Kirby, J.T. and Shao, Z. 2008, A numerical scheme for morphological bed level calculations. An International Journal for Coastal, Harbour and Offshore Engineers, 55 167-180. Doi:10.1016/j.coastaleng.2007.09.009

Lopez, S. J. L. 1978, Mathematical modeling of sediment deposition in reservoirs, In Hydrology Papers, No. 95, Colorado State University, Fort Collins, Colorado, July.

Manson, JR. 1994, The development of a predictive procedure for localized three dimensional river flows. PhD thesis, University of Glasgow.

Martin, H., Pohl, R., eds. 2000, Technische Hydromechanik 4 (Technical hydromechanics). Verlag für Bauwesen, Berlin [in German].

Martinez, R. G., Saavedra, I. C., Power, B. F. D., Valera E. and Villoria, C. 1999, A two-dimensional computational model to simulate suspended sediment transport and bed changes. Journal of Hydraulic Research, 37, No. 3, 327–344.

Mefford, B., Stowell, H. and Heinje, C. 2008, Robles Diversion Dam High Flow and Sediment Bypass Structure Ventura, California, Hydraulic Laboratory Report HL-2008-7, Bureau of Reclamation's Water Resources Research Laboratory, Colorado.

Moody, L. F. 1944, Friction factors for pipe flows, Trans. Am. Soc. Mech. Engrn. 66, pp. 671-684.

Nakato, T. and Ogden, F.L. 1998, Sediment control at water intakes along sand-bed rivers. Journal of Hydraulic Engineering, Vol.124, No. 6, p.589-596.

Neary, V. S., Barkdoll, B., and Odgaard, A. J. 1994, Sandbar formation in side-diversion channels. Proc., Nat. Conf., Hydraulics Division, American Society of Civil Engineers, New York, 1171–1175.

Nezu, I., Nakagawa, A. 1993. Turbulence in open channel flows. IAHR Monograph Series, Balkema, Rotterdam.

Nicholson, J., Broker, I., Roelvink, J.A., Price, D., Tanguy, J. M. and Moreno, L. 1997, Inter comparison of coastal area morphodynamics models. Coastal Engineering 31, 97-123.

Nicklow, J.W. and Mays, L.W. 2000, Optimization of multiple reservoir networks for sedimentation control. Journal of Hydraulic Engineering 126(4).

Noor Shahidan, N.F. and Abu Hasan, Z. 2010, Application of mathematical and physical modeling to resolve sedimentation of Ijok intake. Proceeding of 3rd International Conference on Managing Rivers in 21st Century: Sustainable Solutions for Global Crisis of Flooding, Pollution and Water Scarcity (Rivers 2011), Penang, Malaysia, pp. 784-790, December 6-9, Penang, Malaysia. ISBN: 9789833067350

Norton, W. R., King, I. P. and Orlob, G. T. 1973, A finite element model for Lower Granite Reservoir. Water Resources Engineers, Inc,. Walnut Creek, California.

Novak, P. and Cabelka, J. 1981, Models in hydraulic engineering. Pitman, Boston.

O'Connor, B.A. and Nicholson, J. 1988, A three-dimensional model of suspended particulate sediment transport. Coast. Eng. 12,157-174.

O'Connor, B.A. and Nicholson, J. 1995, Suspended sediment transport equations, Report No. CE/3/95. Department of Civil Engineering, University of Liverpool, p. 11.

Olesen, K.W. 1987, Bed topography in shallow river bends. Report 87-1, Faculty of Civil Engineering, Delft University of Technology, Netherlands.

Olsen, N. R. B. and Skoglund, M. 1994, Three dimensional numerical modelling of water and sediment flow un a sand trap. Journal of Hydraulic Research, IAHR, Vol. 32, pp. 833-844.

Olsen N. R. B. and Kjellesvig, H. M. 1998, A Three-dimensional numerical flow modelling for estimation of maximum local scour depth. IAHR Journal of Hydraulic Research, 36, 579-590.

Olsen, N. R. B. 1999, Two-dimensional numerical modelling of reservoir flushing processes. IAHR Journal of Hydraulic Research, 37, No. 1, 3–16.

Olsen, N. R. B. and Kjellesvig, H. M. 1999, Three-dimensional numerical modelling of bed changes in a sand trap. IAHR Journal of Hydraulic Research, 37, No. 2, 189–197.

Olsen, N. R. B. 2000, CFD Modeling of Bed Change during Flushing of a Reservoir. Hydroinformatic 2000, Iowa, USA.

Olsen N. R. B. 2002, A three dimensional numerical model for simulation of sediment movements in water intakes with multi block option, User's manual.

Olsen, N. R. B. 2003, Three dimensional CFD modelling of free-forming meander channel. Journal of Hydraulic Engineering, 129 (5), 366–372.

Olsen N. R. B. 2011, A three dimensional numerical model for simulation of sediment movements in water intakes with multi block option, Version 1 and 2, User's manual.

Patankar, S. V. 1988, Elliptic Systems: Finite Difference Method I, Handbook of numerical heat transfer, Eds. W. J. Minkowycz, E. M. Sparrow, et al., John Wiley & Sons, Inc., New York.

Péchon, P., Teisson, C. 1996, Numerical modelling of bed evolution behind a detached breakwater. Proceedings of the 25th International Conference on Coastal Engineering, ASCE, New York, pp. 2050–2057.

Pender, G., Keogh, D., Manson, JR. and Addison, P. 1995, Verification of a three-dimensional river flow model with experimental data Hydra 2000, vol. 1: integration of research approach sand applications, Pages: 290-295.

PIANC. 1991, Guidelines for the Design and Construction of Flexible Revetments Incorporating Geotextiles in Marine Environment, Bulletin 7879.

Raghunath, H.M. 1967, Dimensional analysis and hydraulic model testing. Asia Publishing House, London.

Rahuel, J. L., Holly, F. M., Chollet, J. P., Belleudy, P. J., and Yang, G.1989, Modelling of riverbed evolution for bed load sediment mixtures. J. Hydraul. Eng., 115(11), 1521–1542.

Rodi, W. 1984, Turbulence Models and Their Application in Hydraulics. 2nd Edition. IAHR Publication, Delft, 104 pp.

Rodi, W. 1993, Turbulence models and their application in hydraulics - a state of the art review. International Association for Hydraulic Research, Delft, 3rd edition, Balkema.

Rodi, W. 2010, Large eddy simulation of river flows. Proc. International conference on fluvial hydraulics. IAHR, Braunscheweig, Germany, Volume 1, p 23-32.

Roelvink, J. A., van Banning, G.K.F.M. 1994, Design and development of Delft3D and application to coastal morphodynamics. In: Verwey, Minns, Babovic, Maksimovic (Eds.), Hydroinformatics ’94. Balkema, Rotterdam, pp. 451–455.

Roelvink, J. A., Walstra, D.J.R., Chen, Z. 1994, Morphological modelling of Keta lagoon case. Proc. 24th Int. Conf. on Coastal Engineering, ASCE, Kobe, Japan.

Roelvink, J.A. 2006, Coastal morphodynamic evolution techniques. Coast. Eng. 53, 277-287.

Russell, R. C. H. 1964, Methods of choosing scales for models in use at the Hydraulic Research Station, Hydraulics Res. Stn, Wallingford, Report No. INT 40, November.

Rüther, N., Olsen, N. R. B. 2003, CFD modelling of alluvial channel instabilities. Proc. 3rd IAHR Symposium on River, Coastal and Estuarine Morphodynamics. IAHR, Barcelona, Spain.

Rüther, N., Olsen, N. R. B. 2005a, Advances in 3D Modelling of Free forming Meander Formation from Initially Straight Alluvial Channels. 31st IAHR Congress, Seoul, South Korea.

Rüther, N., Olsen, N. R. B. 2005b, Three dimensional modeling of sediment transport in a narrow 90° channel bend. Journal of Hydraulic Engineering 131 (10), 917–920.

Ruether, N., Singh, J. M., Olsen, N. R. B. and Atkinson, E. 2005, 3D computation of sediment transport at water intakes. Proceeding of the institution of civil engineering, water management, Issue WMI, pages 1-8.

Schulz, E.F., Wilde, R. H. and Albertson, M. L. 1954, Influence of shape on the fall velocity of sedimentary particles. MRD Sediment Series, no. 5.

Sharp, J. J. 1981, Hydraulic modeling. Butterworth & Co. (publisher) Ltd, London: 88 Kingsway, WC2B 6AB.

Shen, H. W. 1990, Introductory remarks. In NATO Workshop on Movable Bed Physical Models (SHEN H. W. (ed.)). Kluwer Academic, Dordrecht, The Netherlands, pp. 1-12.

Sloff, C. J., Jagers, H.R.A. and Kitamura, Y.K. 2004, Study on the channel development in a wide reservoir. Proceedings of the 2nd International Conference on Fluvial Hydraulics, River Flow, Napels, Italy, 811-819.

Smith, J. D. and Mclean, S. R. 1977, Spatially averaged flow over a wavy surface. Journal of Geophysical Research, Vol. 82, pp. 1725-1746.

Souza, L.B.S. 2006, Estudo experimental emodelagem numérica do escoamento e doassoreamento em uma armadilha de sedimentos. (Experimental study and numerical simulation of the flow and sedimentation in a sand trap), PhD thesis, Engineering School of Sao Carlos - University of Sao Paulo, Sao Carlos, Brazil (in Portuguese).

Souza, L.B.S., Schulz, H.E., Villela, S.M., Gulliver, J.S. and Souza, L.B.S. 2010, Experimental Study and Numerical Simulation of Sediment Transport in a Shallow Reservoir. Journal of Applied Fluid Mechanics, Vol. 3, No. 2, pp. 9-21, 2010.

Spurk, J.H. 1992, Dimensions analyse in der Strömungslehre (Dimensional analysis in fluid flow). Springer, Berlin [in German].

Steffler, P. and Blackburn, J. 2002, Introduction to depth averaged modelling and User's Manual River 2D. University of Alberta.

Stephan, U. and Hengl, M. 2010, Physical and numerical modeling of sediment transport in river Salzach. Proc. International conference on fluvial hydraulics. IAHR, Braunscheweig, Germany, Volume 2, p 1259-1265.

Struiksma, N. 1985, Prediction of 2-D bed topography in rivers. ASCE Journal of Hydraulic Engineering 111 (8), 1169-1182.

Talmon, A.M. 1992, Bed topography of river bends with suspended sediment transport. Thesis, Delft University of Technology, Netherlands.

Tanguy, J.M., Zhang, B., Hamm, L. 1993, A new Lax–Wendroff algorithm to solve the bed continuity equation with slope effect. Proc. 3rd Int. Conf. on Coastal Estuarine Modelling. ASCE, pp. 134–148.

TELEMAC modeling system. 2007, 3D hydrodynamics, TELEMAC-3D code release 5.8, Operating manual.

Thomas, W. A. 1982, Chapter 18: Mathematical modeling of sediment movement. Gravel-bed rivers, R. D. Hey et al., eds., Wiley, New York.

Tsai, C. T., and Yen, C. L. 1982, Simulation of unsteady flow in movable bed channel. Proc., 3rd Congress of Asian and Pacific Regional Division, IAHR, Bandung, Indonesia.

van Niekerk, A., Vogel, K. R., Slingerland, R. L., and Bridge, J. S. 1992, Routing of heterogeneous sediments over movable bed: Model development. J. Hydraul. Eng., 118(2), 246–262.

van Rijn, L. C. 1984, Sediment transport, part I: bed load transport. J. Hydraulic Eng. (ASCE), 110(10), 1431-1456.

van Rijn, L. C. 1984, Sediment transport, part II: suspended load transport. J. Hydraulic Eng. (ASCE), 110(11), 1613-1641.

van Rijn, L. C. 1986, Mathematical modelling of suspended sediment in non-uniform flows. J. Hydraulic Eng. (ASCE), 112(6), 433-455.

van Rijn, L. C. 1987, Mathematical Modelling of Morphological Processes in the Case of Suspended Sediment Transport. PhD Thesis, Delft Technical University, Delft, The Netherlands.

van Rijn, L. C., van Rossum, H. and Termes, P. 1990, Field verification of 2-D and 3-D suspended sediment models. J. Hydraul. Eng., ASCE, 116(10), 1270-1278.

van Rijn, L. C. 1993, Principles of Sediment Transport in Rivers, Estuaries and Coastal Seas. Aqua Publications, the Netherlands, 673 pp.

Vanoni, V.A., ed. 1975, Sedimentation Engineering: American Society of Civil Engineers, Manuals and Reports on Engineering Practice, no. 54, 745 p.

Versteeg, H. K., Malalasekera, W. 2007, An introduction to computational fluid dynamics the finite volume method. Second edition, Pearson education limited.

Verwey A. 2001, Latest development in floodplain modelling-1D/2D integration. proceedings of the Australia Conference on Hydraulics in Civil Engineering, The Institute of Engineers, Hobart.

Vreugdenhil, C. B., and Wijbenga, J. H. A. 1982, Computation of flow patterns in rivers. J. Hydr. Div., ASCE, 108(11), 1296–1310.

Wang, S. S. Y. and Adeff, S. E. 1986, Three-dimensional modeling of river sedimentation processes. Proceedings of the third international symposium on river sedimentation, The University of Mississippi, Mississippi, USA.

Wang, Z.B. 1989, Mathematical modelling of morphological processes in estuaries. PhD Thesis, Delft University of Technology, Delft, The Netherlands.

Wang, S. S. Y. and Hu, K. K. 1992, Improved methodology for formulating finite element hydrodynamic models. Finite Element in Fluids, edited by T. J. Chung, Vol. 8, Hemisphere Publishing Corp.

Water and Electricity Organization of Khuzestan Province (WEOKP). 2001, Karkhe irrigation network operation company, Bulletin No. 31, p 23-31.

Whitham, G.B. 1974, Linear and Nonlinear Waves. John Wiley and Sons, Inc. Yu, J., Mei, C.C., 2000. Formation of sand bars under surface waves. J. Fluid Mech. 416, 315–348.

Wicks, J., Syme, B., Hassan, M. A. A. M., Lin, B. and Tarrant, O. 2004, 2D modelling of floodplains—is it worth the effort? Proceedings of the River and Coastal Flooding Conference, Defra, UK, pp. 1–10.

Wu, W., Vieira, D.A. and Wang, S. S. Y. 2004, One-Dimensional Numerical Model for Nonuniform Sediment Transport under Unsteady Flows in Channel Networks. J. Hydraulic Eng., ASCE, 130(9), 914-923.

Yalin, M. S. 1971, Theory of hydraulic models. MacMillan, London.

Zanke, U. 1977, Berechnung der Sinkgeschwindigheiten von Sedimenten. Mitt des Franzius-Institutes Fur Wassrbau, Heft 46, Seite 243, Technical University, Hannover, West Deutcheland.

Zegzhda, A. P. 1938, Theory of similarity and method of computation hydraulic models, (in Russian), Gosstrojizdat, Moscow.

Ziegler, C.K. and Nisbet, B.S. 1994, Fine-grained sediment transport in Pawtuxet River, RhodeIsland. Journal of Hydraulic Engineering 120(5), 561-576.

Ziegler, C.K. and Nisbet, B.S. 1995, Long-term simulation of fine-grained sediment transport in large reservoir. Journal of Hydraulic Engineering 121(11).

Zwamborn, J. A. 1966, Reproducibility in Hydraulic Models of Prototype River Morphology. La Houille Blanche, no. 3, pp. 291-298.

Zwamborn, J. A. 1967, Solution of River Problems with Moveable-Bed Hydraulic Models. MEG 597, Council for Scientific and Industrial Research, Pretoria, South Africa.

Zwamborn, J. A. 1969, Hydraulic Models, MEG 795, Council for Scientific and Industrial Research, Stellenbosch, South Africa.